DAMPING INTERAREA AND TORSIONAL OSCILLATIONS USING FACTS DEVICES

A Thesis

Submitted to the College of Graduate Studies and Research

in Partial Fulfillment of the Requirements

For the Degree of

Doctor of Philosophy

in the Department of Electrical Engineering

University of Saskatchewan

Saskatoon, Saskatchewan

By

Amr Adel Eldamaty

To my precious wife, Amira, with thanks and appreciations for her patience and encouragement

PERMISSION TO USE

The author has agreed that the library, University of Saskatchewan, may make this thesis freely available for inspection. Moreover, the author has agreed that permission for extensive copying of this thesis for scholarly purposes may be granted by the professor or professors who supervised the thesis work recorded herein or, in their absence, by the Head of the Department or the Dean of College in which the work was done. It is understood that due recognition will be given to the author of this thesis and to the University of Saskatchewan in any other use of the material in this thesis. Copying or publication or any other use of the thesis for financial gain without approval of the University of Saskatchewan and the author's written permission is prohibited.

Requests for permission to copy or to make any other use of the material in this thesis in whole or in part should be addressed to:

Head of the Department of Electrical Engineering
University of Saskatchewan
Saskatoon, Saskatchewan, S7N 5A9
Canada

ACKNOWLEDGEMENTS

The author would like to express his sincere gratitude and appreciation to his supervisor, Dr. Sherif O. Faried, for his criticisms, valuable guidance and consistent encouragement throughout the course of this research work. The author would also like to acknowledge Dr. Faried's patience and helpful suggestions in the preparation of this thesis. The author would like to express his appreciation to the members of his Advisory Committee.

The author takes this opportunity to express special thanks to his parents, his sister, Abeer and every one in the family for their patience and encouragement. Besides, his appreciations to his wife's family, specially Mama Rawya.

Financial assistance provided by the Natural Sciences and Engineering Research Council of Canada and the University of Saskatchewan in the form of a graduate scholarship is thankfully acknowledged.

ABSTRACT

A problem of interest in the power industry is the mitigation of interarea and torsional oscillations. Interarea oscillations are due to the dynamics of interarea power transfer and often exhibit poor damping when the aggregate power transfer over a corridor is high relative to the transmission strength. These oscillations can severely restrict system operations and, in some cases, can lead to widespread system disturbances. Torsional oscillations are induced due to the interaction between transmission system disturbances and turbine-generator shaft systems. The high torsional stresses induced due to some of these disturbances reduce the life expectancy of the turbine-generators and, in severe cases, may cause shaft damage.

This thesis reports the development of novel control techniques for Flexible AC Transmission System (FACTS) devices for the purpose of damping power system interarea and torsional oscillations. In this context, investigations are conducted on a typical three-area power system incorporating FACTS devices. The Genetic Algorithm (GA) and fuzzy logic techniques are used for designing the FACTS controllers. Although attention is focused in the investigations of this thesis on the Unified Power Flow Controller (UPFC), studies are also conducted on two other FACTS devices, a three voltage-source converter Generalized Unified Power Flow Controller (GUPFC) and a voltage-source converter back-to-back HVdc link.

The results of the investigations conducted in this thesis show that the achieved control designs are effective in damping interarea oscillations as well as the high torsional torques induced in turbine-generator shafts due to clearing and high-speed reclosing of transmission system faults. The controller design procedures adopted in this thesis are general and can be applied to other FACTS devices incorporated in a power system. The results and discussion presented in this thesis should provide valuable information to electric power utilities engaged in planning and operating FACTS devices.

TABLE OF CONTENTS

LIST OF TABLES

LIST OF FIGURES

LIST OF ABBREVIATIONS

EXC	Exciter
FACTS	Flexible AC Transmission Systems
GA	Genetic Algorithm
GEN	Generator rotor
GPS	Global Positioning System
GUPFC	Generalized Unified Power Flow Controller
HP	High-Pressure turbine
IED	Intelligent Electronic Devices
IP	Intermediate-Pressure turbine
IPFC	Interline Power Flow Controller
LP	Low-Pressure turbine
MISO	Multi-Input Single-Output
P-UPFC	Proportional UPFC Controller
PF-UPFC	Proportional fuzzy logic UPFC
HF-UPFC	Hybrid fuzzy logic UPFC
PI	Proportional Integral
PID	Proportional Integral Derivative
PMU	Phasor Measurement Units
PSS	Power System Stabilizer
SISO	Single-Input Single-Output
SSSC	Static Synchronous Series Compensator
STATCOM	Static Synchronous Compensator
SVC	Static VAR Compensator
SVS	Synchronous ac Voltage Source
TCRs	Thyristor Controlled Reactors
TCSC	Thyristor- Controlled Series Capacitor
TSCs	Thyristor-Switched Capacitors
UPFC	Unified Power Flow Controller
VSC BtB	Voltage-Source Converter Back-to-Back HVdc link

1. INTRODUCTION

Growth of electric power transmission facilities is restricted despite the fact that bulk power transfers and use of transmission systems by third parties are increasing. Transmission bottlenecks, non-uniform utilization of facilities and unwanted parallel-path or loop flows are not uncommon. Transmission system expansion is needed, but not easily accomplished. Factors that contribute to this situation include a variety of environmental, land-use and regulatory requirements. As the result, the utility industry is facing the challenge of the efficient utilization of the existing AC transmission lines.

Flexible AC Transmission Systems (FACTS) technology is an important tool for permitting existing transmission facilities to be loaded, at least under contingency situations, up to their thermal limits without degrading system security [1]-[3]. The most striking feature is the ability to directly control transmission line flows by structurally changing parameters of the grid and to implement high-gain type controllers, based on fast switching.

FACTS controllers are power electronic based controllers which can influence transmission system voltage, currents, impedances and/or phase angle rapidly. Thus, such controllers can improve the security of a power system by enhancing its steady-state and transient stability or by damping the subsynchronous resonance oscillations. FACTS application studies require an understanding of the individual FACTS controllers as well as openness to the application of novel approaches.

1.1. FACTS

The development of FACTS controllers has followed two distinctly different technical approaches, both resulting in a comprehensive group of controllers able to address targeted transmission problems. The first group employs reactive impedances or tap-changing transformers with thyristor switches as controlled elements; the second group use self-commutated static converters as controlled voltage sources.

1.1.1. Thyristor controlled FACTS controllers

The first group of controllers, the Static VAR Compensator (SVC), Thyristor-Controlled Series Capacitor (TCSC) and phase shifter, employ conventional thyristors in circuit arrangements which are similar to breaker-switched capacitors and reactors and conventional (mechanical) tap-changing transformers, but have much faster response and are operated by sophisticated control [4]-[17]. Each of these controllers can act on one of the three parameters determining power transmission, voltage (SVC), transmission impedance (TCSC) and transmission angle (phase shifter), as illustrated in Figure 1.1 [2].

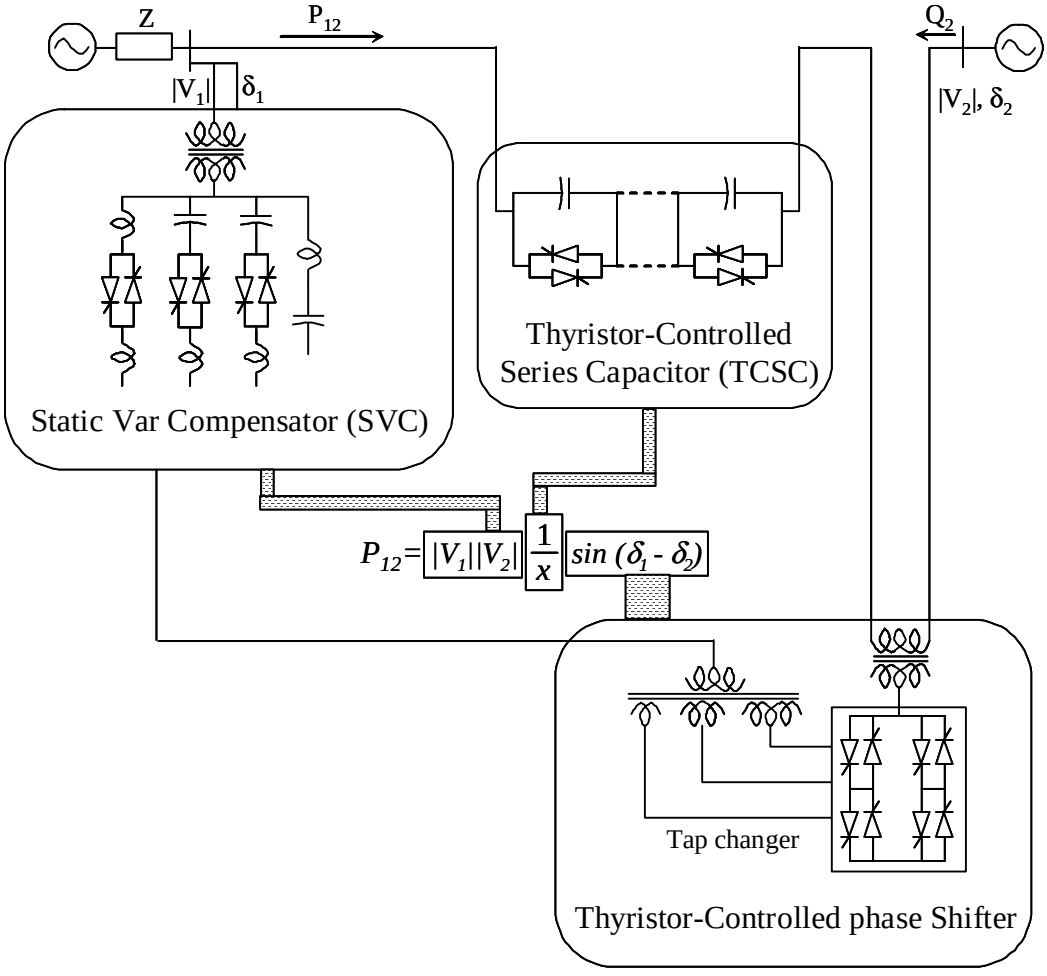

Figure 1.1 Conventional Thyristor-Based FACTS Controller.

Except for the thyristor-controlled phase shifter, all of these controllers have a common characteristic in that the necessary reactive power required for the compensation is generated or absorbed by traditional capacitor or reactor banks, and the thyristor

switches are used only for the control of the combined reactive impedance these banks present to the system. Conventional thyristor-controlled compensators present a variable reactive admittance to the transmission network and, therefore, generally change the character of the system impedance. The SVC is applied as a shunt impedance to produce the required compensating current. Therefore, the shunt compensation provided is a function of the prevailing line voltage. The TCSC is inserted in series with the line for the purpose of developing a compensating voltage to increase the voltage across the series impedance of the given physical line that ultimately determines the line current and power transmitted. This dependence on the line variables is detrimental to the compensation when large disturbances force the TCSC and SVC to operate outside their normal control range. The basic operating principles and characteristics of the conventional thyristor-controlled FACTS controllers can be summarized as follow.

1.1.1.1. Static var compensator

Thyristor-controlled static var compensators are the prototypes of today's FACTS controllers. These controllers were developed in the early 70's for ac furnace compensation, they were later adapted for transmission applications. A typical shunt connected static var compensator is composed of Thyristor-Switched Capacitors (TSCs) and Thyristor Controlled Reactors (TCRs) as shown in Figure 1.2 [2]. The compensator is normally operated to regulate the voltage of the transmission system at a selected terminal. The V-I characteristic of the SVC indicates that regulation with a given slope around the nominal voltage can be achieved in the normal operating range defined by the maximum capacitive and inductive currents of the SVC as shown in Figure 1.3. However, the maximum obtained capacitive current decreases linearly with the system voltage since the SVC becomes a fixed capacitor when the maximum capacitive output is reached. Therefore, the voltage support capability of the conventional thyristor-controlled static var compensator rapidly deteriorates with decreasing system voltage.

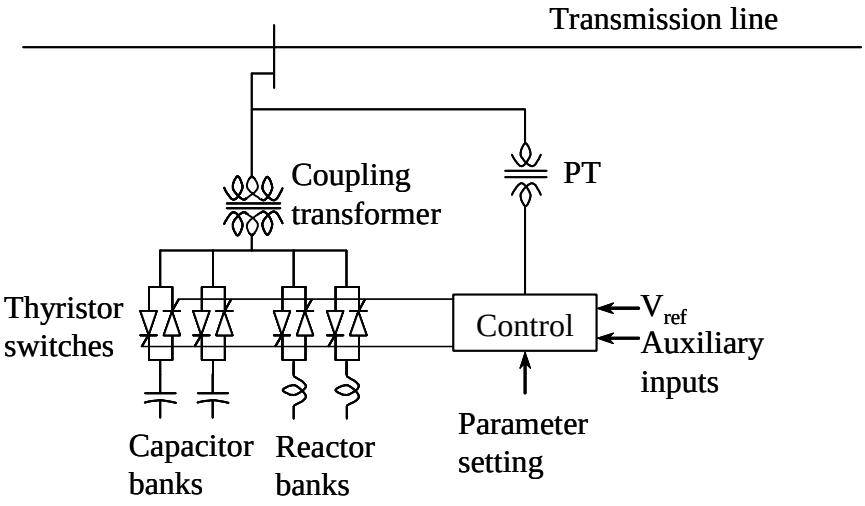

Figure 1.2 Static var compensator employing thyristor-switched capacitors and thyristor-controlled reactors.

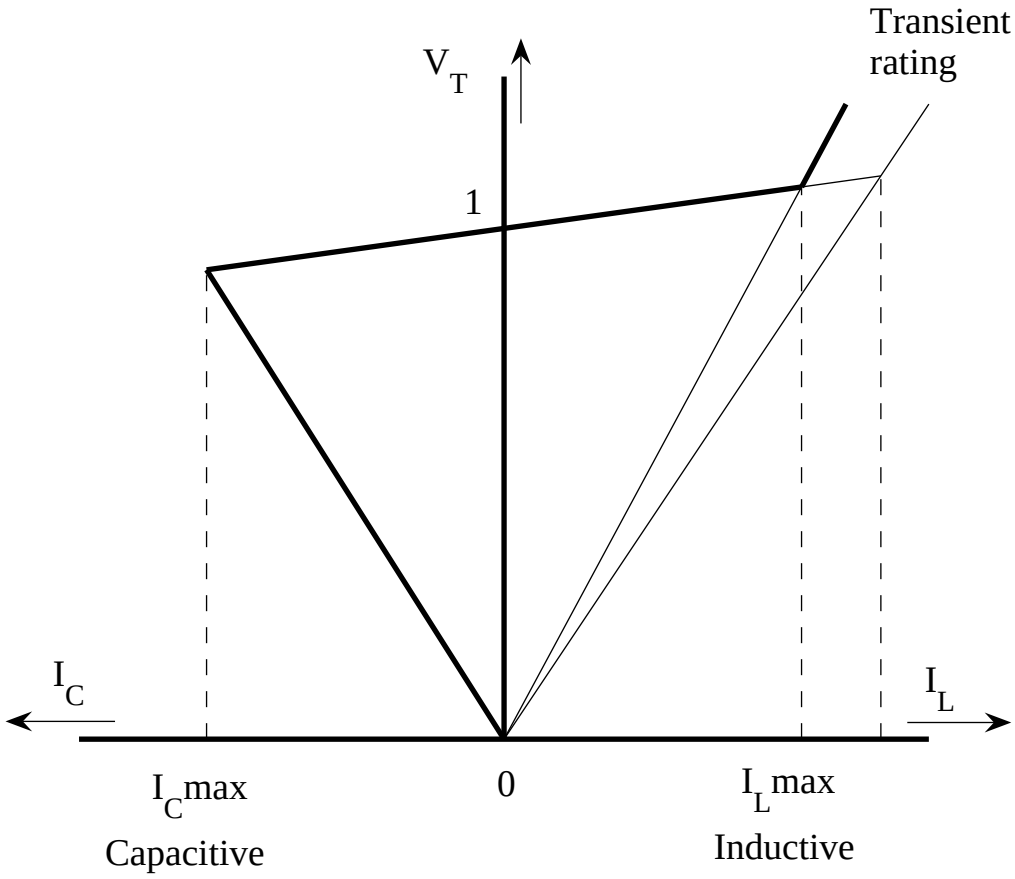

Figure 1.3 V-I characteristic of the Static Var Compensator.

1.1.1.2. Thyristor-controlled series capacitor

Thyristor-switched capacitors and a fixed capacitor in parallel with a thyristor-controlled reactor are the two fundamental types of thyristor-controlled series capacitors. In the thyristor-switched capacitor scheme shown in Figure 1.4 (a), the degree of series compensation is controlled by increasing or decreasing the number of capacitor banks in series. Each capacitor bank is inserted or bypassed by a thyristor switch in order to accomplish certain degree of compensation. The operation of the thyristor switches is coordinated with the voltage and current zero crossing to minimize switching transients. In the fixed-capacitor thyristor-controlled reactor scheme shown in Figure 1.4 (b), the degree of series compensation in the capacitive operating region (the admittance of the TCR is kept below that of the parallel connected capacitor) is increased or decreased by increasing or decreasing the thyristor conduction period and, thereby, the current in the TCR. Minimum series compensation is reached when the TCR is off.

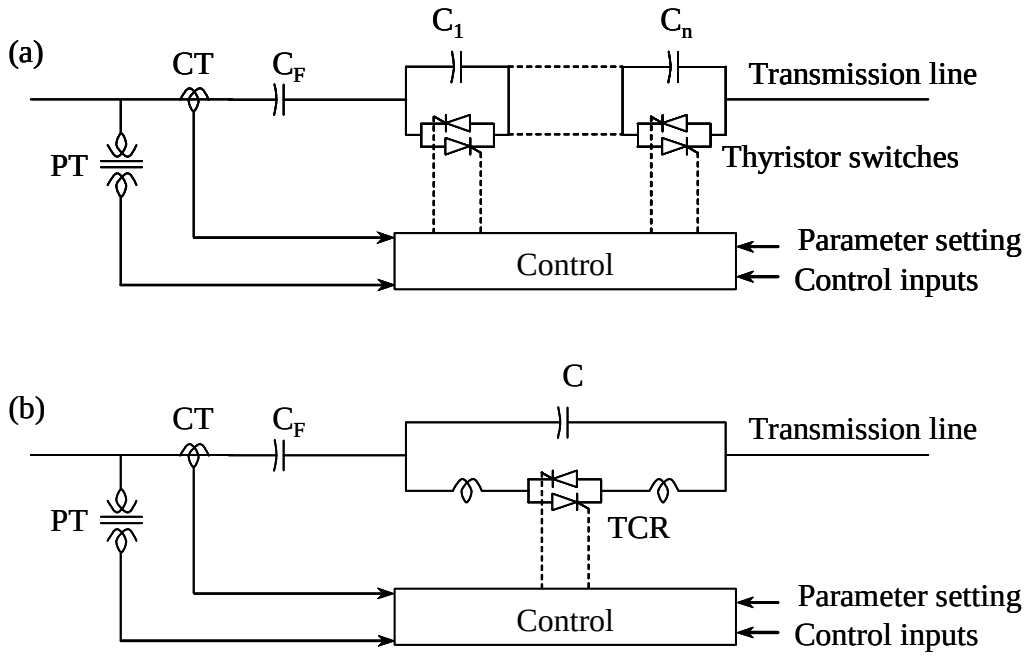

Figure 1.4 (a) Controllable series compensator scheme using thyristor-switched capacitors and (b) a thyristor-controlled reactor in parallel with a series capacitor.

The two schemes may be combined by connecting a number of TCRs plus fixed capacitors in series in order to achieve greater control range and flexibility.

1.1.1.3. Phase-shifter

Figure 1.5 shows a thyristor-controlled phase-shifter transformer arrangement. It consists of a shunt-connected excitation transformer with appropriate taps, a series insertion transformer and a thyristor switch arrangement connecting a selected combination of tap voltages to the secondary of the insertion transformer.

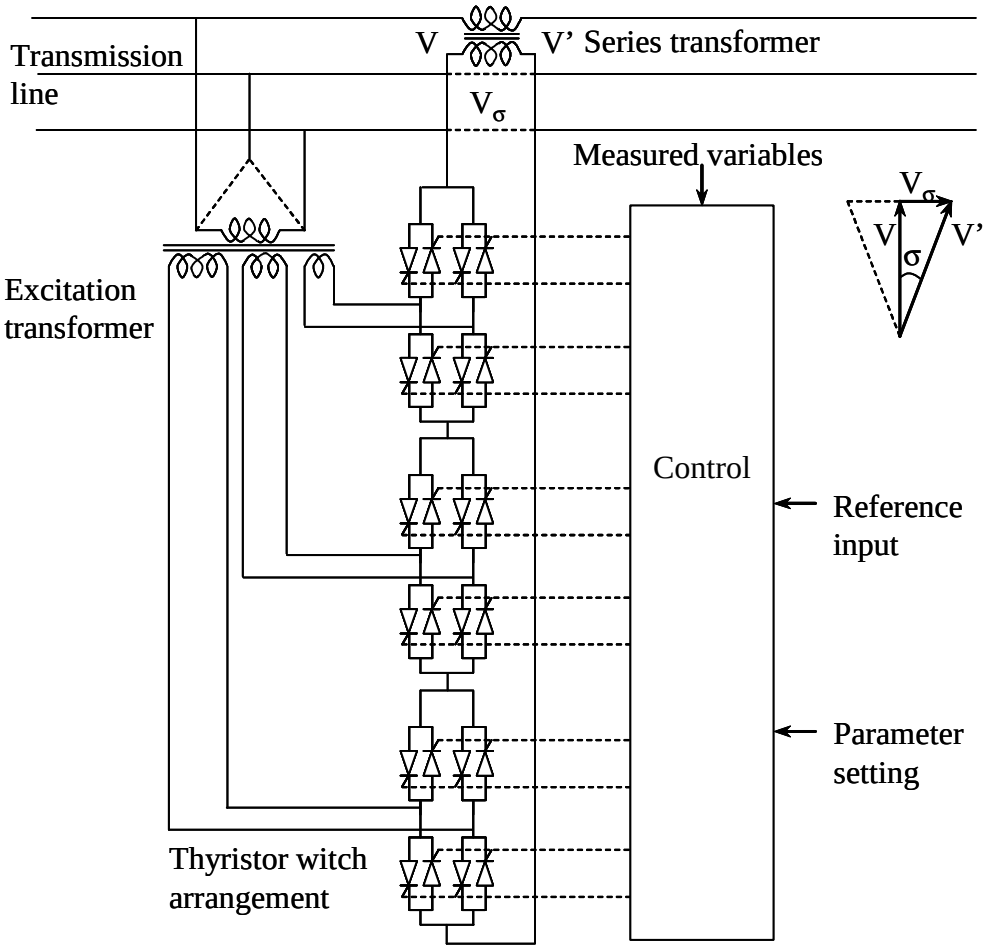

Figure 1.5 Thyristor-controlled phase shifting transformer scheme for transmission angle control.

The phase angle requirements for power flow control can be determined from angle measurements, if available, or from power measurements. The thyristor-controlled phase-shifting transformer could be applied to regulate the transmission angle to maintain balanced power flow in multiple transmission paths, or to control it to increase the transient and dynamic stability of the power system.

1.1.2. Converter-based FACTS controllers

This FACTS controller group employs self-commutated, voltage-sourced switching converters to achieve rapidly controllable, static, Synchronous ac Voltage Source (SVS) or synchronous ac current sources. This approach, when compared to conventional compensation methods using thyristor-switched capacitors and thyristor-controlled reactors, generally provides superior performance characteristics and uniform applicability for transmission voltage, effective line impedance, and angle control. It also offers the unique potential to exchange real power directly with the ac system, in addition to providing the independently controllable reactive power compensation, thereby giving a powerful new option for flow control and the counteraction of dynamic disturbances. Static Synchronous Compensators (STATCOM), Static Synchronous Series Compensators (SSSC), Unified Power Flow Controllers (UPFC), and Interline Power Flow Controllers (IPFC) form the group of FACTS controllers employing switching converter-based synchronous voltage sources. The STATCOM, like its conventional matching part, the SVC, controls transmission voltage by reactive shunt compensation. The SSSC offers series compensation by directly controlling the voltage across the series impedance of the transmission line, thereby controlling the effective transmission impedance. The UPFC can control, individually or in combination, all three effective transmission parameters (voltage, impedance, and angle) or directly, the real and reactive power flow in the line. The IPFC is able to transfer real power between lines, in addition to providing reactive series compensation, and, therefore, can facilitate a comprehensive overall real and reactive power management for a multi-line transmission system.

1.1.2.1. Static synchronous compensator (STATCOM)

If the SVS is used strictly for reactive shunt compensation, like a conventional static var compensator, the dc energy source can be a relatively small dc capacitor, as shown in Figure 1.6. The size of the capacitor is primarily determined by the “ripple” input current encountered with the particular converter design. In this case, the steady-state power exchange between the SVS and the ac system can only be reactive. When the SVS is used for reactive power generation, the converter itself can keep the capacitor charged to the required voltage level. This is achieved by making the output voltages of

the converter lag the system voltage by a small angle. In this way, the converter absorbs a small amount of real power from the ac system to replenish its internal losses and keep the capacitor voltage at the desired value. The same control mechanism can be used to increase or decrease the capacitor voltage, and thereby the amplitude of the output voltage of the converter, for the purpose of controlling the var generation or absorption. The dc capacitor also has the function of establishing an energy balance between the input and output during the dynamic changes of the var output. The SVS, operated as a reactive shunt compensator, exhibits operating and performance characteristics similar to those of an ideal synchronous compensator and for this reason this arrangement is called a Static Synchronous Compensator.

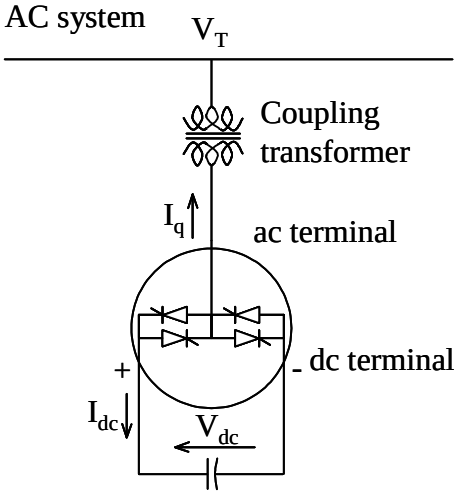

Figure 1.6 Synchronous voltage source operated as a STATCOM.

1.1.2.2. Static synchronous series compensator (SSSC)

The concept of using the solid-state synchronous voltage source for series reactive compensation is based on the fact that the impedance versus frequency characteristic of the conventionally employed series capacitor, in contrast to filter applications, plays no part in accomplishing the desired line compensation. The function of the series capacitor is simply to produce an appropriate voltage at the fundamental ac system frequency to increase the voltage across the inductive line impedance, and, thereby the fundamental line current and the transmitted power. Therefore, if an ac voltage source of fundamental frequency, which is locked with a quadrature (lagging) relationship to the line current and whose amplitude is made proportional to that of the line current, is

injected in series with the line, a series compensation equivalent to that provided by a series capacitor at the fundamental frequency is obtained. Mathematically, this voltage source can be defined as follows:

$$V_c = -jkX\bar{I} \tag{1-1}$$

where, V_c is the injected compensated voltage phasor, $\bar{I}$ is the line current phasor, X is the series reactive line impedance, k is the degree of series compensation, and $j = \sqrt{-1}$. Thus, $kX = X_c$ represents a virtual series capacitor generating the same compensating voltage as its real counterpart. However, in contrast to the real series capacitor, the SVS is able to maintain a constant compensating voltage in the face of variable current, or control the amplitude of the injected compensating voltage independent of the amplitude of the line current.

For normal capacitive compensation, the output voltage lags the line current by 90 degrees. However, the output voltage of the SVS can be reversed by a simple control action to make it lead the line current by 90 degree. In this case, the injected voltage decreases the voltage across the inductive line impedance and, thus, the series compensation has the same effect as if the reactive line impedance was increased. Therefore, a generalized expression for the injected voltage, V_q, can be written:

$$V_q = \pm jV_q(\zeta)\frac{\bar{I}}{I} \tag{1-2}$$

where $V_q(\zeta)$ is the magnitude of the injected compensating voltage ($0 \leq V_q(\zeta) \leq V_{qmax}$), ζ is a chosen control parameter and I is the line current magnitude. The series reactive compensation scheme, based on Equation (1-2), is illustrated in Figure 1.7. Such a series compensation scheme is termed the Static Synchronous Series Compensator (SSSC).

1.1.2.3. Unified Power Flow Controller (UPFC)

The Unified Power flow Controller (UPFC) is the most versatile FACTS device that has emerged for the control and optimization of power flow in electrical power transmission systems. Its concept was proposed by Gyugyi in 1991 [18]. It offers major potential advantages for the static and dynamic operation of transmission lines since it combines the features of both the Static Synchronous Compensator (STATCOM) and the Static Synchronous Series Compensator (SSSC). The UPFC is able to control, simultaneously

or selectively, all the parameters affecting power flow in the transmission line (voltage, impedance, and phase angle), and this unique capability is signified by the adjective "unified" in its name. Alternatively, it can independently control both the real and reactive power flows in the line.

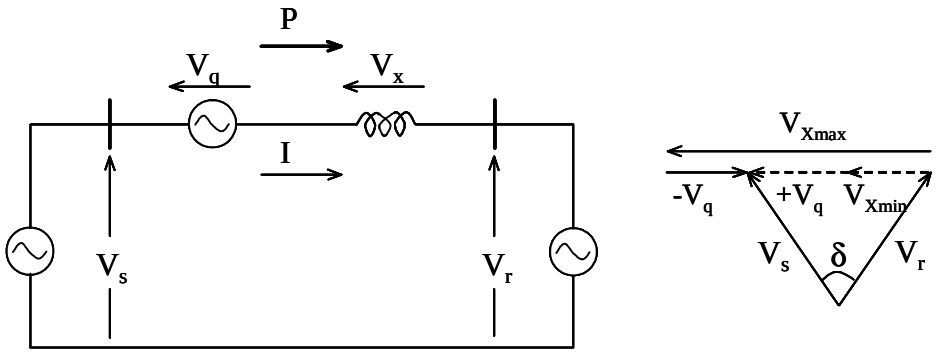

Figure 1.7 A synchronous voltage source operated as a Static Synchronous Series Compensator.

The UPFC can be represented at the fundamental power system frequency by voltage phasor V_{pq} with controllable magnitude V_{pq} $\left(0 \le V_{pq} \le V_{pq\max}\right)$ and angle ρ $\left(0 \le \rho \le 2\pi\right)$, in series with the transmission line.

In the presently used practical implementation, the UPFC consists of two voltage-sourced converters, as illustrated in Figure 1.8. These back-to-back converters, labeled "Converter 1" and "Converter 2" in the figure, are operated from a common dc link provided by a dc storage capacitor. This arrangement functions as an ideal ac-to-ac power converter in which the real power can freely flow in either direction between the ac terminals of the two converters, and each converter can independently generate (or absorb) reactive power at its own ac terminal. Converter 2 provides the main function of the UPFC by injecting the voltage V_{pq} and phase angle ρ in series with the line via an insertion transformer. This injected voltage acts essentially as a synchronous ac voltage source. The transmission line current flows through this voltage source resulting in reactive and real power exchange between it and the ac system. The reactive power exchange at the ac terminal is generated internally by the converter. The real power exchange at the ac terminal is converted into dc power, which appears at the dc link as a positive or negative real power demand.

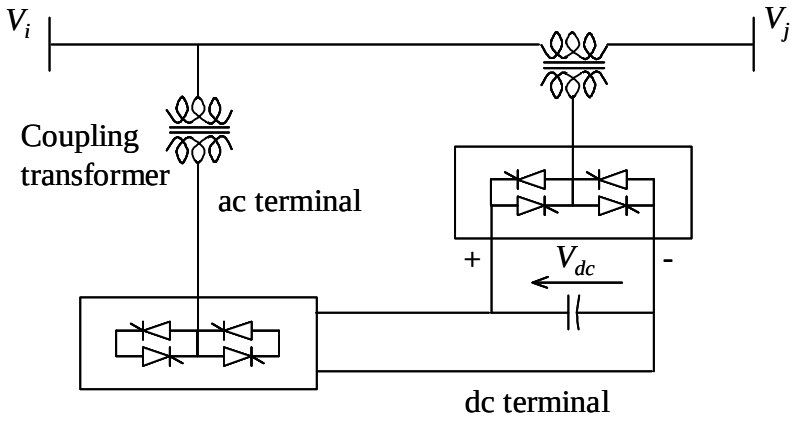

Figure 1.8 Implementation of the UPFC by two back-to-back voltage-sourced converters.

The basic function of Converter 1 is to supply or absorb the real power demanded by Converter 2 at the common dc link to support the real power exchange resulting from the series voltage injection. This dc link power demand of Converter 2 is converted back to ac by Converter 1 and coupled to the transmission line bus via a shunt-connected transformer. In addition to the real power need of Converter 2, Converter 1 can also generate or absorb controllable reactive power, if it is desired, and thereby provide independent shunt reactive compensation for the line.

1.2. Interarea Oscillations

A problem of interest in the power industry in which FACTS controllers could play a major role is the mitigation of low frequency oscillations that often arise between areas in a large interconnected power network [19]-[28]. These oscillations are due to the dynamics of interarea power transfer and often exhibit poor damping when the aggregate power transfer over a corridor is high relative to the transmission strength [29]-[32]. Interarea oscillations can severely restrict system operations by requiring the curtailment of electric power transfers as an operational measure. These oscillations can also lead to widespread system disturbances if cascading outages of transmission lines occur due to oscillatory power swings. As power system reliability became increasingly important, the requirement for a system to be able to recover from a fault cleared by a relay action was added to the system design specifications. Rapid automatic voltage control was used to prevent the system's generators loosing synchronism following a system fault.

Fast excitation systems, however, tend to reduce the damping of system oscillations. Originally, the oscillations most affected were those between electrically closely coupled generators. Special stabilizing controls were designed to damp these oscillations. In 1950s and 1960s, electric power utilities found that they could achieve more reliability and economy by interconnecting to other utilities, often through quite long transmission lines. In some cases, when the utilities connected, low frequency growing oscillations prevented the interconnection from being retained. From an operating point of view, oscillations are acceptable as long as they decay. However, oscillations are a characteristic of the system; they are initiated by the normal small changes in the system's load. There is no warning to the operator if a new operating condition causes an oscillation to increase in magnitude. An increase in tie line flow of a small value may make the difference between decaying oscillations, which are acceptable and increasing oscillations, which have the potential to cause system collapse. Of course, a major disturbance may finally result in growing oscillations and a system collapse. Such was the case in the August 1996 collapse of the Western US/Canada interconnected power system. The progress of this collapse was recorded by the extensive monitoring system which has been installed, and its cause is explained clearly in [33]-[34]. The stability of electromechanical oscillations between interconnected synchronous generators is necessary for secure system operation. The oscillations of one or more generators in an area with respect to the rest of the system are called local modes, while those associated with groups of generators in different areas oscillating against each other are called interarea modes. As an example, in a two-area system, where each area consists of two generators as shown in Figure 1.9, the two local modes of each area and the interarea mode are the three fundamental modes of oscillation. They are each due to the electromechanical torques, which keep the generators in synchronism. The frequencies of the oscillations depend on the strength of the system and on the moment of inertia of the generator rotors. These frequencies are in the range of 0.1-2.5 Hz, in most practical cases. These oscillations are usually observed from generator speed deviations, and they also can be observed in other system variables such as voltage signal at each tie line end. However, the frequencies of the local modes may be very close, and it may not be possible to recognize them separately in the tie bus voltage responses. Local modes are

largely determined and influenced by local states. Interarea modes are more difficult to study as they require detailed representation of the entire interconnected system and are influenced by global states of larger areas of the power network. This has led to an increased interest in the nature of these modes and in developing methods to damp them.

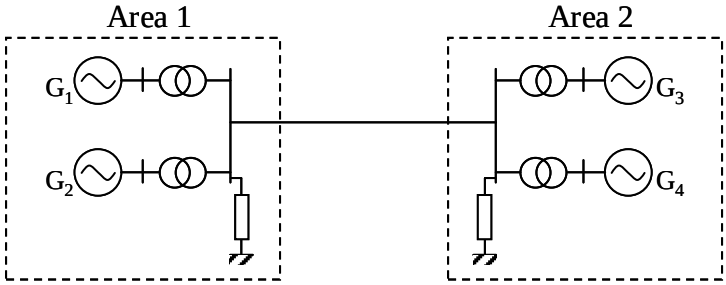

Figure 1.9 A two-area power system.

1.3. Turbine-Generator Shaft Torsional Torques

Until the mid seventies, short circuits in the network or power stations and faulty synchronization were regarded as the only disturbances which could cause severe torsional stresses in the turbine-generator shaft. In this aspect, short circuits are more hazardous the closer to the generator terminal they occur. In most of the international standards, the three-phase terminal short circuit has thus been considered to be the most severe disturbance for which the turbine-generator must be designed to withstand without damage [35]. This criterion has been also applied to the design of the shafts and couplings of both the generator and the turbine.

The occurrence of several incidents in different countries during the seventies and the eighties has put in doubt the validity of the above mentioned practice and promoted investigations into the cause of turbine-generator torsional excitation and the effect of the stimulated oscillations on the machine shafts and couplings. The best known incidents are the two shaft failures that occurred in the Mohave station in Nevada, U.S.A. in 1970 and 1971, which were caused by subsynchronous resonance [36]-[38]. These are the only reported incidents of actual shaft failure in the United States that can be attributed directly to the interaction between the generator unit and the electrical network. These failures were caused by sustained oscillations due to the subsynchronous resonance between the turbine-generator shaft system and the series

compensated transmission network. Because of the resonance phenomenon, transient torques in excess of the high-cycle shaft fatigue limit (a large number of low amplitude oscillations) were sustained long enough to result in the shaft failure.

These incidents and others captured the attention of the industry at large and stimulated greater interest in the interaction between power plants and electric systems [39]-[41]. They also fostered the development of advanced analytical methods and sophisticated computer programs to simulate this interaction under transient conditions. Intensive investigations carried out with these programs during the early seventies have led to the realization that the combination of the larger generating units, extra high voltage transmission systems with fewer exits from power plant sites and closed coupled electrical grids can make it possible for some electrical disturbances to inflict more severe torsional stressing on the turbine-generator shafts than the three-phase terminal short circuit for which the machines are designed [42]-[43]. These disturbances include breaker operations associated with synchronizing, fault clearing and high-speed reclosing.

In the case of clearing a fault close to a turbine-generator in a strong electrical network, an additional torsional shock is superimposed on the already oscillating shaft system due to the fault. This may lead to the amplification of the turbine-generator torsional torques depending on the instant of the superimposition [44].

Similarly, automatic high-speed reclosure, especially unsuccessful reclosure in the case of close-in multi-phase system faults, aggravates the potential impact on the turbine-generator shafts due to the large number of rapidly succeeding torsional shocks when magnified by unfavorable superimposition [45]. Hence, unsuccessful high-speed reclosure can inflict vastly different magnitudes of torsional stresses depending on the actual timing of the breaker operation within the wide spectrum of possible fault clearing and reclosing time combinations.

The basic mechanism of the torsional excitation lies in the sudden change in the turbine-generator electromagnetic torque through alternation in the generator current as it can occur during faults, transmission line switching, load rejection, faulty synchronization, fault clearing and automatic reclosing. Such a torque has many components, namely

unidirectional, exponentially decaying and oscillatory components. The frequencies of the oscillatory components range from subsynchronous to multiples of the network frequency. If one of these frequencies coincides with one of the natural torsional frequencies of the turbine-generator shaft system, torsional torque amplification will develop. However, such coincidence is unusual.

1.4. Scope and Objective of the Thesis

The problem of interarea oscillations in a large interconnected power network is explained in Section 1.2. These oscillations can severely restrict system operations. As it has been pointed out, studying and damping of these oscillations is difficult as they require detailed representation of the entire interconnected system and are influenced by global states of larger areas of the power network. Another problem of concern is the interaction between the turbine-generator shaft system and the electrical network disturbances. This is discussed in Section 1.3. Damping of such oscillations is very low compared with the damping in the electrical system. Therefore, during such events, the shaft connecting the turbine and the generator may undergo heavy stresses and considerable deformation.

The main objectives of this research work are to:

1- Design robust centralized controllers for UPFC for damping interarea oscillations using Genetic Algorithm (GA) and fuzzy logic techniques.

2- Investigate the performance of the designed controllers in damping power system interarea oscillations with respect to their locations in the system.

3- Investigate the performance of a simplified controller for UPFC based on a reduced number of stabilizing signals in damping power system interarea oscillations.

4- Extend the application of the GA technique to design controllers for other voltage source converter FACTS devices. Moreover, the potential of tuning the fuzzy logic controller for the UPFC using the GA technique is investigated.

5- Investigate the possibility of using a GA controller for a VSC back-to-back dc link in damping turbine-generator shaft torsional torques.

1.5. Thesis Outline

The thesis consists of seven chapters. In this chapter, an introduction to the phenomena of interarea oscillations and turbine-generator torsional oscillations is presented. A brief discussion of the different types of FACTS devices is also presented. In Chapter 2, the mathematical model of a single-machine infinite-bus power system equipped with a UPFC is presented. Proposed UPFC controllers based on GA and fuzzy logic techniques are developed and their performances are evaluated.

Chapter 3 presents the application of GA technique in designing a UPFC controller for a multi-area power system. Development of the mathematical model of the multi-area power system equipped with UPFCs is also presented. To demonstrate the effectiveness of the developed controllers, time simulation results for the power system under different system disturbances are presented.

In Chapter 4, a fuzzy logic UPFC controller is developed and its effectiveness in damping interarea oscillations is tested. In Chapter 5, the developed GA technique is utilized to design controllers for two other FACTS devices, namely a Generalized Unified Power Flow Controller (GUPFC) and a Voltage-Source Converter Back-to-Back HVdc link (VSC BtB). The effectiveness of these controllers in damping interarea oscillations is presented.

In Chapter 6, studies are presented on the possibility of using the UPFC and the VSC BtB for damping turbine-generator shaft torsional torques.

Conclusions of this thesis are finally presented in Chapter 7. The work presented in this thesis is summarized in this chapter and some general conclusions are drawn.

2. DAMPING POWER SYSTEM OSCILLATIONS IN A SINGLE-MACHINE INFINITE-BUS POWER SYSTEM USING A UPFC

2.1. Introduction

This chapter presents new control methods based on Genetic Algorithm (GA) and fuzzy logic techniques to control a Unified Power Flow Controller installed in a single-machine infinite-bus power system [46]-[52]. The objective of these controllers is to damp power system oscillations. The Phillips-Herffron model of a single-machine infinite-bus power system equipped with a UPFC is used to model the system in these studies. The GA based UPFC controller is designed based on combining a traditional control technique (eigenvalue shifting technique) with an artificial intelligence technique such as GA. A simple GA using the tournament selection method is used to mimic the GA technique. For this purpose, a GA package is developed using MATLAB. On the other hand, the UPFC based fuzzy controller is based on a simple fuzzy logic controller using the Mamdani-type inference system. The effectiveness of the new controllers is demonstrated through time-domain simulation studies.

2.2. Modeling of a Single-Machine Infinite-Bus Power System Equipped with a UPFC

There are three types of modeling a UPFC. The first model is the electromagnetic model for detailed equipment investigation [53]. The second model is the steady-state model for system steady-state operation evaluation [54]. The third model is the dynamic model which is used in power system stability studies [55]-[56]. The first model is more suitable for studying electromagnetic transients in the range of milliseconds. In this model, the UPFC is represented using switches. This type of modeling is not appropriate for power system oscillation studies.

The steady-state and dynamic models are used to represent the single-machine infinite-bus power system equipped with a UPFC in this chapter. The steady-state model is

developed to study the steady-state performance of the power system as well as calculating the initial operating conditions. The dynamic model is developed based on combining the dynamic equations of the power system with the UPFC dynamic equations. This model is used to simulate the dynamic performance of the power system under study using small signal stability studies.

2.2.1. Steady-state model of the UPFC

A UPFC installed between buses "*i*" and "*j*" can be represented at steady-state by two voltage sources with appropriate impedances as shown in Figure 2.1. The series and shunt UPFC impedances are assumed to be pure reactances. The total real power injected to the power system by the two voltage sources is equal to zero at steady-state. However, there is a real power exchange between the two sources. For power flow studies, the two-voltage source model of the UPFC is converted into three power injections as shown in Figure 2.2. Moreover, the shunt reactance is removed as it has been considered in the injected reactive power Q_{io} and it is removed also from the system admittance matrix. P_{io} and Q_{io} represent the shunt voltage source while P_i, Q_i, P_j and Q_j represent the series voltage source. These injected powers are dependent on the injected voltage as well as on the bus voltages. Buses *i* and *j* are considered to be load buses in the load flow analysis with some modifications as the injected powers are not constant. These injected powers are given as follow:

$$
\begin{aligned}
P_{i(inj)} &= P_i - P_{io} = B_{ij}\left(e_j f_{pq} - f_j e_{pq}\right) \\
Q_{i(inj)} &= Q_i - Q_{io} = B_{ij}\left(e_i e_{pq} + f_i f_{pq}\right) + B_{io}\left(V_i^2 - e_i e_{sh} - f_i f_{sh}\right) \\
P_j &= B_{ij}\left(f_j e_{pq} - e_j f_{pq}\right) \\
Q_j &= -B_{ij}\left(e_j e_{pq} - f_j f_{pq}\right)
\end{aligned}
\qquad (2\text{-}1)
$$

Where: f_i and e_i are the imaginary and real components of the bus voltage V_i respectively. The losses associated with the UPFC operation are typically neglected and, therefore, it neither absorbs nor injects real power with respect to the system during steady-state operation. Physical interpretation of this statement is that the voltage of the dc link capacitor remains constant at the pre-specified value V_{dc}. This constraint that must be satisfied by the UPFC at steady-state is expressed mathematically as:

$$
\mathrm{Re}\left\{V_{sh} I_{sh}^{*} + V_{pq} I_{pq}^{*}\right\} = 0 \qquad (2\text{-}2)
$$

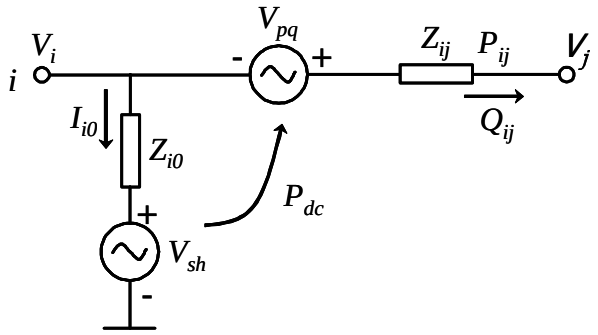

Figure 2.1 A two-voltage source UPFC model.

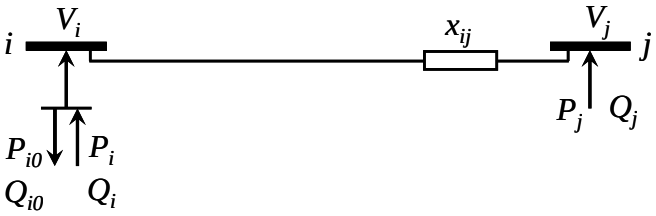

Figure 2.2 UPFC injected voltage model.

The injected real and reactive powers shown in Equation (2-1) can be represented as follows:

$$P_{io} = \frac{|V_i||V_{sh}|}{x_{io}}\sin(\delta_i - \delta_{sh}), \qquad Q_{io} = \frac{|V_i|^2}{x_{io}} - \frac{|V_i||V_{sh}|}{x_{io}}\cos(\delta_i - \delta_{sh})$$

$$P_i = \frac{-|V_i||V_{pq}|}{x_{ij}}\sin(\delta_i - \delta_{pq}), \qquad Q_i = \frac{|V_i||V_{pq}|}{x_{ij}}\cos(\delta_i - \delta_{pq})$$

$$P_j = \frac{|V_j||V_{pq}|}{x_{ij}}\sin(\delta_j - \delta_{pq}), \qquad Q_j = \frac{-|V_j||V_{pq}|}{x_{ij}}\cos(\delta_j - \delta_{pq}) \tag{2-3}$$

With the help of Equations (2-3), the power constraint in Equation (2-2) can be represented as:

$$\delta_{sh} = \delta_i - \sin^{-1}\left\{\frac{|V_{pq}|x_{ij}}{|V_{sh}||V_i|x_{io}}\left[|V_i|\sin(\delta_{pq} - \delta_i) - |V_j|\sin(\delta_{pq} - \delta_j)\right]\right\} \tag{2-4}$$

The Newton-Raphson technique is used to solve the power system load flow. Equation (2-4) is used to modify the power flow program to update the value of δ_{sh} during consecutive iterations in order to satisfy the power constraint of Equation (2-2).

2.2.2. Dynamic model of the UPFC

Figure 2.3 shows a single-machine infinite-bus power system equipped with a UPFC. m_E, m_B and δ_E, δ_B are the amplitude modulation ratio and phase angle of the control signal of each voltage source converter respectively, which are the input control signals of the UPFC.

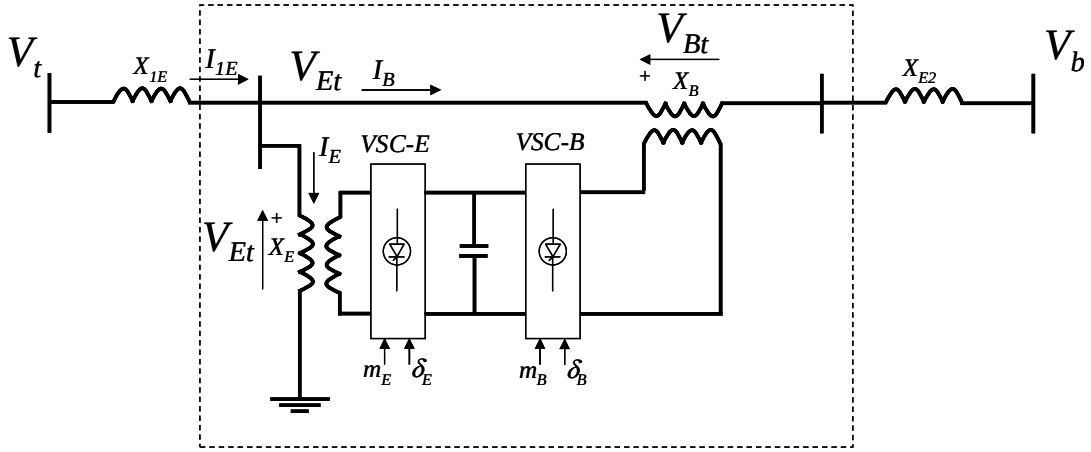

Figure 2.3 A UPFC installed in a single-machine infinite-bus power system.

The three-phase dynamic differential equations of the UPFC can be written as follows:

$$\begin{bmatrix} \frac{di_{Ea}}{dt} \\ \frac{di_{Eb}}{dt} \\ \frac{di_{Ec}}{dt} \end{bmatrix} = \begin{bmatrix} -\frac{r_E}{l_E} & 0 & 0 \\ 0 & -\frac{r_E}{l_E} & 0 \\ 0 & 0 & -\frac{r_E}{l_E} \end{bmatrix} \begin{bmatrix} i_{Ea} \\ i_{Eb} \\ i_{Ec} \end{bmatrix} - \frac{m_E v_{dc}}{2l_E} \begin{bmatrix} \cos(\omega t + \delta_E) \\ \cos(\omega t + \delta_E - 120°) \\ \cos(\omega t + \delta_E + 120°) \end{bmatrix} + \begin{bmatrix} \frac{1}{l_E} & 0 & 0 \\ 0 & \frac{1}{l_E} & 0 \\ 0 & 0 & \frac{1}{l_E} \end{bmatrix} \begin{bmatrix} v_{Eta} \\ v_{Etb} \\ v_{Etc} \end{bmatrix} \tag{2-5}$$

$$\begin{bmatrix} \frac{di_{Ba}}{dt} \\ \frac{di_{Bb}}{dt} \\ \frac{di_{Bc}}{dt} \end{bmatrix} = \begin{bmatrix} -\frac{r_B}{l_B} & 0 & 0 \\ 0 & -\frac{r_B}{l_B} & 0 \\ 0 & 0 & -\frac{r_B}{l_B} \end{bmatrix} \begin{bmatrix} i_{Ba} \\ i_{Bb} \\ i_{Bc} \end{bmatrix}$$
$$-\frac{m_B v_{dc}}{2l_B} \begin{bmatrix} \cos(\omega t + \delta_B) \\ \cos(\omega t + \delta_B - 120°) \\ \cos(\omega t + \delta_B + 120°) \end{bmatrix} + \begin{bmatrix} \frac{1}{l_B} & 0 & 0 \\ 0 & \frac{1}{l_B} & 0 \\ 0 & 0 & \frac{1}{l_B} \end{bmatrix} \begin{bmatrix} v_{Bta} \\ v_{Btb} \\ v_{Btc} \end{bmatrix} \quad (2\text{-}6)$$

$$\frac{dv_{dc}}{dt} = -\frac{m_E}{2C_{dc}} \begin{bmatrix} \cos(\omega t + \delta_E) & \cos(\omega t + \delta_E + 120°) & \cos(\omega t + \delta_E - 120°) \end{bmatrix} \begin{bmatrix} i_{Ea} \\ i_{Eb} \\ i_{Ec} \end{bmatrix}$$
$$+\frac{m_B}{2C_{dc}} \begin{bmatrix} \cos(\omega t + \delta_B) & \cos(\omega t + \delta_B + 120°) & \cos(\omega t + \delta_B - 120°) \end{bmatrix} \begin{bmatrix} i_{Ba} \\ i_{Bb} \\ i_{Bc} \end{bmatrix} \quad (2\text{-}7)$$

By applying Park's transformation, Equations (2-5) to (2-7) are transformed to:

$$\begin{bmatrix} \frac{di_{Ed}}{dt} \\ \frac{di_{Eq}}{dt} \\ \frac{di_{E0}}{dt} \end{bmatrix} = \begin{bmatrix} 0 & \omega & 0 \\ -\omega & 0 & 0 \\ 0 & 0 & 0 \end{bmatrix} \begin{bmatrix} i_{Ed} \\ i_{Eq} \\ i_{E0} \end{bmatrix} + \begin{bmatrix} -\frac{r_E}{l_E} & 0 & 0 \\ 0 & -\frac{r_E}{l_E} & 0 \\ 0 & 0 & -\frac{r_E}{l_E} \end{bmatrix} \begin{bmatrix} i_{Ed} \\ i_{Eq} \\ i_{E0} \end{bmatrix}$$
$$-\frac{m_E v_{dc}}{2l_E} \begin{bmatrix} \cos(\delta_E) \\ \sin(\delta_E) \\ 0 \end{bmatrix} + \begin{bmatrix} \frac{1}{l_E} & 0 & 0 \\ 0 & \frac{1}{l_E} & 0 \\ 0 & 0 & \frac{1}{l_E} \end{bmatrix} \begin{bmatrix} v_{Etd} \\ v_{Etq} \\ v_{Et0} \end{bmatrix} \quad (2\text{-}8)$$

$$\begin{bmatrix} \frac{di_{Bd}}{dt} \\ \frac{di_{Bq}}{dt} \\ \frac{di_{B0}}{dt} \end{bmatrix} = \begin{bmatrix} 0 & \omega & 0 \\ -\omega & 0 & 0 \\ 0 & 0 & 0 \end{bmatrix} \begin{bmatrix} i_{Bd} \\ i_{Bq} \\ i_{B0} \end{bmatrix} + \begin{bmatrix} -\frac{r_B}{l_B} & 0 & 0 \\ 0 & -\frac{r_B}{l_B} & 0 \\ 0 & 0 & -\frac{r_B}{l_B} \end{bmatrix} \begin{bmatrix} i_{Bd} \\ i_{Bq} \\ i_{B0} \end{bmatrix}$$
$$-\frac{m_B v_{dc}}{2l_B} \begin{bmatrix} \cos(\delta_B) \\ \sin(\delta_B) \\ 0 \end{bmatrix} + \begin{bmatrix} \frac{1}{l_B} & 0 & 0 \\ 0 & \frac{1}{l_B} & 0 \\ 0 & 0 & \frac{1}{l_B} \end{bmatrix} \begin{bmatrix} v_{Btd} \\ v_{Btq} \\ v_{Bt0} \end{bmatrix} \tag{2-9}$$

$$\frac{dv_{dc}}{dt} = \frac{3m_E}{4C_{dc}} \begin{bmatrix} \cos(\delta_E) & \sin(\delta_E) & 0 \end{bmatrix} \begin{bmatrix} i_{Ed} \\ i_{Eq} \\ i_{E0} \end{bmatrix} + \frac{3m_B}{4C_{dc}} \begin{bmatrix} \cos(\delta_B) & \sin(\delta_B) & 0 \end{bmatrix} \begin{bmatrix} i_{Bd} \\ i_{Bq} \\ i_{B0} \end{bmatrix} \tag{2-10}$$

A linearized model of the power system can be used in studying power system oscillation stability and control. The dynamic model of the UPFC is required in order to study the effect of the UPFC on enhancing the small signal stability of the power system. For the study of power system oscillation stability, the resistance and transient of the transformers of the UPFC can be ignored. The above equations can then be written as:

$$\begin{bmatrix} v_{Etd} \\ v_{Etq} \end{bmatrix} = \begin{bmatrix} 0 & -x_E \\ x_E & 0 \end{bmatrix} \begin{bmatrix} i_{Ed} \\ i_{Eq} \end{bmatrix} + \begin{bmatrix} \frac{m_E v_{dc} \cos\delta_E}{2} \\ \frac{m_E v_{dc} \sin\delta_E}{2} \end{bmatrix}$$
$$\begin{bmatrix} v_{Btd} \\ v_{Btq} \end{bmatrix} = \begin{bmatrix} 0 & -x_B \\ x_B & 0 \end{bmatrix} \begin{bmatrix} i_{Bd} \\ i_{Bq} \end{bmatrix} + \begin{bmatrix} \frac{m_B v_{dc} \cos\delta_B}{2} \\ \frac{m_B v_{dc} \sin\delta_B}{2} \end{bmatrix} \tag{2-11}$$
$$\frac{dv_{dc}}{dt} = \frac{3m_E}{4C_{dc}} \begin{bmatrix} \cos(\delta_E) & \sin(\delta_E) \end{bmatrix} \begin{bmatrix} i_{Ed} \\ i_{Eq} \end{bmatrix} + \frac{3m_B}{4C_{dc}} \begin{bmatrix} \cos(\delta_B) & \sin(\delta_B) \end{bmatrix} \begin{bmatrix} i_{Bd} \\ i_{Bq} \end{bmatrix}$$

From Figure 2.3:

$$V_t = jx_{1E} I_t + V_{Et}$$
$$V_{Et} = V_{Bt} + jx_{E2} I_B + V_b \tag{2-12}$$

These equations can be expressed in the *d-q* reference frame as:

$$
\begin{aligned}
v_{dt} + jv_{qt} &= jx_{1E}\left(i_{Ed} + i_{Bd} + ji_{Eq} + ji_{Bq}\right) + v_{Etd} + jv_{Etq} \\
&= x_q\left(i_{Eq} + i_{Bq}\right) + j\left[E'_q - x'_d\left(i_{Ed} + i_{Bd}\right)\right] \\
v_{Etd} + jv_{Etq} &= v_{Btd} + jv_{Btq} + jx_{E2}i_{Bd} - x_{E2}i_{Bq} + V_b\sin\delta + jV_b\cos\delta
\end{aligned}
\tag{2-13}
$$

Using Equations (2-11), (2-12) and (2-13) yields

$$
\begin{bmatrix} i_{Ed} \\ i_{Bd} \end{bmatrix} = \begin{bmatrix} x'_d + x_{1E} + x_E & x'_d + x_{1E} \\ x_E & -x_B - x_{E2} \end{bmatrix}^{-1} \begin{bmatrix} E'_q - \dfrac{m_E v_{dc}\sin\delta_E}{2} \\ \dfrac{m_B v_{dc}\sin\delta_B}{2} + V_b\cos\delta - \dfrac{m_E v_{dc}\sin\delta_E}{2} \end{bmatrix}
$$

$$
\begin{bmatrix} i_{Eq} \\ i_{Bq} \end{bmatrix} = \begin{bmatrix} x_q + x_{1E} + x_E & x_q + x_{1E} \\ x_E & -x_B - x_{E2} \end{bmatrix}^{-1} \begin{bmatrix} \dfrac{m_E v_{dc}\cos\delta_E}{2} \\ \dfrac{m_E v_{dc}\cos\delta_E}{2} - V_b\sin\delta - \dfrac{m_B v_{dc}\cos\delta_B}{2} \end{bmatrix}
\tag{2-14}
$$

The complete dynamic model of a single-machine infinite-bus power system equipped with a UPFC can be developed by combining Equations (2-14) with the machine dynamic equations shown below.

$$
\begin{aligned}
\dot{\delta} &= \omega_0\Delta\omega \\
\Delta\dot{\omega} &= \left(P_m - P_e - D\Delta\omega\right)/2H \\
\dot{E}'_q &= \left(-E_q + E_{qe}\right)/T'_{do} \\
\dot{E}_{qe} &= K_A\left(V_{to} - V_t\right)/\left(1 + sT_A\right)
\end{aligned}
\tag{2-15}
$$

Where

$$
\begin{aligned}
T_e &= P_e = V_q I_q + V_d I_d \\
E_q &= E'_q + \left(x_d - x'_d\right)i_{dt} \\
v_t &= \sqrt{v_{dt}^2 + v_{qt}^2} \\
v_{dt} &= x_q i_{qt} \\
v_{qt} &= E'_q - x'_d i_{dt} \\
i_{dt} &= i_{Ed} + i_{Bd} \\
i_{qt} &= i_{Eq} + i_{Bq}
\end{aligned}
\tag{2-16}
$$

By combining and linearizing Equations (2-14), (2-15) and (2-16), the state variable equations of the power system equipped with the UPFC can be represented as:

$$\begin{bmatrix} \Delta\dot{\delta} \\ \Delta\dot{\omega} \\ \Delta\dot{E}'_q \\ \Delta\dot{E}_{qe} \end{bmatrix} = \begin{bmatrix} 0 & \omega_0 & 0 & 0 \\ -\frac{K_1}{M} & -\frac{D}{M} & -\frac{K_2}{M} & 0 \\ -\frac{K_4}{T'_{do}} & 0 & -\frac{K_3}{T'_{do}} & \frac{1}{T'_{do}} \\ -\frac{K_A K_5}{T_A} & 0 & -\frac{K_A K_6}{T_A} & -\frac{1}{T_A} \end{bmatrix} \begin{bmatrix} \Delta\delta \\ \Delta\omega \\ \Delta E'_q \\ \Delta E_{qe} \end{bmatrix} + \begin{bmatrix} 0 \\ -\frac{K_{pd}}{M} \\ -\frac{K_{qd}}{T'_{do}} \\ -\frac{K_A K_{vd}}{T_A} \end{bmatrix} \Delta v_{dc}$$
$$+ \begin{bmatrix} 0 & 0 & 0 & 0 \\ -\frac{K_{pe}}{M} & -\frac{K_{p\delta e}}{M} & -\frac{K_{pb}}{M} & -\frac{K_{p\delta b}}{M} \\ -\frac{K_{qe}}{T'_{do}} & -\frac{K_{q\delta e}}{T'_{do}} & -\frac{K_{qb}}{T'_{do}} & -\frac{K_{q\delta b}}{T'_{do}} \\ -\frac{K_A K_{ve}}{T_A} & -\frac{K_A K_{v\delta e}}{T_A} & -\frac{K_A K_{vb}}{T_A} & -\frac{K_A K_{v\delta b}}{T_A} \end{bmatrix} \begin{bmatrix} \Delta m_E \\ \Delta\delta_E \\ \Delta m_B \\ \Delta\delta_B \end{bmatrix} \quad (2\text{-}17)$$

where Δm_E, Δm_B, $\Delta\delta_E$ and $\Delta\delta_B$ are the deviations of the input control signals of the UPFC. The detailed equations for the state matrix constants are given in Appendix A.

2.3. System under Study

The system used in the investigations in this chapter is shown in Figure 2.4. It consists of a synchronous generator connected via two transformers to an infinite bus system through a transmission line. A UPFC is installed in the midpoint of the transmission line. The system model developed in Section 2.2.2 is used to represent and study the dynamic performance of the single-machine infinite-bus power system.

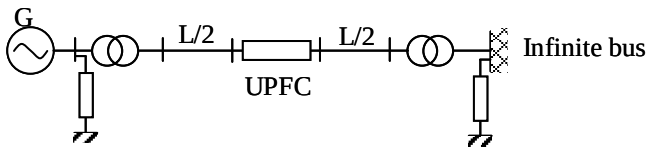

Figure 2.4 Single-machine infinite-bus power system.

From Equations (2-17), the block diagram of the single-machine infinite-bus power system equipped with a UPFC can be represented as shown in Figure 2.5.

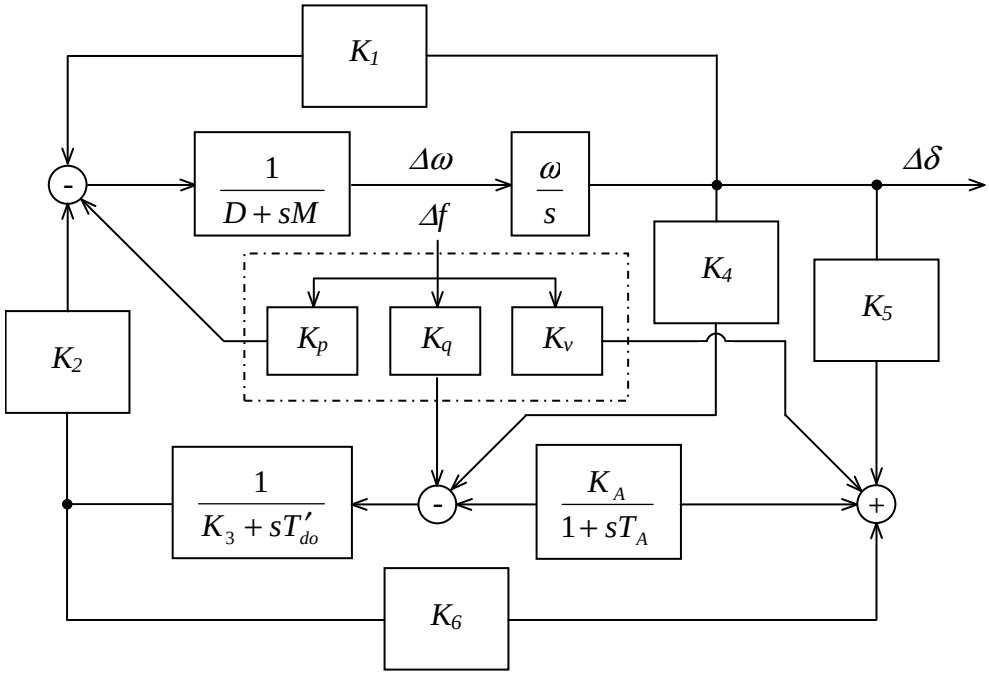

Figure 2.5 Block diagram of a single-machine infinite-bus power system.

Where:

$$\Delta f = \begin{bmatrix} \Delta v_{dc} & \Delta m_E & \Delta \delta_E & \Delta m_B & \Delta \delta_B \end{bmatrix}$$

$$K_p = \begin{bmatrix} \frac{K_{pd}}{M} & \frac{K_{pe}}{M} & \frac{K_{p\delta e}}{M} & \frac{K_{pb}}{M} & \frac{K_{p\delta b}}{M} \end{bmatrix}^T$$

$$K_q = \begin{bmatrix} \frac{K_{qd}}{T'_{do}} & \frac{K_{qe}}{T'_{do}} & \frac{K_{q\delta e}}{T'_{do}} & \frac{K_{qb}}{T'_{do}} & \frac{K_{q\delta b}}{T'_{do}} \end{bmatrix}^T$$

$$K_v = \begin{bmatrix} \frac{K_A K_{vd}}{T_A} & \frac{K_A K_{ve}}{T_A} & \frac{K_A K_{v\delta e}}{T_A} & \frac{K_A K_{vb}}{T_A} & \frac{K_A K_{v\delta b}}{T_A} \end{bmatrix}^T \qquad (2\text{-}18)$$

The block diagram of Figure 2.5 can be used in small signal stability investigations of the power system. The MATLAB Simulink toolbox can be used to study the system performance under different disturbances.

Different controller types are investigated in this chapter to study the potential of the UPFC controller in damping power system oscillations. Controller designs based on both conventional and artificial intelligence techniques are conducted.

2.4. UPFC Controller Performance

Generator angular speed is a commonly used signal to damp power system oscillations. In order to investigate the potential of the UPFC controller in damping power system oscillations, a simple proportional UPFC controller based on the generator angular speed as a stabilizing signal is considered. For simplicity, the UPFC controller is considered to employ a unity feedback proportional controller as shown in Figure 2.6.

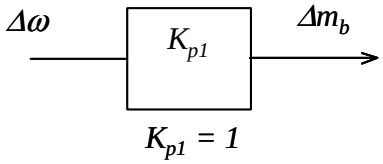

Figure 2.6 A UPFC proportional feedback controller.

The performance of this controller is examined with respect to the performance of the power system without a UPFC installed. Two system disturbances are considered for each case, a step change in the mechanical input power (ΔTm = 0.1 p.u.) and a step change in the reference voltage (ΔVref = 0.1 p.u.). The power system dynamic performances due to these disturbances are shown in Figures 2.7 and 2.8. It can be seen from these figures that the Proportional UPFC Controller (P-UPFC) significantly damps power system oscillations.

2.5. GA Based UPFC Controller Design

The proposed design of the UPFC controller is based on a technique that combines the pole shifting method and the GA principles (a brief GA overview is given in Appendix B). In such a technique, a fitness function is defined such that it will be maximum when the dominant eigenvalues are located in the left half of the s-plane as far from the imaginary axis as the physical constraints permit in order to achieve high damping [57]. The fitness function used by the proposed technique searches for the optimum controller design that depends upon the system parameters. It is selected such that it combines the effect of the real and imaginary parts of the eigenvalues on the time response. Moreover, this fitness function does not depend on the order of the system but on the dominant eigenvalues. In selecting such a fitness function, the closed loop system must satisfy the following requirements:

1- The system is stable.

2- The damping ratio is maximum and preferably greater than a prespecified design value.

3- The settling time is minimum (maximize the negative real part).

The fitness function is defined as follows:

$$F(\sigma_d, \omega_d, \beta) = \begin{cases} 0 & for\ \sigma_d > 0 \\ |\sigma_d| / \left\{1 + [(\omega_d / \sigma_d) / \tan\beta]^2\right\} & for\ \sigma_d > 0 \end{cases} \quad (2\text{-}19)$$

Where:

σ_d is the real part of the dominant eigenvalues

ω_d is the imaginary part of the dominant eigenvalues

$\cos\beta$ is the lower limit of the desired damping coefficient.

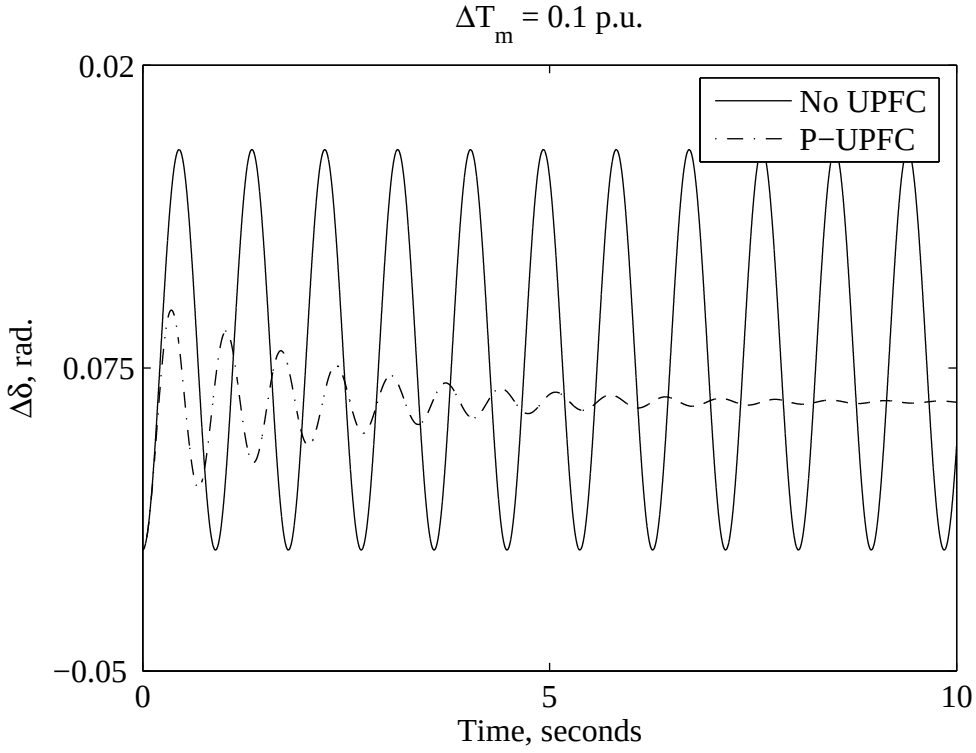

Figure 2.7 Power angle deviation during a step change in the mechanical input power.

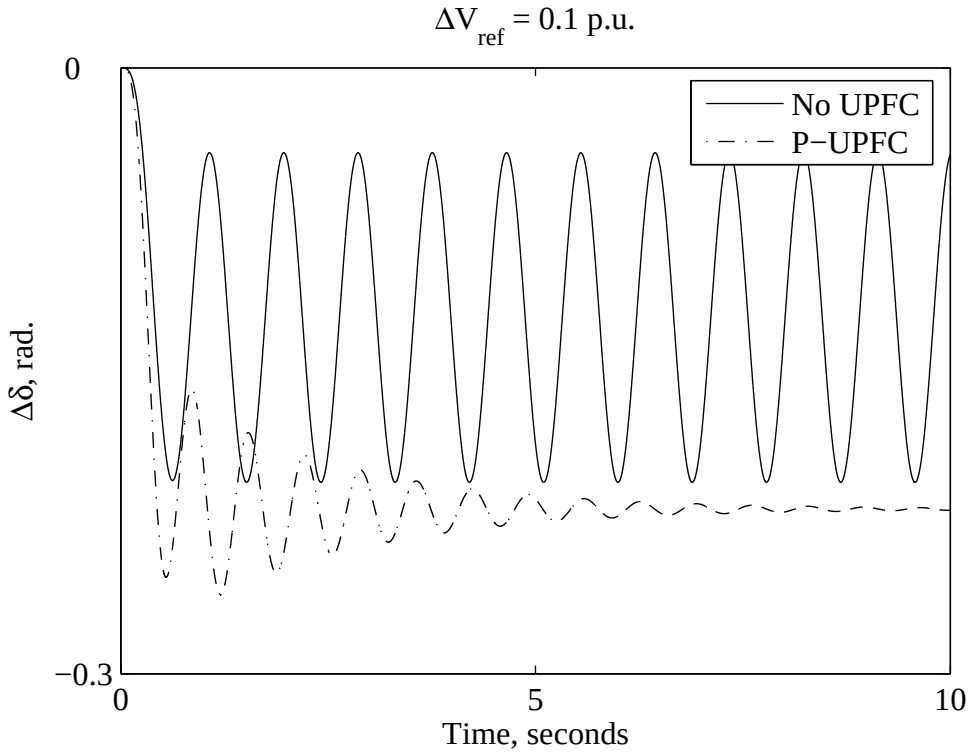

Figure 2.8 Power angle deviation during a step change in the reference voltage.

The area shown in Figure 2.9 represents the design area defined by the fitness function. For a stable system, the second constraint of the fitness function is to maximize the damping ratio. When ω_d/σ_d is less than tanβ, the fitness function will have a bigger value, and when ω_d/σ_d is greater than tanβ, the fitness function will have a smaller value. The second constraint is applied when the most dominant eigenvalues are conjugate complex roots. In the case of a real dominant eigenvalue, the fitness function is $|\sigma_d|$ (maximizing settling time as possible).

Two UPFC controller structures are considered in these investigations. The first controller is a Lead-Lag controller, shown in Figure 2.10. $\Delta\omega$ is used as an input signal for the Lead-Lag controller. The second controller is a Proportional Integral (PI) controller with $\Delta\omega$ and $\Delta\delta$ as input signals as shown in Figure 2.11. The controller parameters are optimized using the GA technique described above. Table 2-1 shows the controller parameters and the corresponding system eigenvalues.

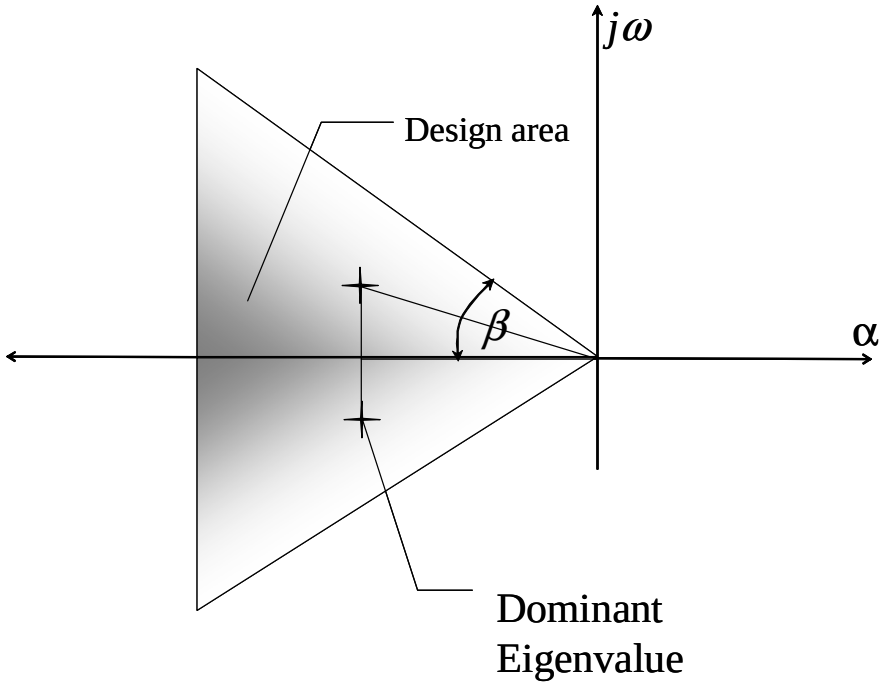

Figure 2.9 Design area for eigenvalues.

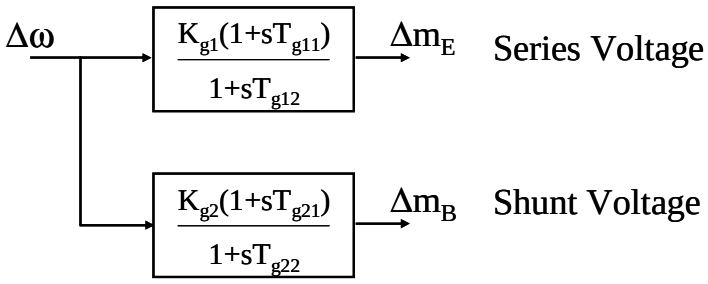

Figure 2.10 GA Lead-Lag controller.

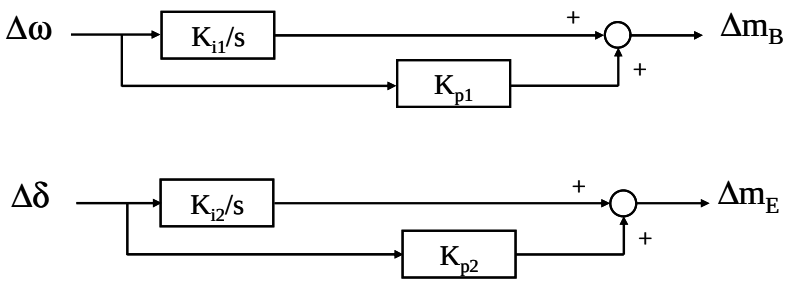

Figure 2.11 GA PI controller.

Table 2-1 GA controller parameters and the corresponding system eigenvalues

Controller parameters			
GA Lead-Lag controller			
$K_{g1} = 1.0673$	$T_{g11} = 5.9818$		$T_{g12} = 0.227$
$K_{g2} = 2.8692$	$T_{g21} = 2.34$		$T_{g22} = 2.4342\times10^{-4}$
GA PI controller			
$K_{i1} = -0.0428$		$K_{p1} = 37.613$	
$K_{i2} = -40.6239$		$K_{p2} = -0.0075$	
System eigenvalues			
No UPFC	P-UPFC	GA Lead-Lag UPFC	GA PI UPFC
$-2.7\times10^{-5} \pm j7.0181$	$-0.4891 \pm j9.31$	-4.5917	-1.6184
-8.3878	-4.1815	$-4.5938 \pm j14.4415$	$-1.6256 \pm j6.5887$
-11.8788	-15.1071	$-5.1427 \pm j2.9786$	-7.4292
		-2667.837	-9.9327

It can be seen from Table 2-1 that the dominant system eigenvalue is shifted from a near critically stable location (-2.7×10^{-5}, in the case of an uncontrolled power system) to a more stable location in the case of the power system equipped with the UPFC controller. It can also be seen that the GA Lead-Lag and the PI UPFC controllers have higher damping coefficients.

2.6. GA Based UPFC Controller Performance

In order to demonstrate the effectiveness of the designed UPFC controllers on damping power system oscillations, the same system disturbances considered in Section 2.4 are used again in this section. It can be seen from Figures 2.12 to 2.15, that the designed UPFC controllers significantly damp power system oscillations compared to the P-UPFC. Moreover, comparing Figures 2.12 and 2.13 with Figures 2.14 and 2.15, shows that the PI controller has the ability to reduce the power angle deviation to zero. This is due to the action of the integral part of such a controller.

2.7. Fuzzy Logic UPFC Controller Design

Fuzzy logic provides a general concept for description and measurement. Most fuzzy logic systems encode human reasoning into a program to make decisions or control a system [51]-[52]. Fuzzy logic comprises fuzzy sets, which are a way of representing non-statistical uncertainty and approximate reasoning, which includes the operations used to make inferences in fuzzy logic [58]-[59].

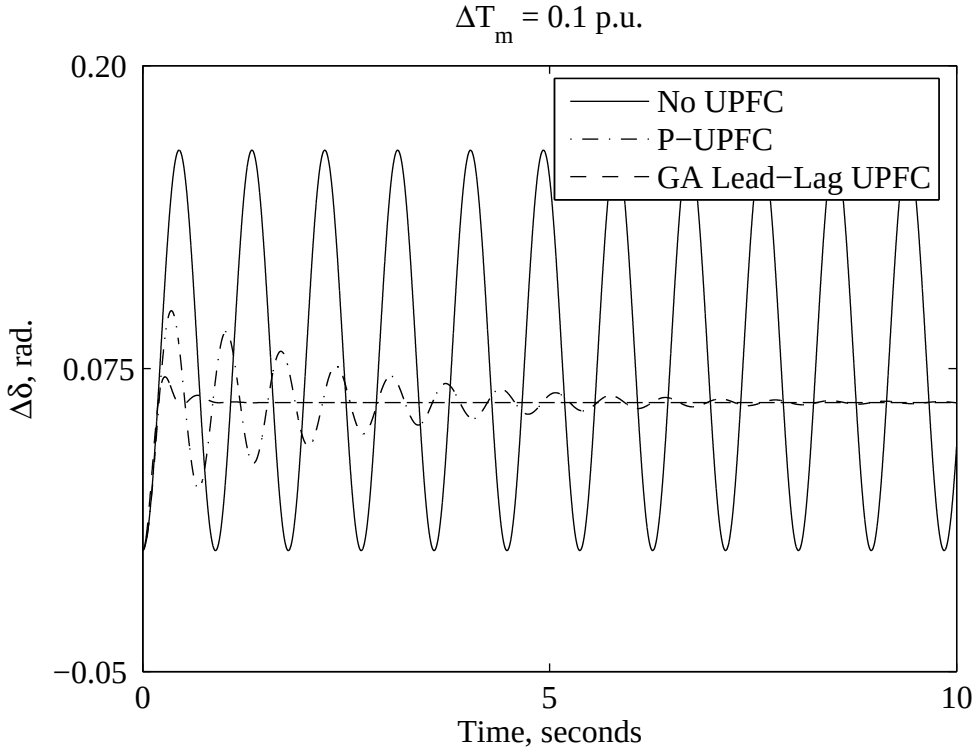

Figure 2.12 Power angle deviation due to a step change in the mechanical input power.

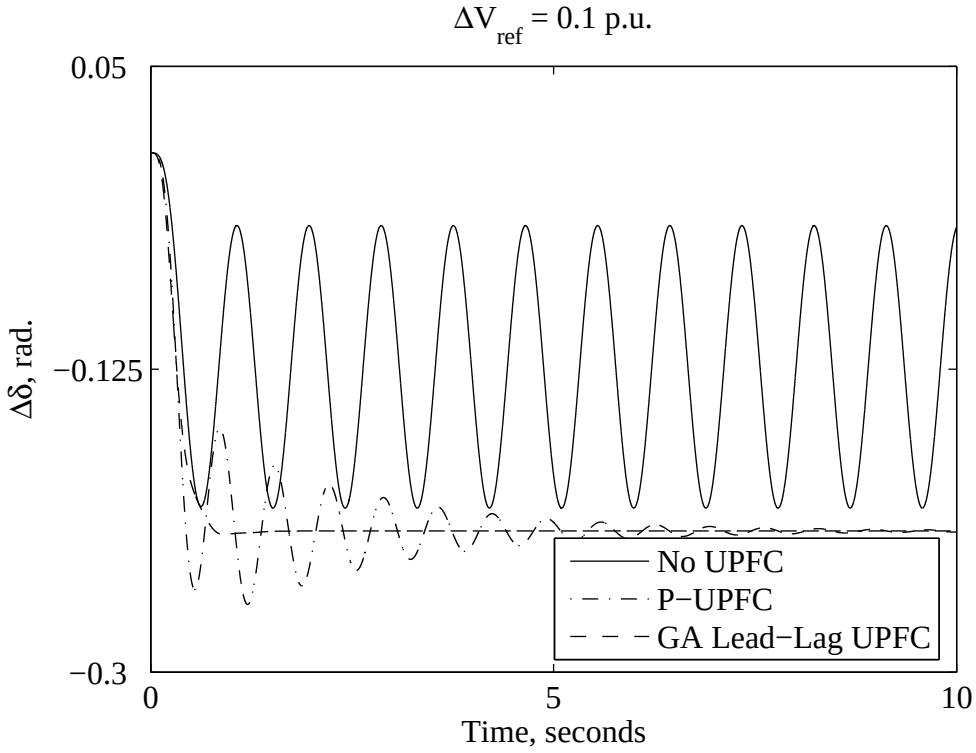

Figure 2.13 Power angle deviation due to a step change in the reference voltage.

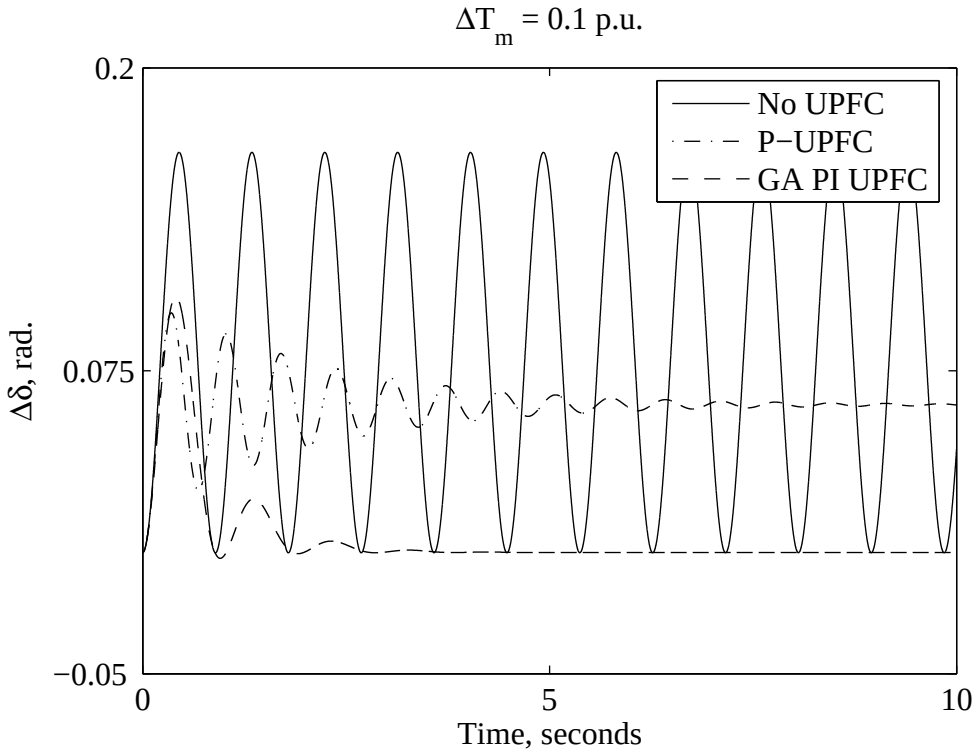

Figure 2.14 Power angle deviation due to a step change in the mechanical input power.

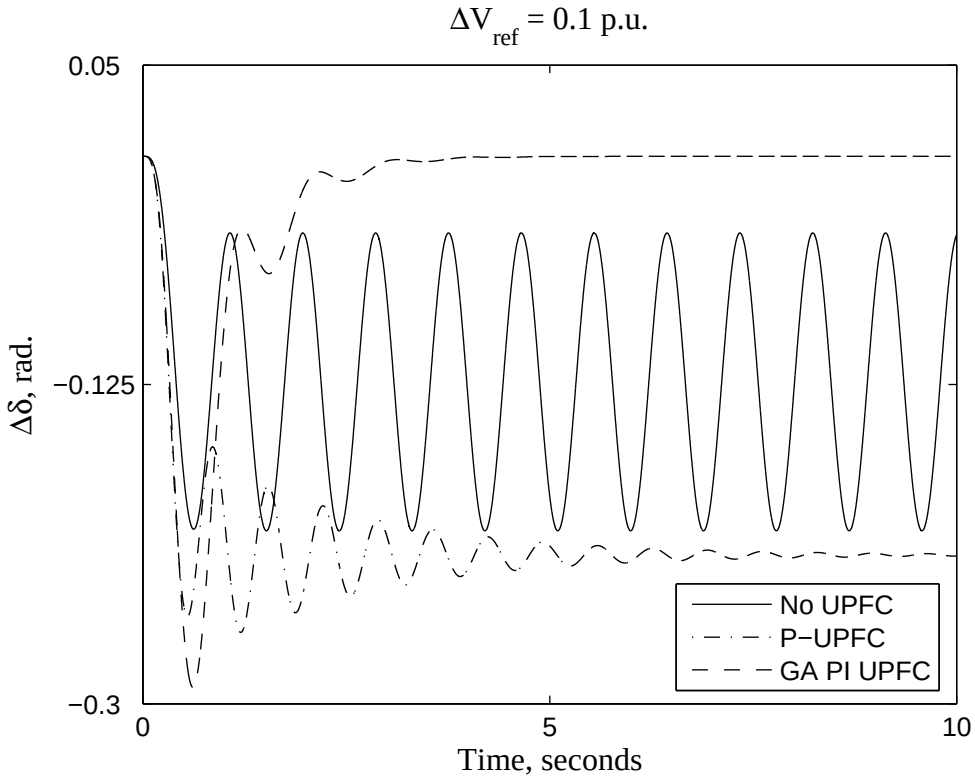

Figure 2.15 Power angle deviation due to a step change in the reference voltage.

2.7.1. Fuzzy control

There are two major types of fuzzy controllers, namely Mamdani type and Takagi-Sugeno (TS) type [60]. The classification depends on the type of fuzzy rules used. If a fuzzy controller uses the TS type of fuzzy rules, it is called a TS fuzzy controller. Otherwise, the controller is named a Mamdani fuzzy controller. Throughout the thesis, attention is focused on the Mamdani type fuzzy controller. Figure 2.16 depicts the structure of a fuzzy control system, which is comprised of a typical Single Input Single Output (SISO) Mamdani fuzzy controller and a system under control. The major components of a typical fuzzy controller are fuzzification, fuzzy rule base, fuzzy inference, and defuzzification.

2.7.1.1. Fuzzification [58]

Fuzzification is the process of decomposing a system input and/or output into one or more fuzzy sets. Many types of curves can be used, but triangular or trapezoidal shaped membership functions are the most common because they are easier to represent in embedded controllers. Each fuzzy set spans a region of input (or output) values graphed with the membership. Any particular input is interpreted from this fuzzy set and a degree of membership is interpreted. The membership functions may overlap to allow smooth mapping of the system. The process of fuzzification allows the system inputs and outputs to be expressed in linguistic terms so that rules can be applied in a simple manner to express a complex system.

2.7.1.2. Fuzzy sets [58]

A fuzzy set is represented by a membership function defined on the universe of discourse. The universe of discourse is the space where the fuzzy variables are defined. The membership function gives the grade, or degree, of membership within the set, of any element of the universe of discourse. The membership function maps the elements of the universe onto numerical values in the interval [0, 1]. A membership function value of zero implies that the corresponding element is definitely not an element of the fuzzy set, while a value of unity means that the element fully belongs to the set. A grade of membership in between corresponds to the fuzzy membership to the set. Figure 2.17 shows four commonly used membership functions.

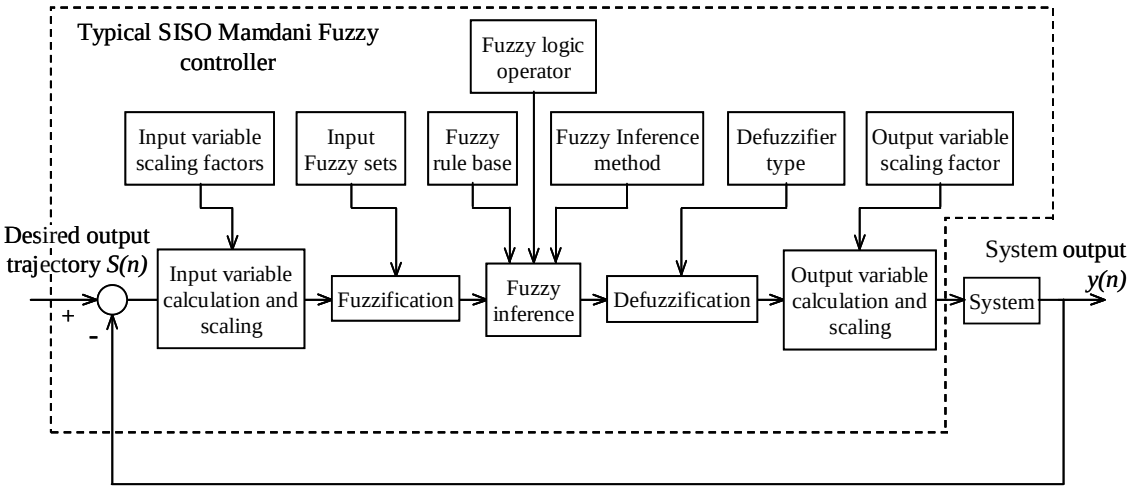

Figure 2.16 Structure of a SISO Mamdani fuzzy control system, which is comprised of a typical Mamdani fuzzy controller and a system under control.

2.7.1.3. Fuzzy rules [58]

Fuzzy rules represent the control strategy. They are linguistic if-then statements involving fuzzy set, fuzzy logic, and fuzzy inference. Fuzzy rules play a key role in representing expert control knowledge and experience and in linking the input variables of fuzzy controllers to output variable (or variables). A general Mamdani fuzzy rule, for *M* input-one output, can be expressed as

If x_1 is $\tilde{A}$ **and … and** x_M is $\tilde{B}$ **Then** U_1 is $\tilde{C}$ (2-20)

where $x_1, \ldots, x_M$ are input variables, U_1 is the output variable, "**and**" is a fuzzy logic AND operator and $\tilde{A}$, $\tilde{B}$ and $\tilde{C}$ are fuzzy sets. Fuzzy sets can also be represented by linguistic terms, for example, "Positive, Negative and Zero". In theory, these variables can be either continuous or discrete; practically speaking, however, they should be discrete because virtually all fuzzy controllers are implemented using digital computers. The first part of the fuzzy rule "**If** x_1 is $\tilde{A}$ **and … and** x_M is $\tilde{B}$" is called the rule antecedent, whereas the remaining part is named the rule consequent.

2.7.1.4. Fuzzy inference [58]

Fuzzy inference is used in a fuzzy rule to determine the rule outcome from the given rule input information. When specific information is assigned to input variables in the rule antecedent, fuzzy inference is needed to calculate the outcome for output variable(s) in

the rule consequent. A number of fuzzy inference methods can be used to accomplish this task, but only four of them are popular in fuzzy control. They are the Mamdani minimum inference method, the Larsen product inference method, the drastic product inference method and the bounded product inference method. These methods are denoted here by R_M, R_L, R_{DP} and R_{BP} respectively. The definitions of these methods are given in Table 2-2, where $\mu_{\tilde{C}}(z)$ is the membership function of the fuzzy set $\tilde{C}$ in the fuzzy rule expressed in Equation (2-20), μ is the combined membership in the rule antecedent and z is the output variable.

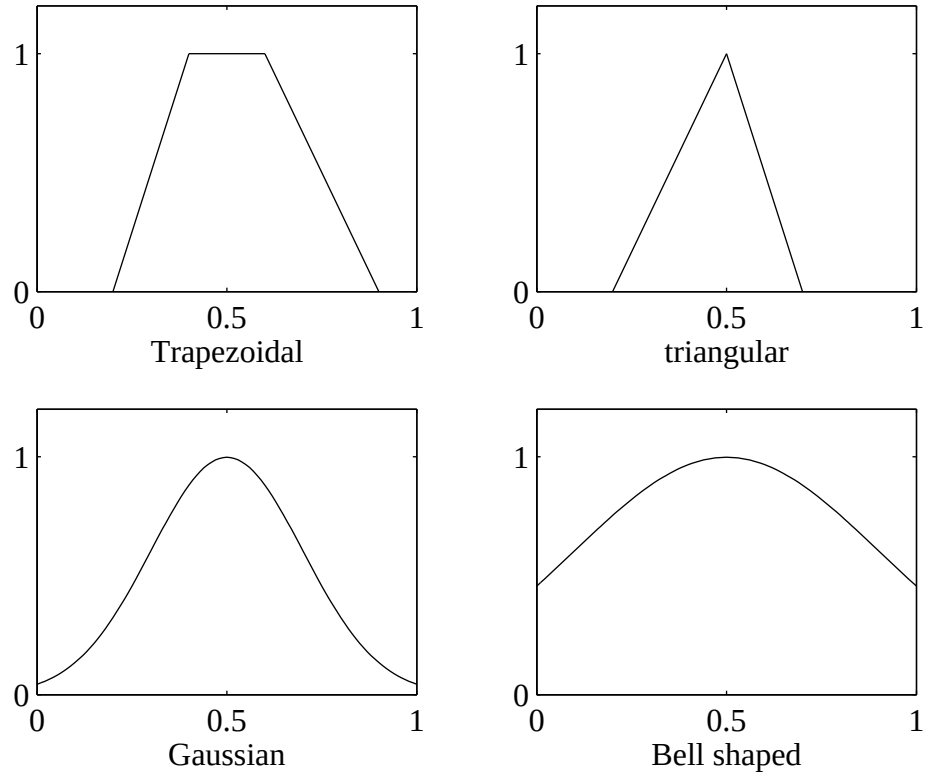

Figure 2.17 Commonly used membership functions.

These definitions are illustrated graphically in Figure 2.18. The results of the four fuzzy inference methods are the fuzzy sets formed by the shaded areas. The resulting fuzzy sets can be explicitly determined since the formulas describing the shaded areas can be derived mathematically. Among the four methods, the Mamdani minimum inference method is used most widely in fuzzy control and is used in the investigations of this thesis.

Table 2-2 Definitions of four popular fuzzy inference methods for fuzzy control

Fuzzy inference method	Definition*
Mamdani minimum inference, R_M	$\min(\mu, \mu_{\tilde{C}}(z))$, *for all z*
Larsen product inference, R_L	$\mu \times \mu_{\tilde{C}}(z)$, *for all z*
Drastic product inference, R_{DP}	$\begin{cases} \mu, & \text{for } \mu_{\tilde{C}}(z)=1 \\ \mu_{\tilde{C}}(z), & \text{for } \mu=1 \\ 0, & \text{for } <1 \text{ and } \mu_{\tilde{C}}(z)<1 \end{cases}$
Bounded product inference, R_{BP}	$\max(\mu + \mu_{\tilde{C}} - 1, 0)$

*General Mamdani fuzzy rule Equation (2-20) is utilized in the definition, $\mu_{\tilde{C}}(z)$ is the membership function of fuzzy set $\tilde{C}$ in the rule consequent, where μ is the final membership yielded by fuzzy logic AND operators in the rule antecedent.

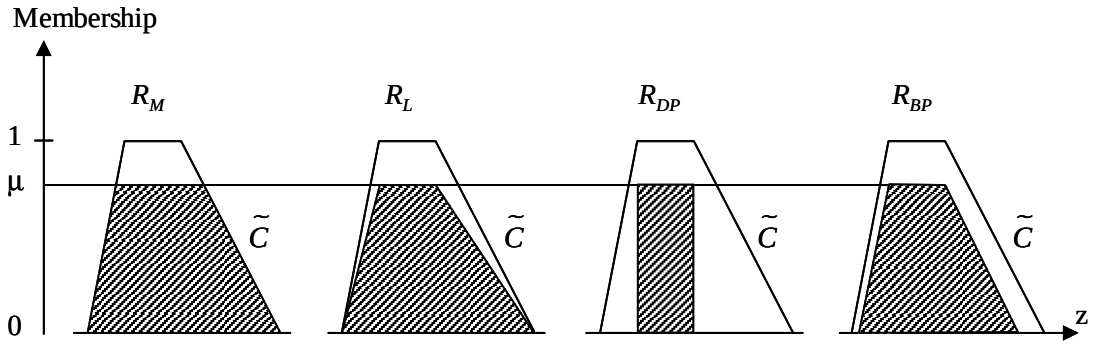

Figure 2.18 Graphical illustration of the definitions of the four popular fuzzy inference methods.

2.7.1.5. Defuzzification [58]

Fuzzy inference yields a linguistic output variable which needs to be translated into a crisp value. The objective is to derive a single crisp numeric value that best represents the inferred fuzzy values of the linguistic output variable. Defuzzification is such inverse transformation which maps the output from the fuzzy domain back into the crisp domain. Some defuzzification methods tend to produce an integral output considering all the elements of the resulting fuzzy set with the corresponding weights. Other methods take into account just the elements corresponding to the maximum points of the resulting membership functions. The following defuzzification methods are of practical importance:

Center-of-Area

The Center-of-Area method is often referred to as the Center-of-Gravity method because it computes the centroid of the composite area representing the output fuzzy term.

Center-of-Maximum

In the Center-of-Maximum method only the peaks of the membership functions are used. The defuzzified crisp compromise value is determined by finding the place where the weights are balanced. Thus the areas of the membership functions play no role and only the maxima (singleton memberships) are used. The crisp output is computed as a weighted mean of the term membership maxima, weighted by the inference results.

Mean-of-Maximum

The Mean-of-Maximum is used only in some cases where the Center-of-Maximum approach does not work. This occurs whenever the maxima of the membership functions are not unique and the question is as to which one of the equal choices one should take.

2.7.2. Controller design

A simple fuzzy logic controller based on a Mamdani type fuzzy logic controller is used in this section to damp power system oscillations in the study system. Two controller structures are considered in this study. The first is a proportional fuzzy logic controller using generator speed as a stabilizing signal. Figure 2.19 shows the Proportional fuzzy logic UPFC (PF-UPFC) controller structure. Single-input single-output fuzzy logic controller is considered. The membership functions of the input and output signals are shown in Figure 2.20.

The rules used in this controller are chosen as follows:

If $\Delta\omega$ is P **then** Δm_b is P.

If $\Delta\omega$ is N **then** Δm_b is N.

The second controller is a Hybrid fuzzy logic UPFC (HF-UPFC) controller. The structure of this controller is similar to the PF-UPFC controller with the addition of a conventional integrator. The HF-UPFC controller structure is shown in Figure 2.21.

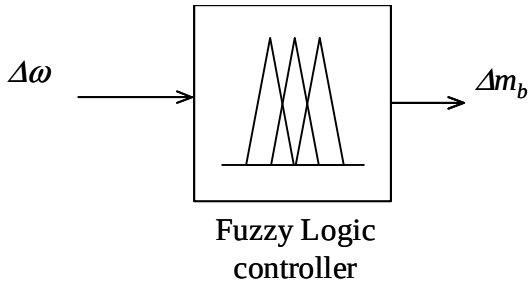

Figure 2.19 Proportional fuzzy logic controller structure.

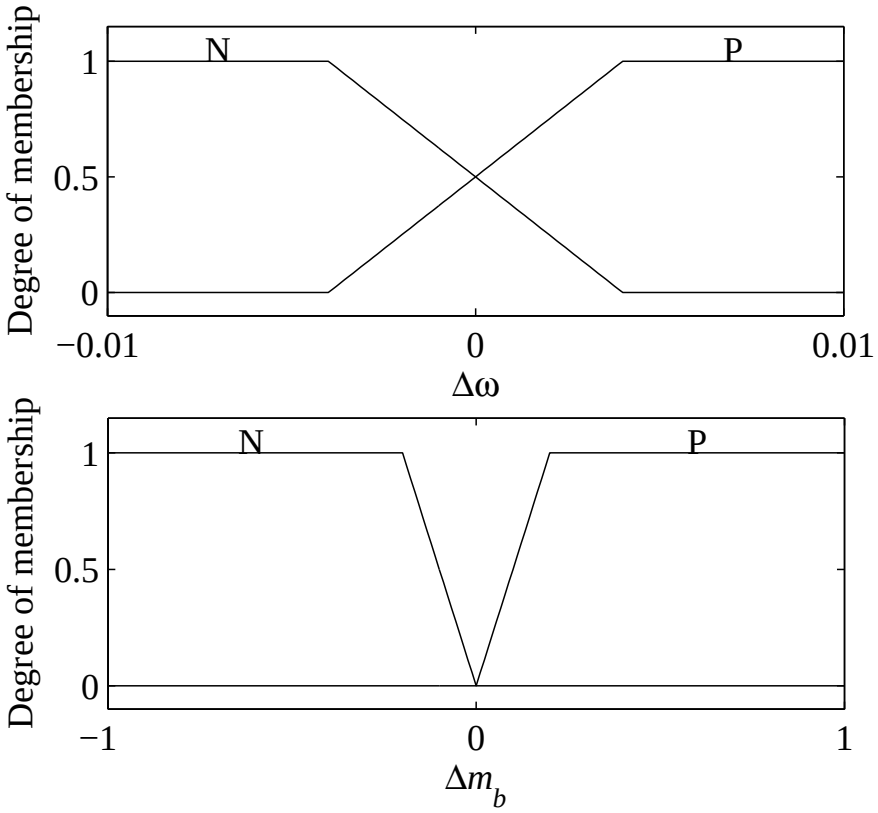

Figure 2.20 Input and output membership functions.

2.8. Fuzzy Logic UPFC Controller Performance

The performance of the designed PF-UPFC and HF-UPFC controllers after sudden changes in the reference mechanical power and reference voltage are shown in Figures 2.22 to 2.25. It can be seen from these figures, that the designed fuzzy logic UPFC controllers significantly damp power system oscillations compared to the P-UPFC.

Moreover, comparing Figures 2.22 and 2.23 with Figures 2.24 and 2.25, shows that the HF-UPFC controller has the ability to reduce the power angle deviation to zero. This is again due to the action of the integral part of such a controller.

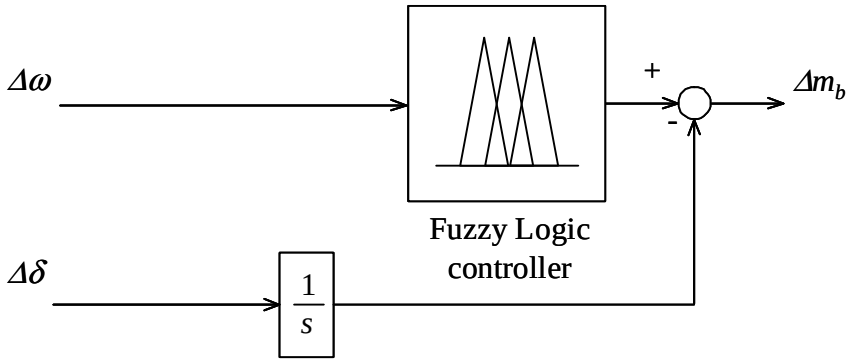

Figure 2.21 Hybrid fuzzy logic controller structure.

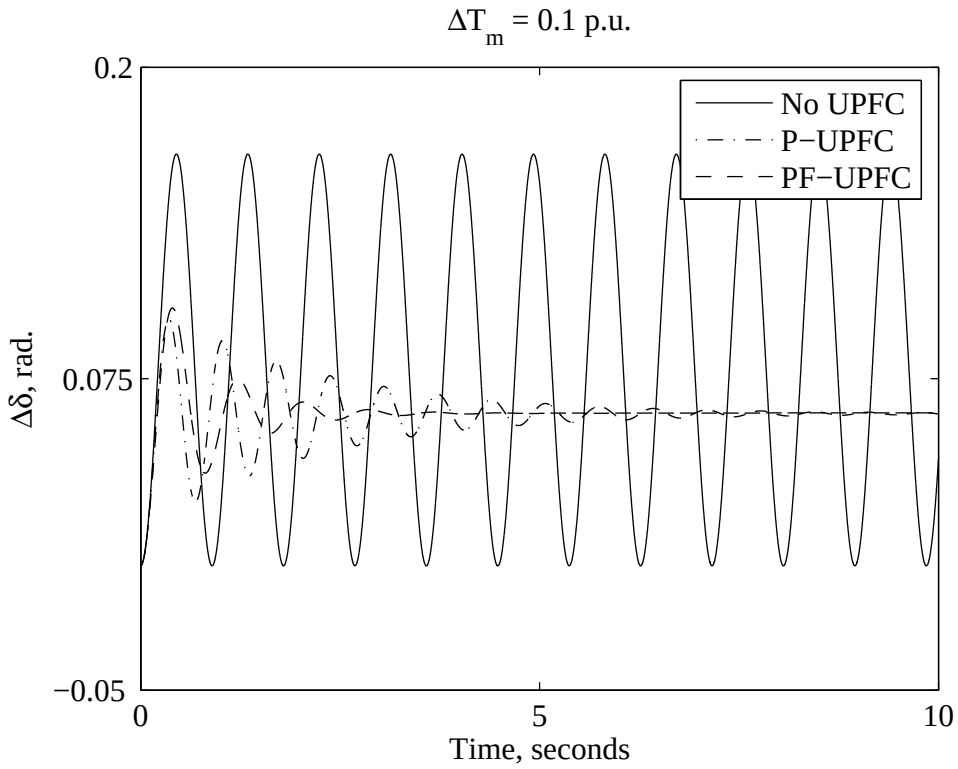

Figure 2.22 Power angle deviation due to a step change in the mechanical input power.

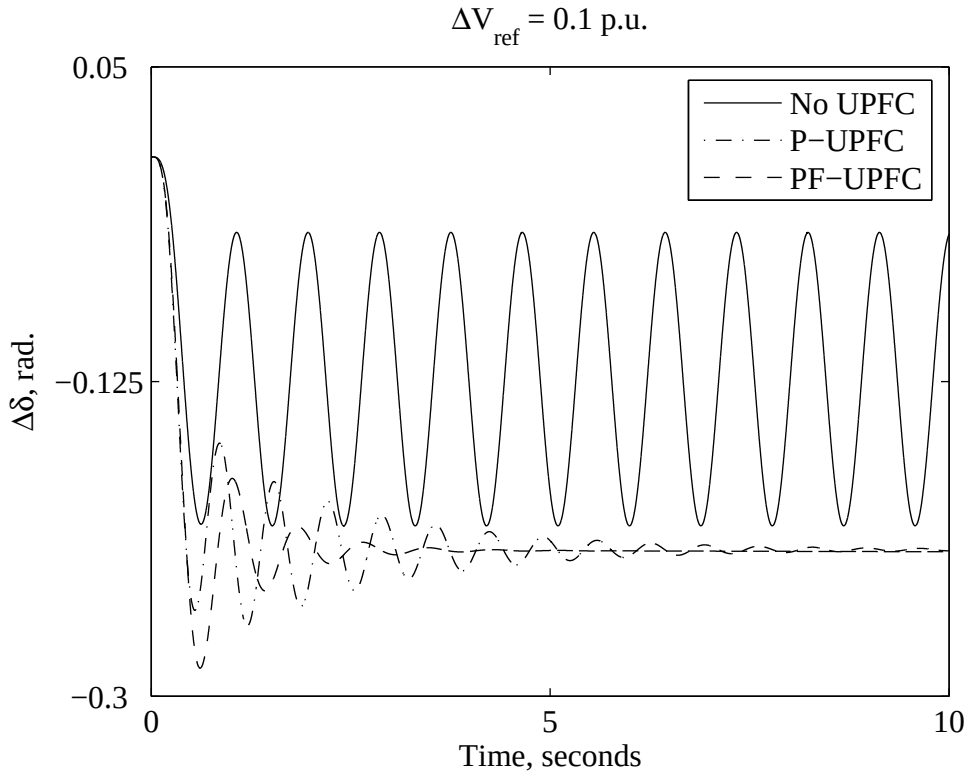

Figure 2.23 Power angle deviation due to a step change in the reference voltage.

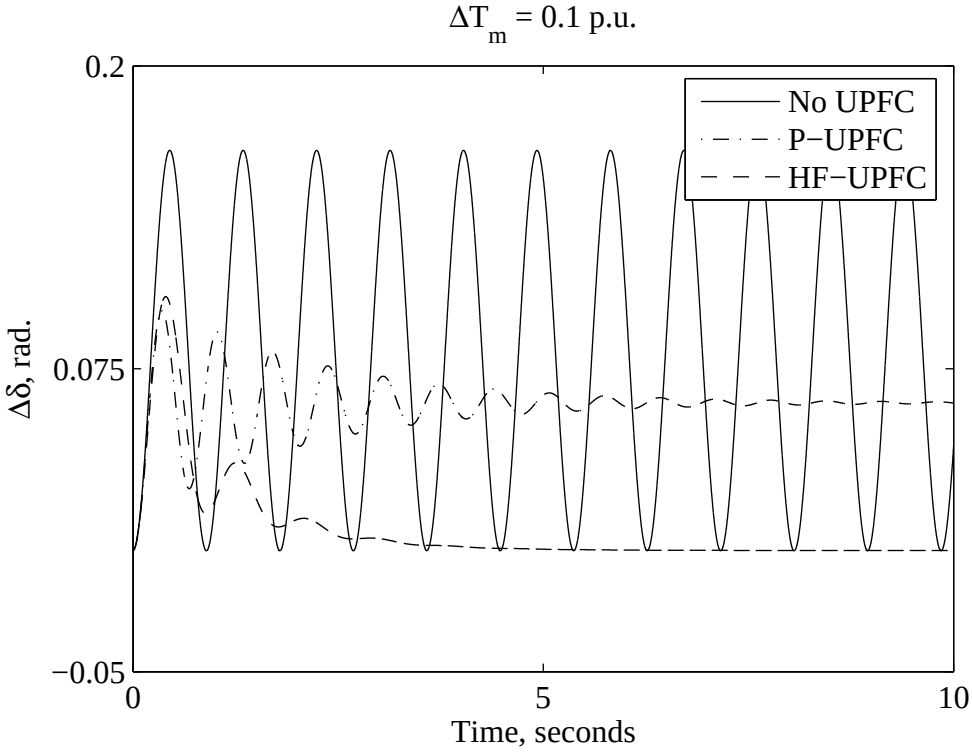

Figure 2.24 Power angle deviation due to a step change in the mechanical input power.

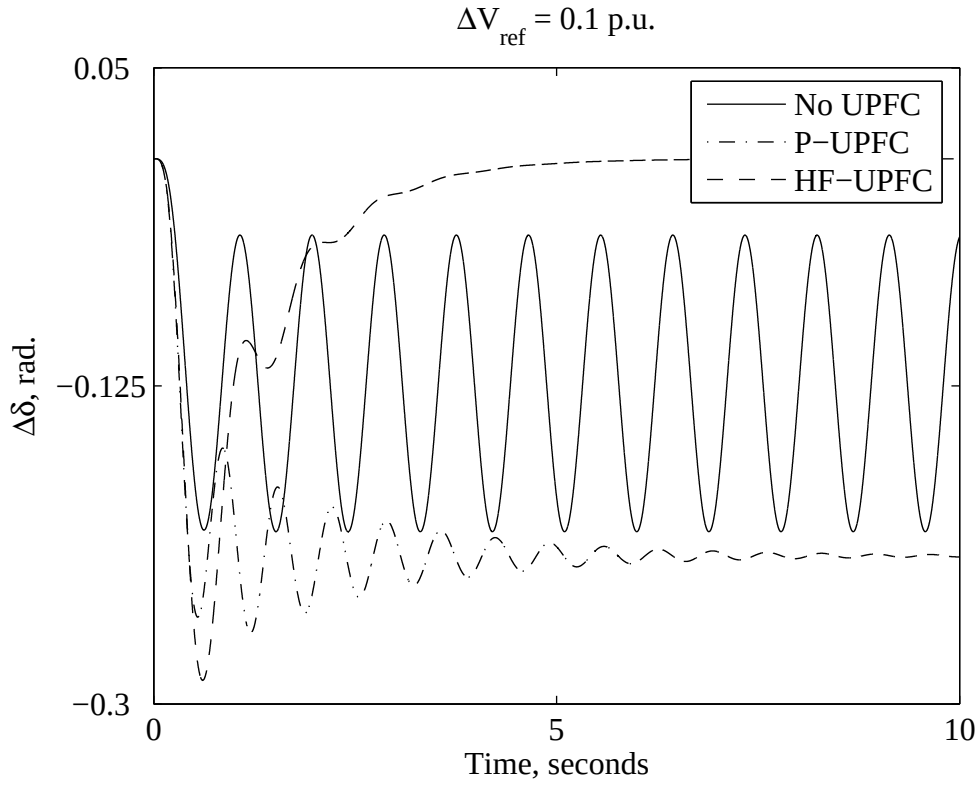

Figure 2.25 Power angle deviation due to a step change in the reference voltage.

2.9. Summary

In this chapter, a complete state-space model for a single-machine infinite-bus power system equipped with a UPFC is developed to study power system oscillations. Different controllers based on both conventional and artificial intelligence techniques have been developed and investigated. Novel control techniques based on GA and fuzzy logic were examined. Eigenvalue analysis as well as time simulations based on small system disturbances show the effectiveness of these controllers in damping power system oscillations. It should be noted that a system block diagram based on a linearized model is not suitable for simulating large system disturbances such as system faults. Large system disturbances are required to validate the controller's ability to damp power system oscillations. These types of disturbances are considered in the subsequent chapters.

3. DAMPING INTERAREA OSCILLATIONS USING GA BASED UPFC CONTROLLERS

3.1. Introduction

Large power systems typically exhibit multiple dominant interarea swing modes, which are associated with the dynamics of power transfers and involve groups of machines oscillating relative to each other. With the power industry moving toward deregulation, long-distance power transfers are steadily increasing, outpacing the addition of new transmission facilities and causing the interarea oscillations to become more lightly damped [61]. Power System Stabilizers (PSSs) have been used to damp interarea oscillations using different methodologies such as GA, small signal stability and robust control [62]-[64]. However, PSSs are designed individually for each generator that is likely to be affected by these oscillations. Due to the complexity of present day power systems, the number of modes of oscillation experienced by a particular generator has become large and the frequency of these modes has begun to vary over a wide range. Therefore, the design of an effective PSS has become extremely complex and difficult. During the last decade, FACTS based stabilizers have been employed to damp power system swing oscillations [12]-[23], [65]-[70]. Several approaches were used to design and control FACTS devices, for example, H_∞ and nonlinear PID control [65]-[67].

In this chapter, the GA technique is used to design centralized UPFC controllers to damp interarea oscillations in a typical three-area power system. Digital simulation studies on the study system are conducted to investigate the effectiveness of the designed controllers during system disturbances.

3.2. Modeling of a Multi-Area Power System Incorporating UPFCs

Without loss of generality, assume that in an n-machine power system, a UPFC is installed between nodes *i* and *j* in the network as shown in Figure 3.1. In order to include the function of the UPFC in the network admittance matrix *Y*, where only n

generator nodes are kept, an initial system admittance matrix Y_t containing nodes *i* and *j* is formed according to the following equation [2]:

$$\begin{bmatrix} 0 \\ 0 \\ I_g \end{bmatrix} = \begin{bmatrix} Y_{ii} & Y_{ij} & Y_{ik} \\ Y_{ji} & Y_{jj} & Y_{jk} \\ Y_{ki} & Y_{kj} & Y_{kk} \end{bmatrix} \begin{bmatrix} V_i \\ V_j \\ V_g \end{bmatrix} = Y_t \begin{bmatrix} V_i \\ V_j \\ V_g \end{bmatrix} \tag{3-1}$$

where

$$I_g = \begin{bmatrix} I_{g1} & I_{g2} & \cdots & I_{gn} \end{bmatrix}^T, \quad V_g = \begin{bmatrix} V_{g1} & V_{g2} & \cdots & V_{gn} \end{bmatrix}^T, \quad k = 1,2,...,n. \text{ and } k \neq i, k \neq j$$

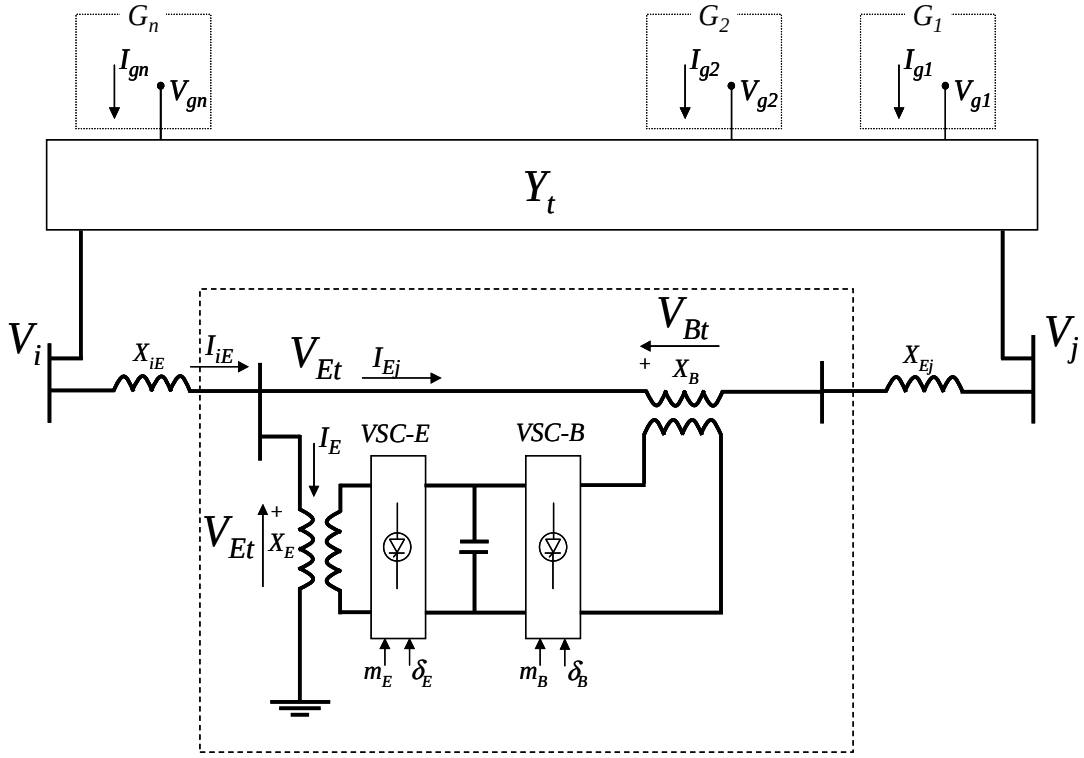

Figure 3.1 An n-machine power system incorporating a UPFC.

After installing the UPFC between nodes *i* and *j*, the network equation of the power system given by Equation (3-1) becomes:

$$\begin{aligned} Y'_{ii}V_i + I_{iE} + Y_{ik}V_g &= 0 \\ Y'_{jj}V_j - I_{Ej} + Y_{jk}V_g &= 0 \\ Y_{ki}V_i + Y_{kj}V_j + Y_{kk}V_g &= I_g \end{aligned} \tag{3-2}$$

where Y'_{ii} and Y'_{jj} are obtained from Y_{ii} and Y_{jj} by excluding $x_{ij} = x_{iE} + x_{Ej}$. The following equations can be also obtained from Figure 3.1:

$$V_i = jx_{iE} I_{iE} + V_{Et},\ I_E = I_{iE} - I_{Ej}$$
$$V_{Et} = jx_{Ej} I_{Ej} + V_{Bt} + V_j \tag{3-3}$$

Equation (2-11) can be written as:

$$V_{Et} = jx_E I_E + V_E$$
$$V_{Bt} = jx_B I_{Ej} + V_B \tag{3-4}$$

where

$$V_E = \frac{m_E v_{dc}}{2}\left(\cos\delta_E + j\sin\delta_E\right), \qquad V_B = \frac{m_B v_{dc}}{2}\left(\cos\delta_B + j\sin\delta_B\right)$$

The following equation can be obtained from Equations (3-3) and (3-4):

$$\begin{bmatrix} I_{iE} \\ I_{Ej} \end{bmatrix} = \frac{1}{x_\Sigma}\begin{bmatrix} -j\left(x_E + x_{Ej} + x_B\right) & jx_E \\ -jx_E & j\left(x_{iE} + x_E\right) \end{bmatrix}\begin{bmatrix} V_i \\ V_j \end{bmatrix} + \frac{1}{x_\Sigma}\begin{bmatrix} j\left(x_{Ej} + x_B\right) & jx_E \\ -jx_{iE} & j(x_{iE} + x_E) \end{bmatrix}\begin{bmatrix} V_E \\ V_B \end{bmatrix} \tag{3-5}$$

where $x_\Sigma = \left(x_{iE} + x_E\right)\left(x_E + x_{Ej} + x_B\right) - x_E^2$.

By substituting Equation (3-5) into Equation (3-2), the generator currents can be represented as:

$$I_g = CV_g + F_E V_E + F_B V_B \tag{3-6}$$

where

$$C = Y_{kk} + \begin{bmatrix} Y_{ki} & Y_{kj} \end{bmatrix} N^{-1}\begin{bmatrix} -Y_{ik} \\ Y_{jk} \end{bmatrix}$$

$$F_E = -\begin{bmatrix} Y_{ki} & Y_{kj} \end{bmatrix} N^{-1}\begin{bmatrix} \dfrac{j\left(x_{Ej} + x_B\right)}{x_\Sigma} \\ -\dfrac{jx_{iE}}{x_\Sigma} \end{bmatrix}, \quad F_B = -\begin{bmatrix} Y_{ki} & Y_{kj} \end{bmatrix} N^{-1}\begin{bmatrix} -\dfrac{jx_E}{x_\Sigma} \\ \dfrac{j\left(x_{iE} + x_E\right)}{x_\Sigma} \end{bmatrix}$$

$$N = \begin{bmatrix} Y'_{ii} - \dfrac{j\left(x_E + x_{Ej} + x_B\right)}{x_\Sigma} & \dfrac{jx_E}{x_\Sigma} \\ -\dfrac{jx_E}{x_\Sigma} & -Y'_{jj} + \dfrac{j\left(x_{iE} + x_E\right)}{x_\Sigma} \end{bmatrix}$$

The generator terminal voltages of the n-machine power system can also be expressed in the *d-q* reference frame as:

$$V_g = E'_q - jx'_d I_g - j\left(x_q - x'_d\right)I_q \tag{3-7}$$

where

$$E'_q = \begin{bmatrix} E'_{q1} & E'_{q2} & \cdots & E'_{qn} \end{bmatrix}^T,\ I_q = \begin{bmatrix} I_{q1} & I_{q2} & \cdots & I_{qn} \end{bmatrix}^T$$

$$x'_d = \begin{bmatrix} x'_{d1} & 0 & \cdots & 0 \\ 0 & x'_{d2} & \cdots & 0 \\ \vdots & \vdots & \ddots & \vdots \\ 0 & 0 & \cdots & x'_{dn} \end{bmatrix}, \qquad x_q = \begin{bmatrix} x_{q1} & 0 & \cdots & 0 \\ 0 & x_{q2} & \cdots & 0 \\ \vdots & \vdots & \ddots & \vdots \\ 0 & 0 & \cdots & x_n \end{bmatrix}$$

Using Equations (3-6) and (3-7), generator currents can be expressed as:

$$I_g = C_d\left[E'_q - j\left(x_q - x'_d\right)I_q + C_E V_E + C_B V_B\right] \tag{3-8}$$

Where $C_d = \left(C^{-1} + jx'_d\right)^{-1}$, $C_E = C^{-1}F_E$, $C_B = C^{-1}F_B$

Equation (3-8) can also be represented in the *d-q* reference frame as:

$$\begin{aligned} I_{Gi} = I_{gi}e^{j\delta_i} = \sum_{k=1}^{n} C_{dik}[E'_{qk}e^{j(90+\delta_k-\delta_i)} + \left(x_{qk} - x'_{dk}\right)e^{j(\delta_k-\delta_i)}I_{qk} \\ + C_{Ek}V_E e^{j\delta_i} + C_{Bk}V_B e^{j\delta_i}] \end{aligned} \tag{3-9}$$

Assuming that

$$C_{dik} = C_{dik}e^{j\beta_{dik}},\quad C_{Ek} = C_{Ek}e^{j\beta_{Ek}},\quad C_{Bk} = C_{Bk}e^{j\beta_{Bk}}$$

Equation (3-9) becomes

$$\begin{aligned} I_{di} &= \sum_{k=1}^{n} C_{dik}[-E'_{qk}\sin\delta_{ikd} + \left(x_{qk} - x'_{dk}\right)I_{qk}\cos\delta_{ikd} \\ &\quad + C_{Ek}V_E\cos\delta_{Ek} + C_{Bk}V_B\cos\delta_{Bk}] \\ I_{qi} &= \sum_{k=1}^{n} C_{dik}[E'_{qk}\cos\delta_{ikd} + \left(x_{qk} - x'_{dk}\right)I_{qk}\sin\delta_{ikd} \\ &\quad + C_{Ek}V_E\sin\delta_{Ek} + C_{Bk}V_B\sin\delta_{Bk}] \end{aligned} \tag{3-10}$$

where

$$\begin{aligned} \delta_{ikd} &= \delta_k - \delta_i + \beta_{dik} \\ \delta_{Ek} &= \delta_E + \delta_i + \beta_{dik} + \beta_{Ek} \\ \delta_{Bk} &= \delta_B + \delta_i + \beta_{dik} + \beta_{Bk} \end{aligned}$$

Linearizing Equation (3-10) gives

$$\begin{aligned}\Delta I_d &= Y_d\Delta\delta + F_d\Delta E'_q + G_d\Delta v_{dc} + H_{Ed}\Delta m_E + H_{Bd}\Delta m_B + R_{Ed}\Delta\delta_E + R_{Bd}\Delta\delta_B \\ \Delta I_q &= Y_q\Delta\delta + F_q\Delta E'_q + G_q\Delta v_{dc} + H_{Eq}\Delta m_E + H_{Bq}\Delta m_B + R_{Eq}\Delta\delta_E + R_{Bq}\Delta\delta_B\end{aligned} \tag{3-11}$$

The linearized equations model of an n-machine power system can be written as follows:

$$\begin{aligned}\Delta\dot{\delta} &= \omega_0\Delta\omega \\ \Delta\dot{\omega} &= \left(-\Delta T_e - D\Delta\omega\right)/2H \\ \Delta\dot{E}'_q &= \left[-\Delta E'_q - \left(x_d - x'_d\right)\Delta I_d + \Delta E_{fd}\right]/T'_{d0} \\ \Delta\dot{E}_{fd} &= \left(-\Delta E_{fd} - K_A\Delta V_T\right)/T_A \\ \Delta T_e &= \Delta I_q E'_{q0} + I_{q0}\Delta E'_q + \Delta I_q\left(x_q - x'_d\right)I_{d0} + \Delta I_d\left(x_q - x'_d\right)I_{q0} \\ \Delta V_{Td} &= x_q\Delta I_q, \quad \Delta V_{Tq} = \Delta E'_q - x'_d\Delta I_d\end{aligned} \tag{3-12}$$

where variables with prefix Δ are n-order vectors. Others are n-order diagonal matrices.

Substituting Equations (3-11) into Equations (3-12) yields

$$\begin{aligned}\Delta T_e &= K_1\Delta\delta + K_2\Delta E'_q + K_{pd}\Delta v_{dc} + K_{pe}\Delta m_E + K_{pde}\Delta\delta_E + K_{pb}\Delta m_B + K_{pdb}\Delta\delta_B \\ \Delta E_q &= K_4\Delta\delta + K_3\Delta E'_q + K_{qd}\Delta v_{dc} + K_{qe}\Delta m_E + K_{qde}\Delta\delta_E + K_{qb}\Delta m_B + K_{qdb}\Delta\delta_B \\ \Delta V_T &= K_5\Delta\delta + K_6\Delta E'_q + K_{vd}\Delta v_{dc} + K_{ve}\Delta m_E + K_{vde}\Delta\delta_E + K_{vb}\Delta m_B + K_{vdb}\Delta\delta_B\end{aligned} \tag{3-13}$$

The linearized model for the n-machine power system can be obtained by substituting Equations (3-13) into Equations (3-12) as follows:

$$\begin{bmatrix}\Delta\dot{\delta}\\ \Delta\dot{\omega}\\ \Delta\dot{E}'_q\\ \Delta\dot{E}_{fd}\end{bmatrix} = \begin{bmatrix}0 & \omega_0 I & 0 & 0\\ -\frac{K_1}{M} & -\frac{D}{M} & -\frac{K_2}{M} & 0\\ -\frac{K_4}{T'_{do}} & 0 & -\frac{K_3}{T'_{do}} & \frac{1}{T'_{do}}\\ -\frac{K_A K_5}{T_A} & 0 & -\frac{K_A K_6}{T_A} & -\frac{1}{T_A}\end{bmatrix}\begin{bmatrix}\Delta\delta\\ \Delta\omega\\ \Delta E'_q\\ \Delta E_{fd}\end{bmatrix} + \begin{bmatrix}0 & 0 & 0 & 0 & 0\\ -\frac{K_{pd}}{M} & -\frac{K_{pe}}{M} & -\frac{K_{p\delta e}}{M} & -\frac{K_{pb}}{M} & -\frac{K_{p\delta b}}{M}\\ -\frac{K_{qd}}{T'_{do}} & -\frac{K_{qe}}{T'_{do}} & -\frac{K_{q\delta e}}{T'_{do}} & -\frac{K_{qb}}{T'_{do}} & -\frac{K_{q\delta b}}{T'_{do}}\\ -\frac{K_A K_{vd}}{T_A} & -\frac{K_A K_{ve}}{T_A} & -\frac{K_A K_{v\delta e}}{T_A} & -\frac{K_A K_{vb}}{T_A} & -\frac{K_A K_{v\delta b}}{T_A}\end{bmatrix}\begin{bmatrix}\Delta v_{dc}\\ \Delta m_E\\ \Delta\delta_E\\ \Delta m_B\\ \Delta\delta_B\end{bmatrix} \tag{3-14}$$

Equation (3-14) has the general form of the state-space equation

$$\left[\dot{X}\right] = [A][X] + [B][U] \tag{3-15}$$

3.3. System under Study

The multi-area power system used in the investigations of this thesis is shown in Figure 3.2. It consists of three control areas connected through three tie lines. Each area is represented by an equivalent generator and a local load.

The transient model for the generators, a first-order simplified model for the excitation systems and linear models for the loads and AC network are used. UPFCs are assumed to be installed at different locations on the tie lines. The system data and the detailed equations for the state matrix [A] and the input matrix [B] are given in Appendix C.

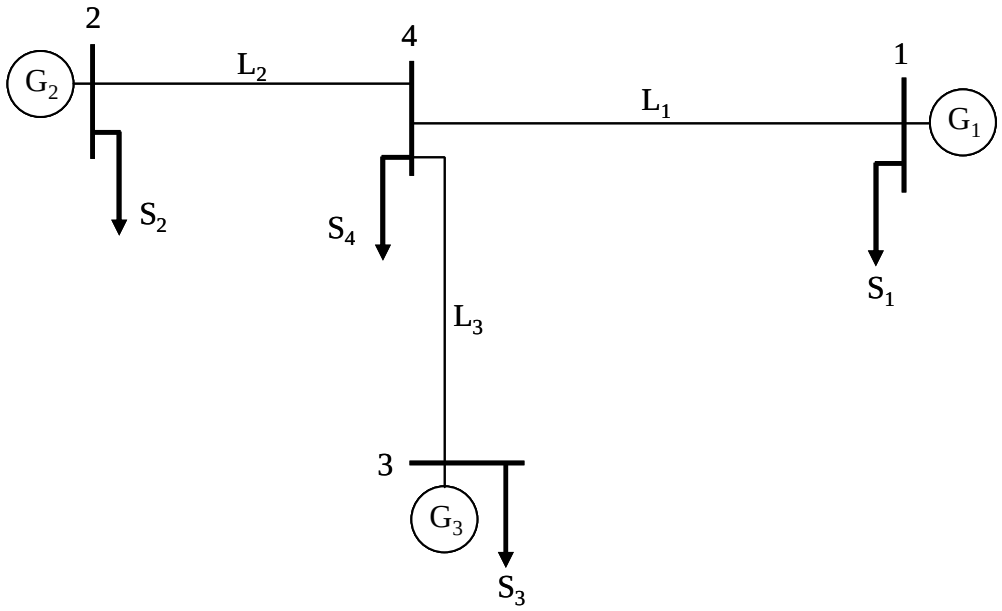

Figure 3.2 System under study.

3.4. GA Based UPFC Controller Design

Figure 3.3 shows the transfer function of a PI controller whose output U_i controls the magnitude $|V_{inj}|$ and the phase angle δ_{inj} of the injected voltage V_{inj} of a voltage-source converter. A UPFC, therefore, would have two such controllers. The PI controller parameters are assumed to be adjustable. The GA technique developed in this thesis is used to adjust these parameters.

The selection of the appropriate stabilizing signal is a fundamental issue in the design of an effective and robust controller. The variation in generator speeds ($\Delta\omega_1$, $\Delta\omega_2$ and $\Delta\omega_3$) are selected in the controller design as they are the best stabilizing signals to

observe the interarea modes. With this selection, the UPFC controller is a centralized three-input, four-output controller with global signals.

With the help of the Global Positioning System (GPS), time synchronization between Intelligent Electronic Devices (IED) is achievable with an accuracy of less than 1 μs. Measurements of electrical values taken at different locations that received a time-tag when they were recorded permit complete phasor information exchange in real-time [71]. Existing Phasor Measurement Units (PMU) are able to exchange phasor information with a frequency up to 60 Hz.

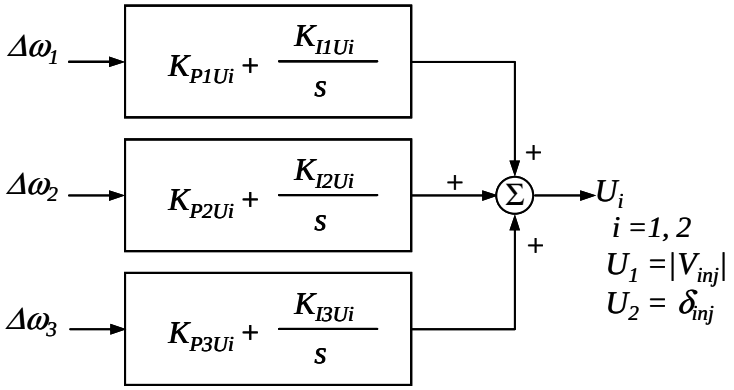

Figure 3.3 A PI controller structure for each voltage-source converter of the UPFC.

3.4.1. GA parameters selection

The choice of the GA parameters is application dependent. The suitable values of these parameters are selected by trial and error.

Consider the case of a UPFC installed in the middle of tie-line L_1. Figures 3.4 to 3.6 depict respectively the results of parametric studies carried out to investigate the effect of the population size (P_s), the crossover probability (P_c) and the mutation probability (P_m) on the final optimized value of the fitness function. As it can be seen from Figure 3.4, increasing the population size over 100 strings does not significantly affect the controller design as the differences among the final values of the fitness function are relatively small. It can also be seen from Figure 3.4 that the value of the fitness function converges to its optimum value within 40 to 60 generations when using a population size greater than 100 strings. It can be seen from Figure 3.5 that, a crossover probability between 0.5 and 0.9 results in small differences in the final value of the fitness function.

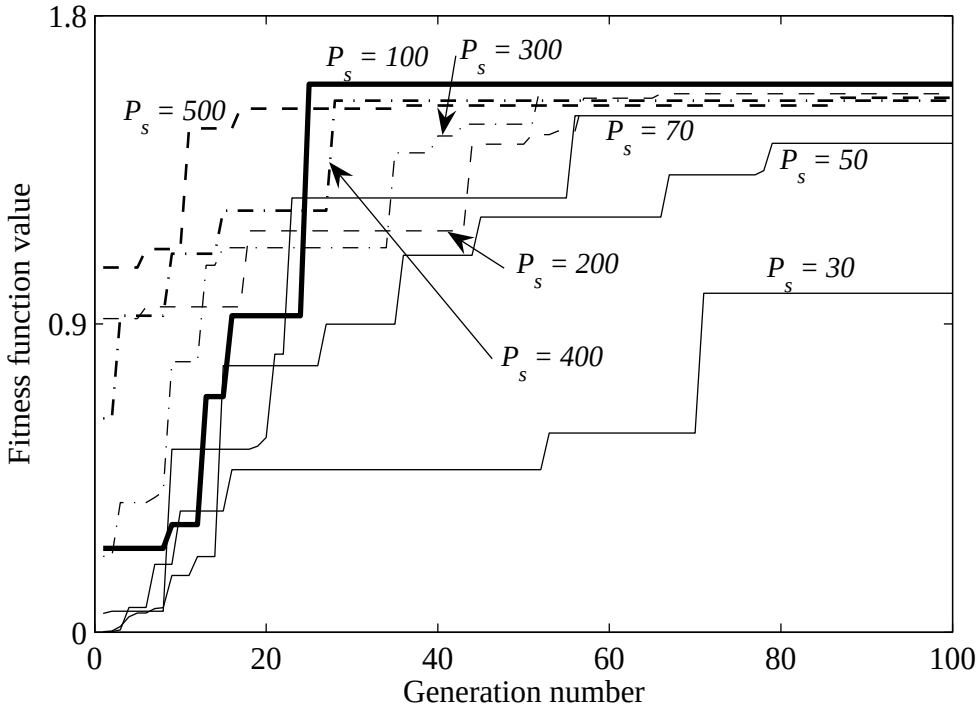

Figure 3.4 Effect of the population size on the variation of the fitness function with the number of generations (a UPFC is installed in the middle of tie-line L_1).

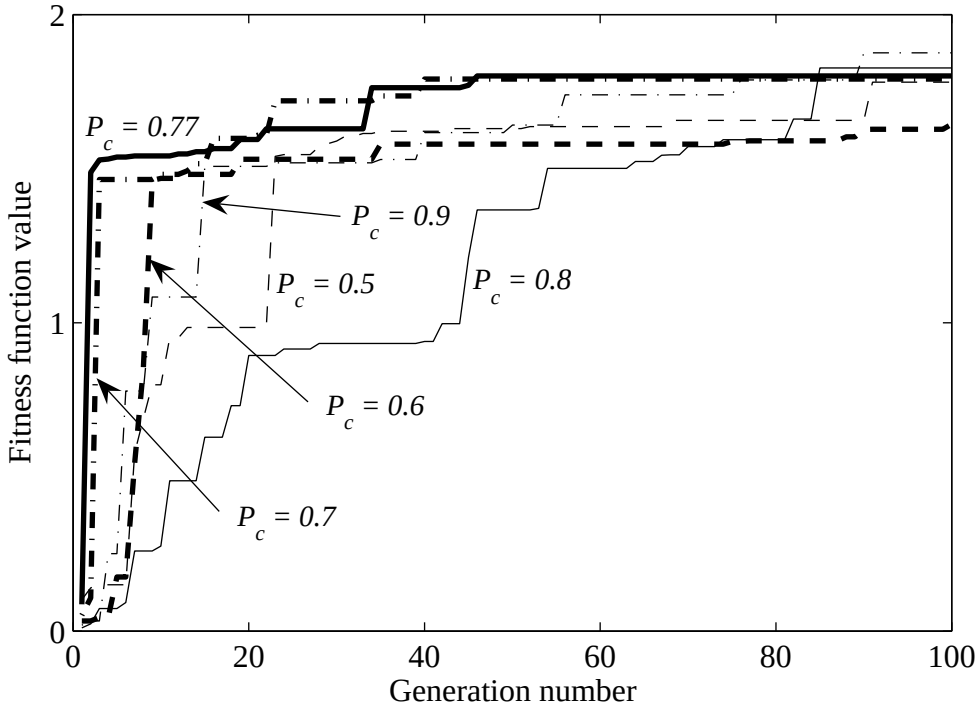

Figure 3.5 Effect of the crossover probability on the variation of the fitness function with the number of generations (a UPFC is installed in the middle of tie-line L_1).

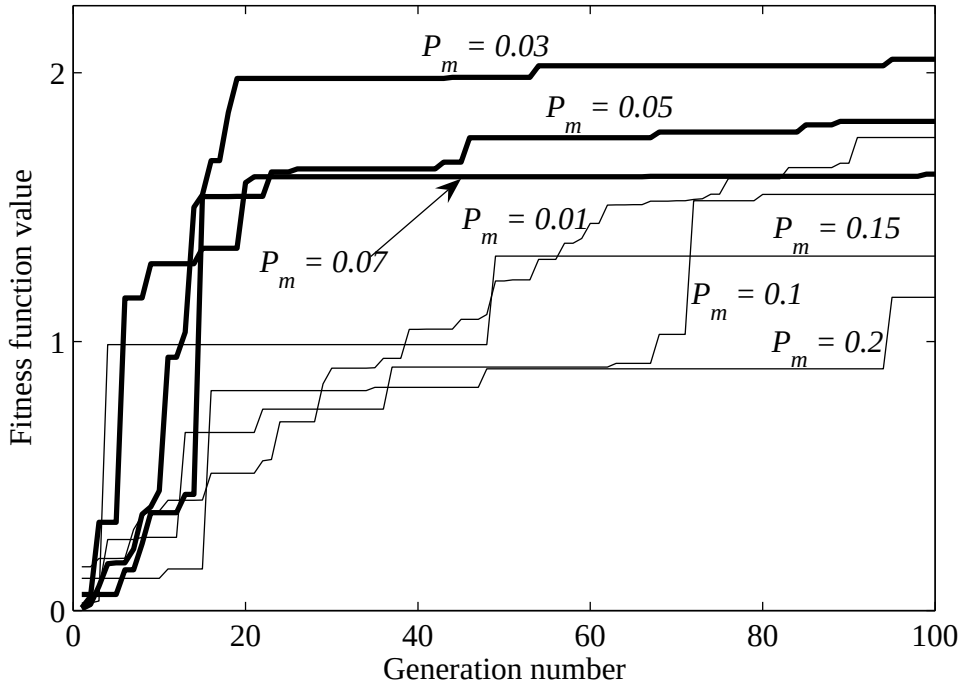

Figure 3.6 Effect of the mutation probability on the variation of the fitness function with the number of generations (a UPFC controller is installed in the middle of tie-line L_1).

From the control point of view, a crossover probability in the range of 0.7 to 0.77 results in a good system response. Regarding the effect of the mutation probability on the final value of the fitness function, Figure 3.6 shows that, selecting a mutation probability between 0.03 and 0.07 results in a desirable convergence for the fitness function and, therefore, a better design for the UPFC controller. The effect of selecting the value of the angle β on the controller design and consequently on the system response is illustrated in Figure 3.7. This figure shows the relative generator speeds due to a three-cycle three-phase fault at bus 1. As can be seen from the figure, the value of β does not significantly affect the system response.

During the course of this research, the GA operators are selected as follows [46]-[50]:

- Population size = 100 to 500 strings (each string represents a controller design).
- Maximum number of generations = 30 to 100 (iterations).
- Crossover probability = 0.77
- Mutation probability = 0.05

- Selection method is tournament selection.
- β = 45° (cosβ = 0.707) [57].

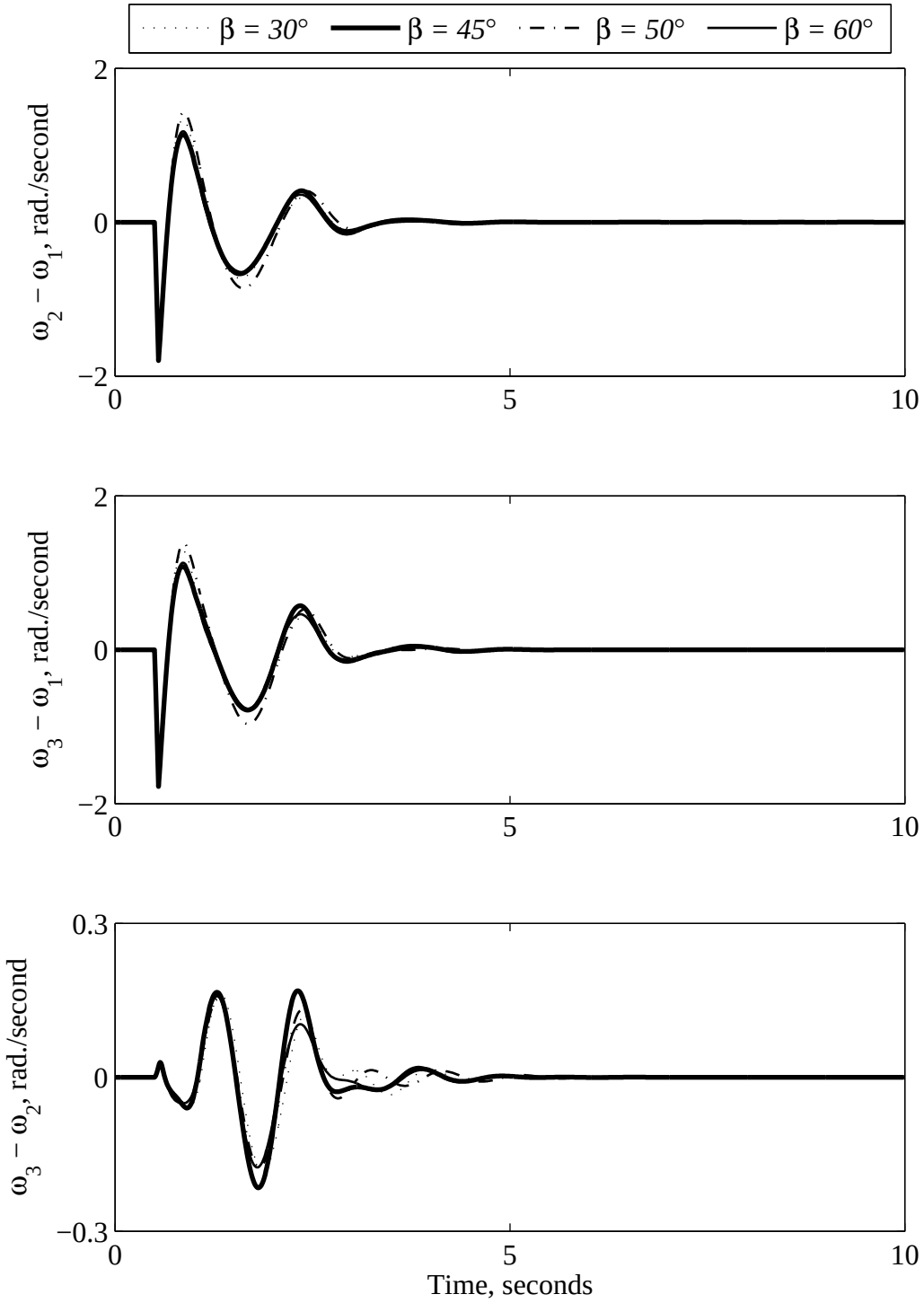

Figure 3.7 Effect of the angle β on the relative generator speeds due to a 3-cycle three-phase fault at bus 1 (a UPFC controller is installed in the middle of tie-line L_1).

3.5. GA Based UPFC Controller Performance during System Faults

To demonstrate the effectiveness of the designed UPFC controller, several simulation studies representing small and large disturbances are carried out on the system under investigations. The system pre-disturbance operating condition is such that area 1 is importing 440 MW through tie-line L_1. The detailed system pre-disturbance operating condition is given in Appendix D.

3.5.1. Effect of the Fault Location

In this case, a UPFC controller is assumed to be installed in the middle of tie-line L_1 (LOC1). Table 3-1 shows the system eigenvalues with and without employing the designed UPFC controller. It can be seen from Table 3-1 that the dominant eigenvalues are shifted to the left, which results in a better system performance. To validate the eigenvalues analysis, the designed UPFC controller is tested through simulating large system disturbances, namely three-phase faults at different system locations. These faults are assumed to occur on a weak tie-line and to be cleared by circuit breaker operations that leave the main tie-lines intact.

Table 3-1 System eigenvalues with the UPFC controller installed in tie-line L_1

System eigenvalues	
No UPFC	GA PI UPFC
$-0.1649 \pm j4.6393$	-1.6088
$-0.2309 \pm j6.6423$	$-1.6213 \pm j5.7847$
$-0.5410 \pm j5.2272$	$-1.8029 \pm j1.2063$
-1.4757	$-2.8255 \pm j7.0481$
-2.0865	$-3.2365 \pm j1.9593$
-4.6719	-16.3615
-14.7535	-16.7835
-17.7718	-18.6242
-18.7702	

Figures 3.8 to 3.11 illustrate the time responses of the generator speeds measured with respect to the speed of generators G_1 and G_2 due to a 3-cycle three-phase fault at the different system buses. It can be seen from these figures that, without the UPFC controller, the system is first-swing stable but the post-contingency oscillations are poorly damped. It can also be seen that the UPFC controller significantly damps the

system oscillations at all fault locations. It can be seen, however, from the same figures that the fault location affects the performance of the UPFC. Comparing Figure 3.8 with

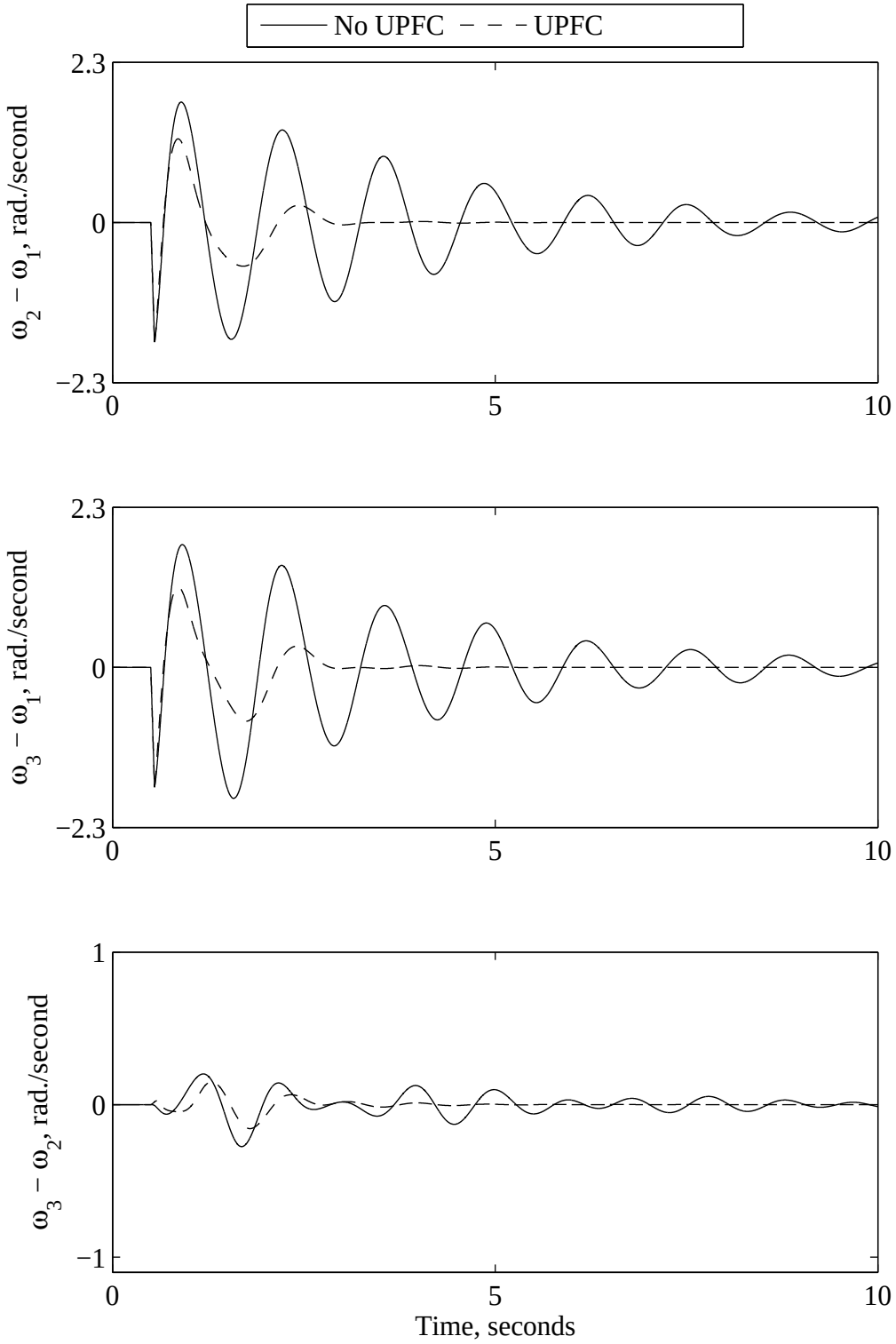

Figure 3.8 Relative generator speeds due to a 3-cycle three-phase fault at bus 1 (a UPFC is installed at LOC1).

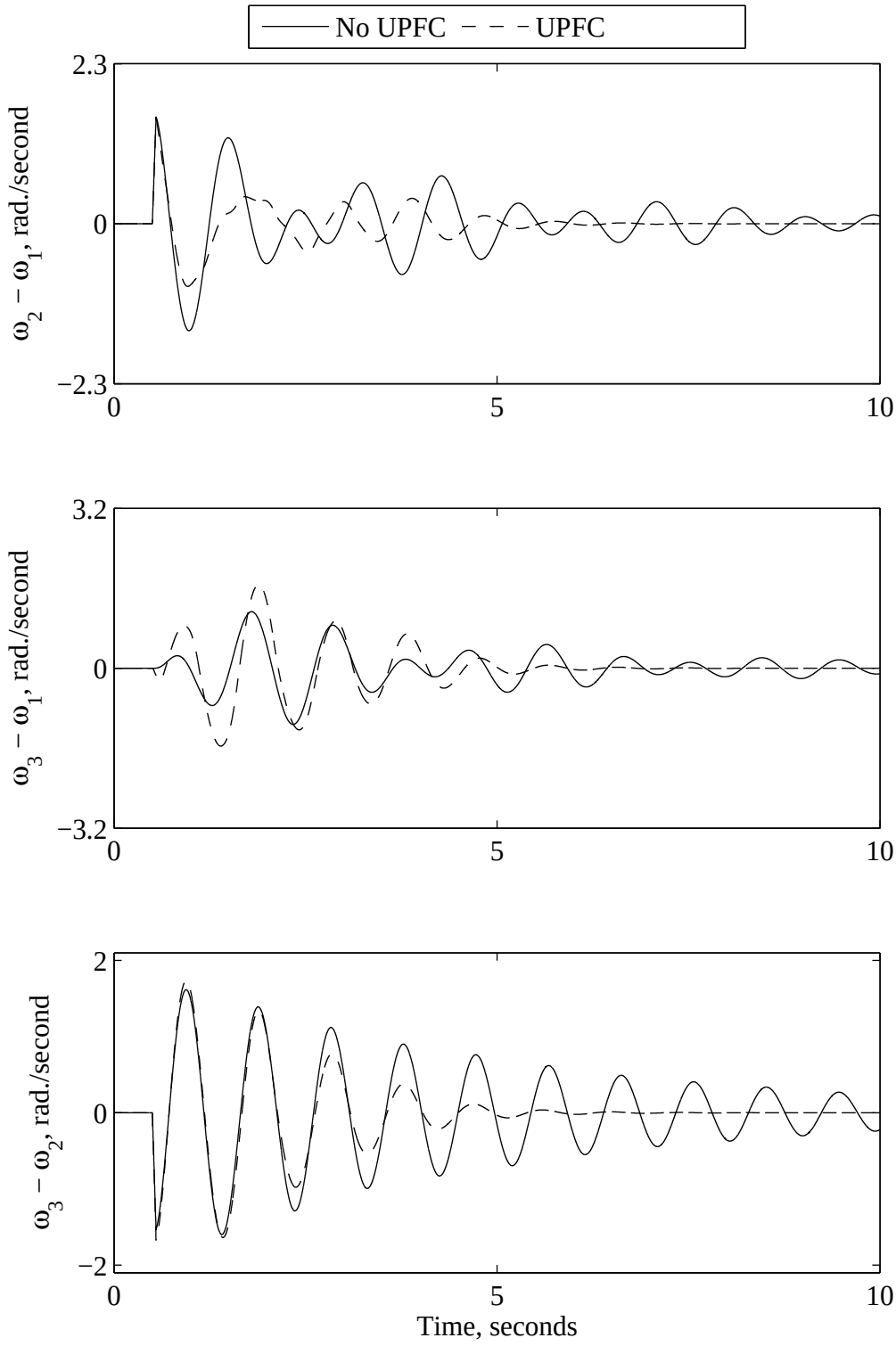

Figure 3.9 Relative generator speeds due to a 3-cycle three-phase fault at bus 2 (a UPFC is installed at LOC1).

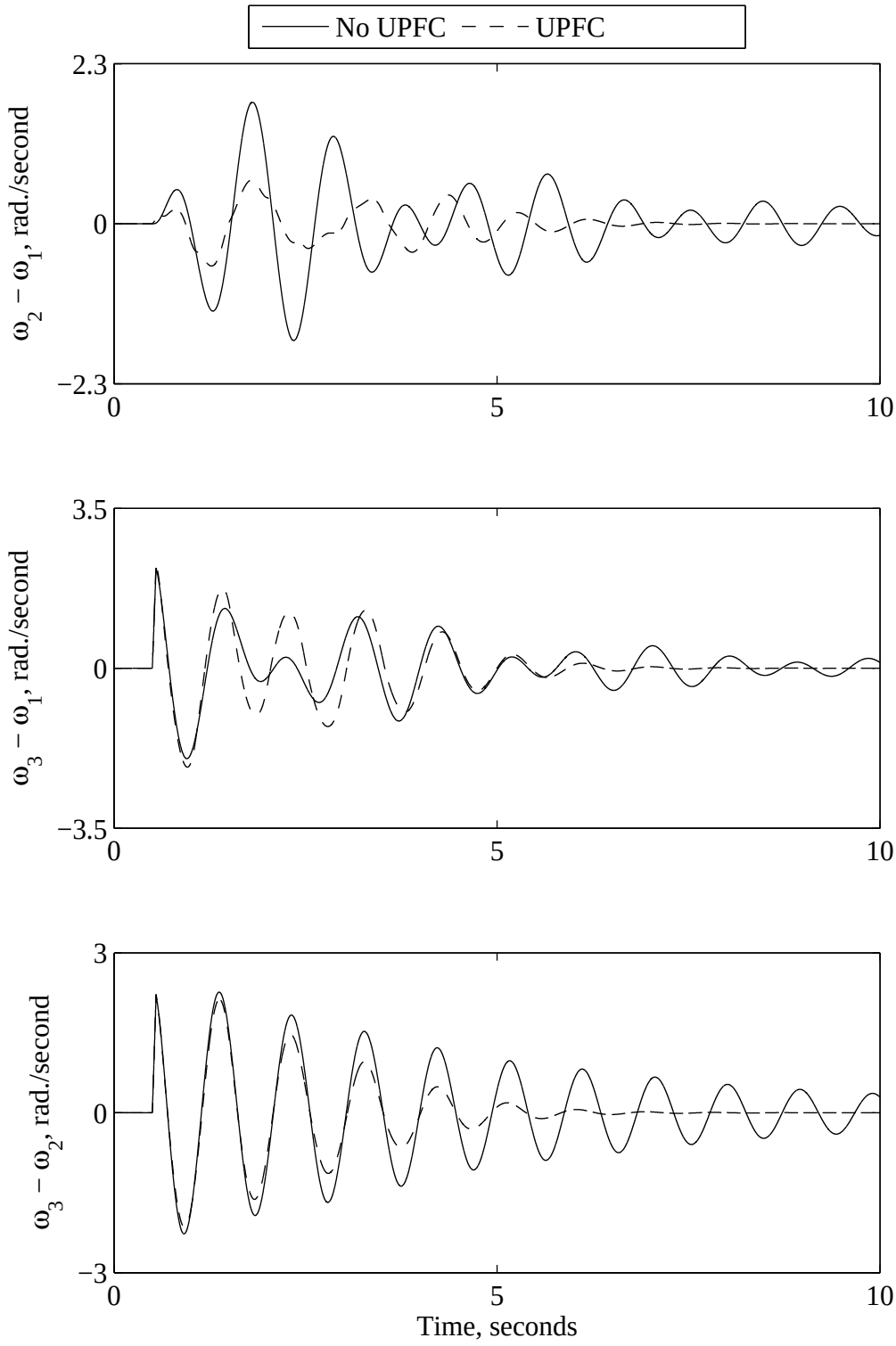

Figure 3.10 Relative generator speeds due to a 3-cycle three-phase fault at bus 3 (a UPFC is installed at LOC1).

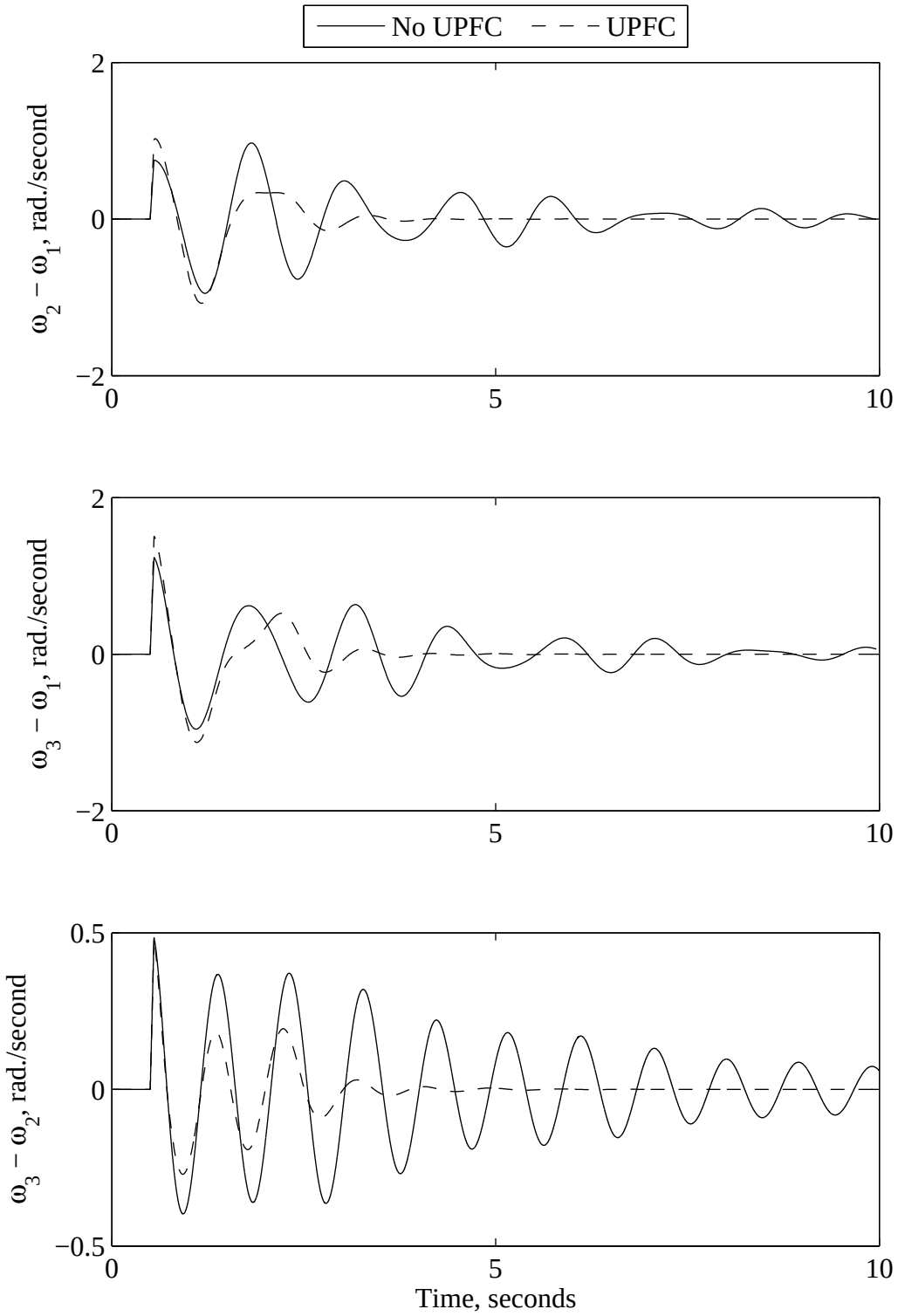

Figure 3.11 Relative generator speeds due to a 3-cycle three-phase fault at bus 4 (a UPFC is installed at LOC1).

Figures 3.9 and 3.10, shows that the UPFC controller is more effective in damping the system oscillations in the case of a three-phase fault at bus 1. This is due to the closeness of bus 1 to the UPFC location.

Figures 3.12 and 3.13 show the injected voltages of the UPFC due to the three-phase fault at bus 1. The upper and lower limits of the injected shunt voltage are 1.1 p.u. and 0.9 p.u. respectively while the series injected voltage is limited to ± 0.1 p.u. Figure 3.14 shows the variation of the dc-link capacitor voltage due to the same disturbance.

3.5.2. Effect of the UPFC Location

It has been reported that FACTS devices derive maximum benefit from their stabilized voltage support when sited at the mid-point of the transmission line [72]. In some situations, however, it might be desirable to install the FACTS device at one end of the transmission line if maintaining the voltage level at that end around its nominal value is essential [73]. In this section, the effect of the location of the UPFC controller on the damping of the interarea oscillations is examined. Beside the middle of tie-line L_1 (LOC1), which has been investigated in the previous section, three other locations (LOC2, LOC3 and LOC4) are selected as shown in Figure 3.15.

Figures 3.16 to 3.24 illustrate the transient time responses of the relative generator speeds due to 3-cycle three-phase faults at buses 1, 2 and 3 with a UPFC installed respectively at LOC2, LOC3 and LOC4. Examining these figures along with Figures 3.8 to 3.11 reveals that the location of the UPFC affects its performance. In general, the UPFC controller is more effective in damping interarea oscillations in the case of a fault occurring, relatively, close to it. This is demonstrated in Figures 3.8, 3.17 and 3.21. Moreover, Figures 3.22 to 3.24 show that the fault location does not significantly affect the damping performance of the UPFC controller if it is installed at LOC4. This is due to the central position of bus 4 in the power system. Furthermore, comparing Figures 3.8 to 3.11 with Figures 3.16 to 3.24 shows that, a UPFC installed at (LOC1 or LOC3) provides the most damping to the interarea oscillations. This can be explained as tie-lines L_1 and L_3 transfer more power than tie-line L_2. It can be concluded, therefore, that the best location for the UPFC controller is at the middle of the tie-line that transfers the highest amount of power.

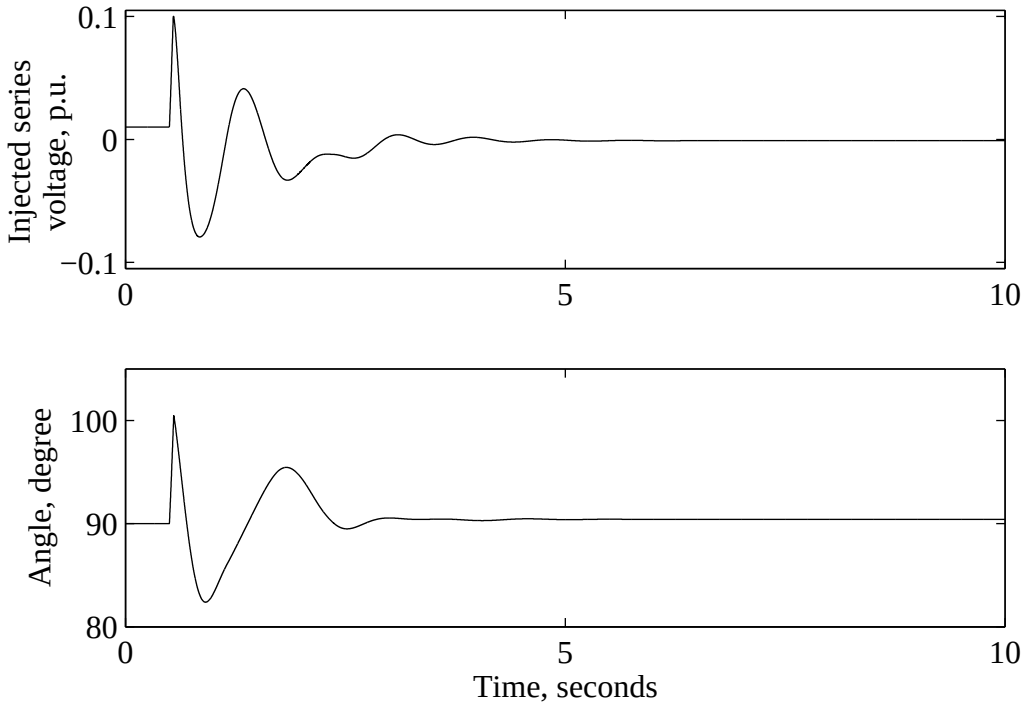

Figure 3.12 UPFC injected series voltage due to a 3-cycle three-phase fault at bus 1 (a UPFC is installed at LOC1).

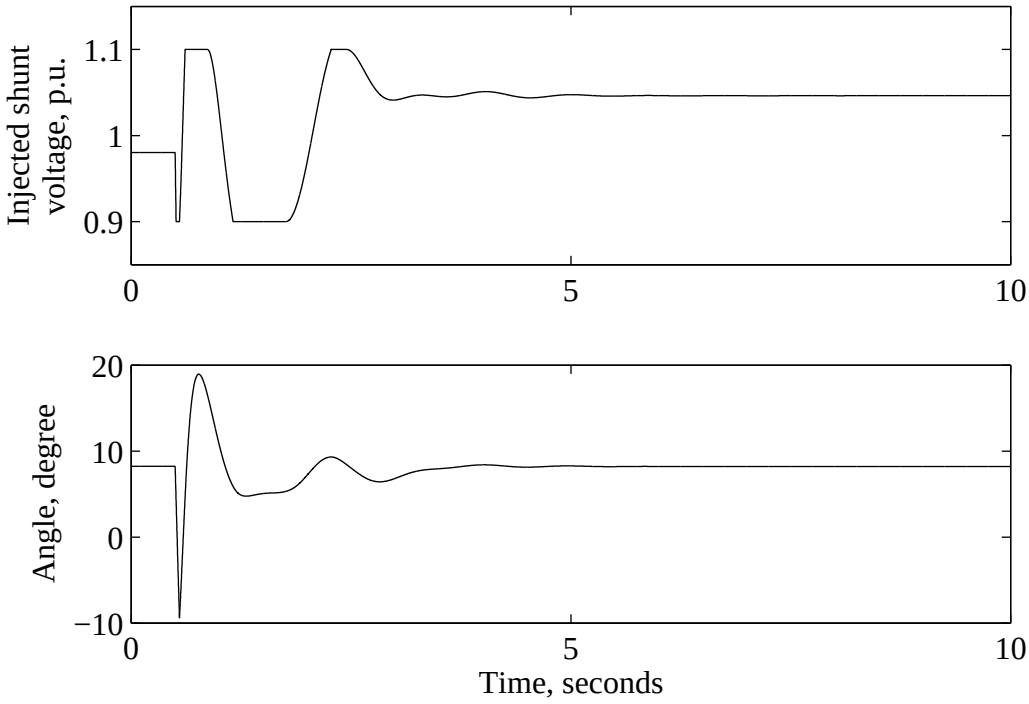

Figure 3.13 UPFC injected shunt voltage due to a 3-cycle three-phase fault at bus 1 (a UPFC is installed at LOC1).

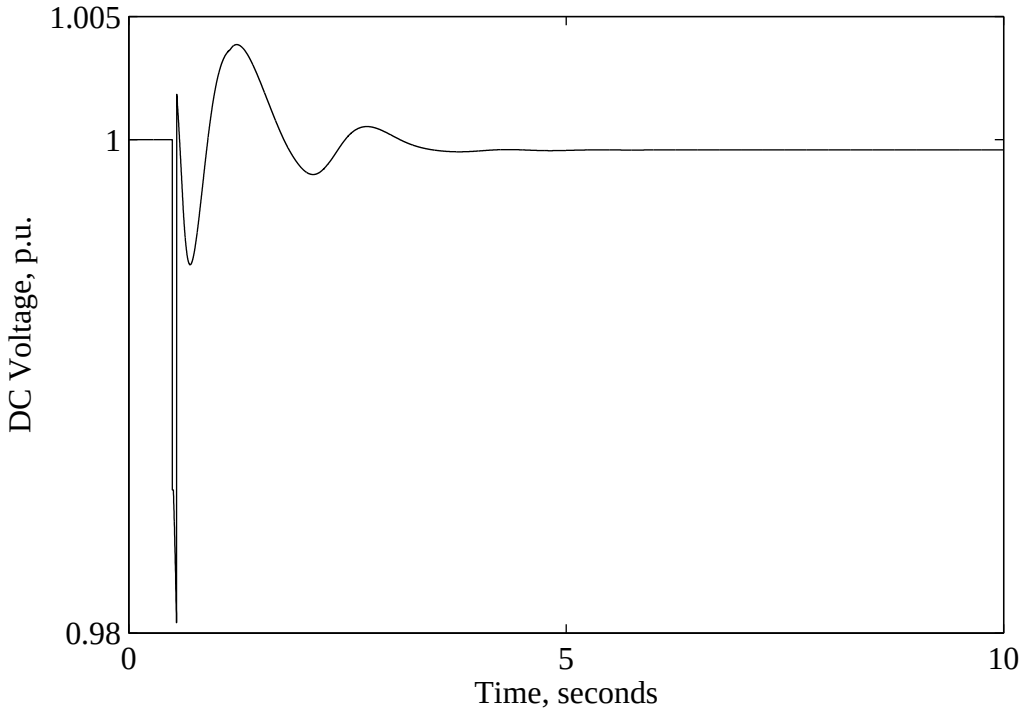

Figure 3.14 UPFC dc-link capacitor voltage due to a 3-cycle three-phase fault at bus 1 (a UPFC is installed at LOC1).

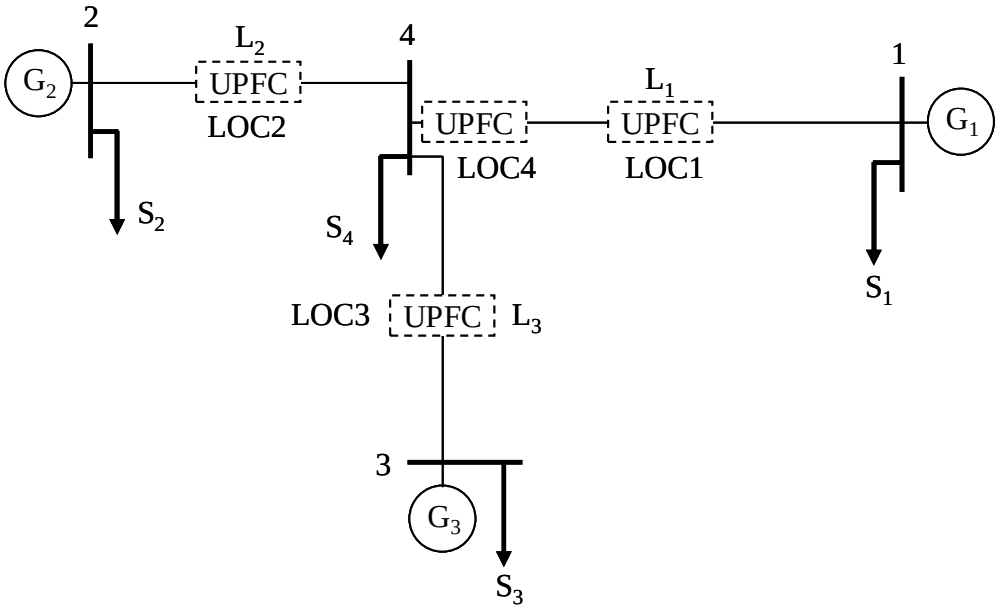

Figure 3.15 UPFC studied locations.

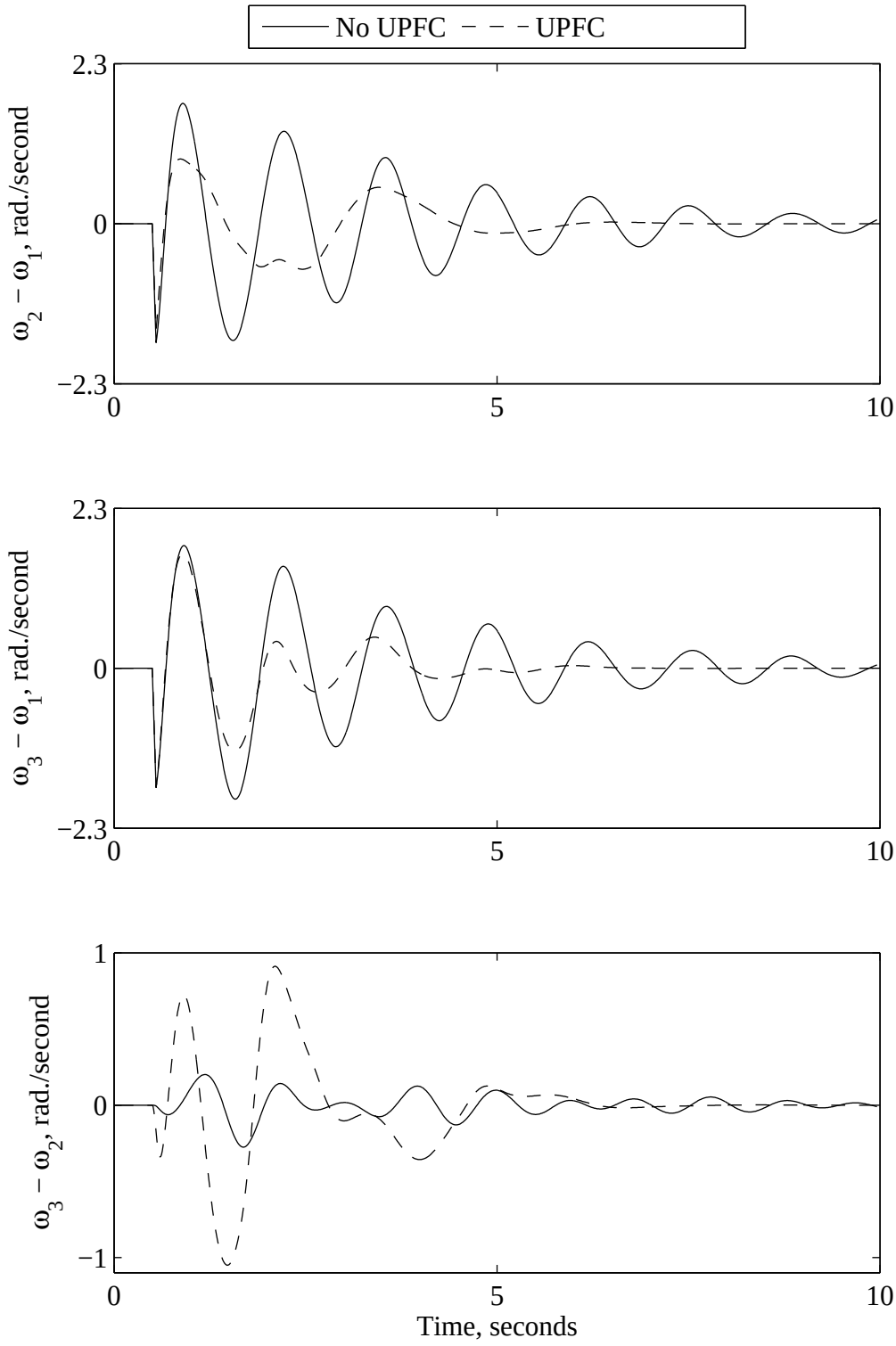

Figure 3.16 Relative generator speeds due to a 3-cycle three-phase fault at bus 1 (a UPFC is installed at LOC2).

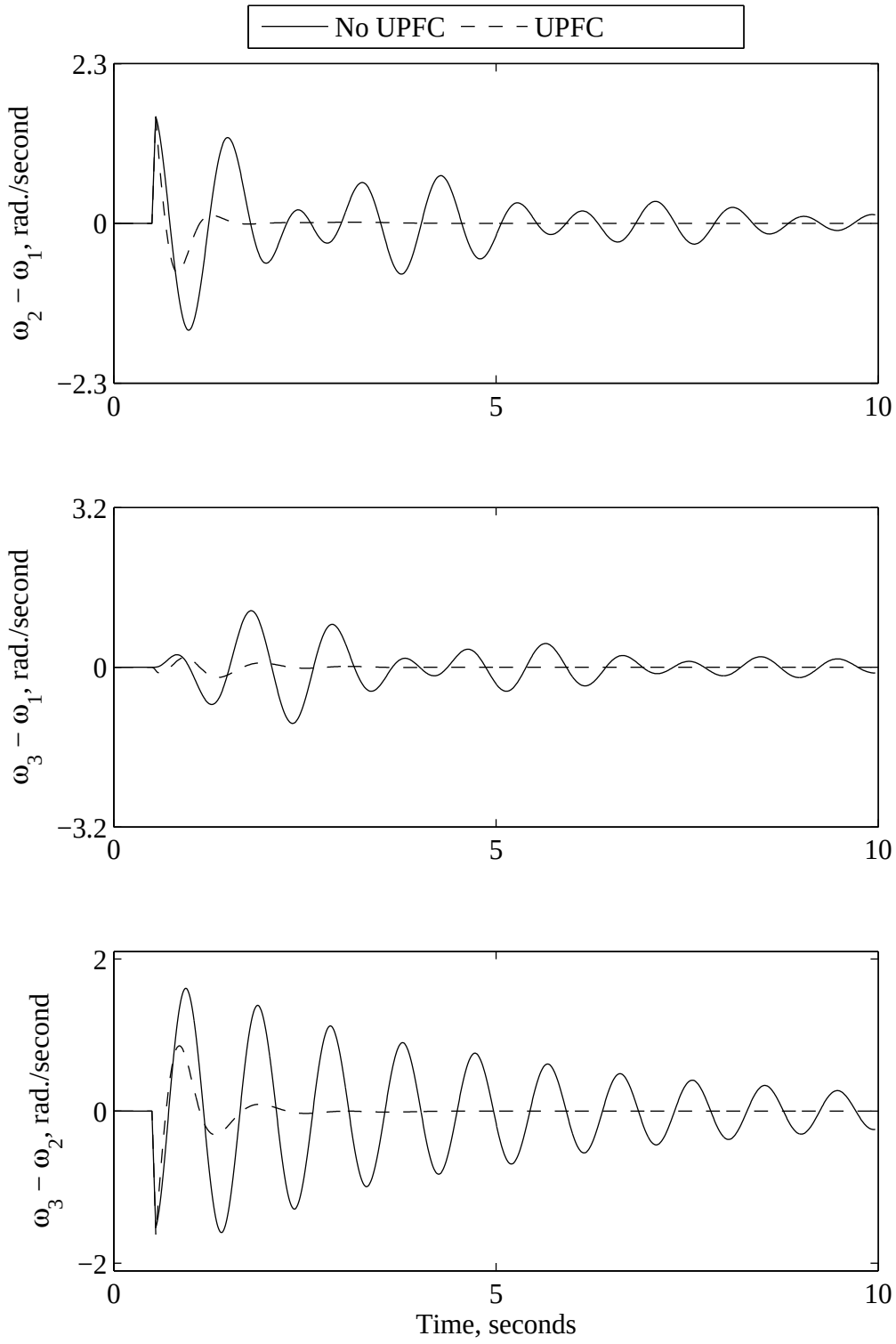

Figure 3.17 Relative generator speeds due to a 3-cycle three-phase fault at bus 2 (a UPFC is installed at LOC2).

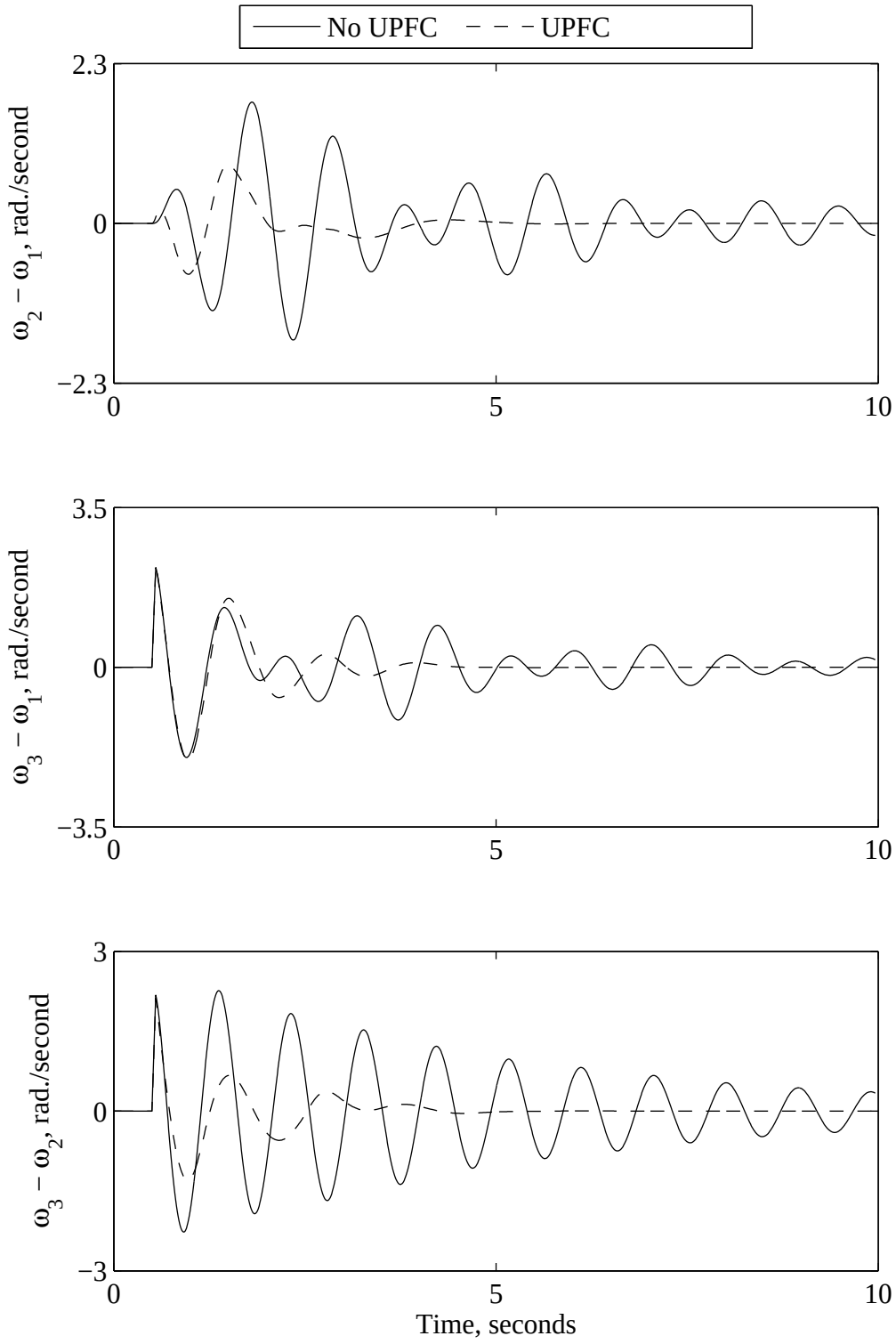

Figure 3.18 Relative generator speeds due to a 3-cycle three-phase fault at bus 3 (a UPFC is installed at LOC2).

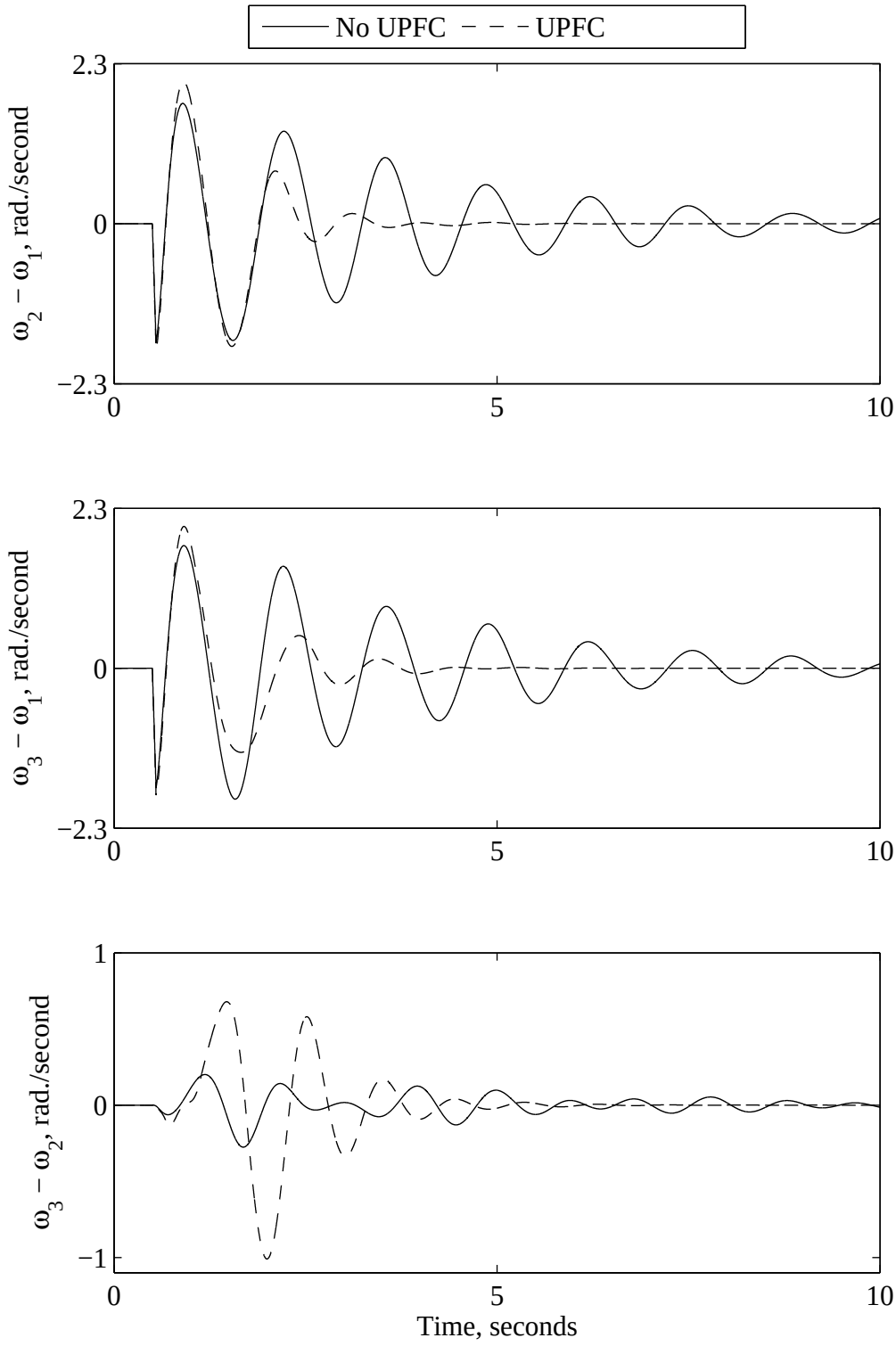

Figure 3.19 Relative generator speeds due to a 3-cycle three-phase fault at bus 1 (a UPFC is installed at LOC3).

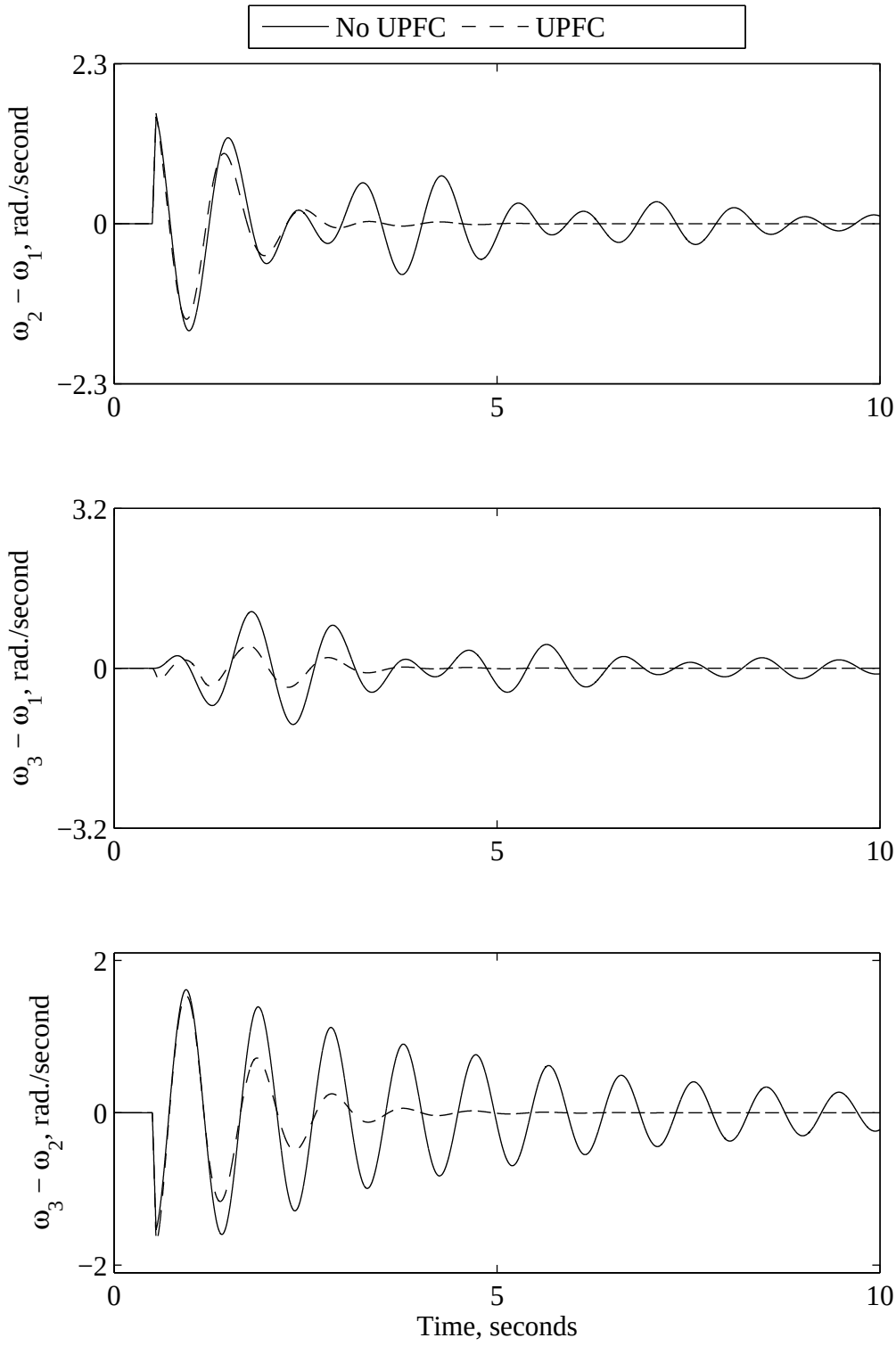

Figure 3.20 Relative generator speeds due to a 3-cycle three-phase fault at bus 2 (a UPFC is installed at LOC3).

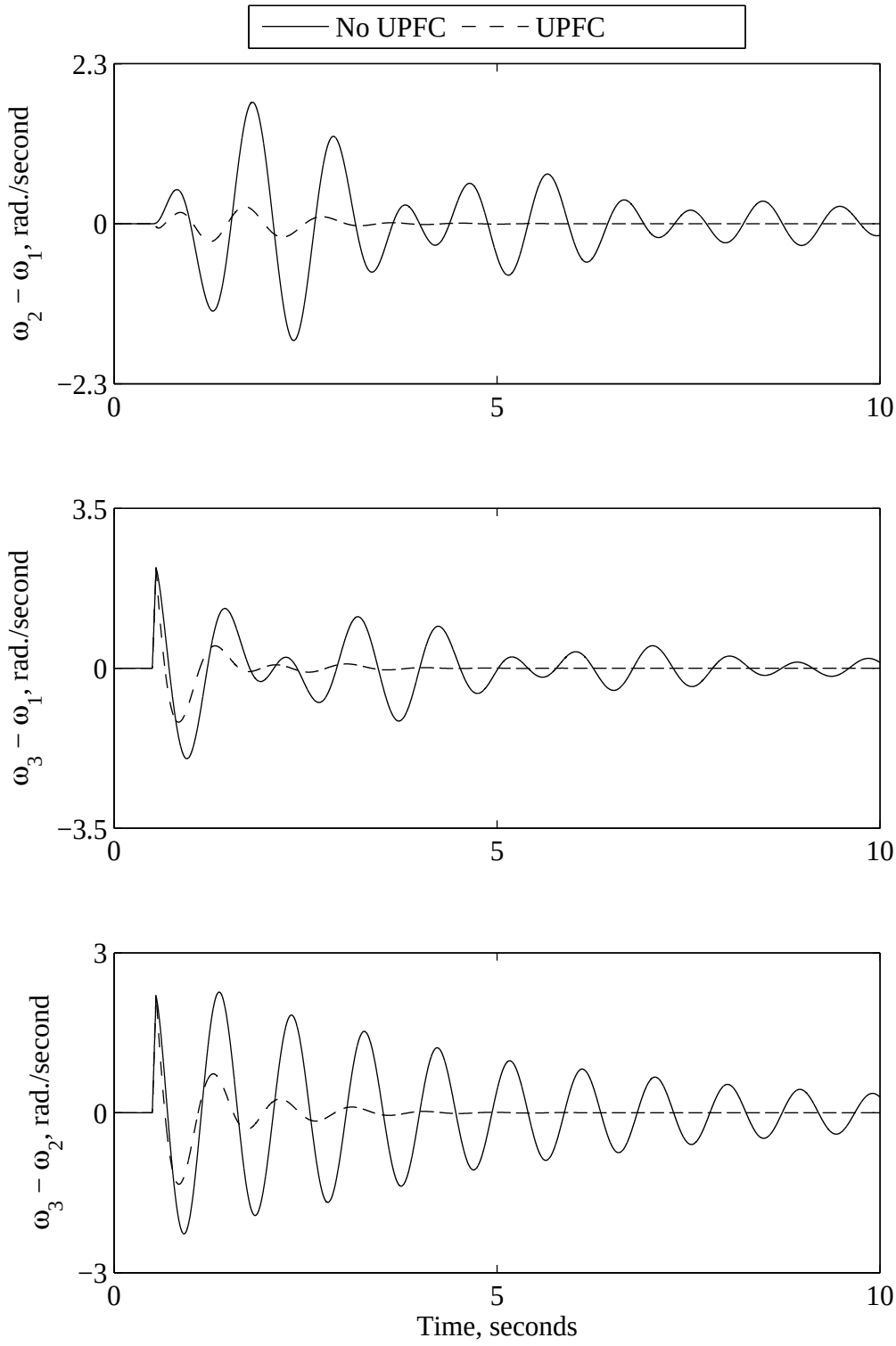

Figure 3.21 Relative generator speeds due to a 3-cycle three-phase fault at bus 3 (a UPFC is installed at LOC3).

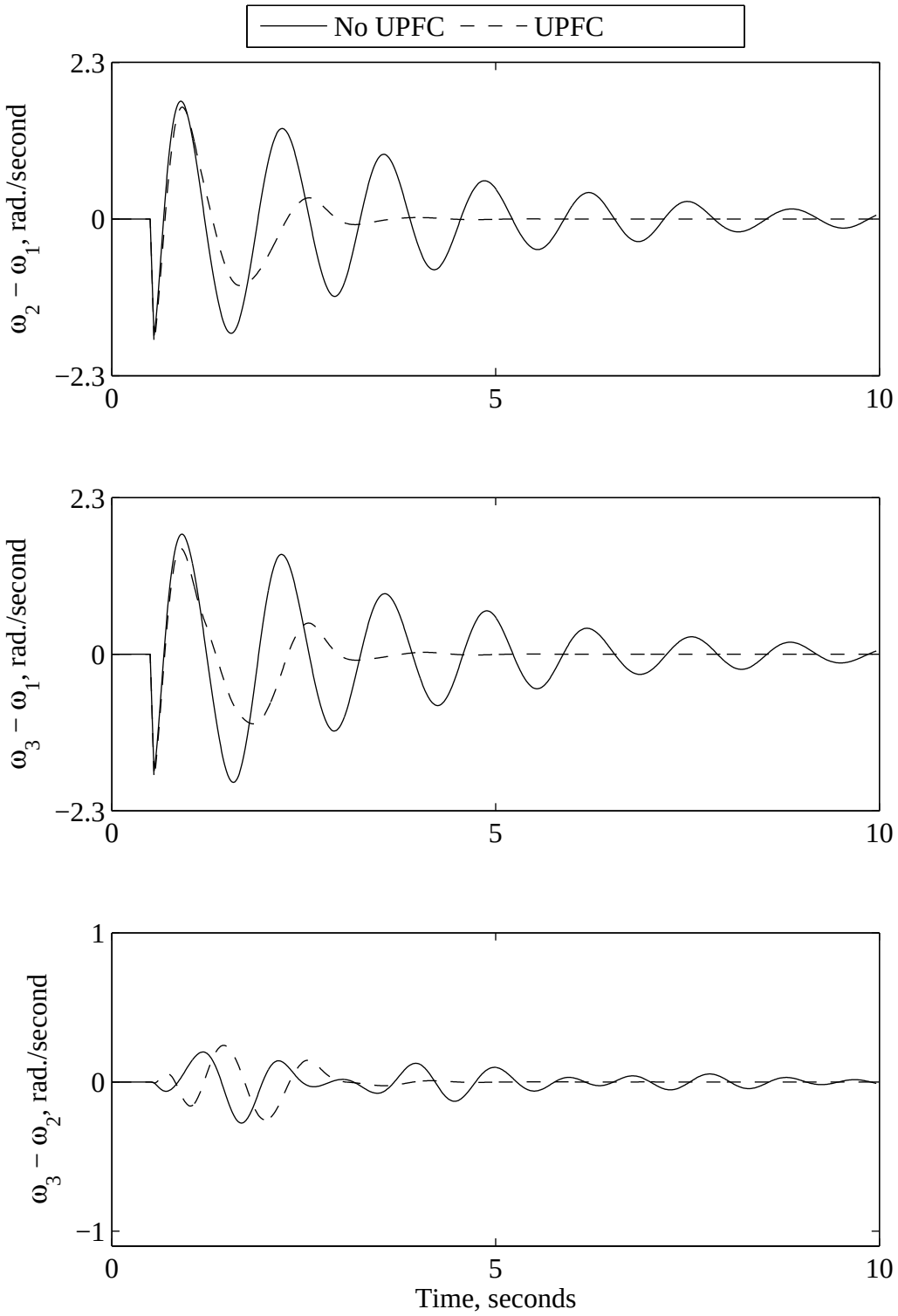

Figure 3.22 Relative generator speeds due to a 3-cycle three-phase fault at bus 1 (a UPFC is installed at LOC4).

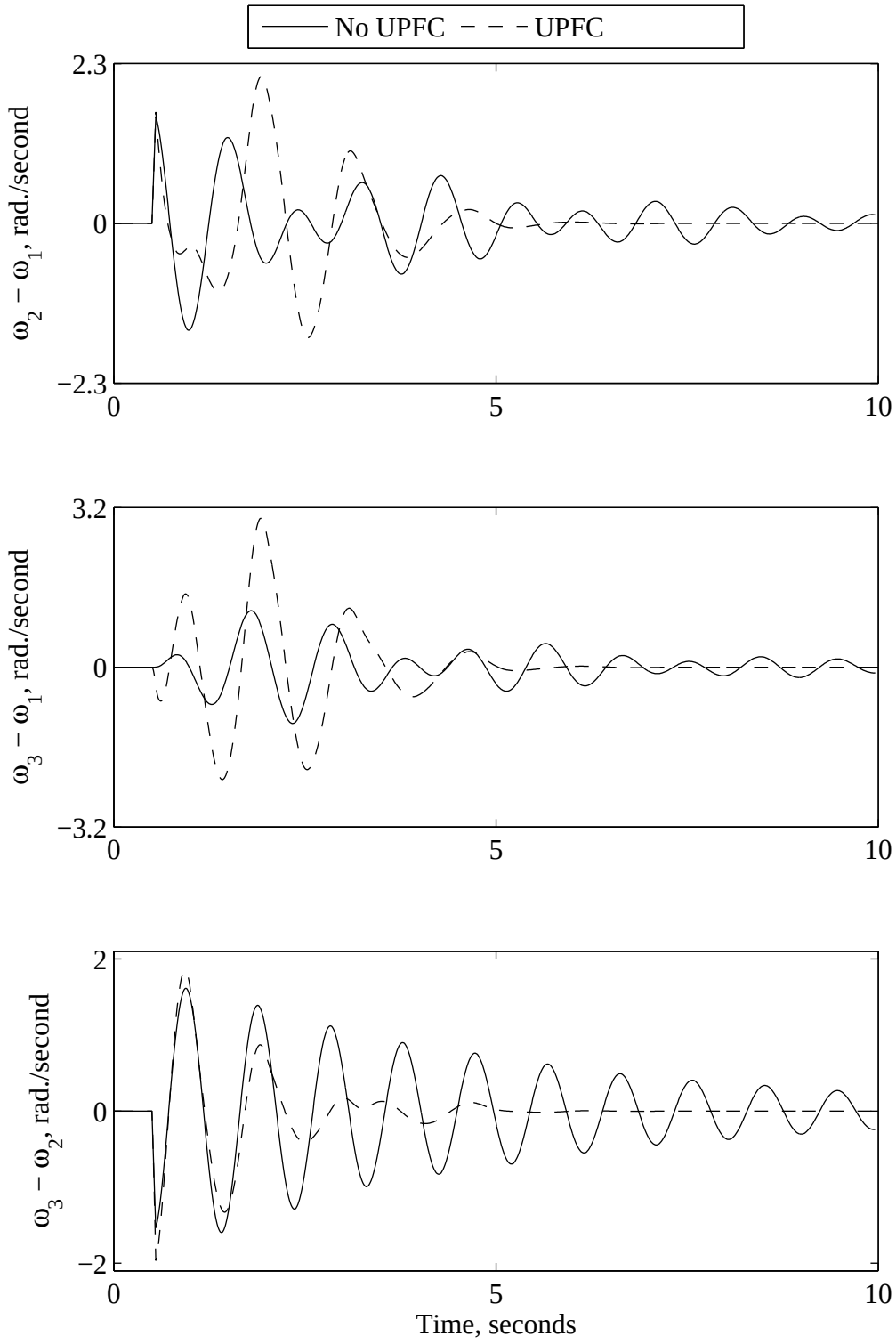

Figure 3.23 Relative generator speeds due to a 3-cycle three-phase fault at bus 2 (a UPFC is installed at LOC4).

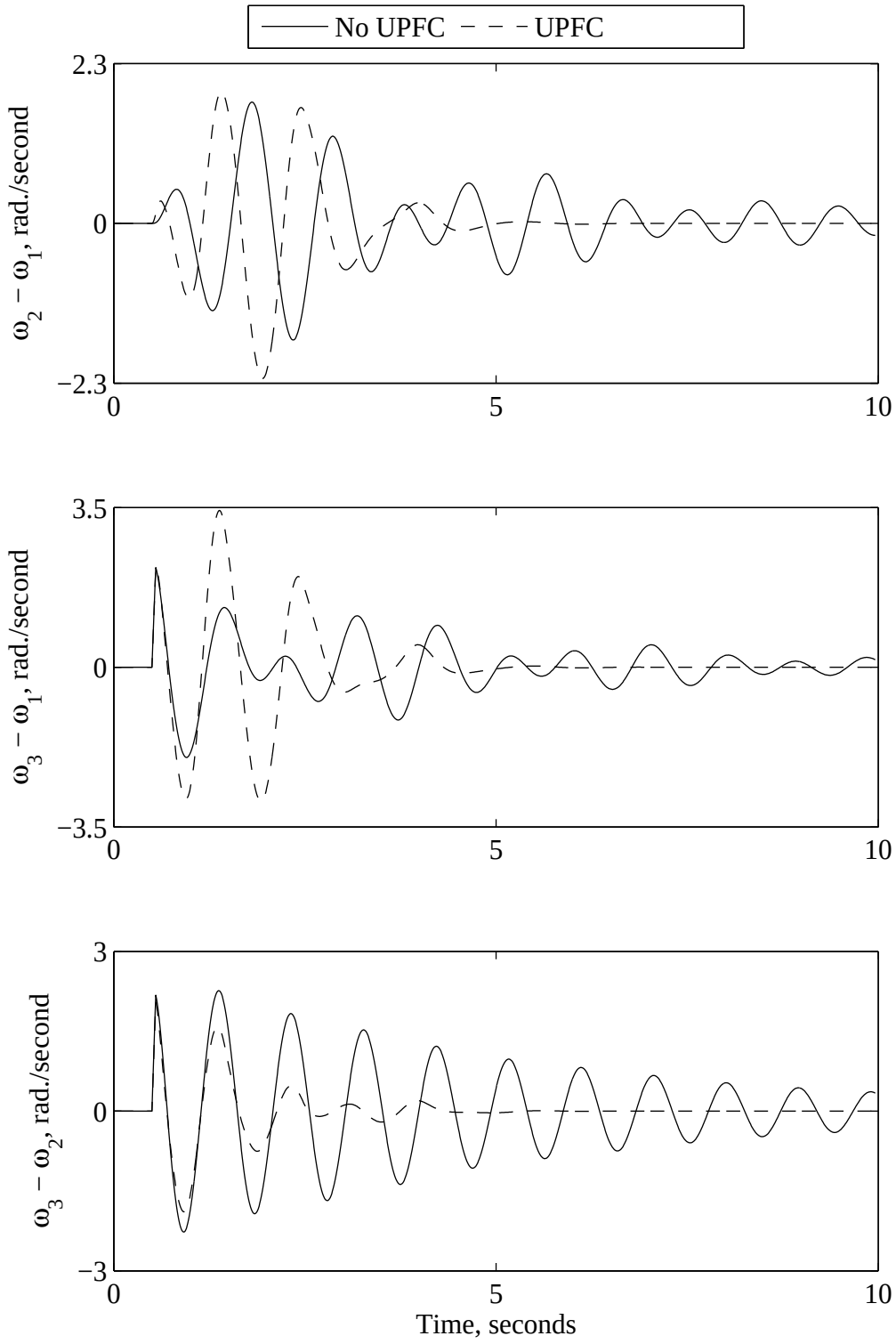

Figure 3.24 Relative generator speeds due to a 3-cycle three-phase fault at bus 3 (a UPFC is installed at LOC4).

It is worth noting here that the response of the relative generator speed ($\omega_3 - \omega_2$) in Figures 3.16 and 3.19 might be misinterpreted that the UPFC is not effective in damping these oscillations. This can be, however, clarified with the help of Figures 3.25 and 3.26 which show the speed of generators 2 and 3 due to the same disturbances considered in Figures 3.16 and 3.19. As it can be seen from Figures 3.25 and 3.26, in the case of no UPFC installed in the system, the generator speeds ω_2 and ω_3 are almost in phase and exhibit poor damping. This indicates that areas 2 and 3 oscillate with respect to area 1. It can also be seen from the same figures that the UPFC effectively damps the generator speeds ω_2 and ω_3.

3.5.3. Effect of Adding another UPFC

Multiple FACTS controllers, if properly designed, will enhance the damping of the system oscillations. This section investigates the effect on the damping of interarea oscillations of installing two UPFCs in the system under study. Based on the simulation results of the previous section, the two UPFCs are installed at LOC1 and LOC3. The controller design in this case is based on a linearized model of a power system incorporating two UPFCs. Such a design eliminates the possible adverse interaction between the two UPFCs. A PI controller is considered again in these investigations. Figures 3.27 to 3.29 illustrate the time responses of the generator relative speeds due to 3-cycle three-phase faults at buses 1, 2 and 3 with two UPFCs installed at LOC1 and LOC3. As it can be seen from these figures, damping of the system oscillations is slightly improved compared to the case when a single UPFC is installed in the system (Figure 3.8). This observation clearly concludes that, for the system under investigation, a single UPFC is sufficient to effectively damp interarea oscillations.

3.6. UPFC Performance during Other Disturbances

Although three-phase faults are the most severe disturbances in a power system, the probabilities of their occurrence are relatively low (3% to 5%) [74]. In this section, the performance of the designed UPFC controllers is examined due to several large and small system disturbances. In this context, a sudden load decrease of 95% is considered as the simulated large disturbance while a 5% decrease in the input reference mechanical power is considered as the simulated small disturbance. Figures 3.30 and 3.31 show the

power system time response following a 5% sudden decrease in the input reference mechanical power of generator G_1 with the UPFC installed at LOC1 and with two UPFCs installed at LOC1 and LOC3 respectively. It can be seen from these figures that the designed controller for the UPFC is capable of damping small disturbances. It can also be seen from Figures 3.30 and 3.31 that more damping to the interarea oscillations is achieved with two UPFCs.

Figures 3.32 and 3.33 respectively show the system response due to a 95%, 3-cycle sudden decrease in loads S_1 and S_2 with the UPFC installed at LOC1. System responses due to the same disturbance with two UPFCs installed at LOC1 and LOC3 are shown in Figures 3.34 and 3.35. It can be seen from these figures that, the UPFCs exhibit excellent performance in damping the system oscillations.

3.7. Performance of a Simplified Centralized PI UPFC Controller

The designed centralized PI UPFC damps sufficiently the interarea oscillations. However, reducing the number of global signals in such a controller would result in a simple and cost effective one. In this context, investigations have been conducted to examine the effect of using two stabilizing signals on the performance of the designed UPFC controllers. Figure 3.36 shows the transfer function of a simplified centralized PI controller. The variation in only two generator speeds $\Delta\omega_{k1}$ and $\Delta\omega_{k2}$ are selected as stabilizing signals. With this selection, the UPFC controller is a centralized two-input, four-output controller with global signals. Figure 3.37 illustrates the time responses of the relative generator speeds due to a 3-cycle three-phase fault at bus 1 in the case of the UPFC installed at LOC1. It can be seen from this figure that, using only two stabilizing signals effectively damps system oscillations. It can also be seen that the centralized PI UPFC controller performance is better than the simplified centralized PI UPFC controller.

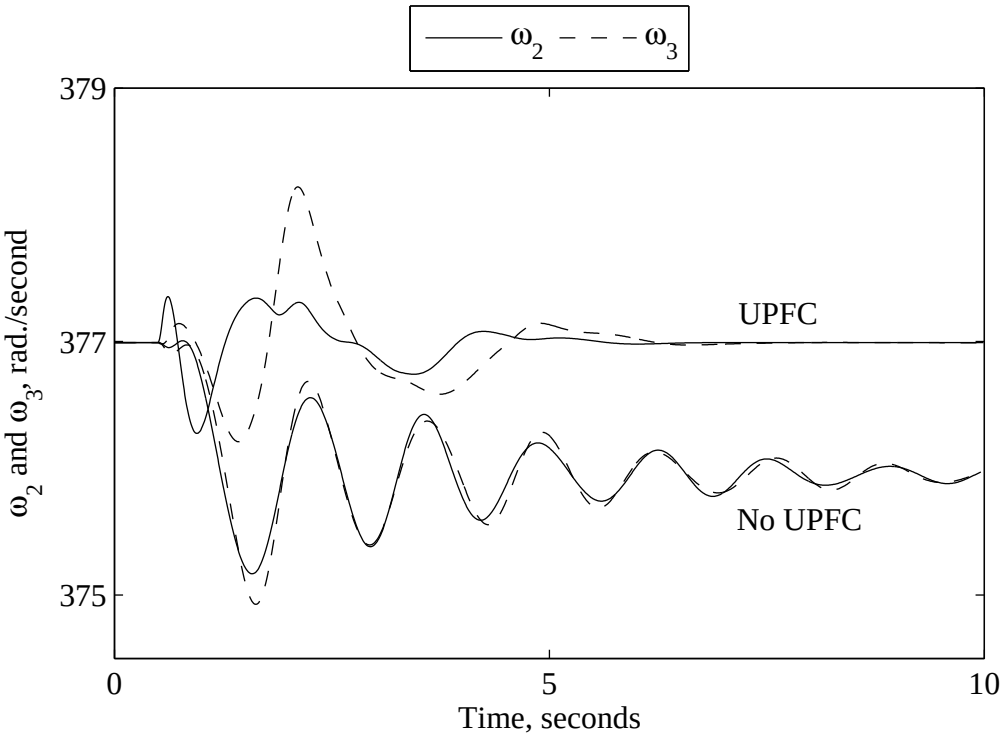

Figure 3.25 Generators 2 and 3 speeds due to a 3-cycle three-phase fault at bus 1 (a UPFC is installed at LOC2).

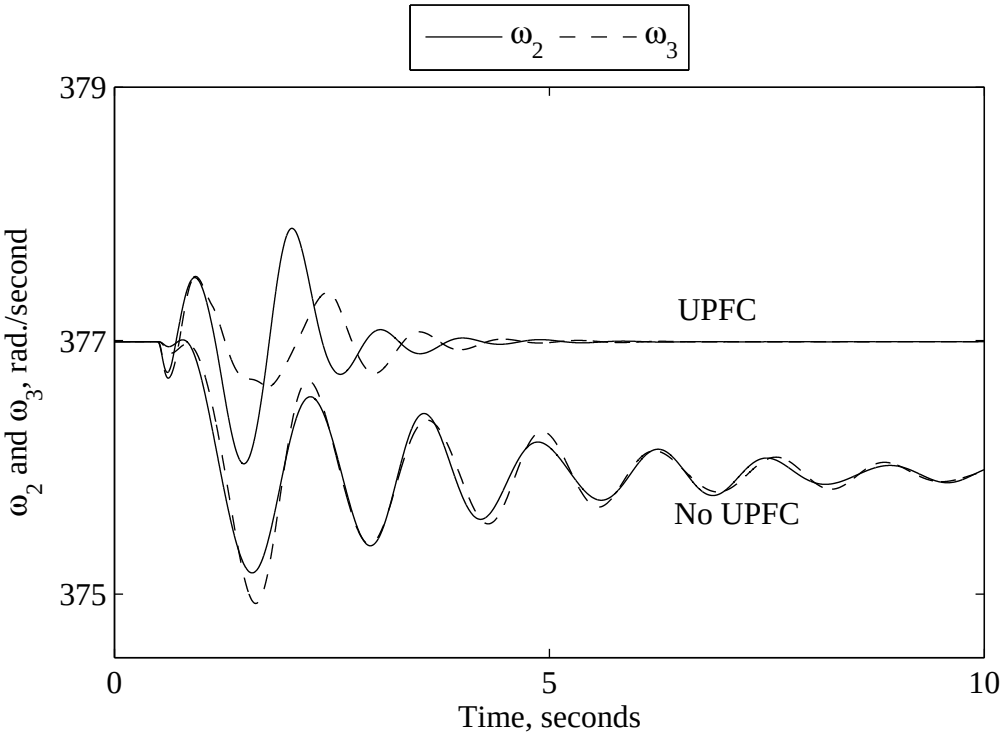

Figure 3.26 Generators 2 and 3 speeds due to a 3-cycle three-phase fault at bus 1 (a UPFC is installed at LOC3).

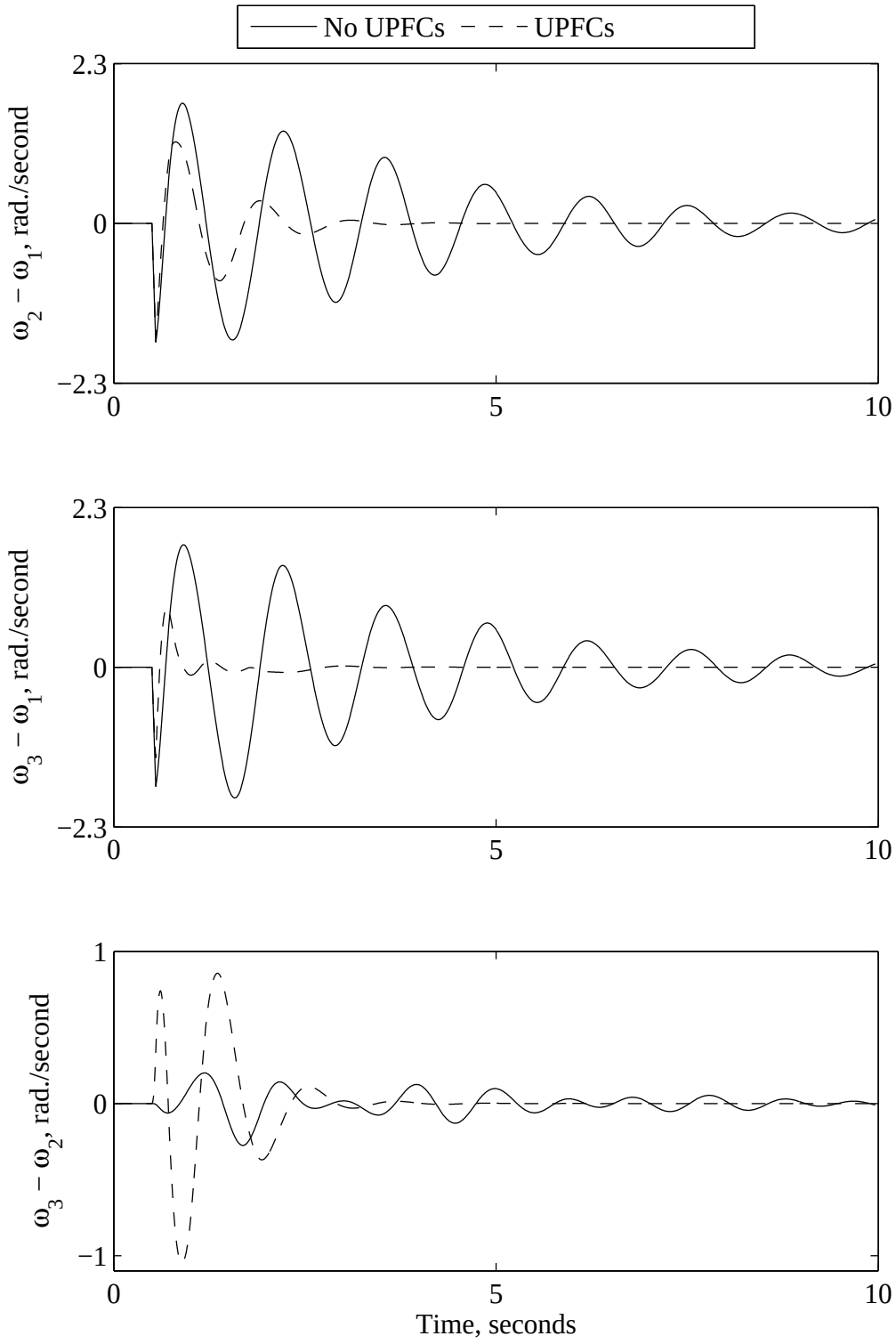

Figure 3.27 Relative generator speeds due to a 3-cycle three-phase fault at bus 1 (two UPFCs are installed at LOC1 and LOC3).

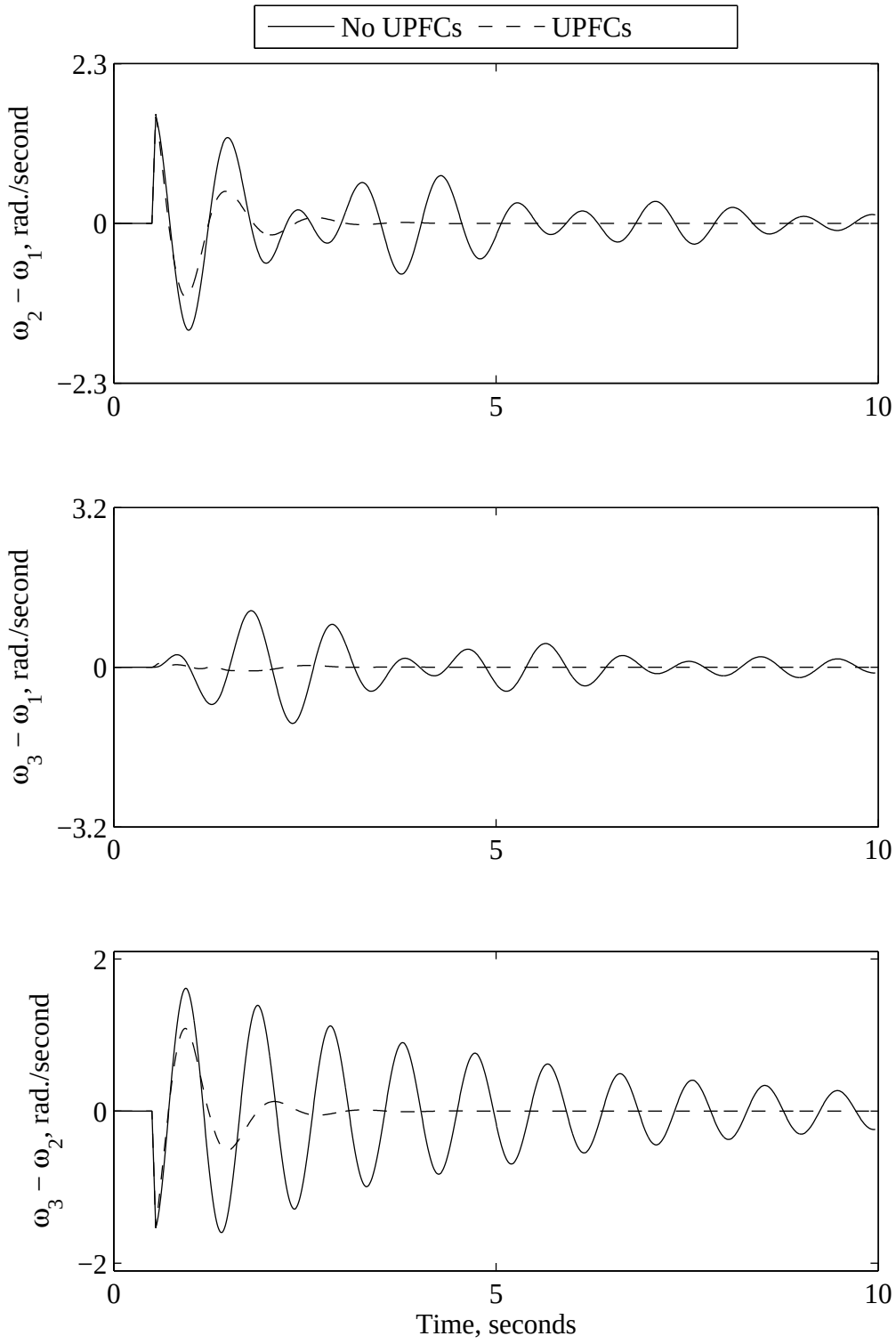

Figure 3.28 Relative generator speeds due to a 3-cycle three-phase fault at bus 2 (two UPFCs are installed at LOC1 and LOC3).

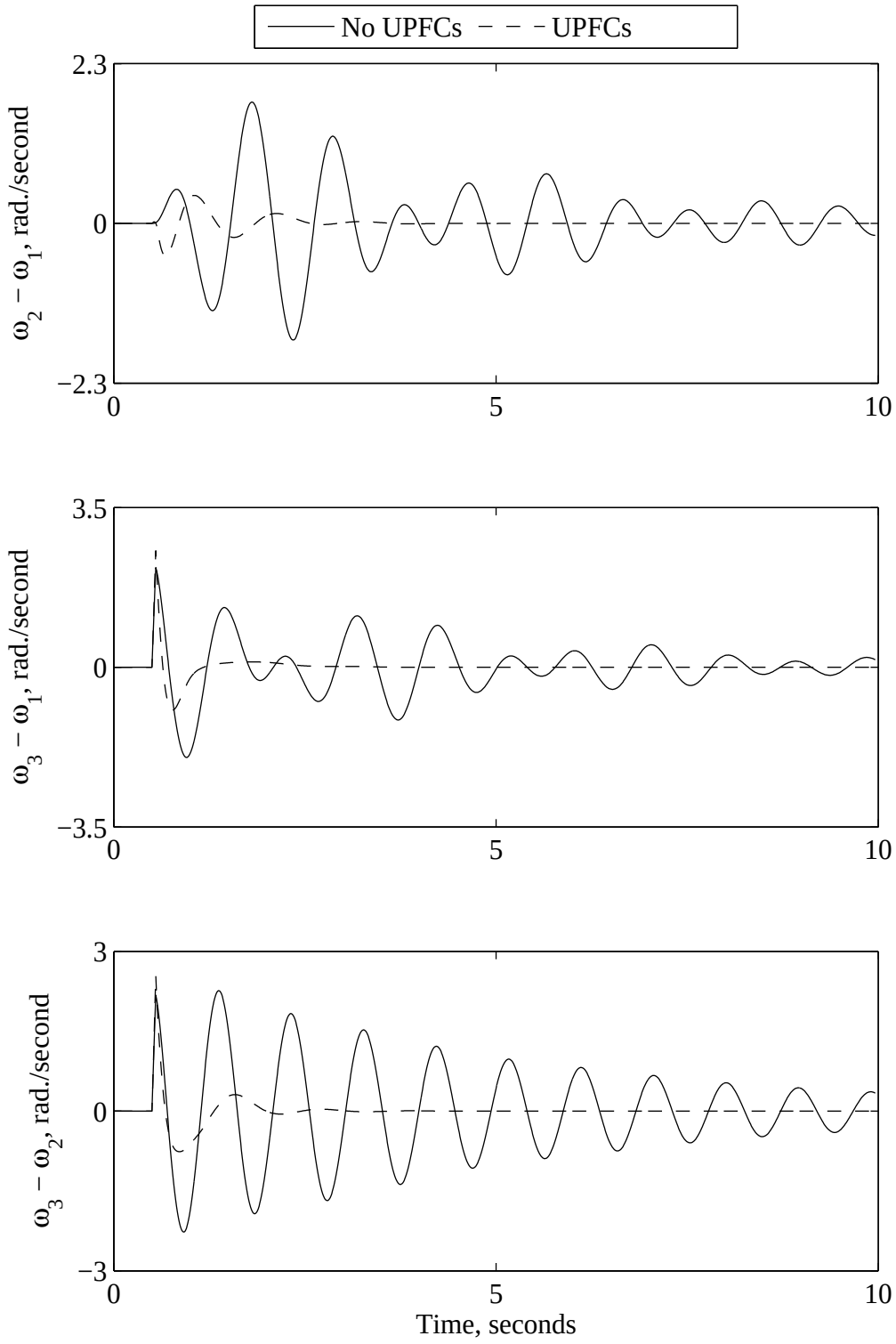

Figure 3.29 Relative generator speeds due to a 3-cycle three-phase fault at bus 3 (two UPFCs are installed at LOC1 and LOC3).

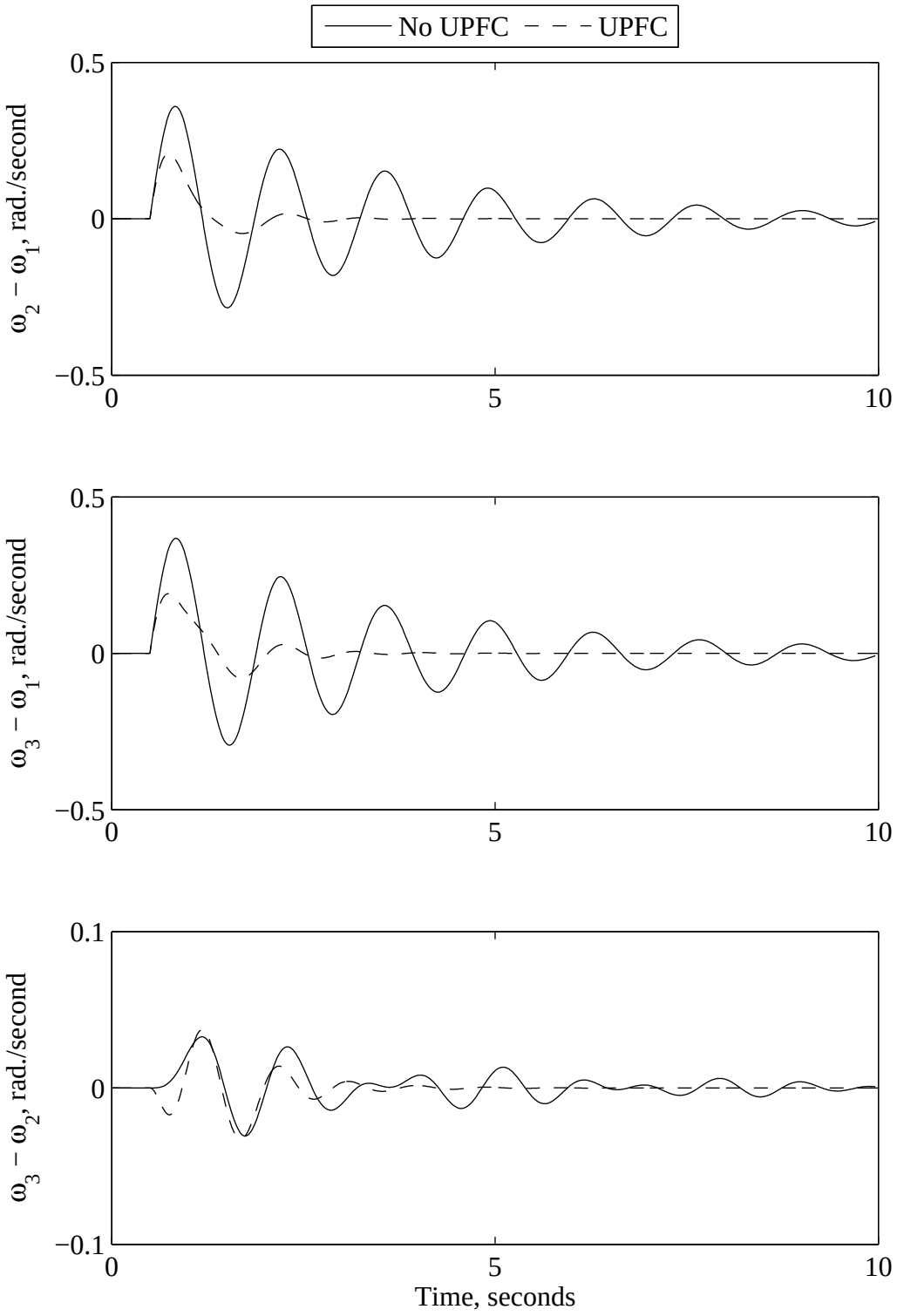

Figure 3.30 Relative generator speed responses for a 5% sudden decrease in the reference power of generator G_1 (a UPFC is installed at LOC1).

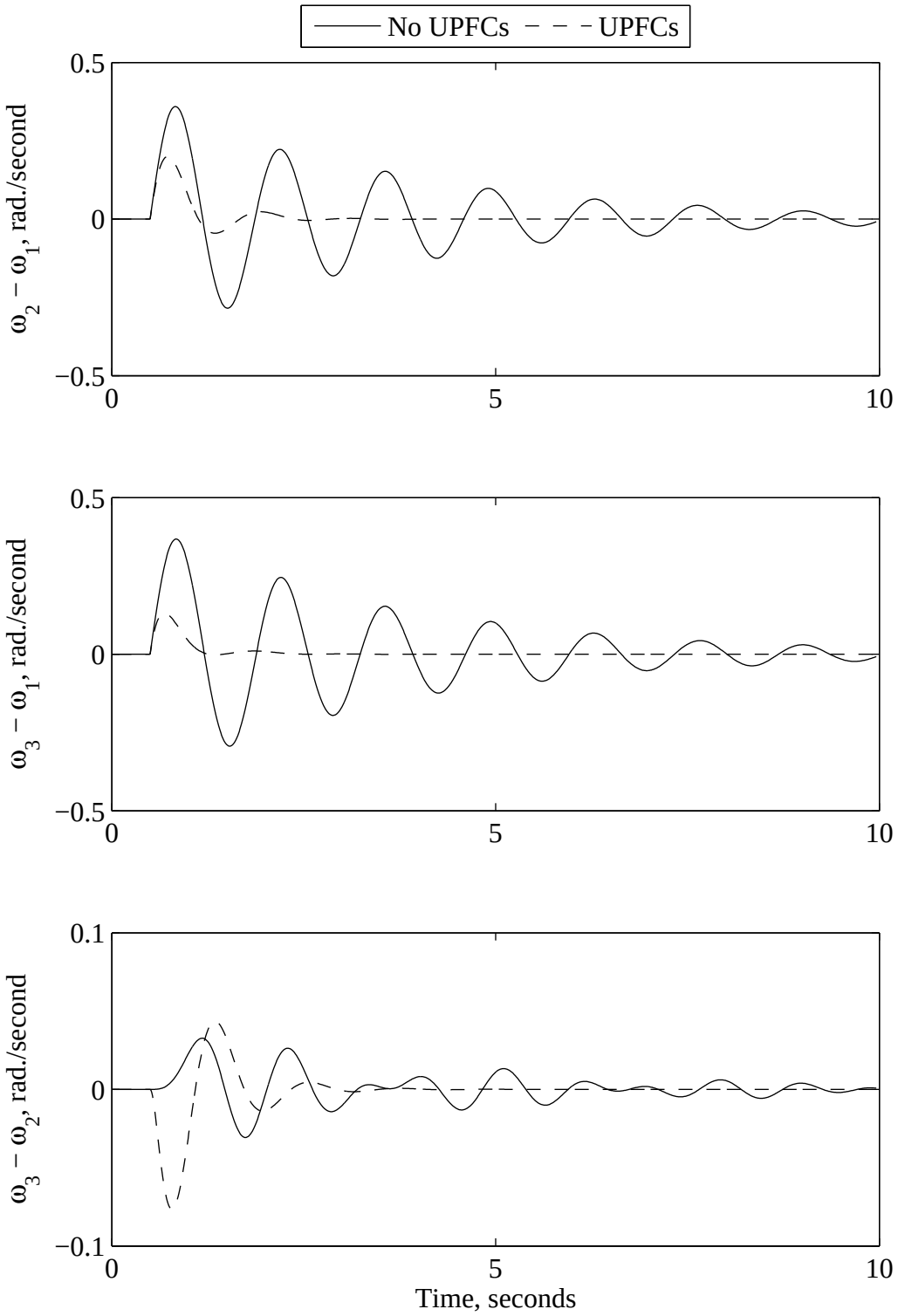

Figure 3.31 Relative generator speed responses for a 5% sudden decrease in the reference power of generator G_1 (two UPFCs are installed at LOC1 and LOC3).

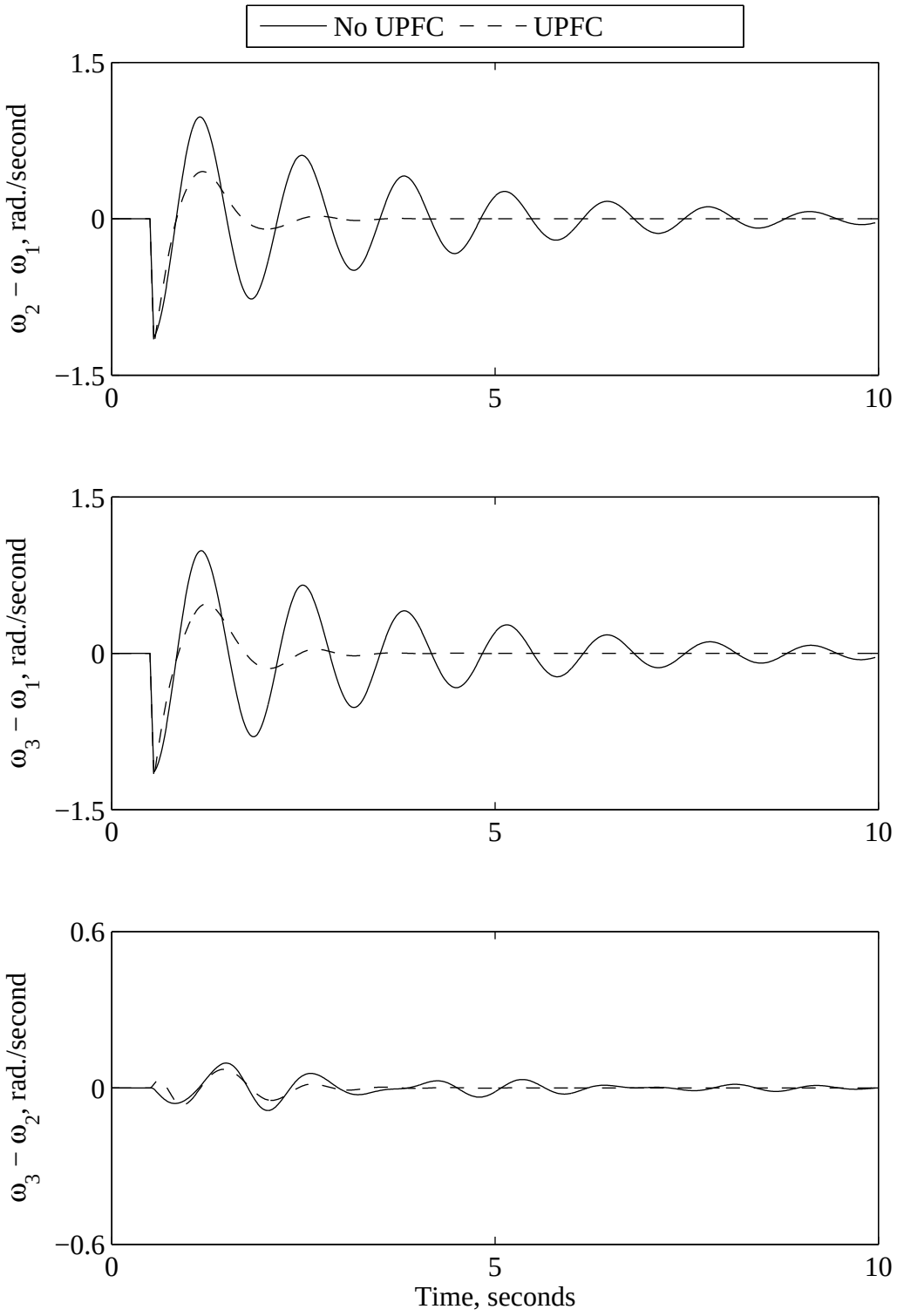

Figure 3.32 Relative generator speed responses due to a 3-cycle 95% sudden load decrease at bus 1 (a UPFC is installed at LOC1).

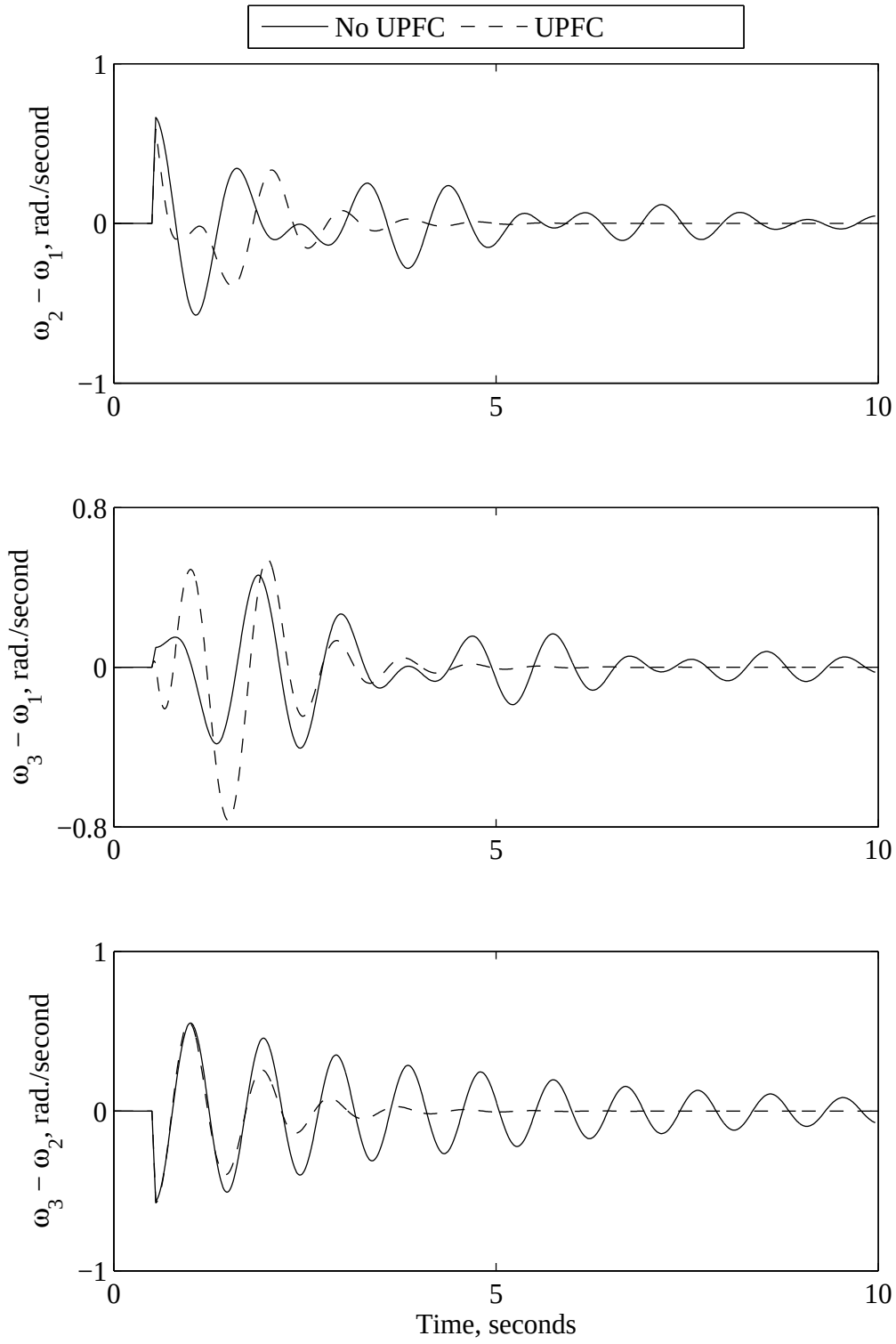

Figure 3.33 Relative generator speed responses due to a 3-cycle 95% sudden load decrease at bus 2 (a UPFC is installed at LOC1).

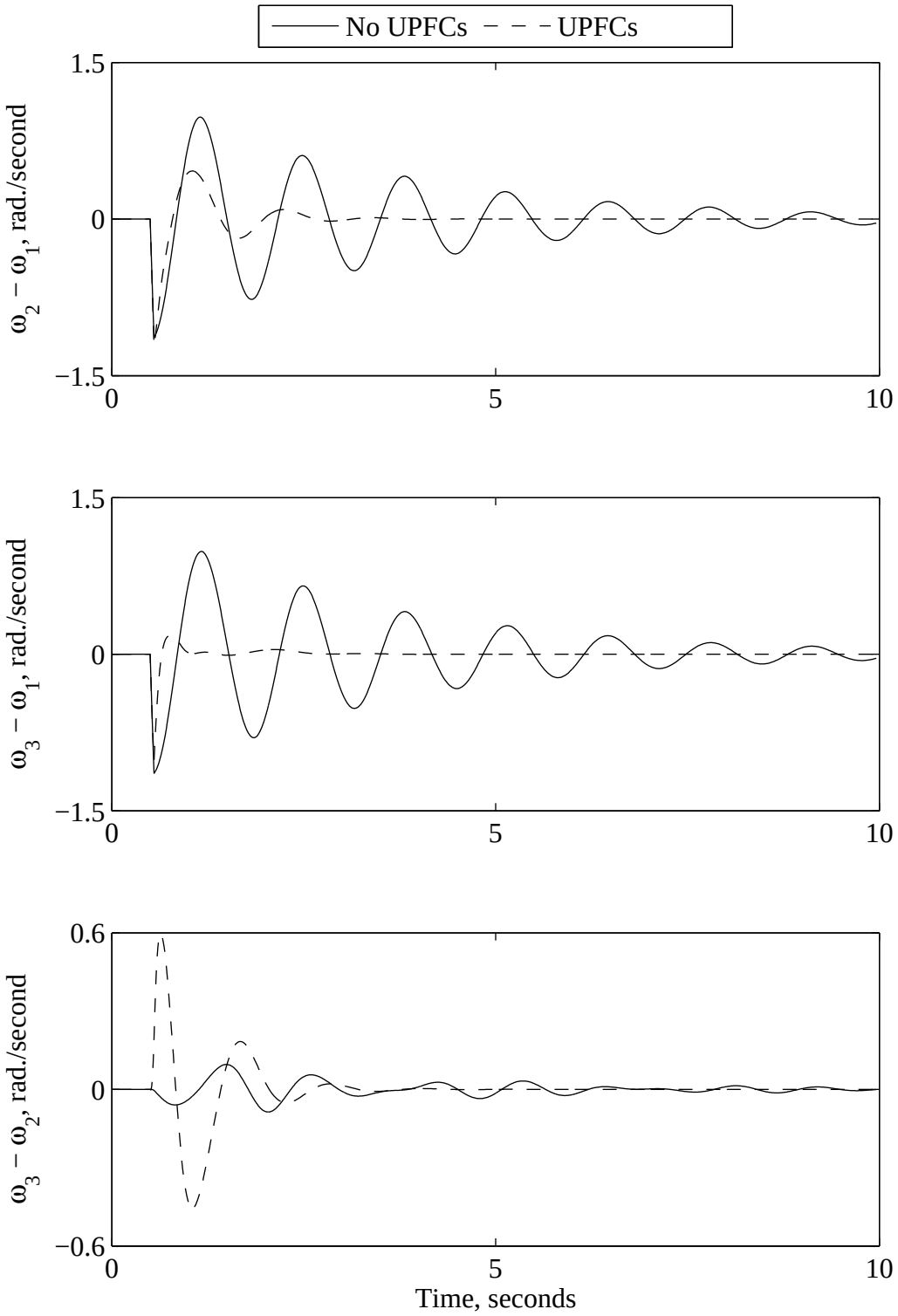

Figure 3.34 Relative generator speed responses due to a 3-cycle 95% sudden load decrease at bus 1 (two UPFCs are installed at LOC1 and LOC3).

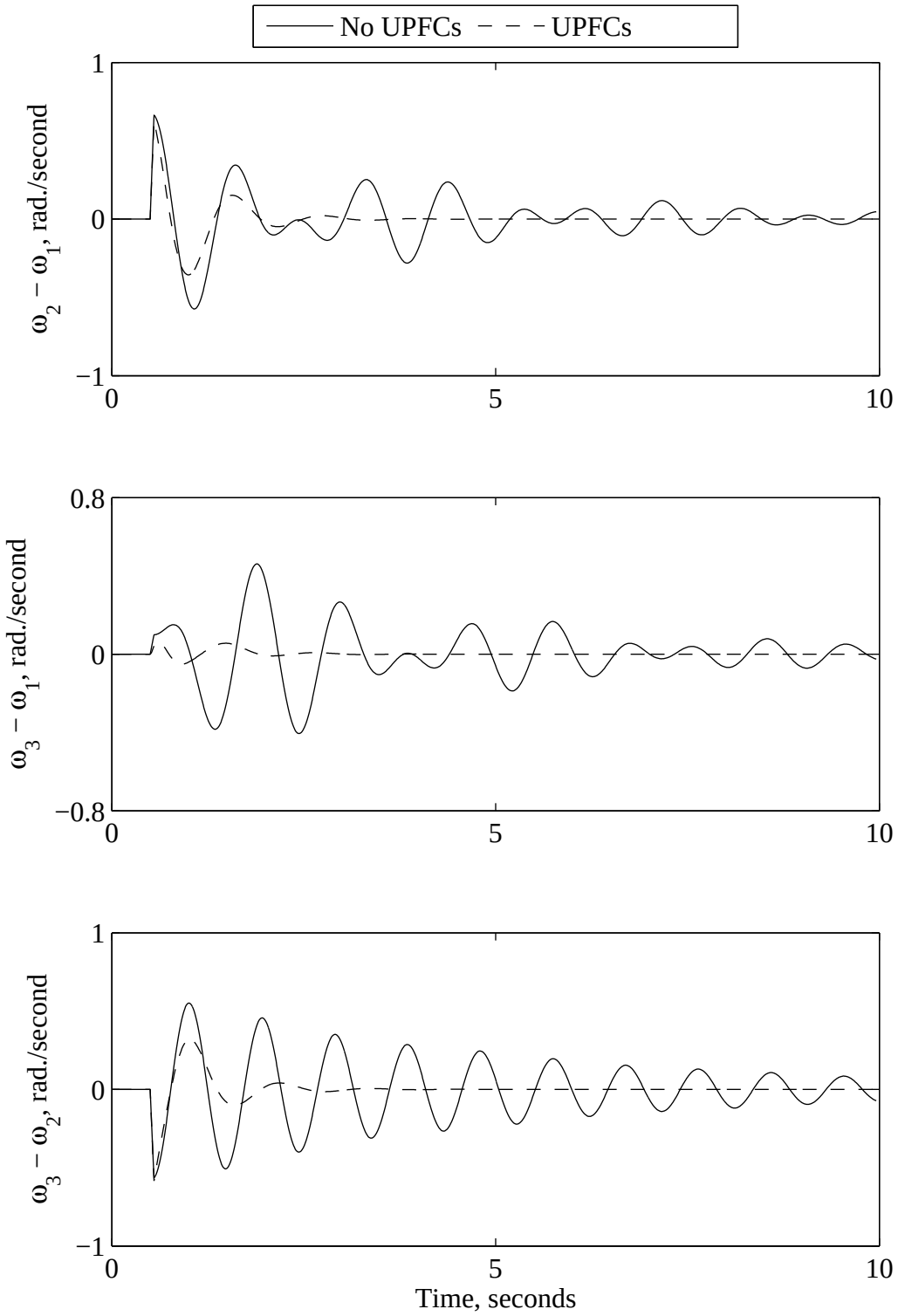

Figure 3.35 Relative generator speed responses due to a 3-cycle 95% sudden load decrease at bus 2 (two UPFCs are installed at LOC1 and LOC3).

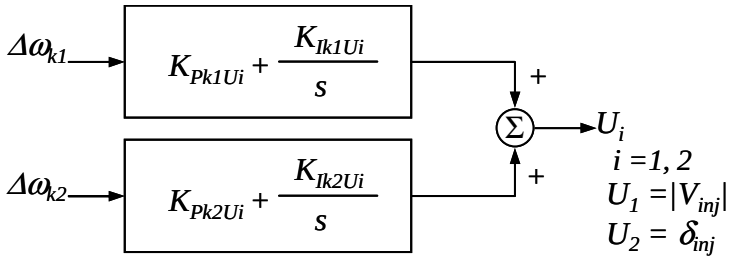

Figure 3.36 A simplified centralized PI UPFC controller structure.

3.8. Effect of the Operating Condition and the Fault Clearing Time

To demonstrate the robustness of the designed controller, simulation studies under various operating conditions were carried out without making any adjustment to the controller parameters. Two operating conditions designated as Case 1 and Case 2 are reported in this thesis. The system pre-disturbance operating conditions in Cases 1 and 2 are such that area 1 is exporting respectively, 66 MW and 265 MW through tie-line L_1 (Appendix C). Figure 3.38 illustrates the time responses of the relative generator speeds due to a 3-cycle three-phase fault at bus 1 for Case 1 with UPFC(s) installed at different locations. As it can be seen from this figure, the UPFCs effectively damp the system oscillations. It is worth noting here that simulation results of Case 2 (Figure E.1, Appendix E) and other cases not reported in this thesis yield the same conclusion. Therefore, it can be concluded that the designed controller is robust.

Regarding the effect of the fault clearing time, the simulation results given in Appendix F show that the controller is effective.

3.9. Summary

In this chapter, a GA based optimization scheme for designing UPFC controllers capable of enhancing the damping of interarea oscillations in a sample three-area power system is developed. The selection of suitable GA parameters for the study system is studied. The results of the investigations have shown that the achieved control laws are effective both for damping large and small disturbances and are robust with respect to fault location and operating condition. The controller design procedure is very general and can be applied to power system damping control design employing other FACTS

devices. The conducted investigations have shown also that the simplified centralized UPFC controllers are effective in damping interarea oscillations.

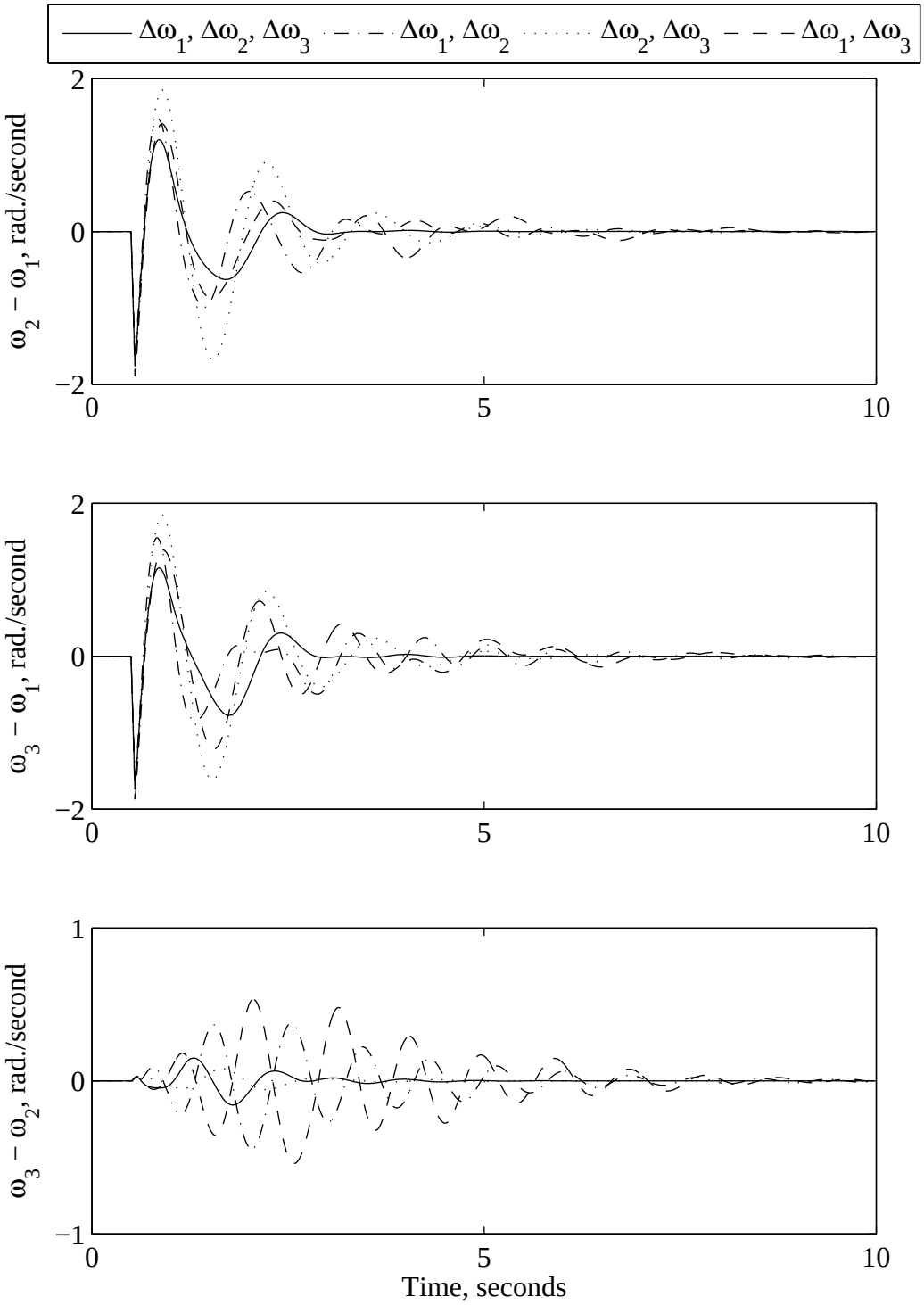

Figure 3.37 Effect of the global stabilizing signal on the relative generator speeds due to a 3-cycle three-phase fault at bus 1 (a UPFC controller is installed at LOC1).

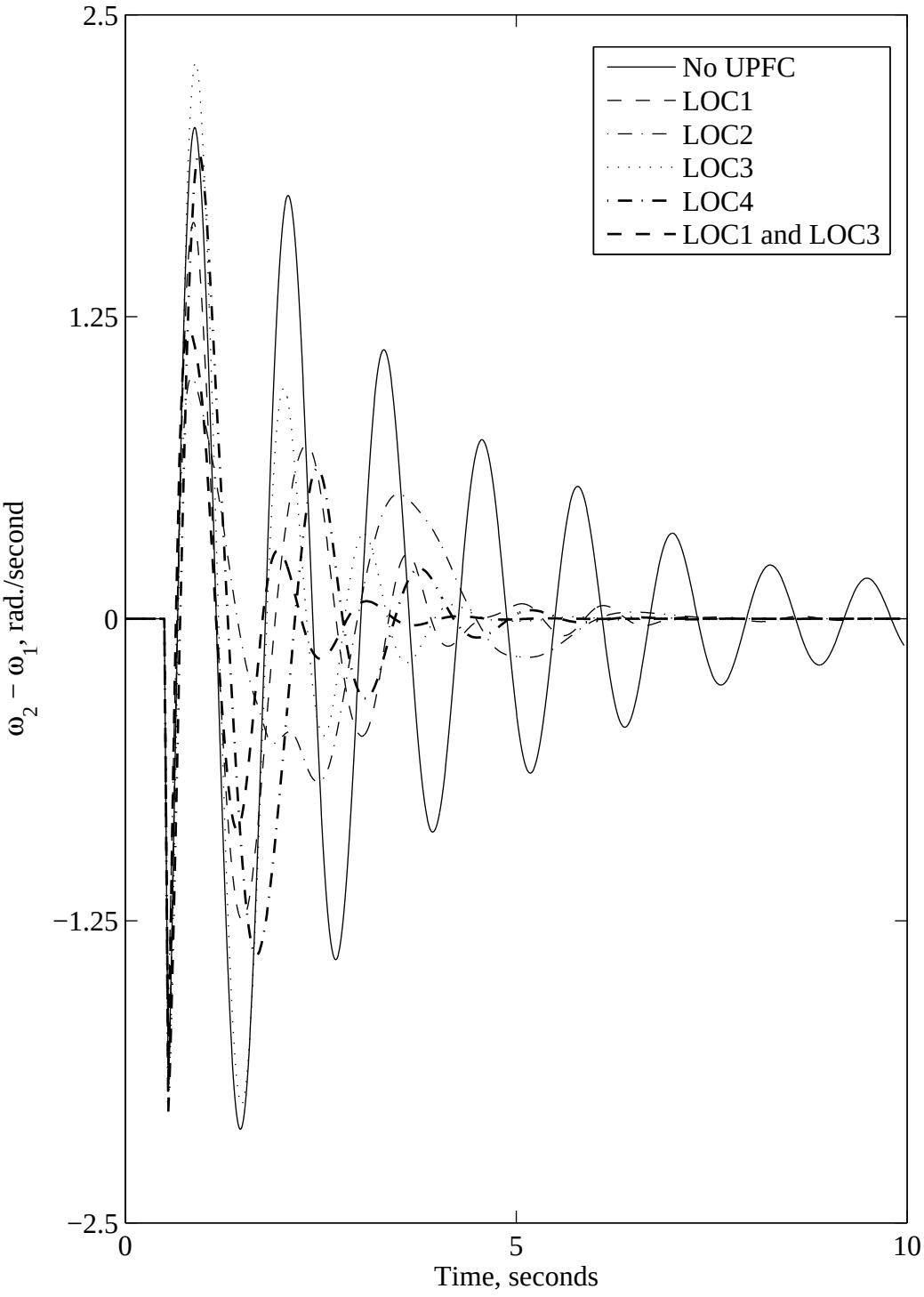

Figure 3.38 Effect of the operating condition on the relative generator speeds due to a 3-cycle three-phase fault at bus 1.

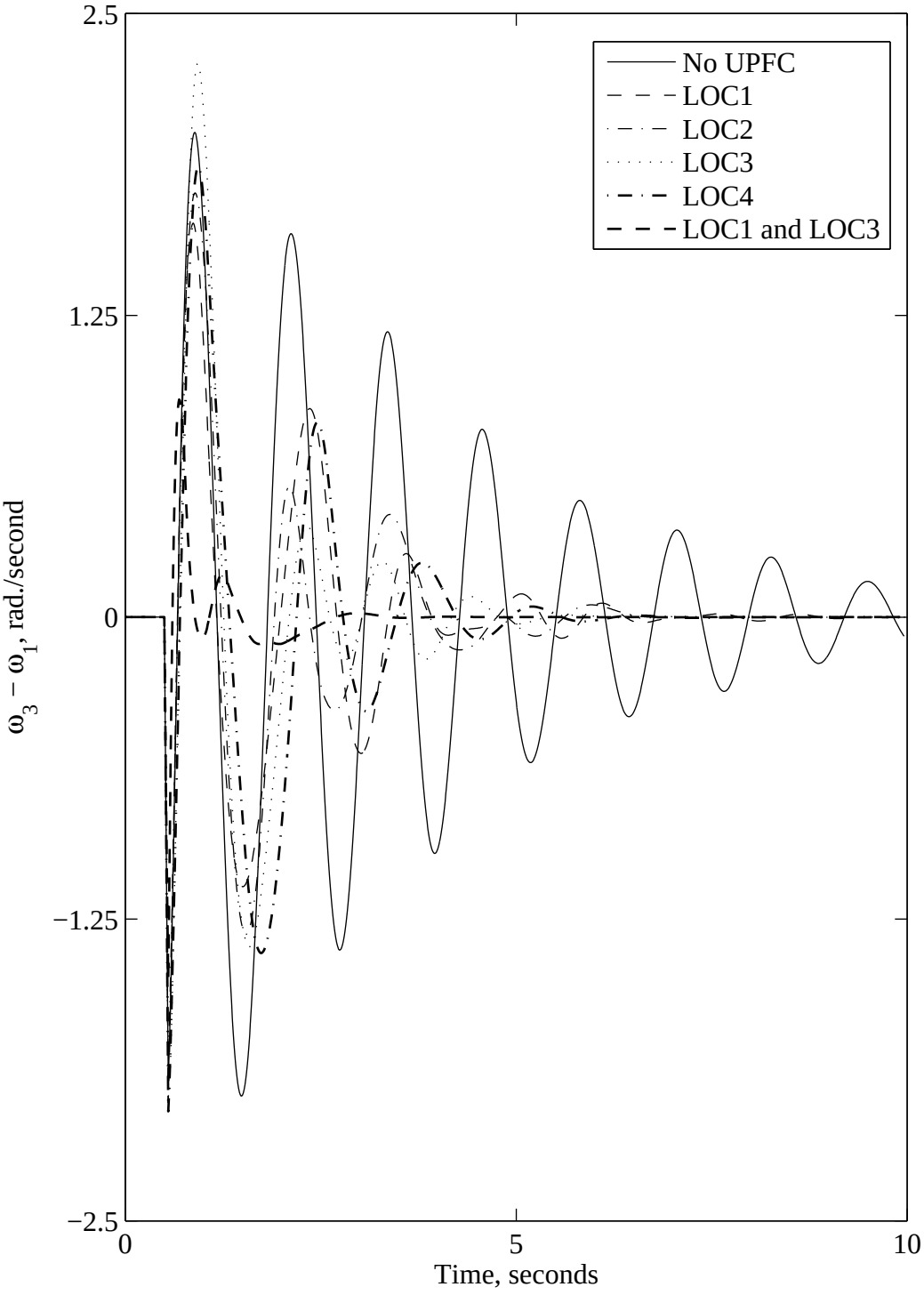

Figure 3.38, continued.

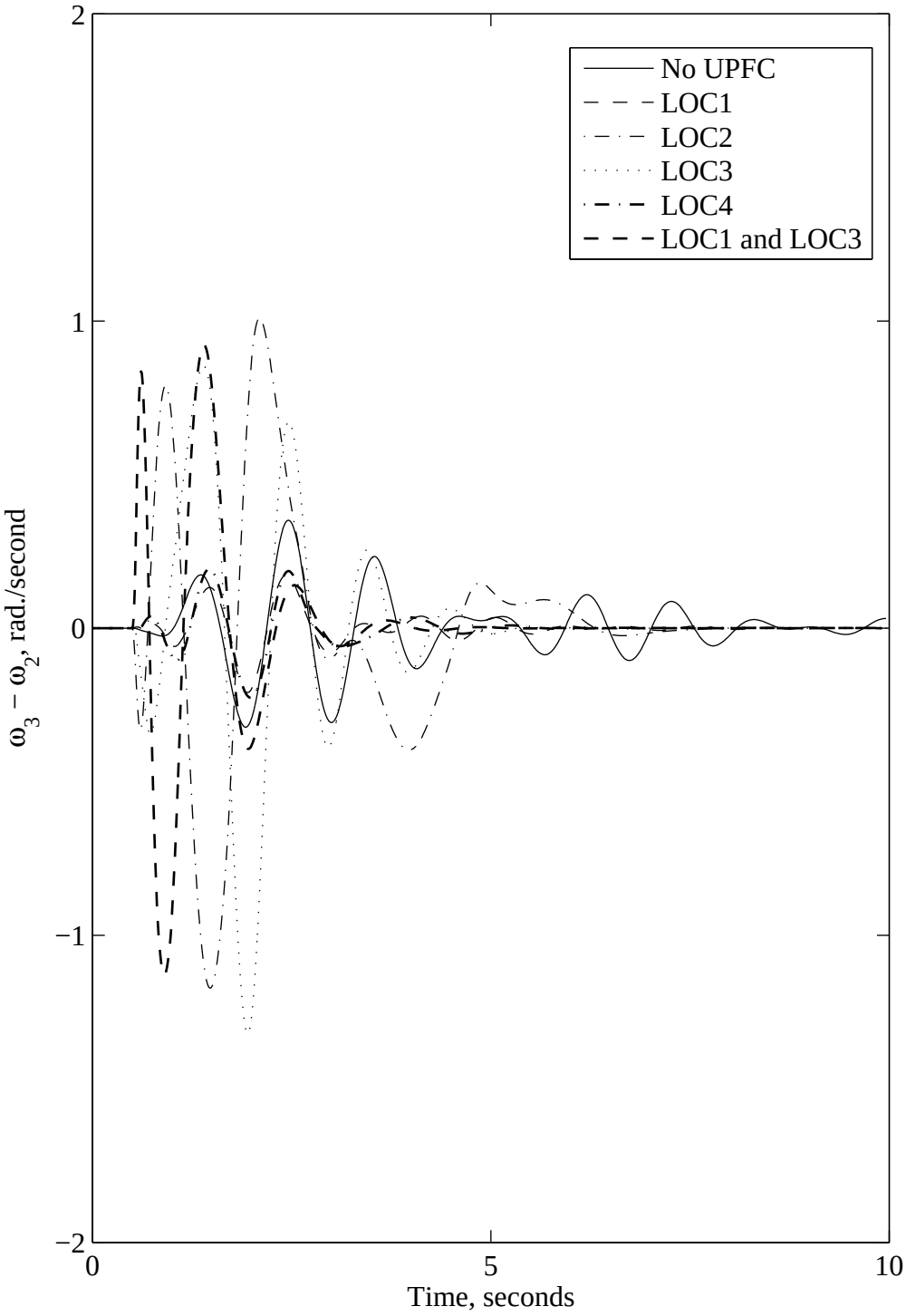

Figure 3.38, continued.

4. DAMPING INTERAREA OSCILLATIONS USING FUZZY LOGIC UPFC CONTROLLERS

4.1. Introduction

Fuzzy control has gained a great acceptance in the academic and industrial world. The worldwide success of numerous commercial products and applications has proved the fuzzy control to be not only practical and powerful, but also cost effective. Real world systems are nonlinear and accurate modeling is difficult and even impossible in some cases [58]. Fuzzy control has the unique ability to successfully accomplish control tasks without knowing the mathematical model of the system, even if it is nonlinear and complex. On the other hand, fuzzy controller design needs a good understanding of the physics of the system under study [59]. In this chapter, fuzzy logic controllers for UPFC are developed. Controllers design is conducted based on the knowledge of the system dynamics as well as GA tuning. The effectiveness of these controllers is examined throughout several system disturbances.

4.2. Fuzzy Logic UPFC Controller Design

A Multi-Input Single-Output (MISO) Mamdani type fuzzy controller using a centroid defuzzification method is used to design a PI fuzzy controller for the UPFC. The variation in generator speeds $\Delta\omega_1$, $\Delta\omega_2$ and $\Delta\omega_3$ are selected again as input signals. Figure 4.1 shows a PI fuzzy controller structure. A centralized PI fuzzy controller uses 12 of such a controller is considered to control the UPFC. The variables g_{1i} and g_{2i} represent the input variable scaling factors. These variables are adjustable and are chosen, normally, based on the designer experience and the system dynamic performance. The values of g_{1i} and g_{2i}, selected for the PI fuzzy controller in the case of a UPFC installed at LOC1, are given in Table 4-1. The membership functions for the premises (inputs) and consequents (outputs) are shown respectively in Figures 4.2 and 4.3. N, Z and P are linguistic values representing “Negative”, “Zero” and “Positive”

respectively. The output signal ΔU_i is used to control the UPFC series and shunt injected voltage magnitudes and angles.

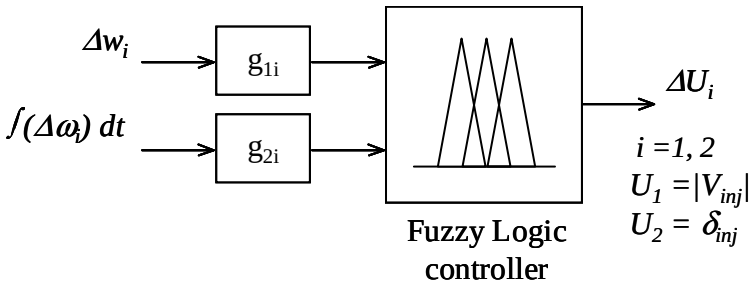

Figure 4.1 PI fuzzy controller structure.

The PI fuzzy controller uses four simplified rules as

If $\Delta\omega_i$ is P **and** $\int\Delta\omega_i$ is P **Then** ΔU_i is P

If $\Delta\omega_i$ is P **and** $\int\Delta\omega_i$ is N **Then** ΔU_i is Z

If $\Delta\omega_i$ is N **and** $\int\Delta\omega_i$ is P **Then** ΔU_i is Z

If $\Delta\omega_i$ is N **and** $\int\Delta\omega_i$ is N **Then** ΔU_i is N

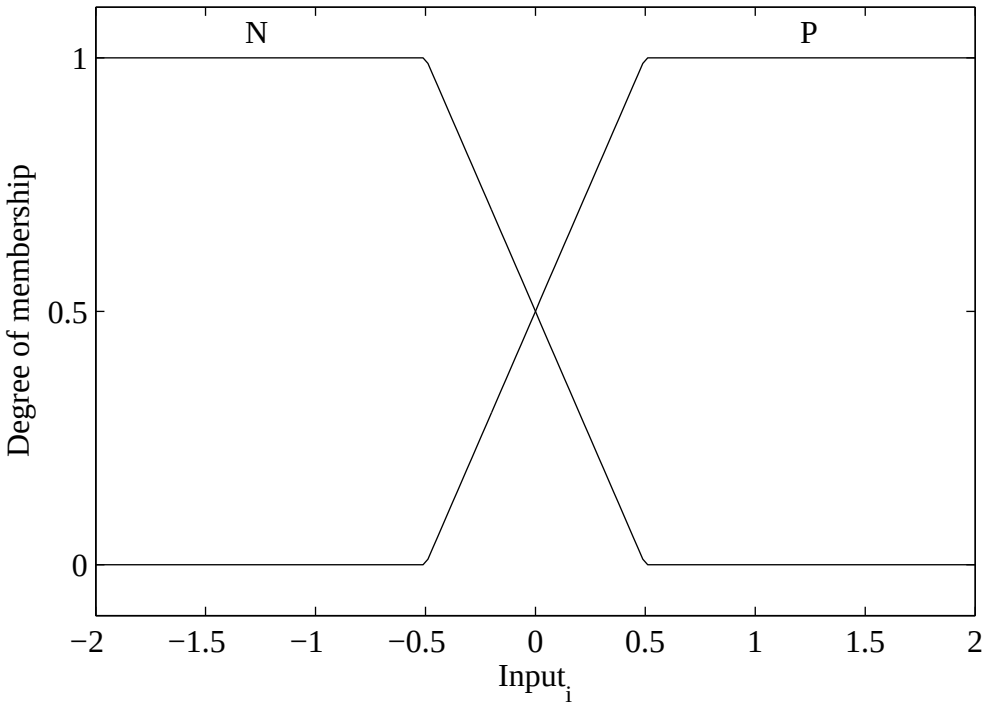

Figure 4.2 Membership functions for $\Delta\omega_i$.

Table 4-1 The input gains g_{1i} and g_{2i} values

i	g_1	g_2	i	g_1	g_2
1	2	1	7	-1	2
2	1	1	8	1	-1
3	1	-2	9	1	2
4	2	-2	10	-1	-1
5	1	-2	11	2	1
6	-2	-1	12	1	0

The variation in the UPFC injected voltages and angles are chosen to be

$$\Delta V_B = \sum_{i=1}^{12} K_{Bi}\Delta U_i \,, \qquad \Delta \delta_B = \sum_{i=1}^{12} K_{dBi}\Delta U_i$$

$$\Delta V_E = \sum_{i=1}^{12} K_{Ei}\Delta U_i \,, \qquad \Delta \delta_E = \sum_{i=1}^{12} K_{dEi}\Delta U_i$$

where,

i	K_{Bi}	K_{dBi}	K_{Ei}	K_{dEi}
1	1	0	0	0
2	0	1	0	0
3	0	0	1	0
4	0	0	0	1
5	1	0	0	0
6	0	1	0	0
7	0	0	1	0
8	0	0	0	1
9	1	0	0	0
10	0	1	0	0
11	0	0	1	0
12	0	0	0	1

4.3. Fuzzy Logic UPFC Controller Performance during System Faults

The performance of the developed PI fuzzy controller is examined due to three-phase faults at different locations. The system pre-disturbance operating condition is, selected again, such that area 1 is importing 440 MW through tie-line L_1. The UPFC is considered to be installed at LOC1. Figures 4.4 to 4.7 show the time responses of the relative generator speeds due to 3-cycle three-phase faults at buses 1, 2, 3 and 4

respectively. It can be seen from these figures that the PI fuzzy controller of the UPFC significantly damps system oscillations at all fault locations.

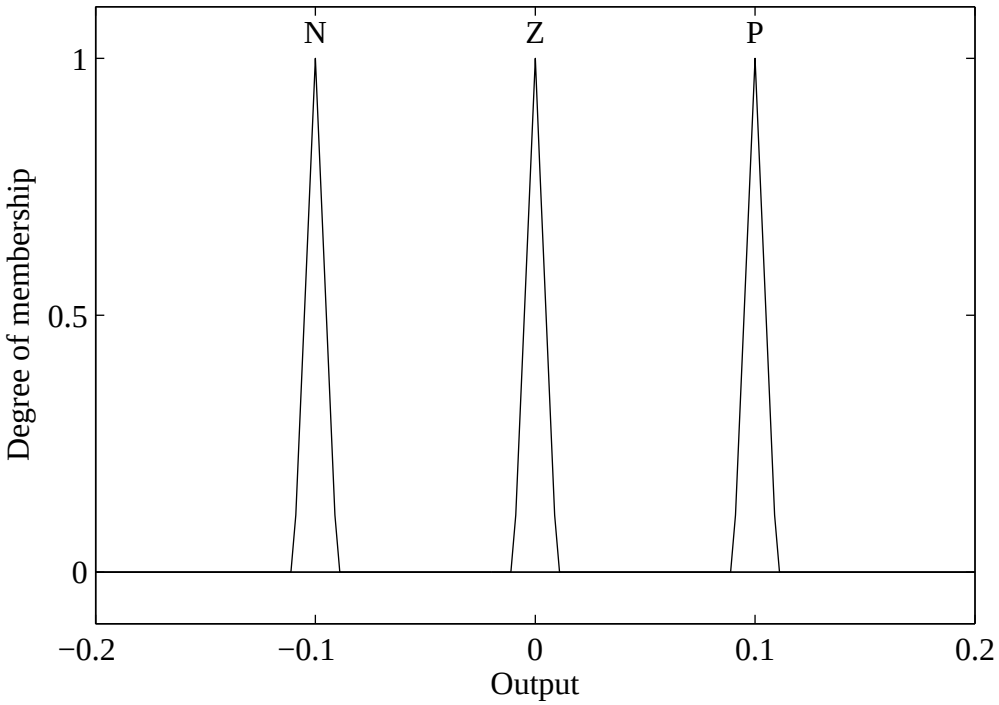

Figure 4.3 Membership functions for output signals.

4.4. Fuzzy Logic UPFC Performance during Other Disturbances

Two system disturbances are considered to examine the designed controller performance under different large and small disturbances. A sudden load decrease of 95% is considered as the simulated large disturbance while a 5% decrease in the input reference mechanical power is considered as the simulated small disturbance. Figure 4.8 shows the system response following a 5% sudden decrease in the input reference mechanical power of generator G_1 with the UPFC installed in LOC1 while Figures 4.9 and 4.10 show the system response due to a 95%, 3-cycle sudden decrease in loads S_1 and S_2 with the UPFC installed in the same location. It can be seen from Figures 4.8 to 4.10 that the developed controller revels excellent performance in damping the system oscillations due to both small and large disturbances.

To examine the effect of the UPFC location and the operating condition on the UPFC controller performance, simulation studies were carried out under various operating

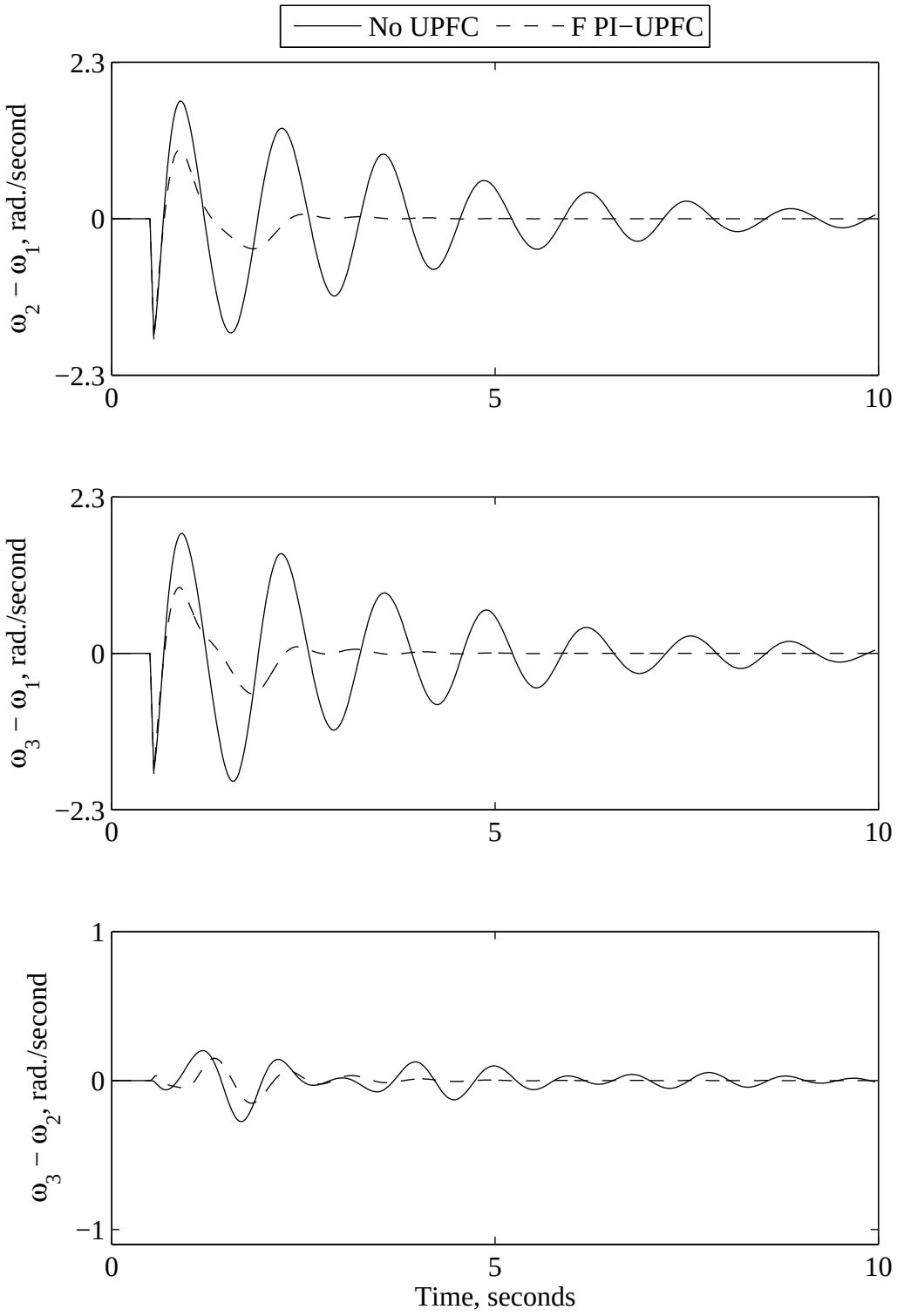

Figure 4.4 Relative generator speeds due to a 3-cycle three-phase fault at bus 1 (a UPFC is installed at LOC1).

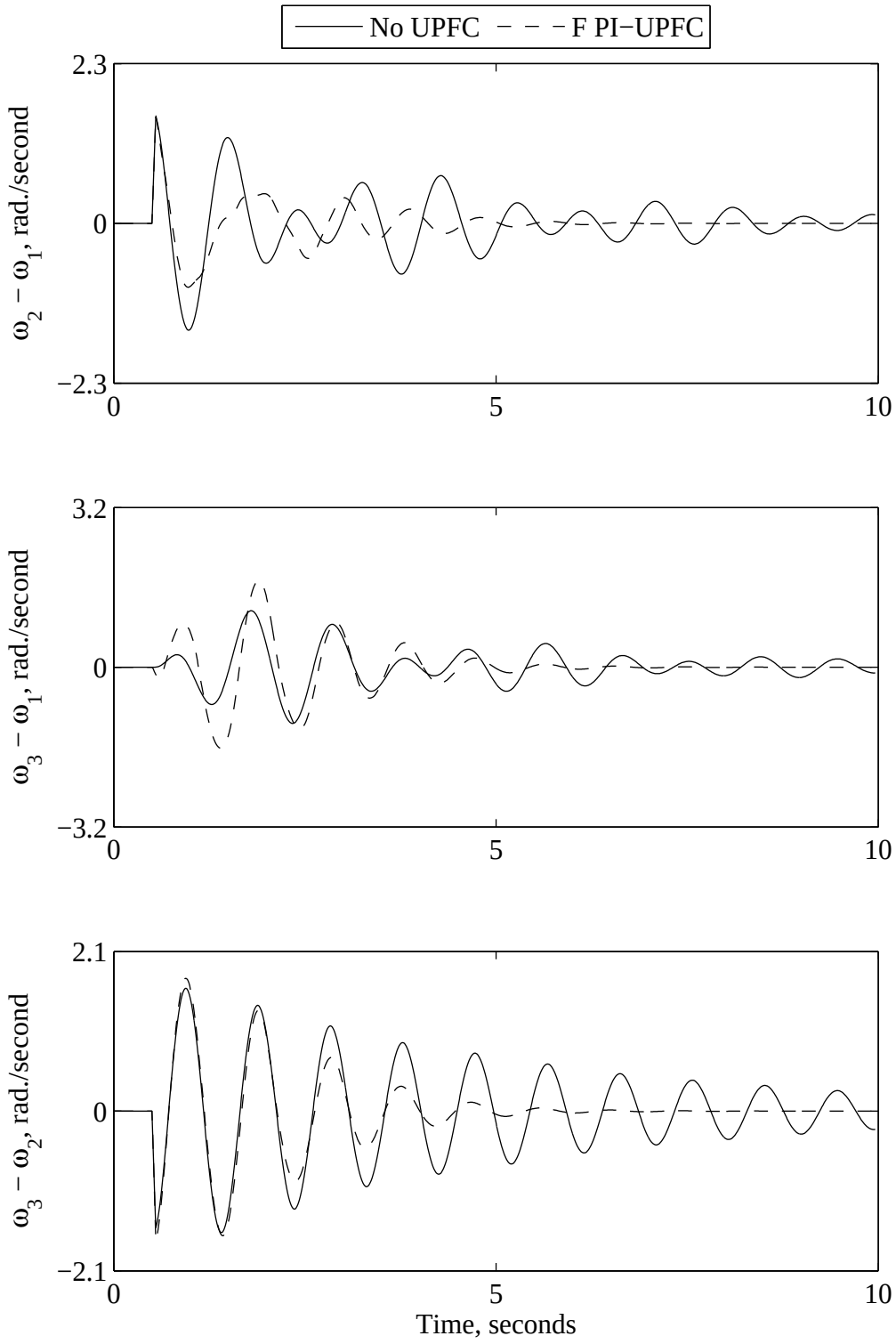

Figure 4.5 Relative generator speeds due to a 3-cycle three-phase fault at bus 2 (a UPFC is installed at LOC1).

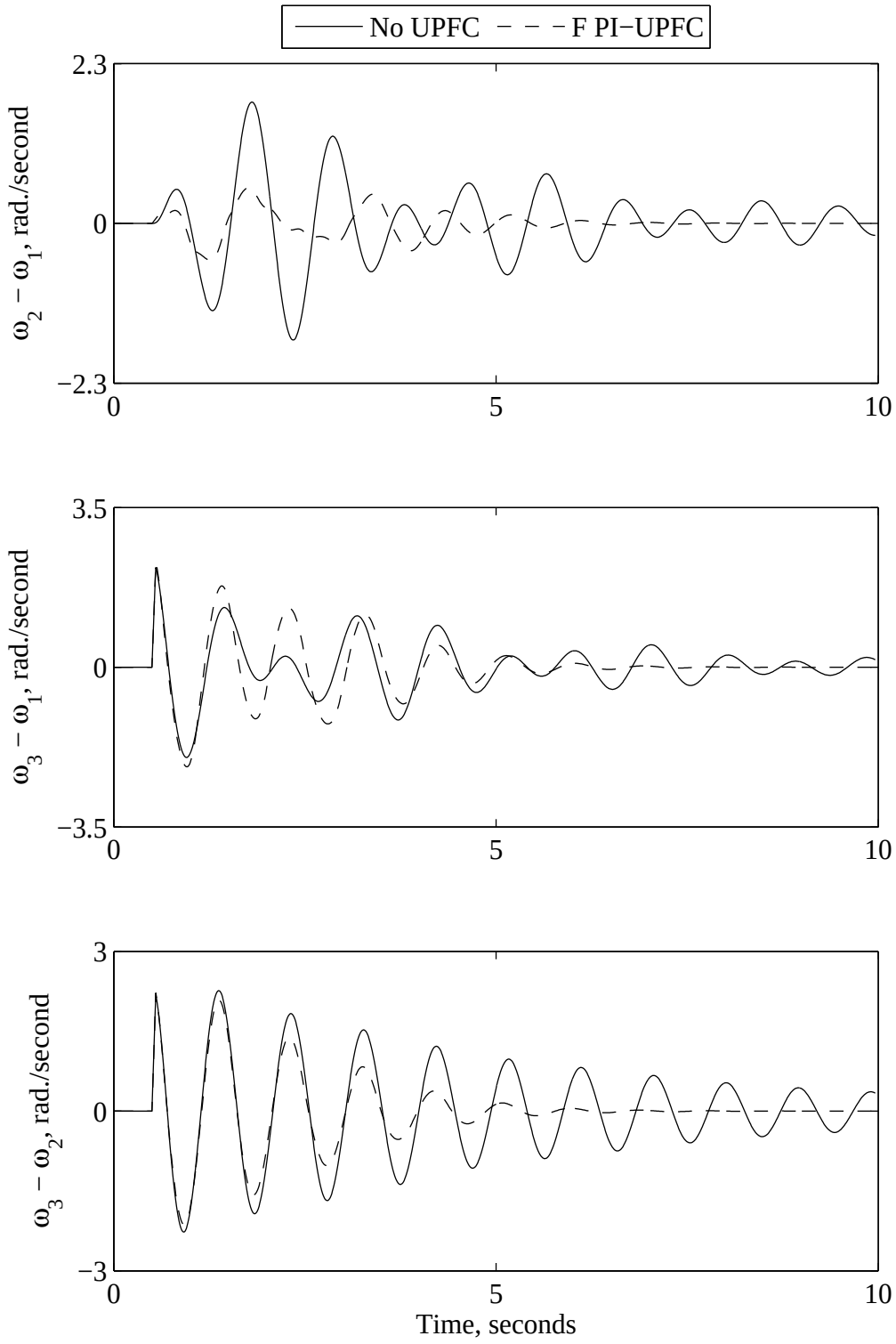

Figure 4.6 Relative generator speeds due to a 3-cycle three-phase fault at bus 3 (a UPFC is installed at LOC1).

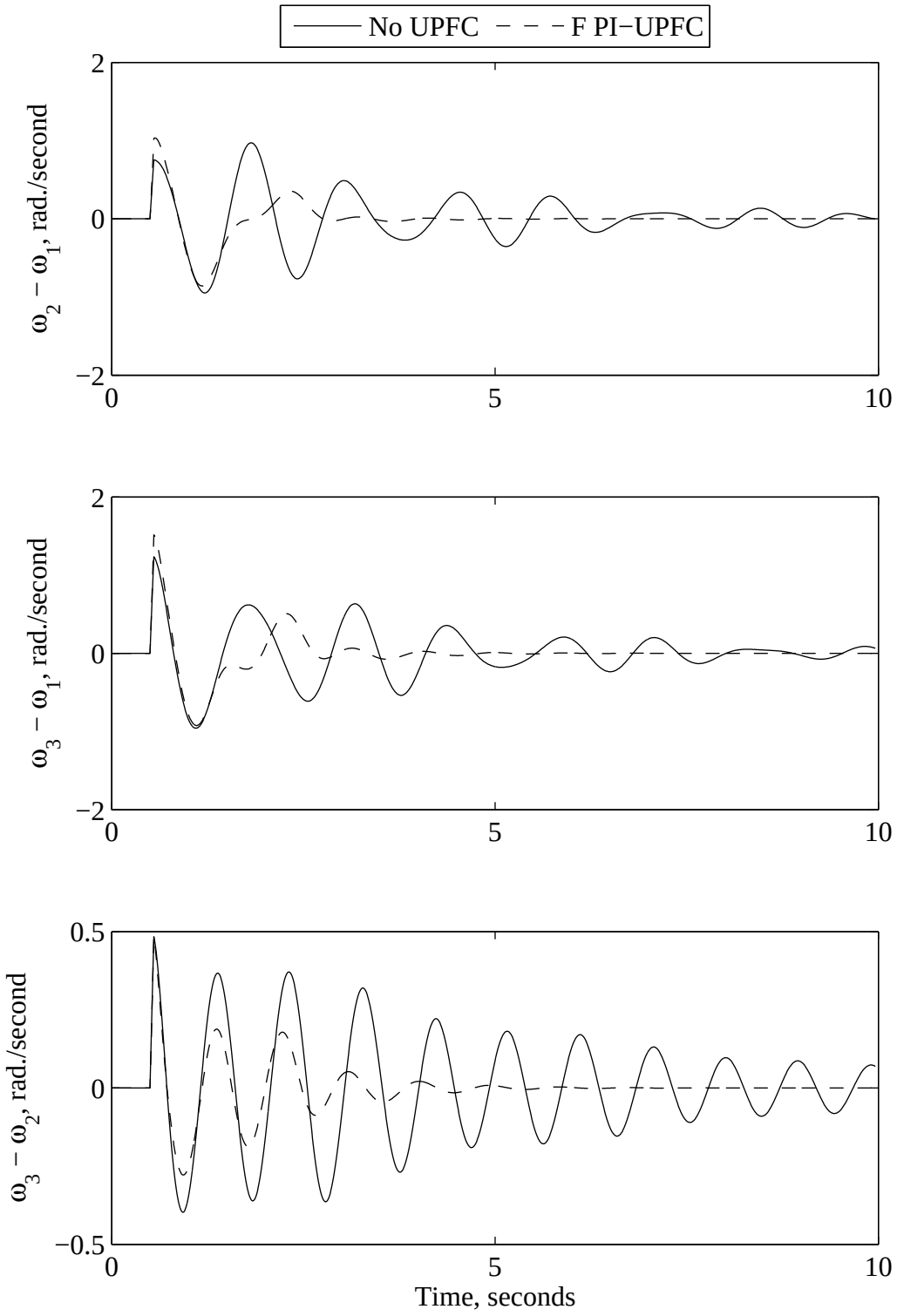

Figure 4.7 Relative generator speeds due to a 3-cycle three-phase fault at bus 4 (a UPFC is installed at LOC1).

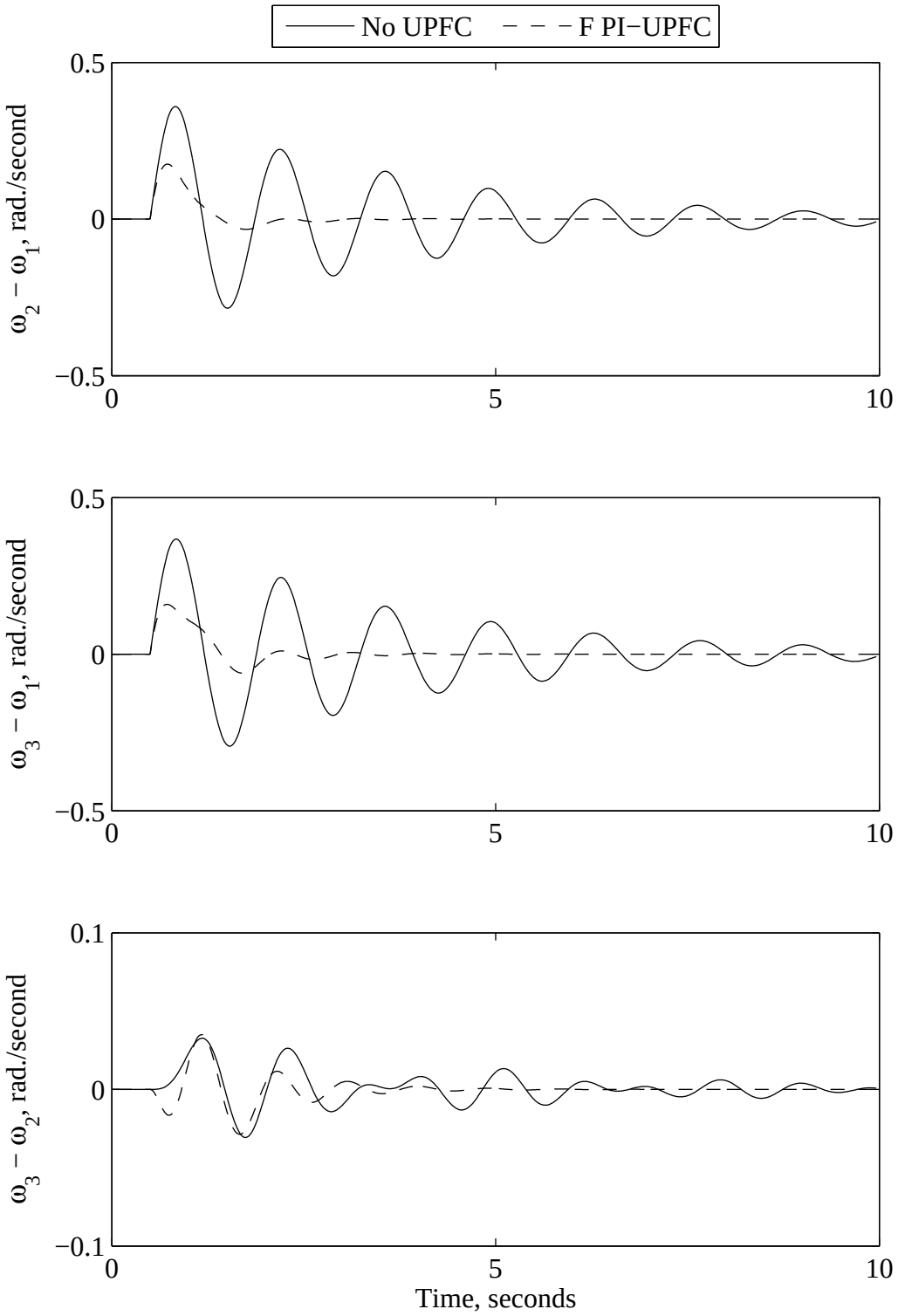

Figure 4.8 Relative generator speed responses for a 5% sudden decrease in the reference power of generator G_1 (a UPFC is installed at LOC1).

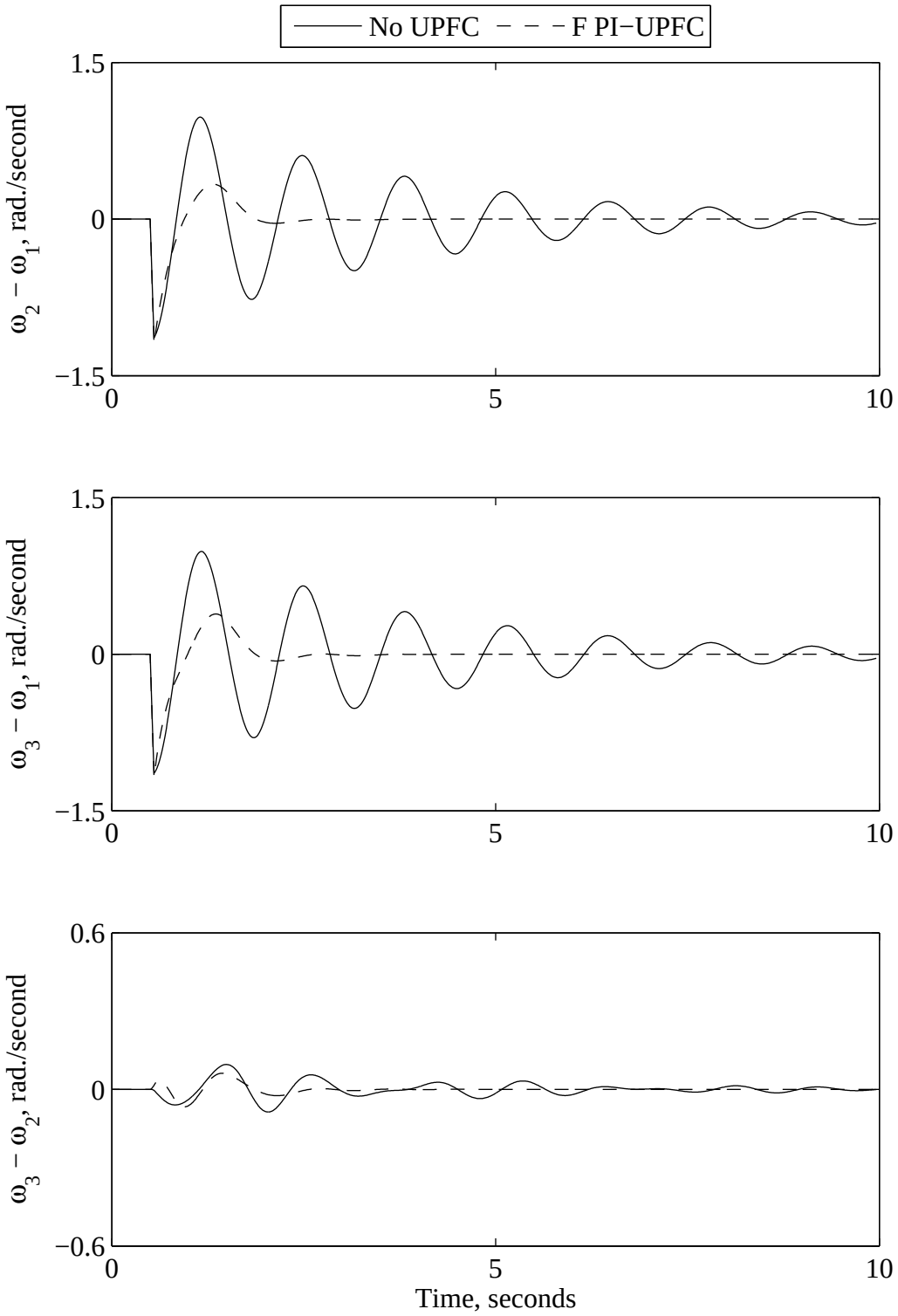

Figure 4.9 Relative generator speed responses due to a 3-cycle 95% sudden load decrease at bus 1 (a UPFC is installed at LOC1).

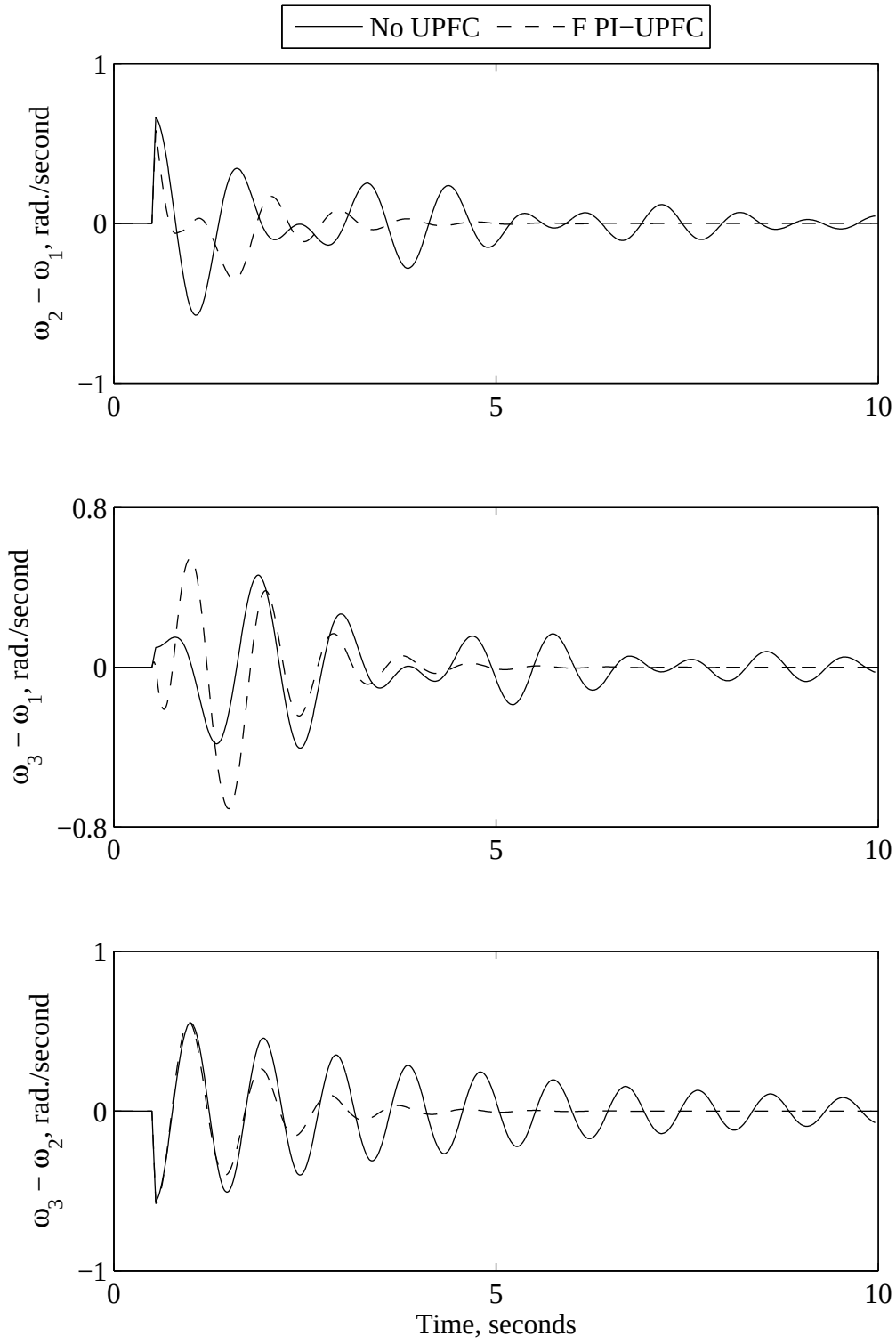

Figure 4.10 Relative generator speed responses due to a 3-cycle 95% sudden load decrease at bus 2 (a UPFC is installed at LOC1).

conditions with the UPFC installed in different locations; two cases are reported in this thesis. Figures 4.11 to 4.13 illustrate the time responses of the relative generator speeds due to 3-cycle three-phase faults at buses 1, 2 and 3 with the UPFC installed at LOC3 while Figure 4.14 shows the relative generator speeds due to a 3-cycle three-phase fault at bus 1 with the UPFC installed at LOC1 for Case 1 (Section 3.8). As can be seen from these figures, the designed controller for the UPFC effectively damps the system oscillations.

4.5. GA Tuned Fuzzy Logic UPFC Controller

This section discusses a new approach for designing a controller for the UPFC based on combining GA technique with the fuzzy logic. In this approach, a GA objective function is chosen to tune the input membership functions, output membership functions and the fuzzy set rules and their weights. The structure of the input and output membership functions is shown in Figures 4.15 and 4.16 respectively where L_i, M_i, X_i and K_i are adjustable parameters. The controller design is based on minimizing the generator speeds due to three-phase faults. The steps of the controller design procedure are as follows:

1- Decoding:

Each GA individual is a binary decoded string represents a fuzzy controller design. Figure 4.17 shows the structure of the GA string used in this section. Such a string consists of three parts. The first part contains the input membership function parameters while the second part contains the output membership function parameters, where *Nin* and *Nout* are the number of inputs and outputs respectively. The third part of the string contains the fuzzy rules, where *Nr* is the number of rules. Each of these rules consists of *Nin* + *Nout* + 2 columns as follows:

> Each variable, input, or output, has an index number, and each membership function has an index number. The rules are built from statements having the following form:
>
> **If** $input_1$ is mf_{1in} **or** $input_2$ is mf_{3in} **Then** $output_1$ is mf_{2out} (weight = 0.5) (4-1)

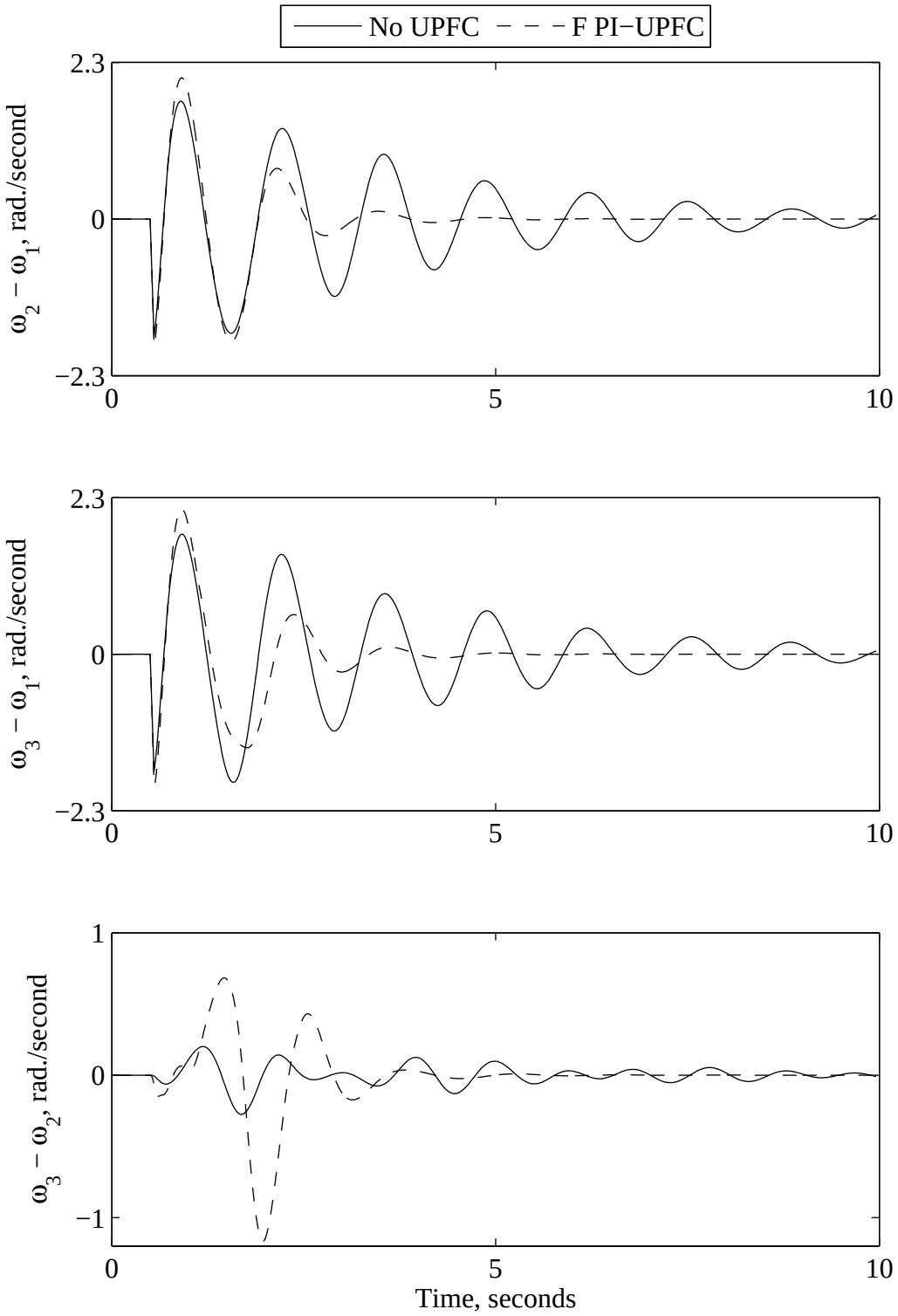

Figure 4.11 Relative generator speeds due to a 3-cycle three-phase fault at bus 1 (a UPFC is installed at LOC3).

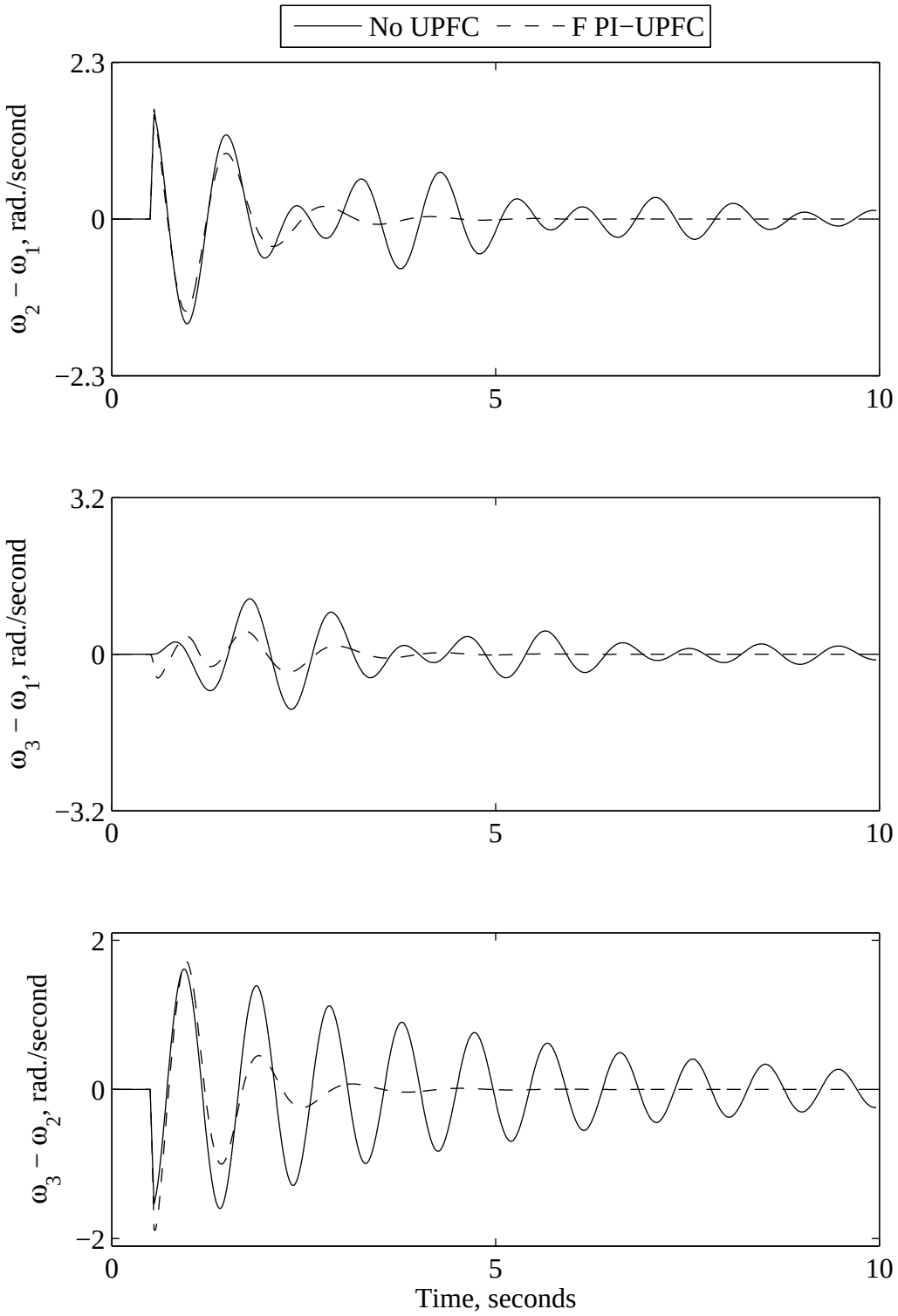

Figure 4.12 Relative generator speeds due to a 3-cycle three-phase fault at bus 2 (a UPFC is installed at LOC3).

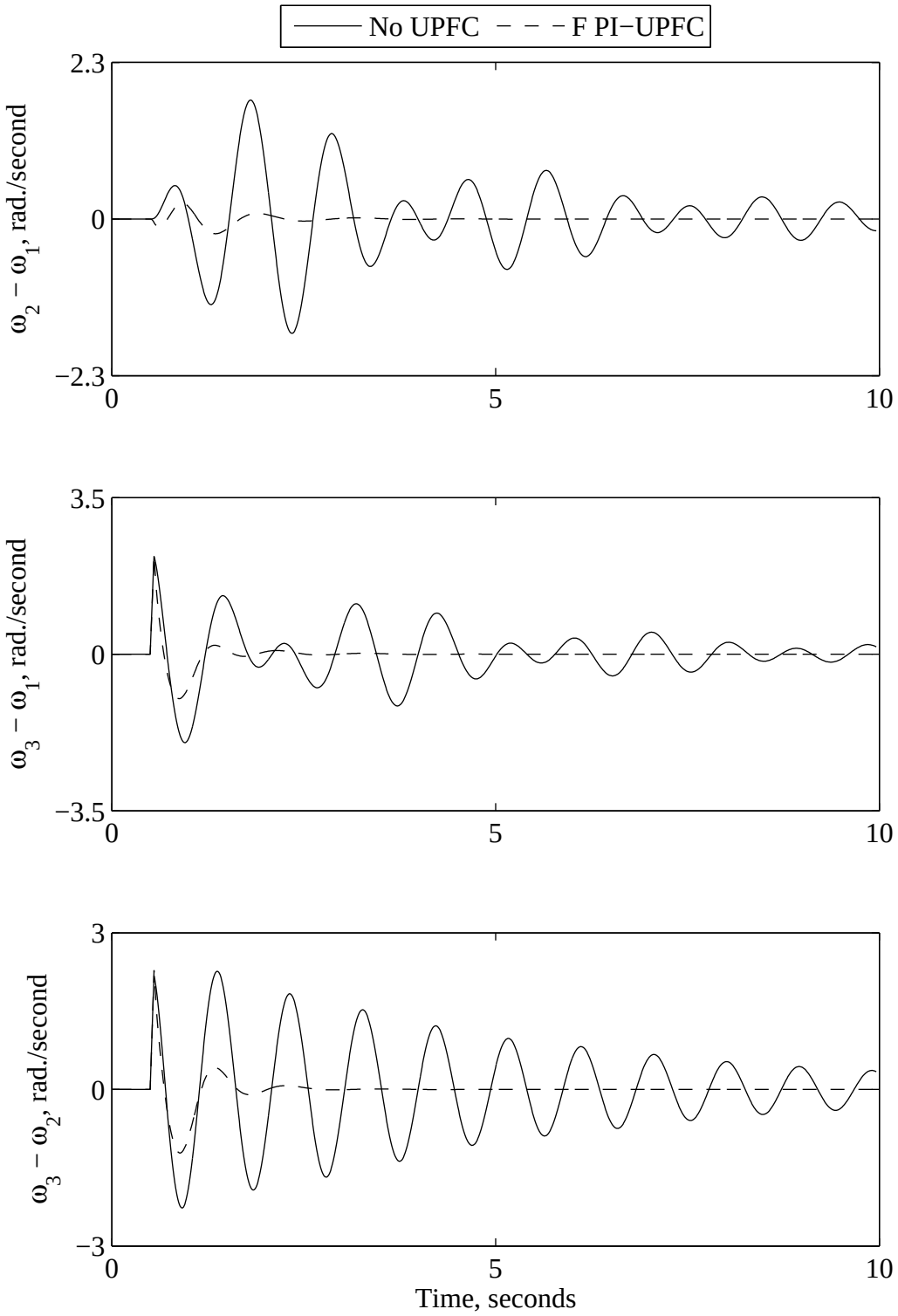

Figure 4.13 Relative generator speeds due to a 3-cycle three-phase fault at bus 3 (a UPFC is installed at LOC3).

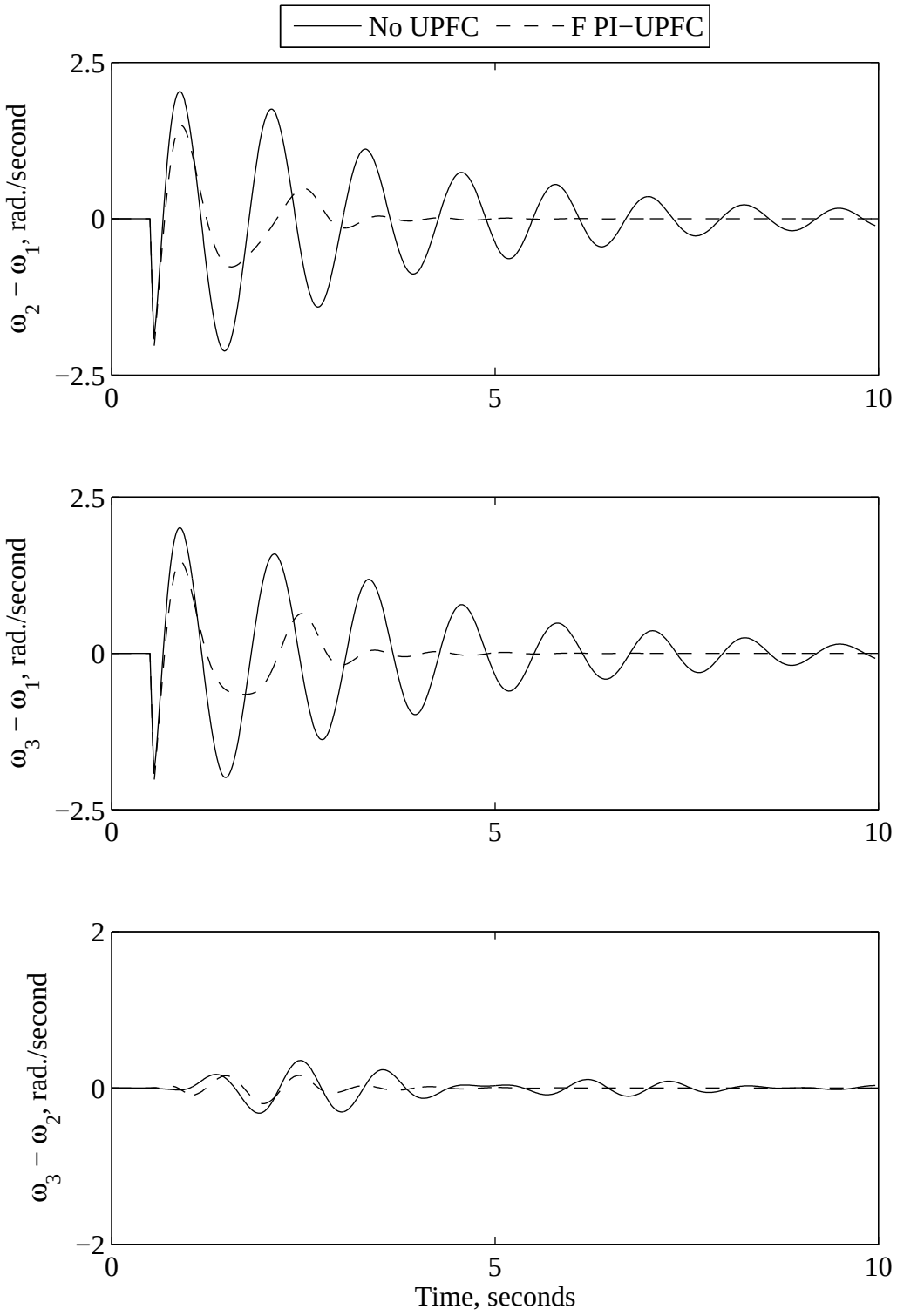

Figure 4.14 Effect of the operating condition on the relative generator speeds due to a 3-cycle three-phase fault at bus 1 (a UPFC is installed at LOC1).

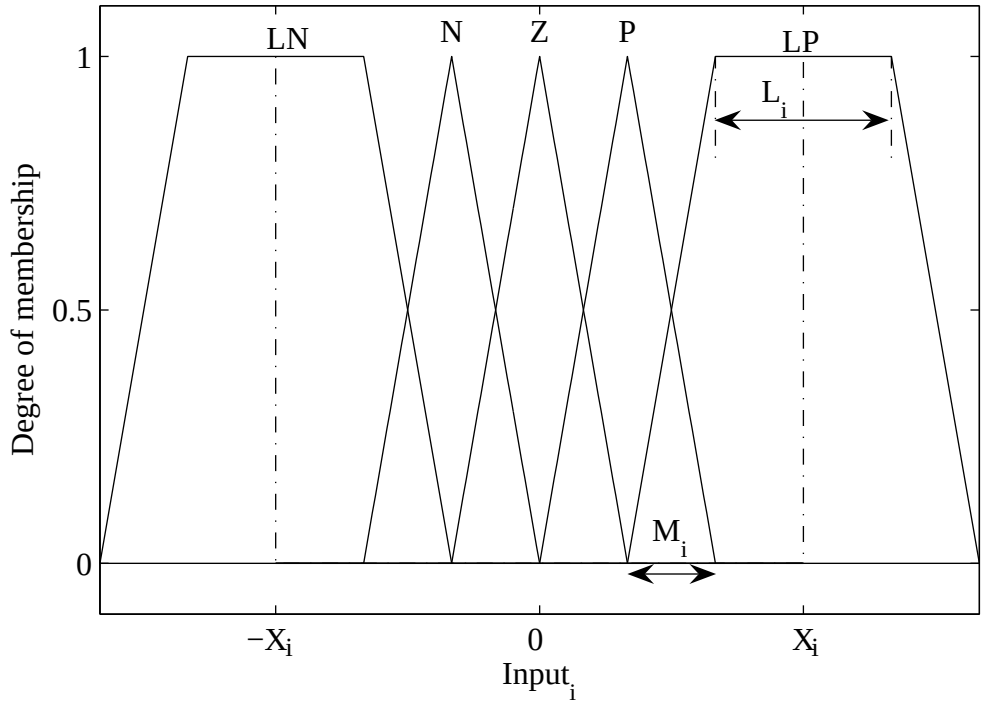

Figure 4.15 GA tuned fuzzy controller input membership function.

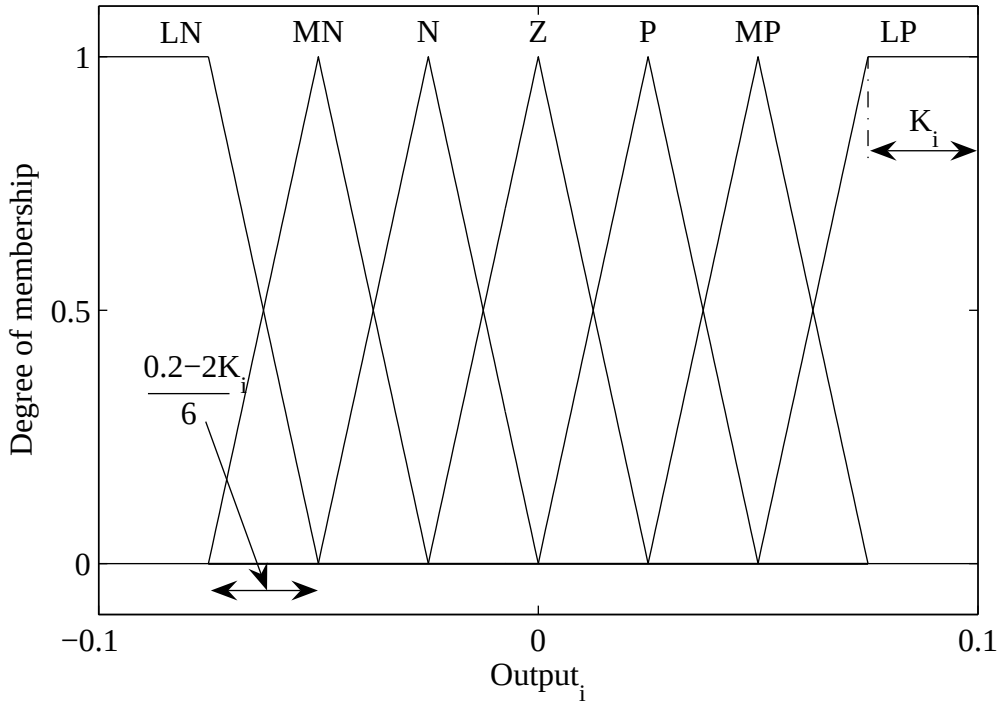

Figure 4.16 GA tuned fuzzy controller output membership function.

This rule is turned into a structure according to the following logic. If there are *Nin* inputs to the system and *Nout* outputs, then the first *Nin* vector entries of the rule structure correspond to inputs 1 through *Nin*. The entry in column 1 is the index number for the membership function associated with input 1. The entry in column 2 is the index number for the membership function associated with input 2, and so on. The next *Nout* columns work the same way for the outputs. Column *Nin* + *Nout* + 1 is the weight associated with the rule (0 to 1) and column *Nin* + *Nout* + 2 specifies the connective used (where AND = 1 and OR = 2). The structure associated with the rule shown in Equation (4-1) is

[1 3 2 0.5 2]

2- Initialization:

An initial generation (a population of initial controller design) is created using a random generator. The fitness value of each member (string) in the initial population is calculated using the following fitness function:

$$F = \max\left(f_{ij}\right), \qquad i = 1, 2, 3 \quad and \quad j = 1, 2, 3$$

where $f_{ij} = \int_0^{Tsim} \left(\omega_j - 1\right)^2 dt$, and i represents the fault location, j represents generator number and *Tsim* represents the total simulation time.

The maximum value of f_{ij} is used to consider the least effective performance of such controller due to several faults. It is worth noting here that individuals with lower values of F are the fittest. The definition of f_{ij} is illustrated graphically in Figure 4.18.

3- Reproduction:

Three GA operators, namely selection, crossover and mutation are implemented to create a new population. The selection operation determines which parents participate in producing offspring for the next generation, and it is analogous to "survival of the fittest" in natural selection. To exploit the potential of the current population, the crossover operator generates new chromosomes. One point crossover is used in the investigation of this section, where a crossover point on the genetic code is selected at

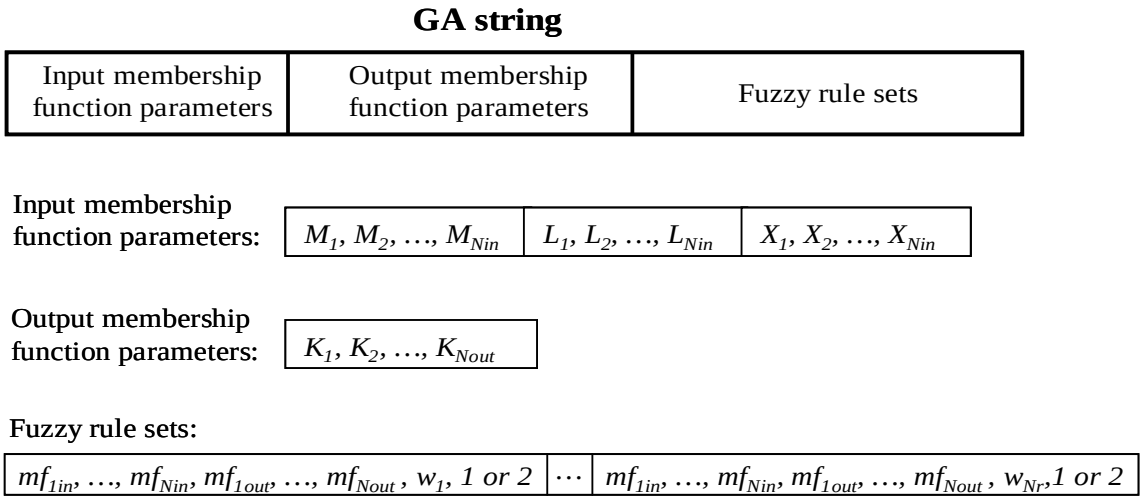

Figure 4.17 GA string structure.

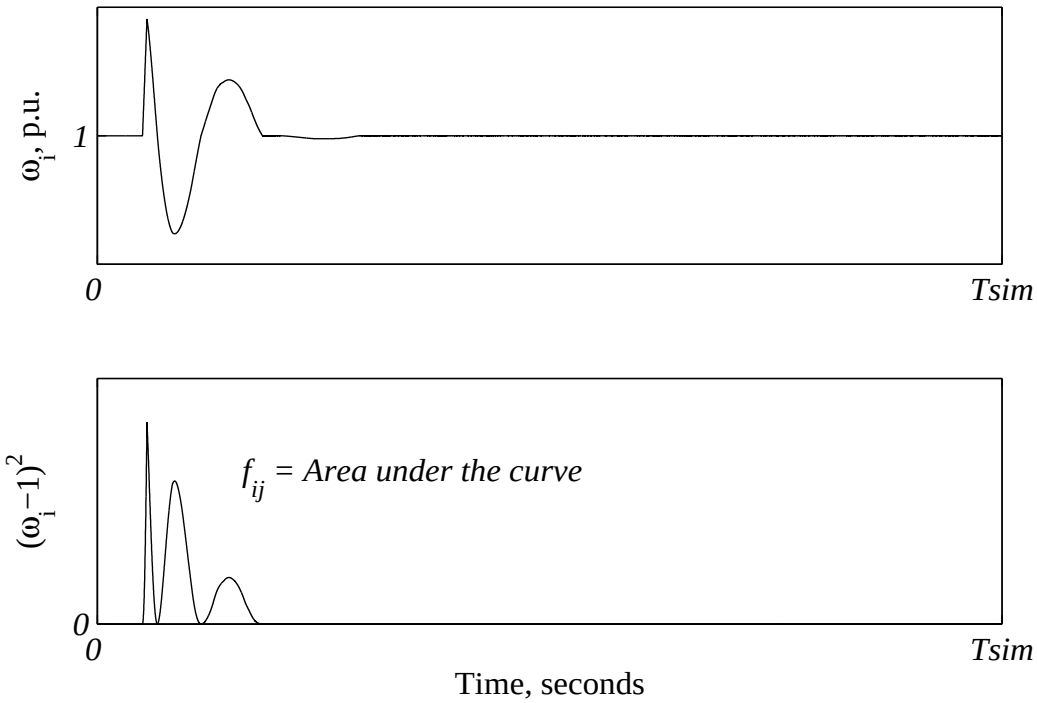

Figure 4.18 Graphical illustration of the definitions of f_{ij}.

random and two parent chromosomes are interchanged at this point to generate two children. While crossover exploits current gene potentials, mutation operator is capable of spontaneously generating new chromosomes. A mutation operator can prevent any single bit from converging to a value throughout the entire population, and more

important, it can prevent the population from converging and stagnating any local optima. The fitness values of the new population are revaluated.

4- Termination:

If the termination criterion (in this case, a predetermined maximum number of generations) is not satisfied, then step three is repeated. Otherwise, the algorithm is terminated and the best controller design is selected.

The variation in generator speeds $\Delta\omega_1$, $\Delta\omega_2$ and $\Delta\omega_3$ and the deviation of the generator power angles $\Delta\delta_1$, $\Delta\delta_2$ and $\Delta\delta_3$ are used as input signals. The centralized GA tuned fuzzy controller has six inputs and four outputs as shown in Figure 4.19.

4.6. GA Tuned Fuzzy Logic UPFC Controller Performance

Figures 4.20 to 4.22 show the time responses of the system due to various system disturbances with the UPFC installed at LOC1. It can be seen from these figures that the GA tuned fuzzy UPFC controller damps significantly the system oscillations. The controller performance, however, is relatively less effective in the case of a small disturbance especially if compared with the controller of Figure 4.8. This is due to the fact that such a controller is designed based on tuning its parameters due to large disturbances.

4.7. Summary

In this chapter, a fuzzy logic controller for UPFC is designed and its potential in damping interarea oscillations in the three-area power system is examined. The results of the investigations have shown that the developed controllers are effective both in damping large and small disturbances and are robust with respect to fault location and operating condition. The conducted investigations have shown also that the GA tuned fuzzy controller for UPFC is effective in damping interarea oscillations.

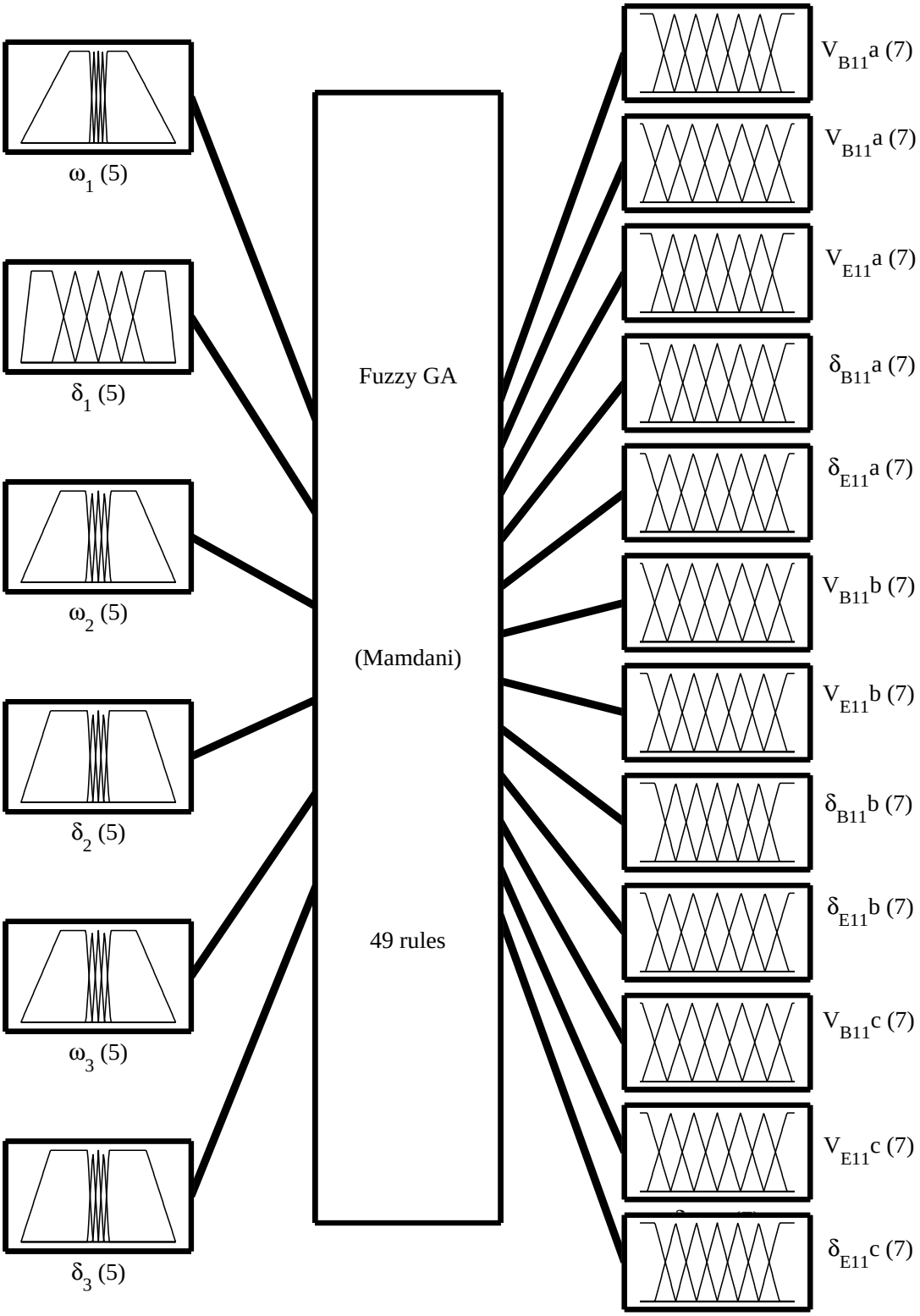

System Fuzzy GA: 6 inputs, 12 outputs, 49 rules

Figure 4.19 GA tuned fuzzy controller structure.

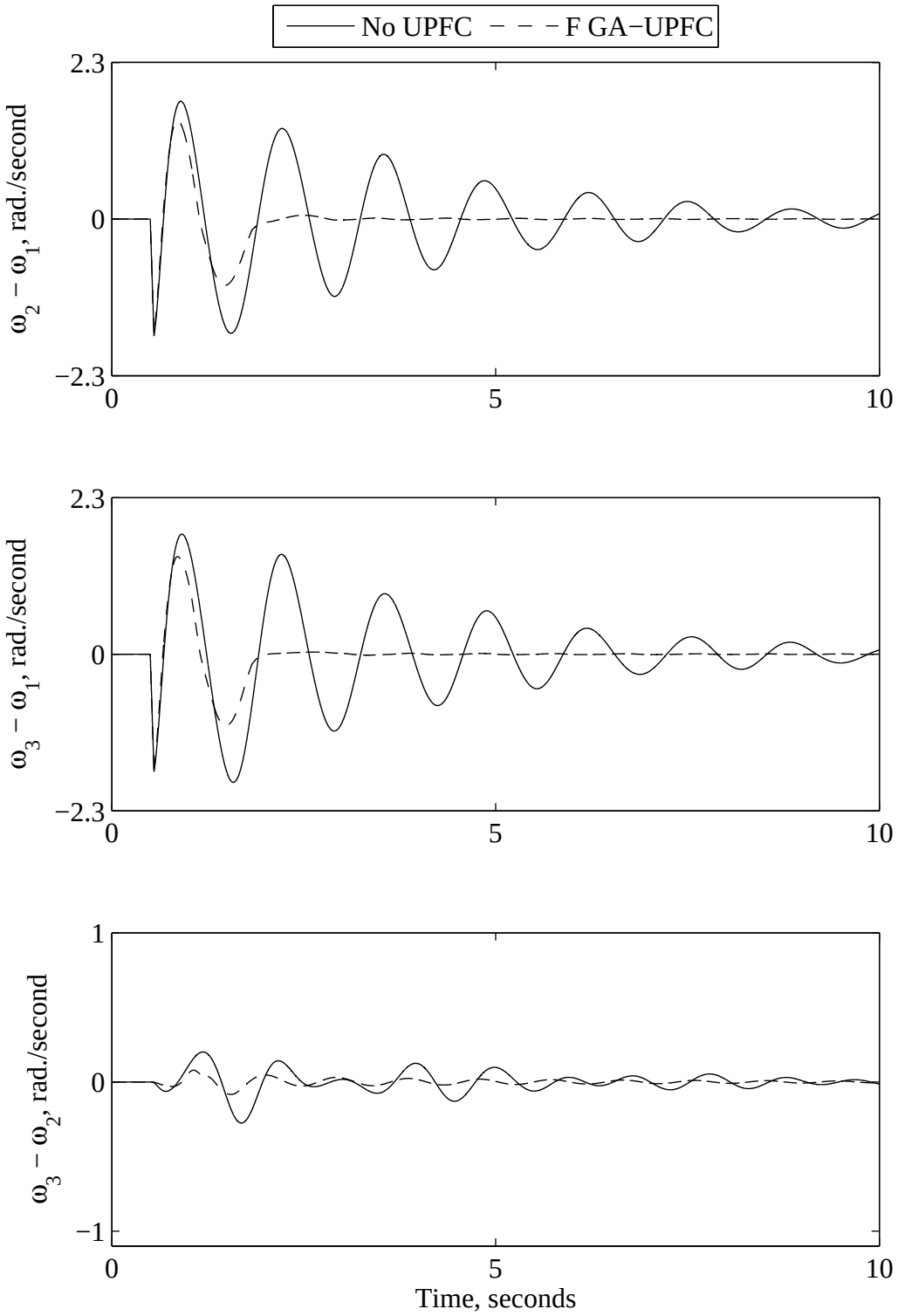

Figure 4.20 Relative generator speeds due to a 3-cycle three-phase fault at bus 1 (a UPFC is installed at LOC1).

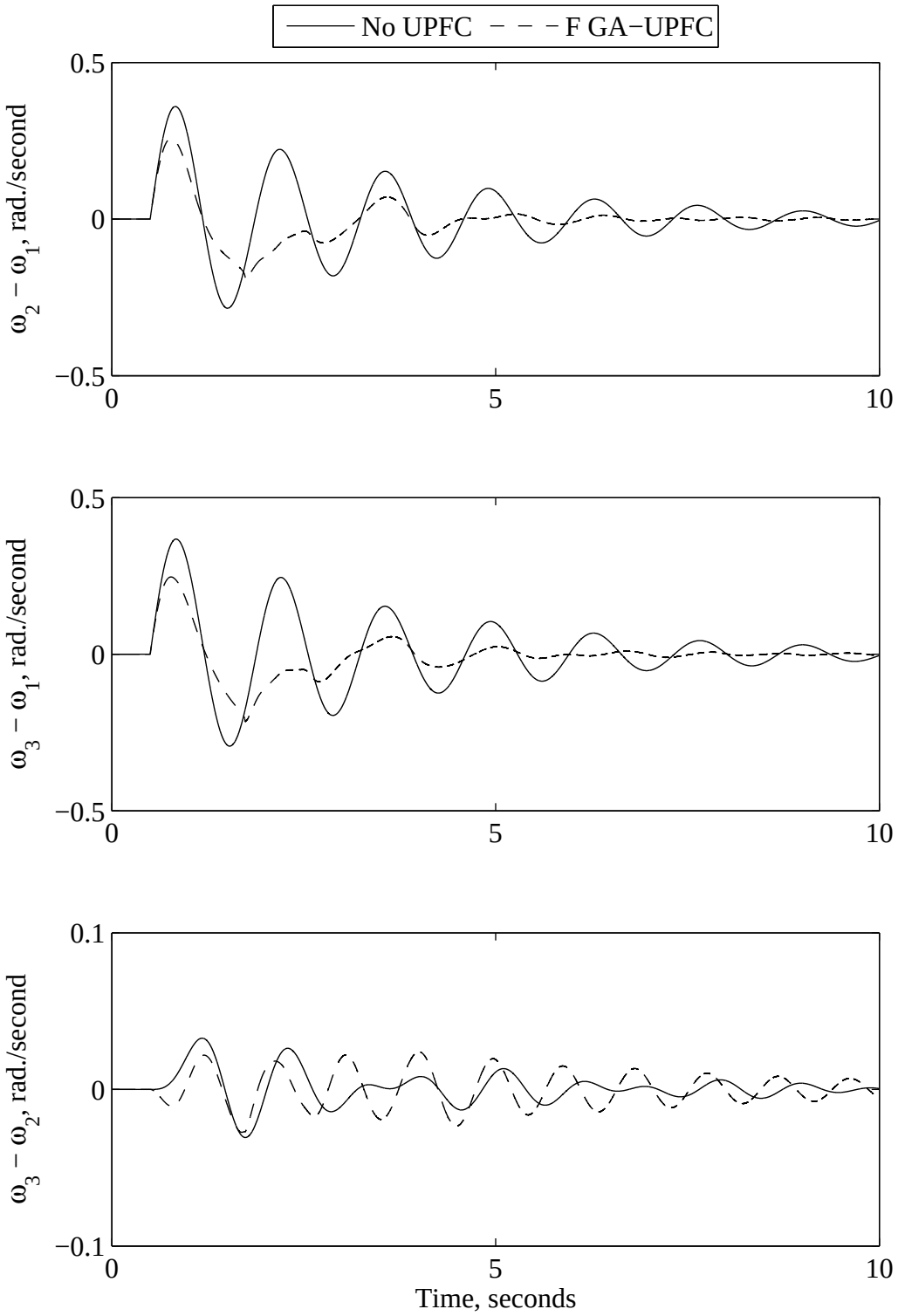

Figure 4.21 Relative generator speed responses for a 5% sudden decrease in the reference power of generator G_1 (a UPFC is installed at LOC1).

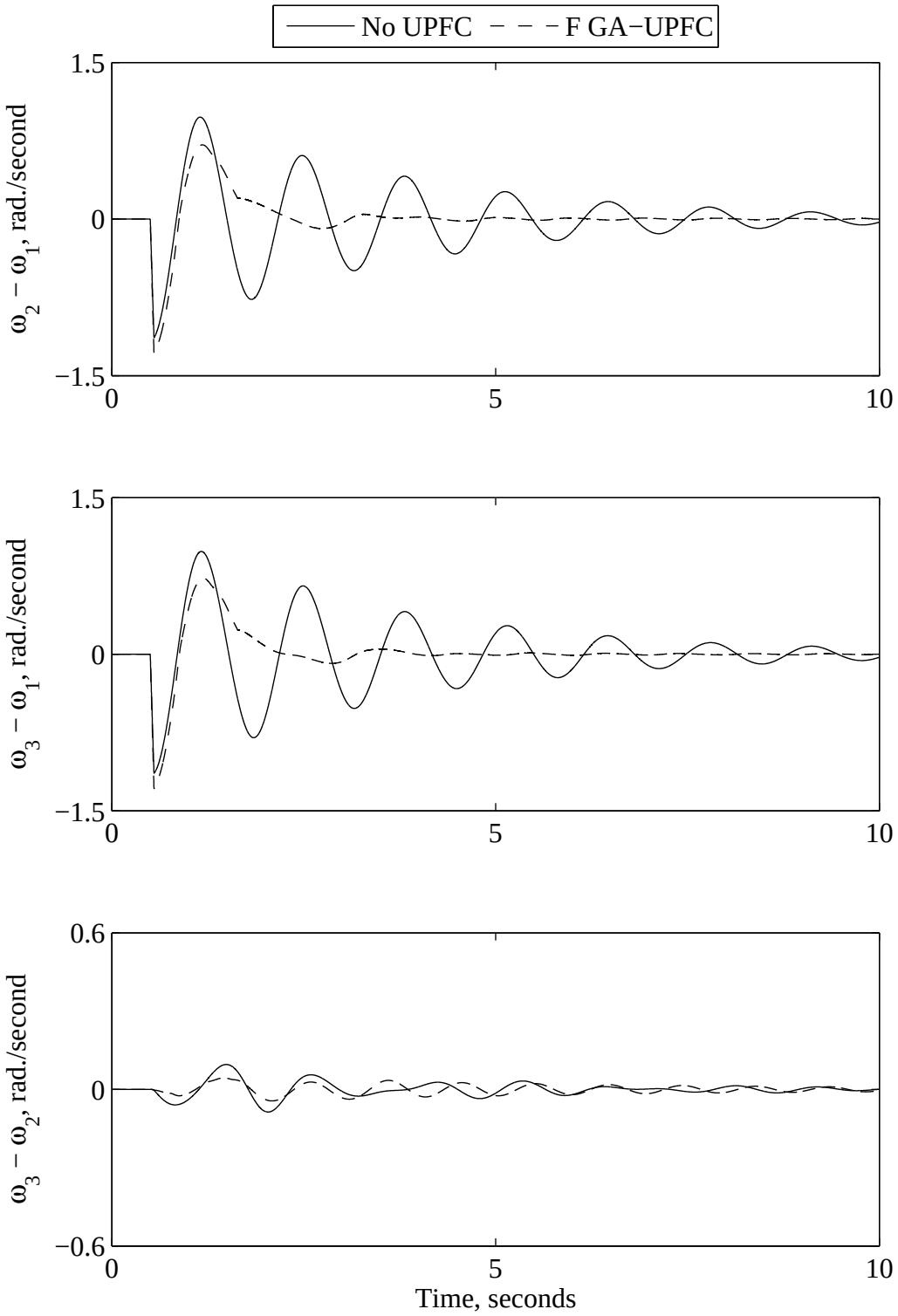

Figure 4.22 Relative generator speed responses due to a 3-cycle 95% sudden load decrease at bus 1 (a UPFC is installed at LOC1).

5. DAMPING INTERAREA OSCILLATIONS USING A GENERALIZED UNIFIED POWER FLOW CONTROLLER AND A VOLTAGE-SOURCE CONVERTER BACK-TO-BACK HVDC LINK

5.1. Introduction

In this chapter, the GA based optimization technique used previously for designing controllers for the UPFC is utilized to design PI controllers for two FACTS devices. These controllers are also aimed at enhancing the damping of interarea oscillations. The two FACTS devices considered are, a three-converter Generalized Unified Power Flow Controller (GUPFC) and a Voltage-Source Converter Back-to-Back HVdc link (VSC BtB). The three-area power system of Figure 3.2 is considered again in the investigations in this chapter with the FACTS controllers installed at different locations. The effectiveness of the proposed GA FACTS controllers in damping interarea oscillations is demonstrated through eigenvalue analysis as well as simulation results of typical time responses of different system disturbances.

5.2. GUPFC Controller Design

The proposed GUPFC shown schematically in Figures 5.1 and 5.2 consists of three voltage source converters operated from a common dc link provided by a dc storage capacitor. The shunt converters can be seen as independent Static Synchronous Compensators (STATCOM). The real power can flow between the three converters through the dc link providing great capability for power flow control as well as for damping power system oscillations. The real power constraint that must be satisfied by the GUPFC at steady-state is expressed mathematically as:

$$\mathrm{Re}\left\{V_{sh-i}I^{*}_{sh-i} + V_{sh-j}I^{*}_{sh-j} + V_{pq}I^{*}_{pq}\right\} = 0 \qquad (5\text{-}1)$$

For power flow studies, the three-voltage source model of the GUPFC is converted into four power injections as shown in Figure 5.3. These four power injections are similar to the case of the UPFC given in Section 2.2.1 with the addition of P_{j0}.

It is worth noting that the GUPFC can be regarded as two UPFCs connected back-to-back.

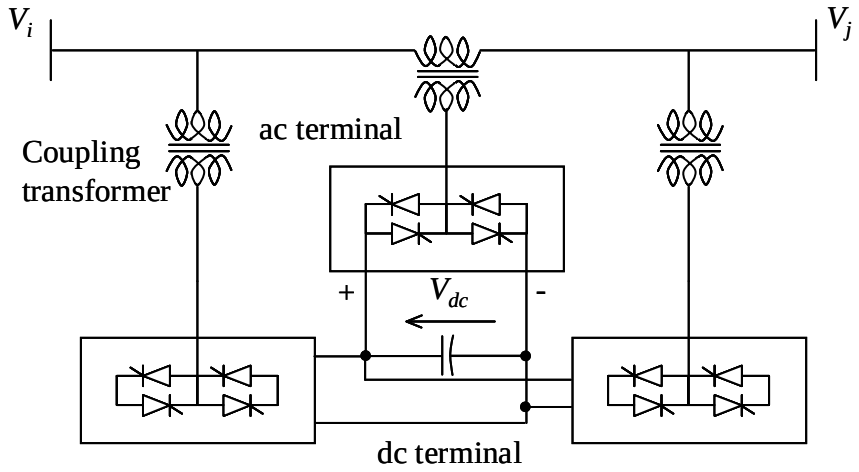

Figure 5.1 The GUPFC structure model.

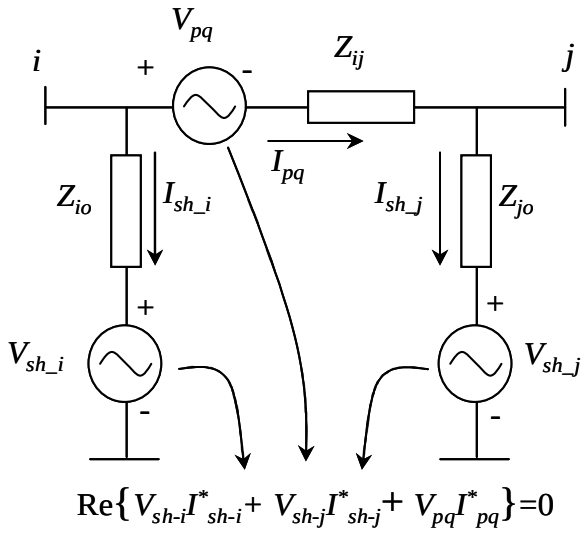

Figure 5.2 The GUPFC three voltage source model.

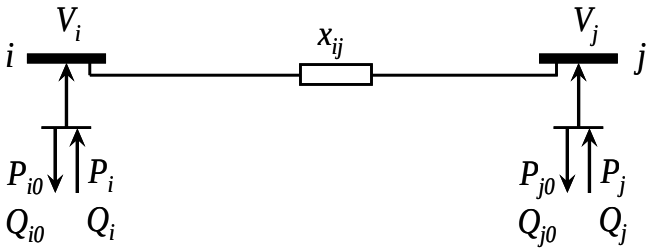

Figure 5.3 The GUPFC injected voltage model.

Tuning of power system damping controllers typically uses a small-signal model represented by the well-known state-space equations. The system state-space model is developed by linearizing the combined power system dynamic equations and the dynamic equations representing the GUPFC. These dynamic equations are expressed in the *d-q* reference frame as follow:

$$\begin{bmatrix} v_{sh-id} \\ v_{sh-iq} \end{bmatrix} = \begin{bmatrix} 0 & -x_E \\ x_E & 0 \end{bmatrix} \begin{bmatrix} i_{sh-id} \\ i_{sh-iq} \end{bmatrix} + \begin{bmatrix} \frac{m_{E-i} v_{dc} \cos \delta_{E-i}}{2} \\ \frac{m_{E-i} v_{dc} \sin \delta_{E-i}}{2} \end{bmatrix}$$

$$\begin{bmatrix} v_{sh-jd} \\ v_{sh-jq} \end{bmatrix} = \begin{bmatrix} 0 & -x_E \\ x_E & 0 \end{bmatrix} \begin{bmatrix} i_{sh-jd} \\ i_{sh-jq} \end{bmatrix} + \begin{bmatrix} \frac{m_{E-j} v_{dc} \cos \delta_{E-j}}{2} \\ \frac{m_{E-j} v_{dc} \sin \delta_{E-j}}{2} \end{bmatrix}$$

$$\begin{bmatrix} v_{pqd} \\ v_{pqq} \end{bmatrix} = \begin{bmatrix} 0 & -x_B \\ x_B & 0 \end{bmatrix} \begin{bmatrix} i_{pqd} \\ i_{pqq} \end{bmatrix} + \begin{bmatrix} \frac{m_B v_{dc} \cos \delta_B}{2} \\ \frac{m_B v_{dc} \sin \delta_B}{2} \end{bmatrix}$$

$$\begin{aligned} \frac{dv_{dc}}{dt} = {} & \frac{3m_{E-i}}{4C_{dc}} \begin{bmatrix} \cos(\delta_{E-i}) & \sin(\delta_{E-i}) \end{bmatrix} \begin{bmatrix} i_{sh-id} \\ i_{sh-iq} \end{bmatrix} + \frac{3m_{E-j}}{4C_{dc}} \begin{bmatrix} \cos(\delta_{E-j}) & \sin(\delta_{E-j}) \end{bmatrix} \begin{bmatrix} i_{sh-jd} \\ i_{sh-jq} \end{bmatrix} \\ & + \frac{3m_B}{4C_{dc}} \begin{bmatrix} \cos(\delta_B) & \sin(\delta_B) \end{bmatrix} \begin{bmatrix} i_{pqd} \\ i_{pqq} \end{bmatrix} \end{aligned} \tag{5-2}$$

Figure 5.4 shows the transfer function of a PI controller whose output U_i controls the magnitude $|V_{inj}|$ and the phase angle δ_{inj} of the injected voltage V_{inj} of a voltage-source converter. The GUPFC controller, therefore, has three such controllers. The GA technique developed in this thesis is used again to adjust the PI controller parameters. The variation in generator speeds $\Delta\omega_1$, $\Delta\omega_2$ and $\Delta\omega_3$ are selected again in the controller design as stabilizing signals. With this selection, the GUPFC controller is a centralized three-input, three-output controller with global signals.

Table 5-1 shows the effect on the system eigenvalues of employing the GUPFC at LOC1. For the sake of comparison, the system eigenvalues in the case of a UPFC

installed at the same location are also given in Table 5-1. It can be seen from Table 5-1 that the system eigenvalues are shifted to the left with the employment of the GUPFC and UPFC resulting in better system performance. It can also be seen from the same table that the GUPFC provides slightly a better system performance than the UPFC.

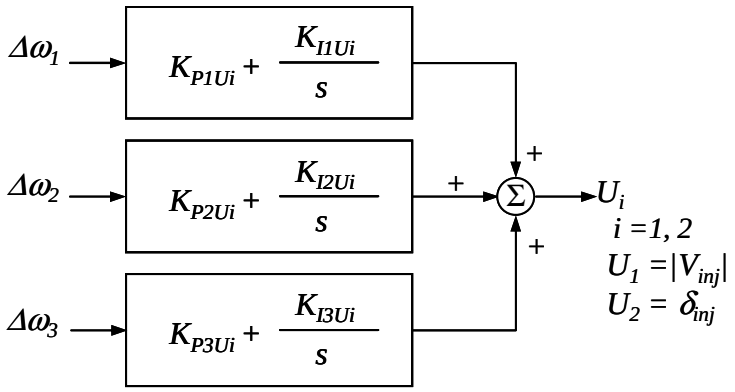

Figure 5.4 A PI controller structure for each voltage-source converter.

Table 5-1 System eigenvalues for GUPFC controller

System eigenvalues		
No FACTS	GA PI GUPFC	GA PI UPFC
-0.1649 ± *j*4.6393	-1.7877 ± *j*0.0518	-1.6088
-0.2309 ± *j*6.6423	-2.1280 ± *j*4.9780	-1.6213 ± *j*5.7847
-0.5410 ± *j*5.2272	-2.1612 ± *j*3.3170	-1.8029 ± *j*1.2063
-1.4757	-2.3056 ± *j*7.9171	-2.8255 ± *j*7.0481
-2.0865	-3.2811	-3.2365 ± *j*1.9593
-4.6719	-15.0031	-16.3615
-14.7535	-17.9412	-16.7835
-17.7718	-18.6018	-18.6242
-18.7702		

5.3. VSC BtB Controller Design

The HVdc Back-to-Back system shown in Figures 5.5 and 5.6 is known as HVdc Light [75]-[81]. It consists of two voltage-source converters operated from a common dc link provided by a dc storage capacitor. The fundamental difference between a voltage source converter and a current source converter (used in conventional HVdc systems) makes the performances of the HVdc Light different from that of the conventional HVdc

system [82]. In general, the VSC HVdc has the following advantages compared with the current source converter HVdc:

1- Active and reactive power exchange can be controlled flexibly and independently.

2- The power quality and system stability can be improved via continuously adjustable reactive power support with AC voltage feedback control.

3- Possible to feed AC systems with low short circuit power or even passive networks with no local power generation.

4- Power flow direction can be easily changed without changing the polarity of DC link.

This arrangement virtually isolates dynamically the two sides of the system by controlling the voltage at both sides. Thus, the VSC BtB decouples the interarea dynamics as well as provides damping to the system. The real power constraint that must be satisfied by the VSC BtB at steady-state is expressed mathematically as:

$$\mathrm{Re}\left\{ V_{sh-i} I^{*}_{sh-i} + V_{sh-j} I^{*}_{sh-j} \right\} = 0 \tag{5-3}$$

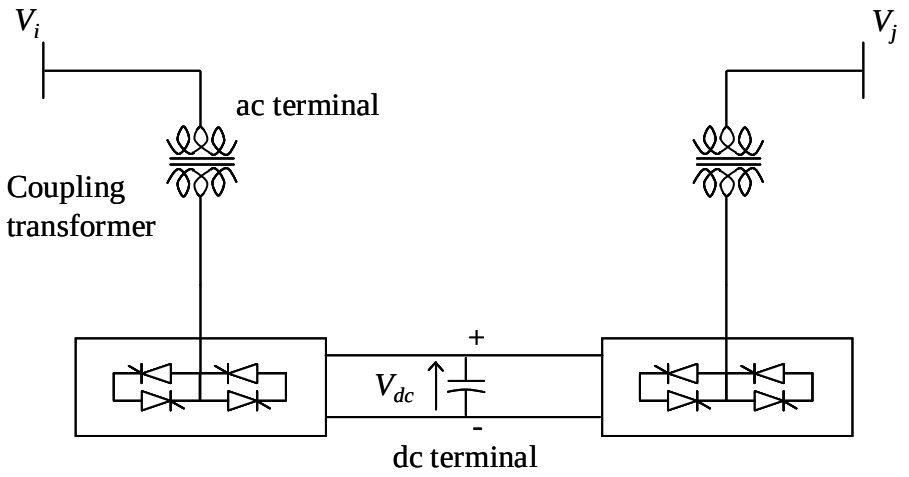

Figure 5.5 The VSC BtB Structure model.

For power flow studies, the two-voltage source model of the VSC BtB is converted into two power injections as shown in Figure 5.7. In order to fulfill this constraint, one of the

two shunt voltages is adjusted according to the other shunt voltage as well as the voltage at buses *i* and *j*. In the studies conducted in this chapter, the phase angle of the voltage $V_{sh\text{-}i}$ is adjusted according to the following equation:

$$\delta_{sh-i} = \delta_j - \sin^{-1}\left[\frac{|V_i||V_{sh-i}|x_{jo}}{|V_j||V_{sh-j}|x_{io}}\sin(\delta_{sh-i} - \delta_i)\right] \tag{5-4}$$

Where, $V_{sh\text{-}i} = |V_{sh\text{-}i}|\angle\delta_{sh\text{-}i}$, $V_{sh\text{-}j} = |V_{sh\text{-}j}|\angle\delta_{sh\text{-}j}$ and $Z_{io}=jx_{io}$, $Z_{jo}=jx_{jo}$

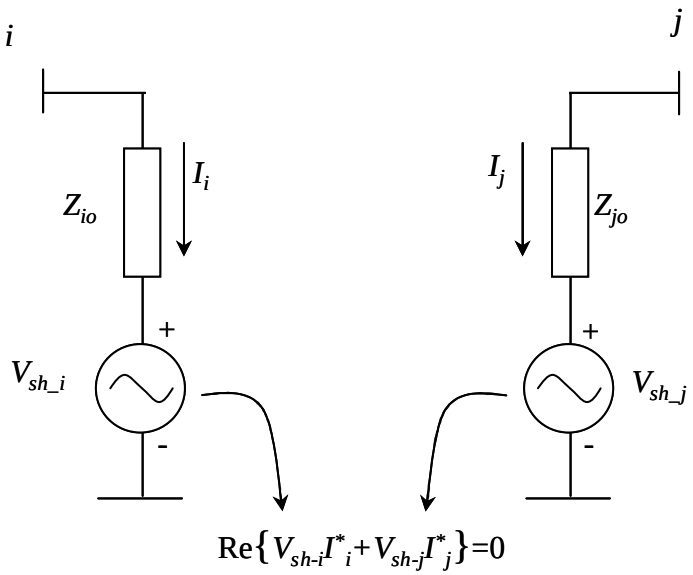

Figure 5.6 The VSC BtB voltage source model.

Figure 5.7 The VSC BtB injected voltage model.

A small-signal model represented by state-space equations is used again in this section to tune the VSC BtB controller parameters. The system state-space model is developed by linearizing the combined power system dynamic equations and the dynamic equations representing the VSC BtB device. These dynamic equations are expressed in the *d-q* reference frame as follows:

$$\begin{bmatrix} v_{sh-id} \\ v_{sh-iq} \end{bmatrix} = \begin{bmatrix} 0 & -x_E \\ x_E & 0 \end{bmatrix} \begin{bmatrix} i_{sh-id} \\ i_{sh-iq} \end{bmatrix} + \begin{bmatrix} \frac{m_{E-i} v_{dc} \cos \delta_{E-i}}{2} \\ \frac{m_{E-i} v_{dc} \sin \delta_{E-i}}{2} \end{bmatrix}$$

$$\begin{bmatrix} v_{sh-jd} \\ v_{sh-jq} \end{bmatrix} = \begin{bmatrix} 0 & -x_E \\ x_E & 0 \end{bmatrix} \begin{bmatrix} i_{sh-jd} \\ i_{sh-jq} \end{bmatrix} + \begin{bmatrix} \frac{m_{E-j} v_{dc} \cos \delta_{E-j}}{2} \\ \frac{m_{E-j} v_{dc} \sin \delta_{E-j}}{2} \end{bmatrix}$$

$$\frac{dv_{dc}}{dt} = \frac{3m_{E-i}}{4C_{dc}} \begin{bmatrix} \cos(\delta_{E-i}) & \sin(\delta_{E-i}) \end{bmatrix} \begin{bmatrix} i_{sh-id} \\ i_{sh-iq} \end{bmatrix} + \frac{3m_{E-j}}{4C_{dc}} \begin{bmatrix} \cos(\delta_{E-j}) & \sin(\delta_{E-j}) \end{bmatrix} \begin{bmatrix} i_{sh-jd} \\ i_{sh-jq} \end{bmatrix} \quad (5\text{-}5)$$

The same PI controller structure used in the previous section is considered in this study. The VSC BtB controller has two such PI controllers. The adjustment of the controller parameters is done again by employing the developed GA technique. The variation in generator speeds $\Delta\omega_1$, $\Delta\omega_2$ and $\Delta\omega_3$ are selected also in the controller design as stabilizing signals. With this selection, the FACTS controller is a centralized three-input, two-output controller with global signals. Table 5-2 shows the effect on the system eigenvalues of employing the VSC BtB at LOC1. The system eigenvalues in the case of a UPFC installed at the same location are also given in Table 5-2. It can be seen from Table 5-2 that the system eigenvalues are shifted to the left with the employment of the VSC BtB and UPFC, resulting in a better system performance. It can also be seen from the same table that the VSC BtB provides a slightly better system performance than the UPFC.

Table 5-2 System eigenvalues for VSC BtB controller

System eigenvalues		
No FACTS	GA PI VSC BtB	GA PI UPFC
$-0.1649 \pm j4.6393$	-1.6781	-1.6088
$-0.2309 \pm j6.6423$	$-1.7024 \pm j7.5179$	$-1.6213 \pm j5.7847$
$-0.5410 \pm j5.2272$	$-1.8723 \pm j2.5965$	$-1.8029 \pm j1.2063$
-1.4757	-2.2415	$-2.8255 \pm j7.0481$
-2.0865	$-2.2443 \pm j4.3791$	$-3.2365 \pm j1.9593$
-4.6719	-6.9194	-16.3615
-14.7535	-13.7851	-16.7835
-17.7718	-17.7972	-18.6242
-18.7702	-18.564	

5.4. GA Based GUPFC Controller Performance during System Faults

To demonstrate the effectiveness of the proposed GUPFC controller, several simulation studies representing small and large disturbances are carried out on the system under investigation. The system pre-disturbance operating condition presented in Section 3.5 is considered again in these studies. Moreover, for all these disturbances the performance of the GUPFC is compared with the performance of a UPFC installed at the same location.

5.4.1. Effect of the Fault Location

The effectiveness of the proposed GUPFC controller in damping interarea oscillations during large system disturbances is examined through simulating three-phase faults at generator buses with the GUPFC installed at LOC1. Figures 5.8 to 5.10 illustrate the time responses of the relative generator speeds due to a 3-cycle three-phase fault at buses 1, 2 and 3 respectively. The time responses of the generator terminal voltages and real powers are shown respectively in Figures 5.11 and 5.12. The dc link capacitor voltage and the dc power of the GUPFC are illustrated respectively in Figures 5.13 and 5.14. It can be seen from these figures that the GUPFC controller significantly damps the system oscillations. These figures show also that the GUPFC performs relatively better than the UPFC. It can also be seen that the fault location affect the performance of the FACTS devices. Comparing Figure 5.8 with Figures 5.9 and 5.10, shows that the GUPFC controller is again more effective in damping the system oscillations in the case of the three-phase fault at bus 1. This is again due to the closeness of bus 1 to the GUPFC location.

5.4.2. Effect of the GUPFC Location

In this section, the effect of the location of the GUPFC controller on the damping of the interarea oscillations is examined. The locations presented in Section 3.5.2 are considered again in these investigations. The time responses of the relative generator speeds in case of the GUPFC device installed at LOC1 were illustrated in Figures 5.8 to 5.10 while the time responses of the other locations are shown in Figures 5.15 to 5.23. It can be seen from Figures 5.8 to 5.10 and Figures 5.15 to 5.23 that the location of the

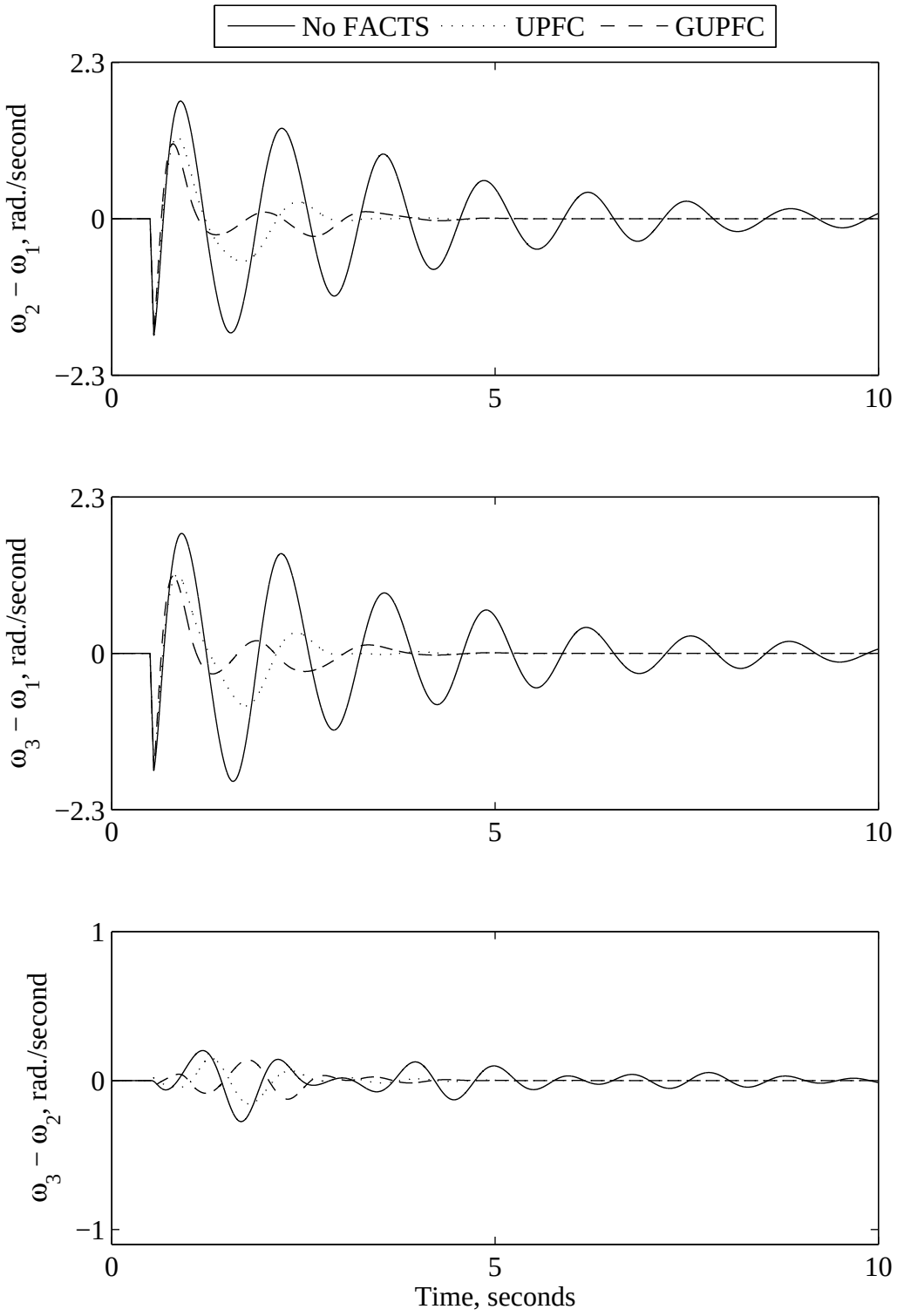

Figure 5.8 Relative generator speeds due to a 3-cycle three-phase fault at bus 1 (a GUPFC is installed at LOC1).

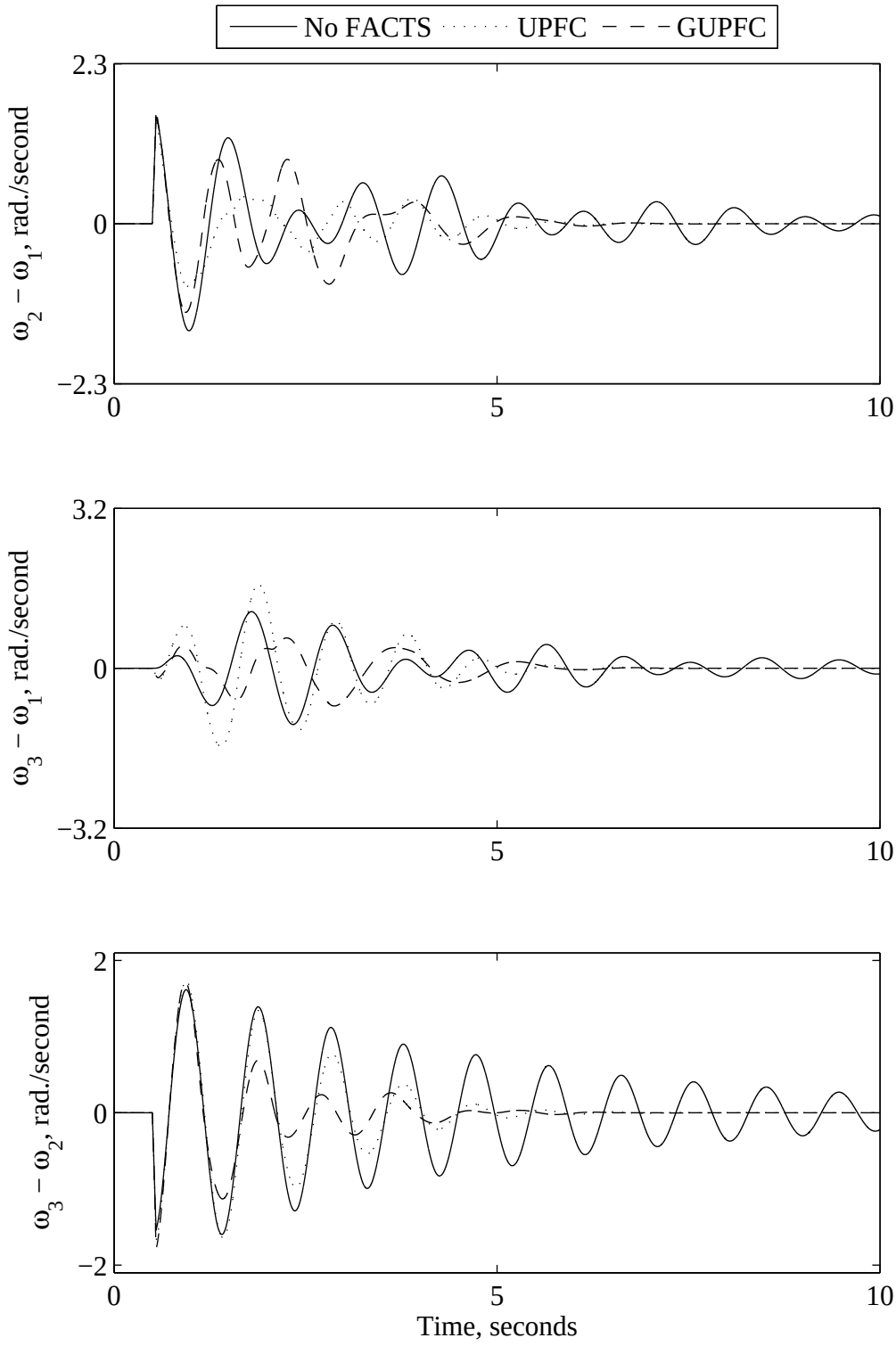

Figure 5.9 Relative generator speeds due to a 3-cycle three-phase fault at bus 2 (a GUPFC is installed at LOC1).

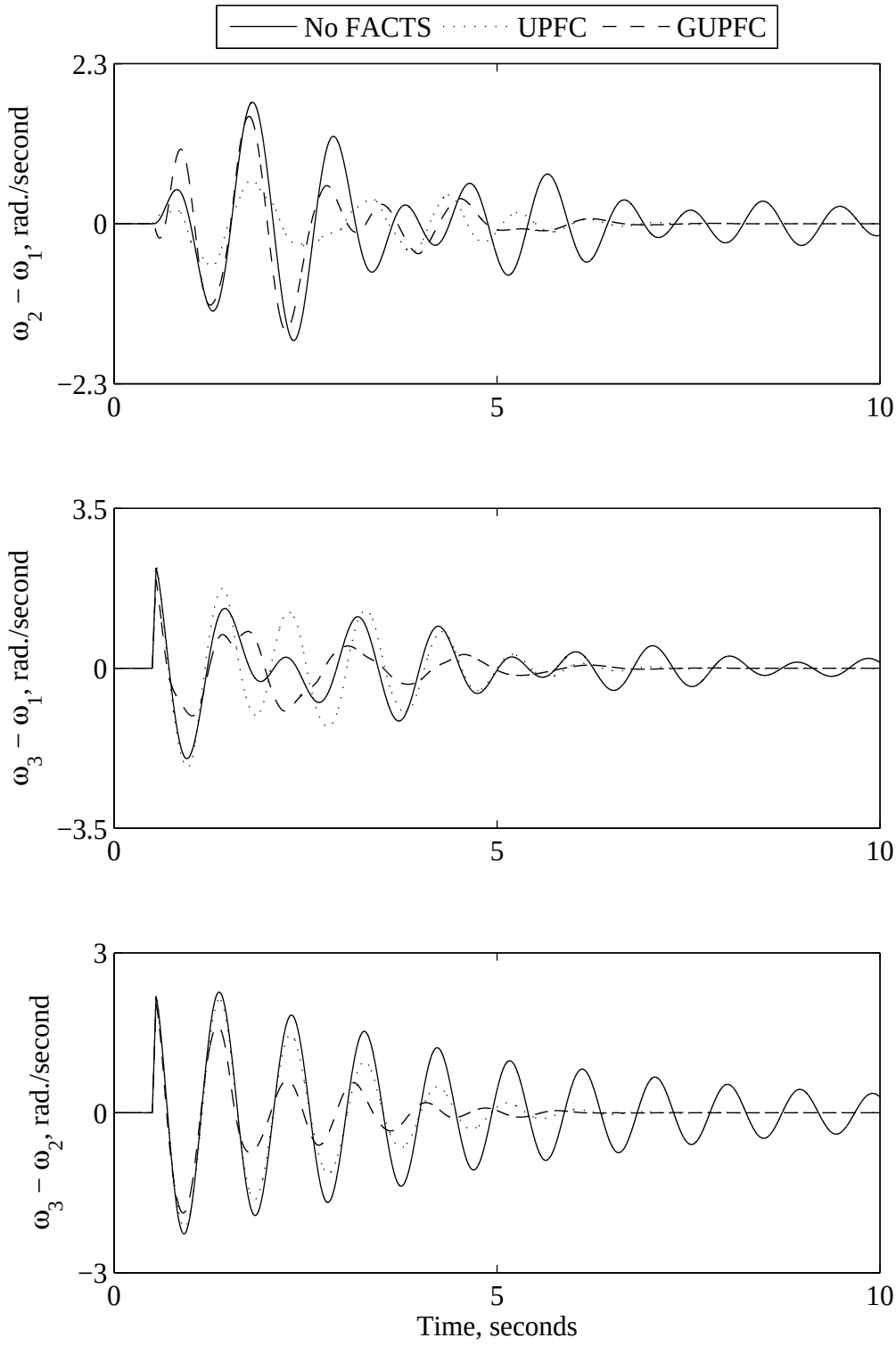

Figure 5.10 Relative generator speeds due to a 3-cycle three-phase fault at bus 3 (a GUPFC is installed at LOC1).

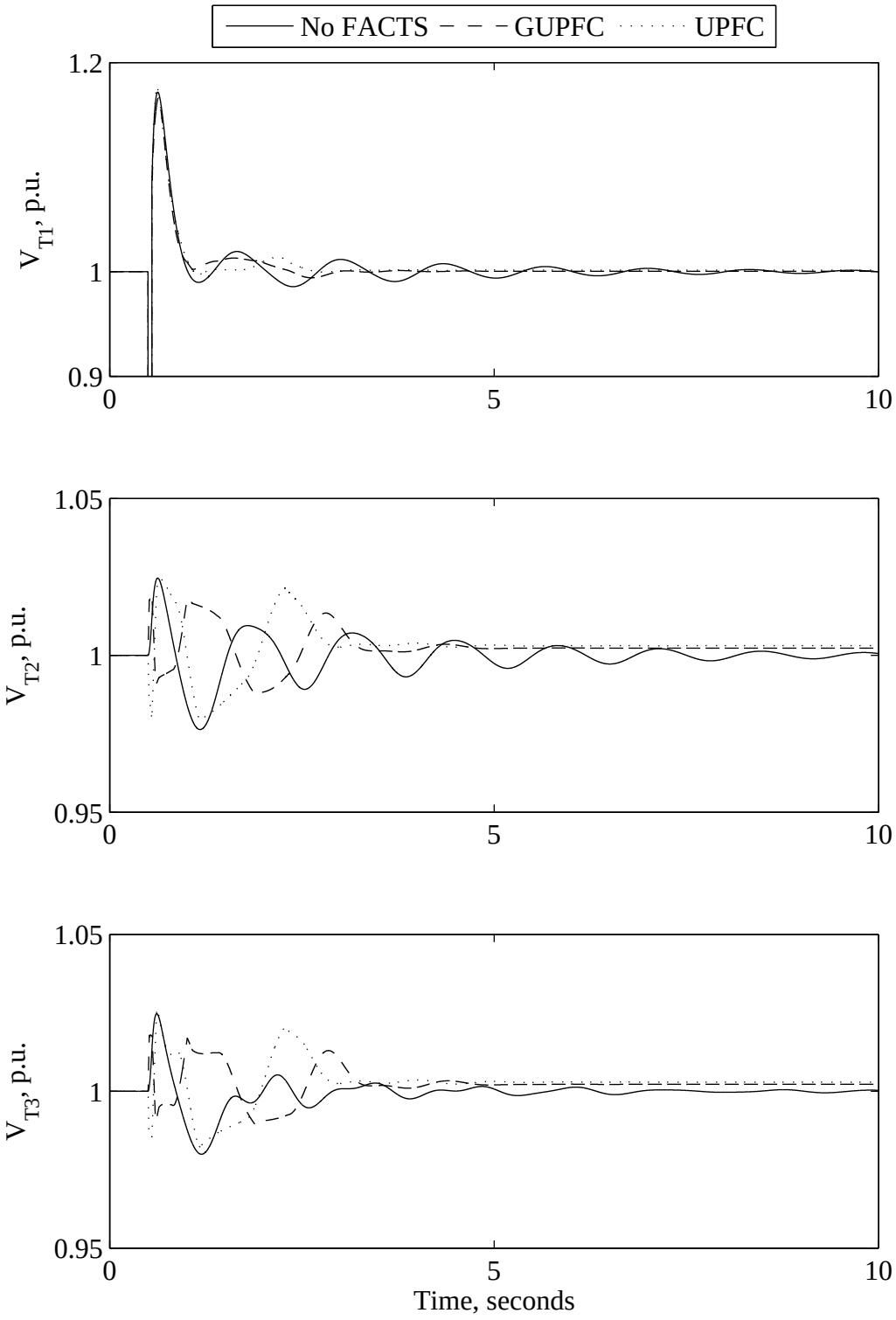

Figure 5.11 Generator terminal voltages due to a 3-cycle three-phase fault at bus 1 (a GUPFC is installed at LOC1).

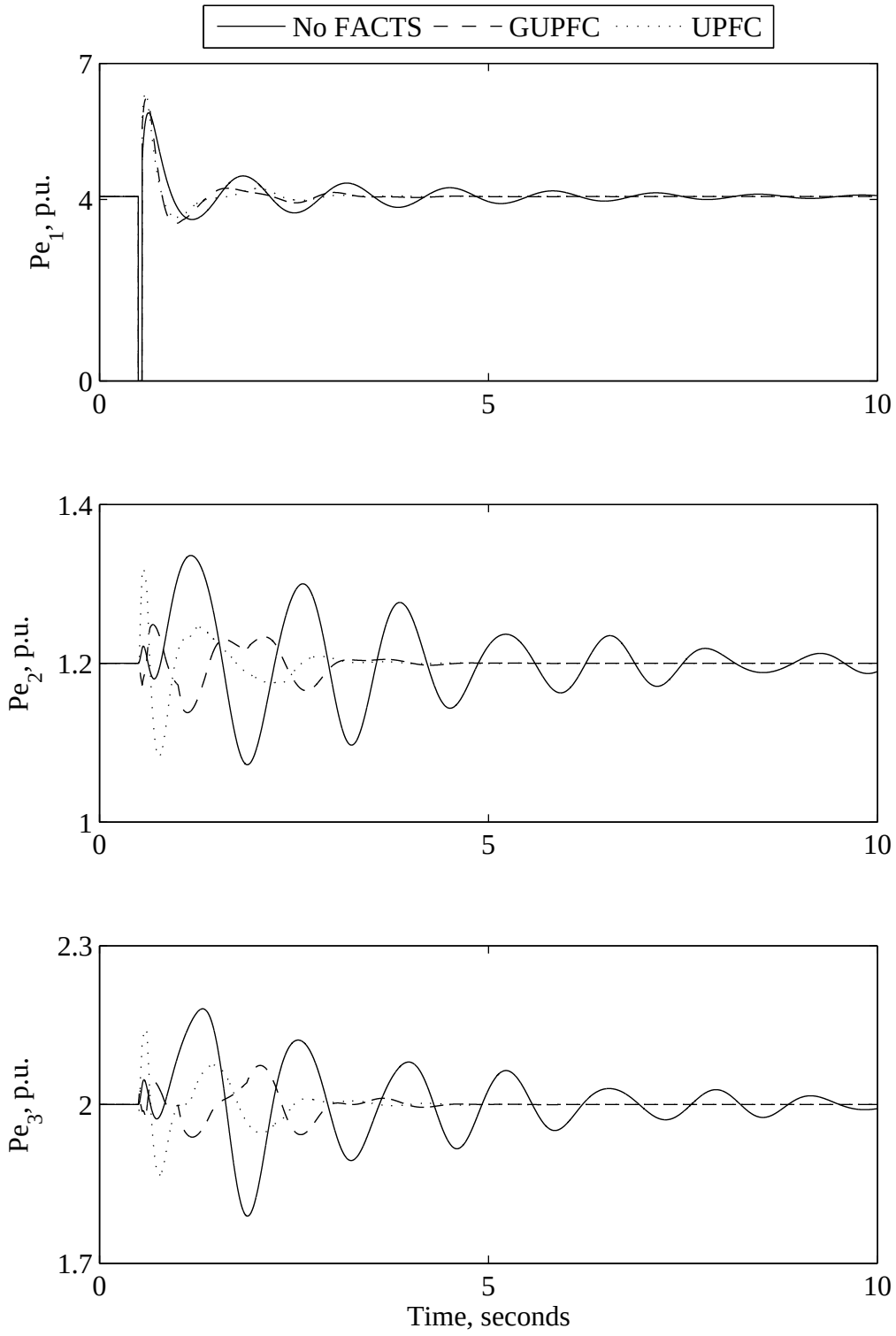

Figure 5.12 Generator real powers due to a 3-cycle three-phase fault at bus 1 (a GUPFC is installed at LOC1).

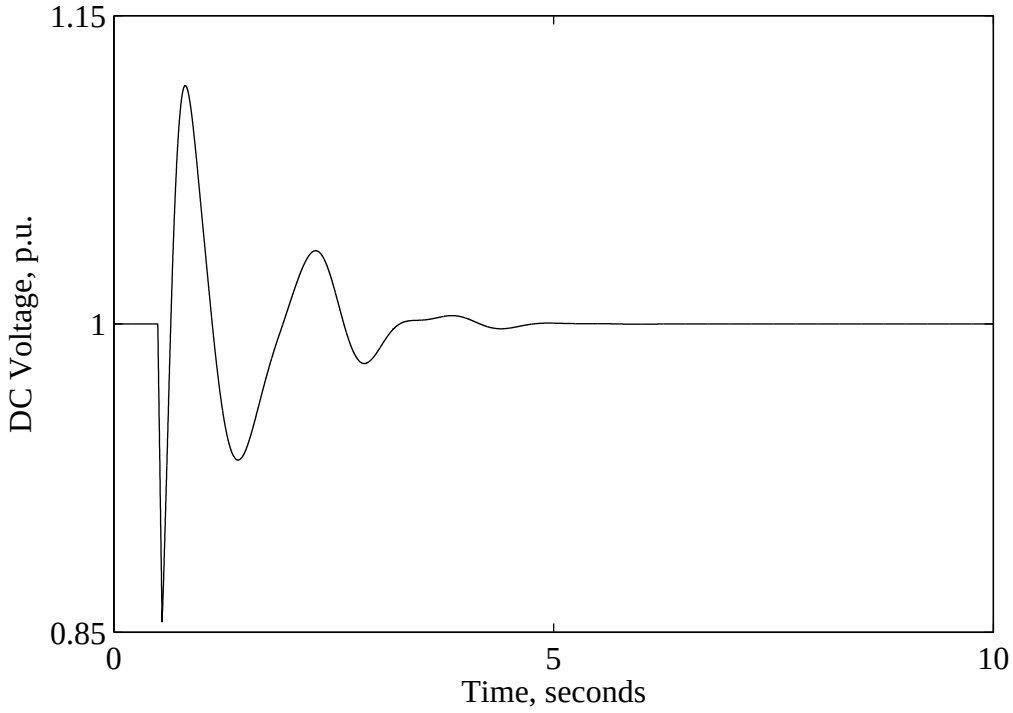

Figure 5.13 GUPFC dc-link capacitor voltage due to a 3-cycle three-phase fault at bus 1 (a GUPFC is installed at LOC1).

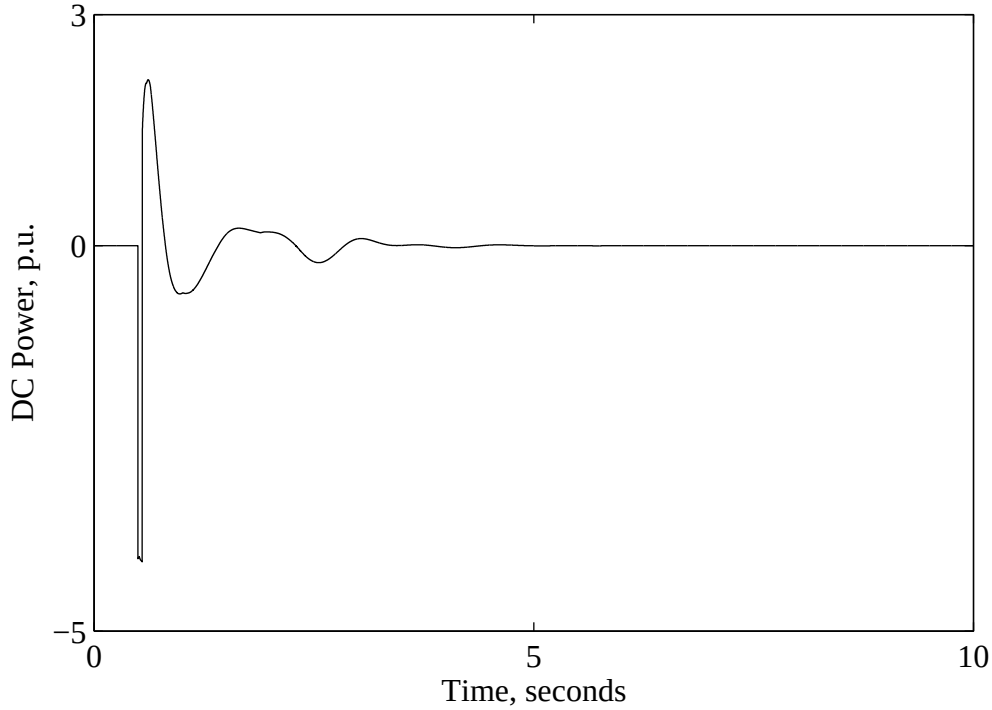

Figure 5.14 GUPFC dc power due to a 3-cycle three-phase fault at bus 1 (a GUPFC is installed at LOC1).

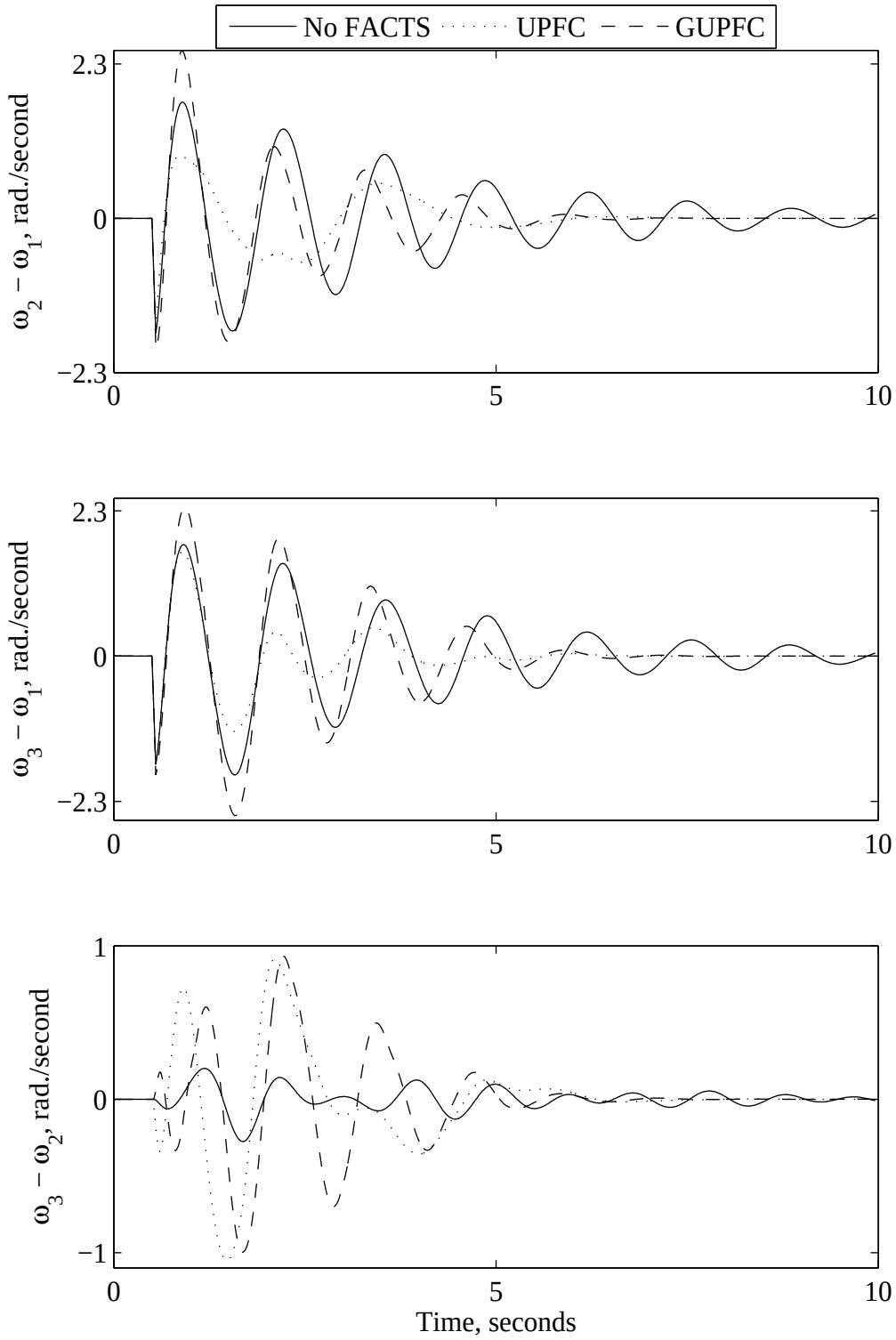

Figure 5.15 Relative generator speeds due to a 3-cycle three-phase fault at bus 1 (a GUPFC is installed at LOC2).

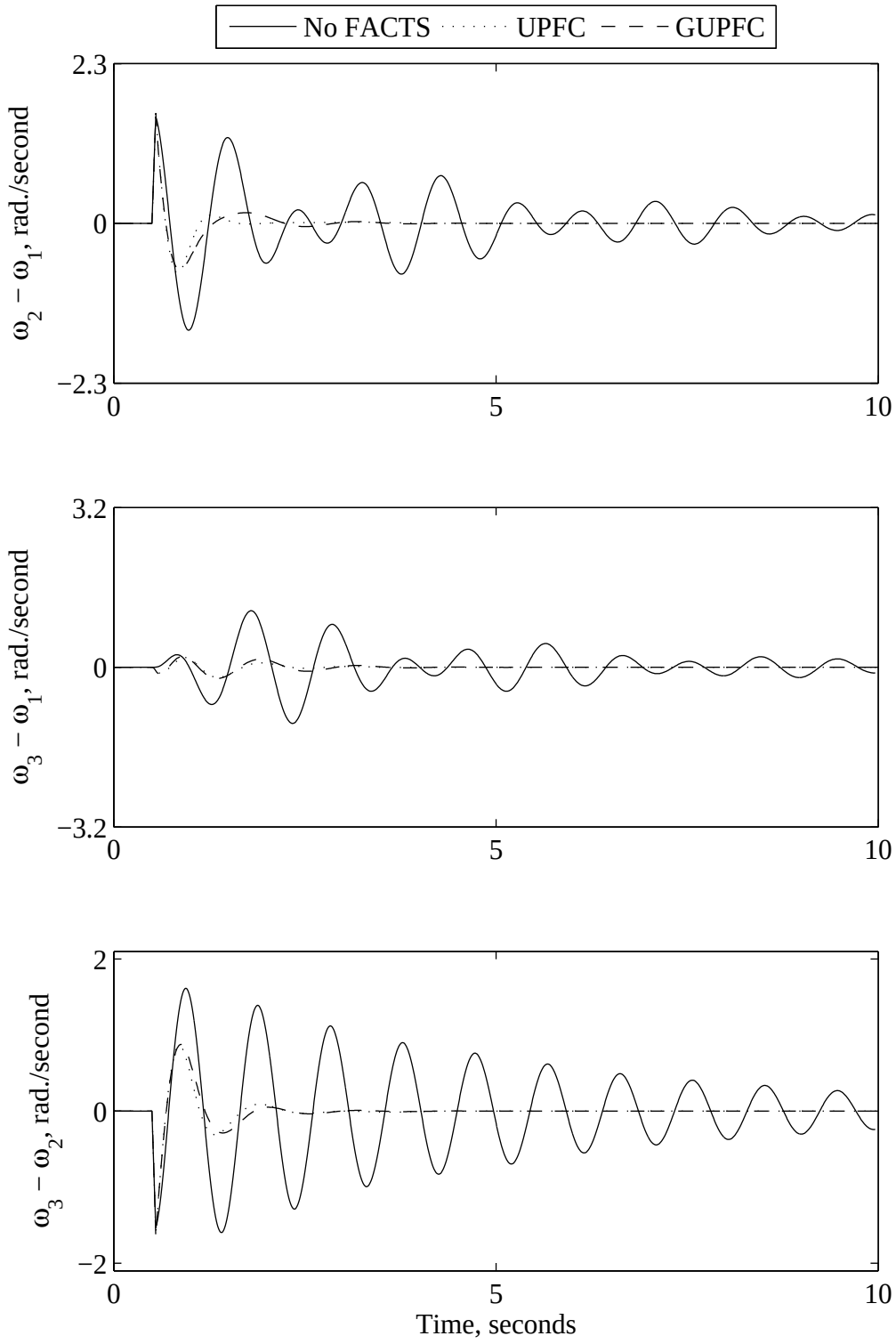

Figure 5.16 Relative generator speeds due to a 3-cycle three-phase fault at bus 2 (a GUPFC is installed at LOC2).

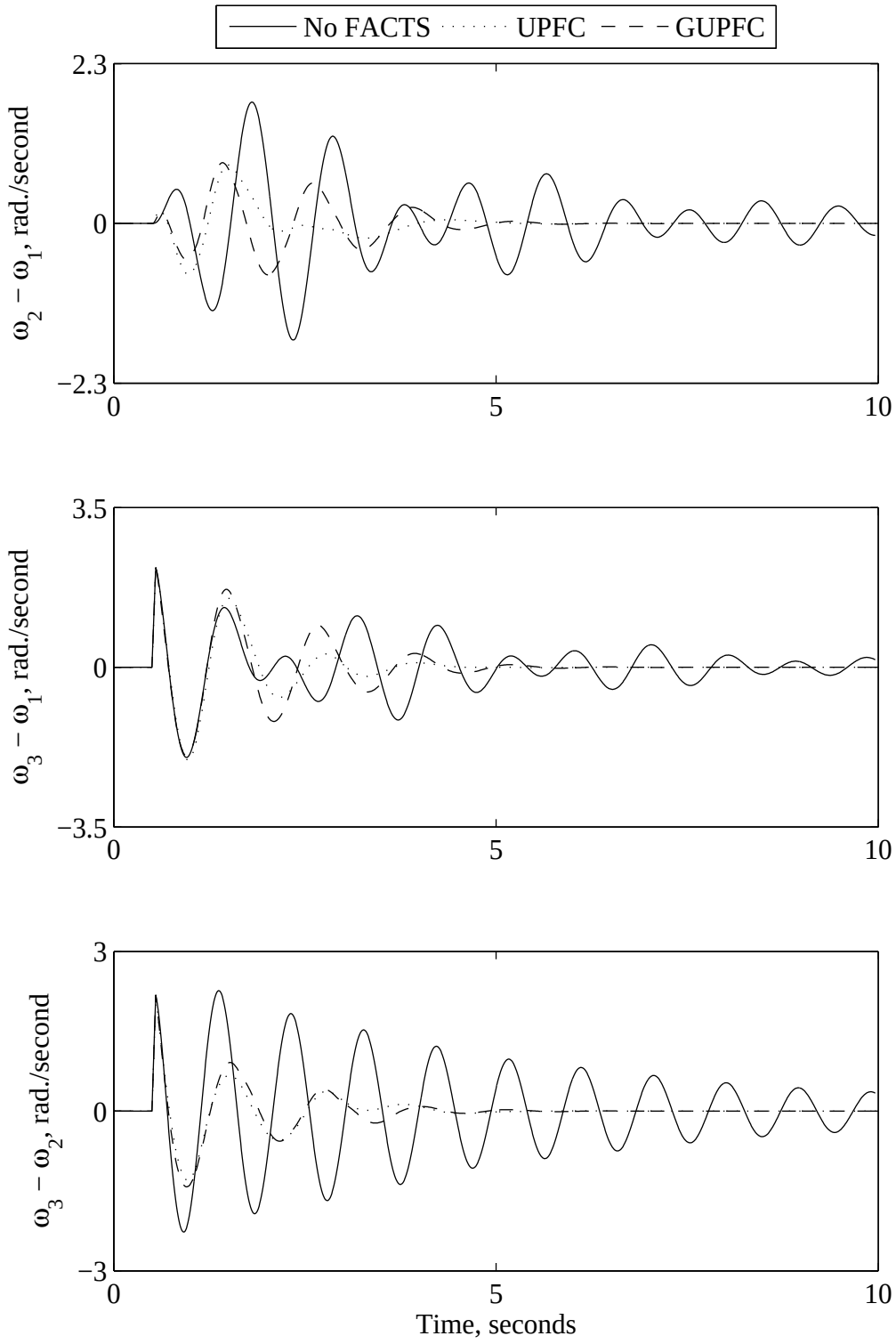

Figure 5.17 Relative generator speeds due to a 3-cycle three-phase fault at bus 3 (a GUPFC is installed at LOC2).

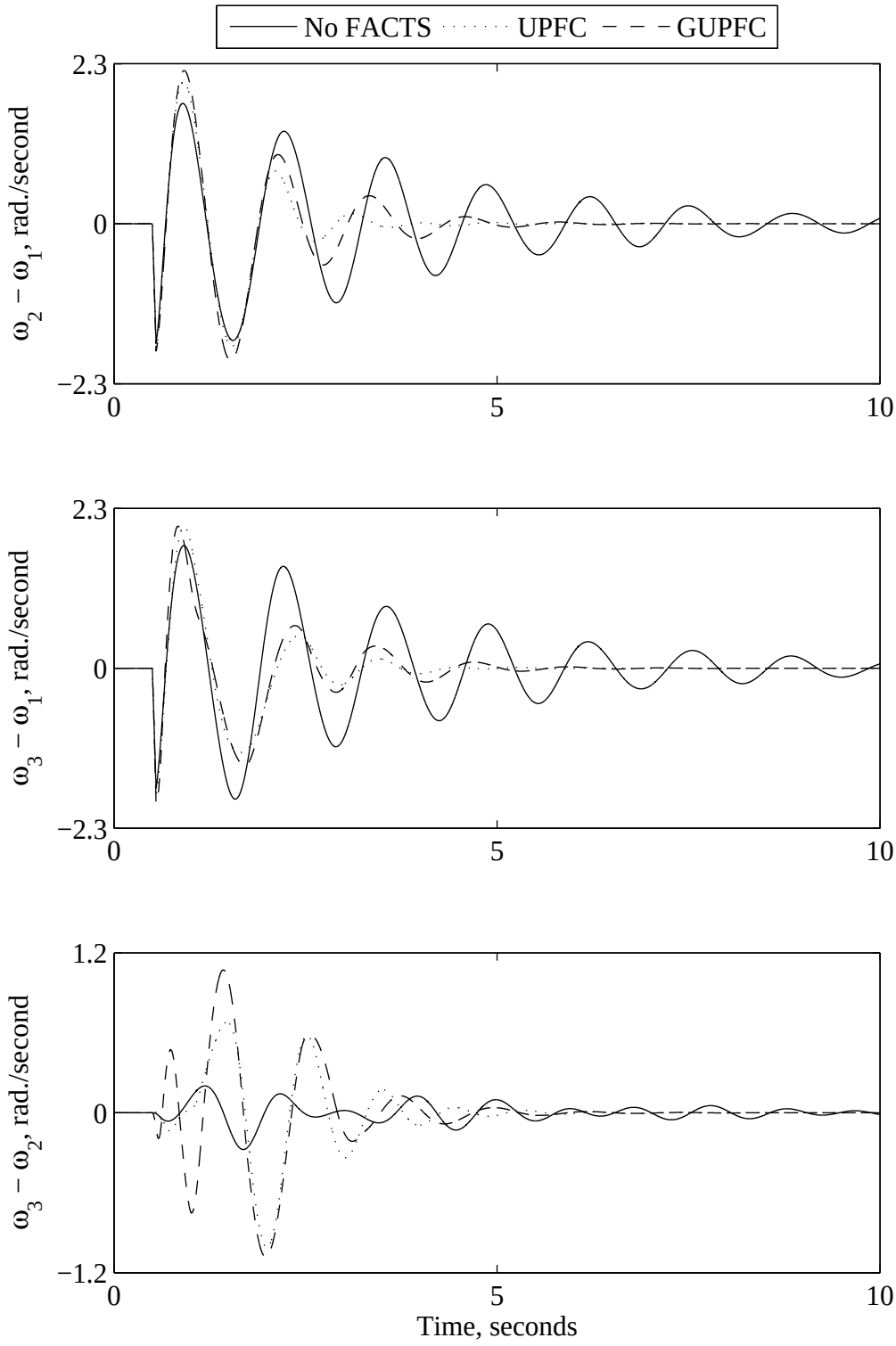

Figure 5.18 Relative generator speeds due to a 3-cycle three-phase fault at bus 1 (a GUPFC is installed at LOC3).

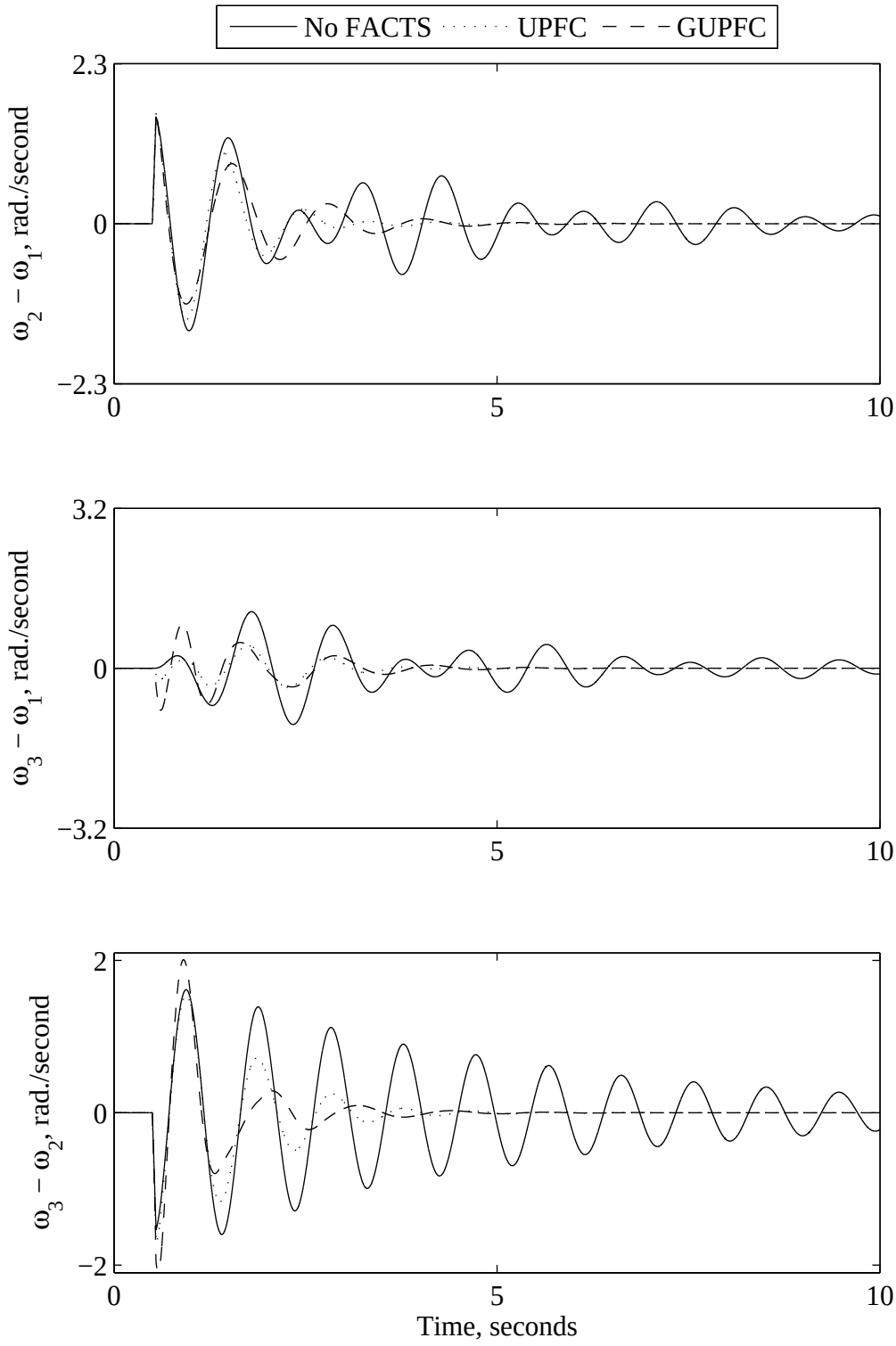

Figure 5.19 Relative generator speeds due to a 3-cycle three-phase fault at bus 2 (a GUPFC is installed at LOC3).

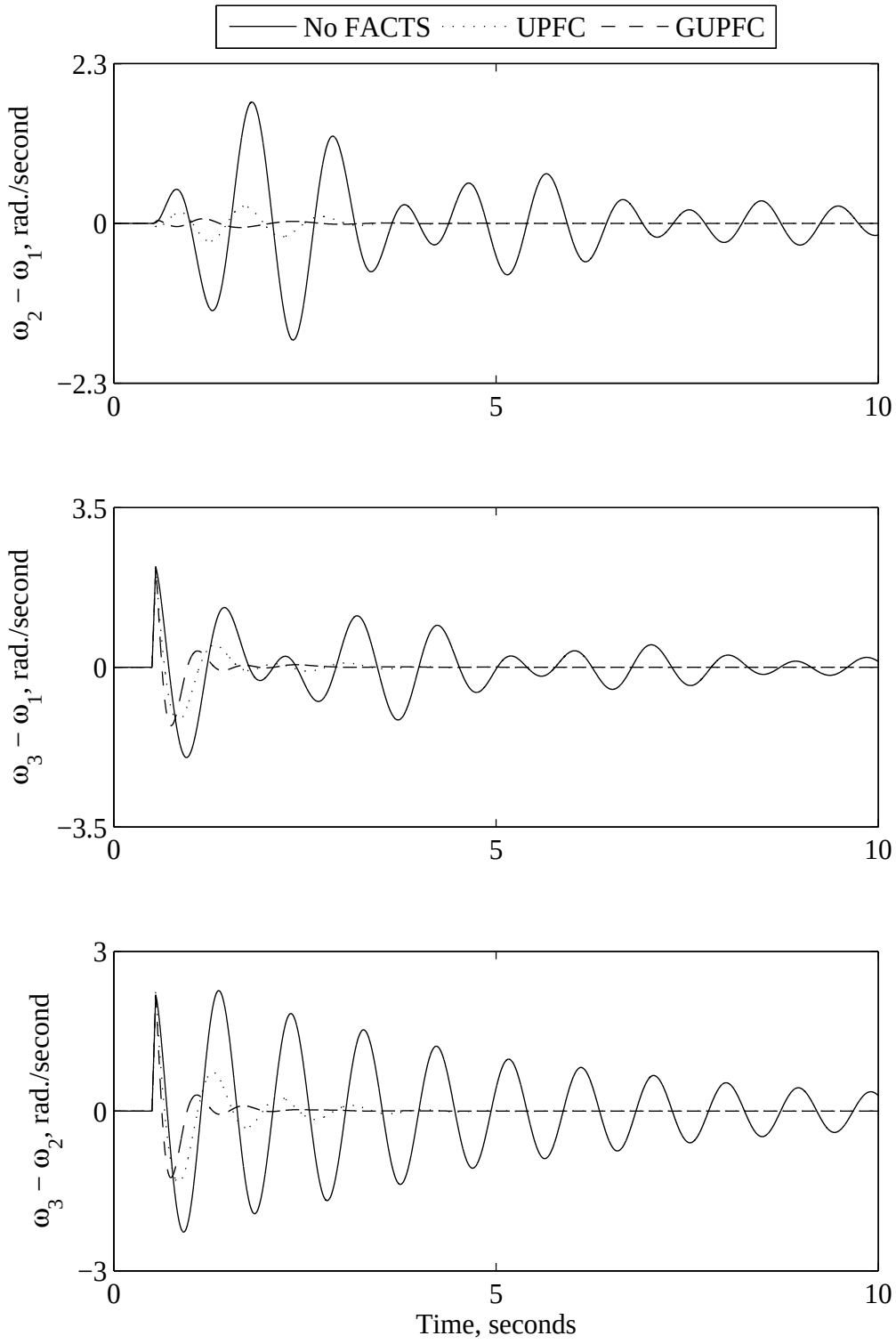

Figure 5.20 Relative generator speeds due to a 3-cycle three-phase fault at bus 3 (a GUPFC is installed at LOC3).

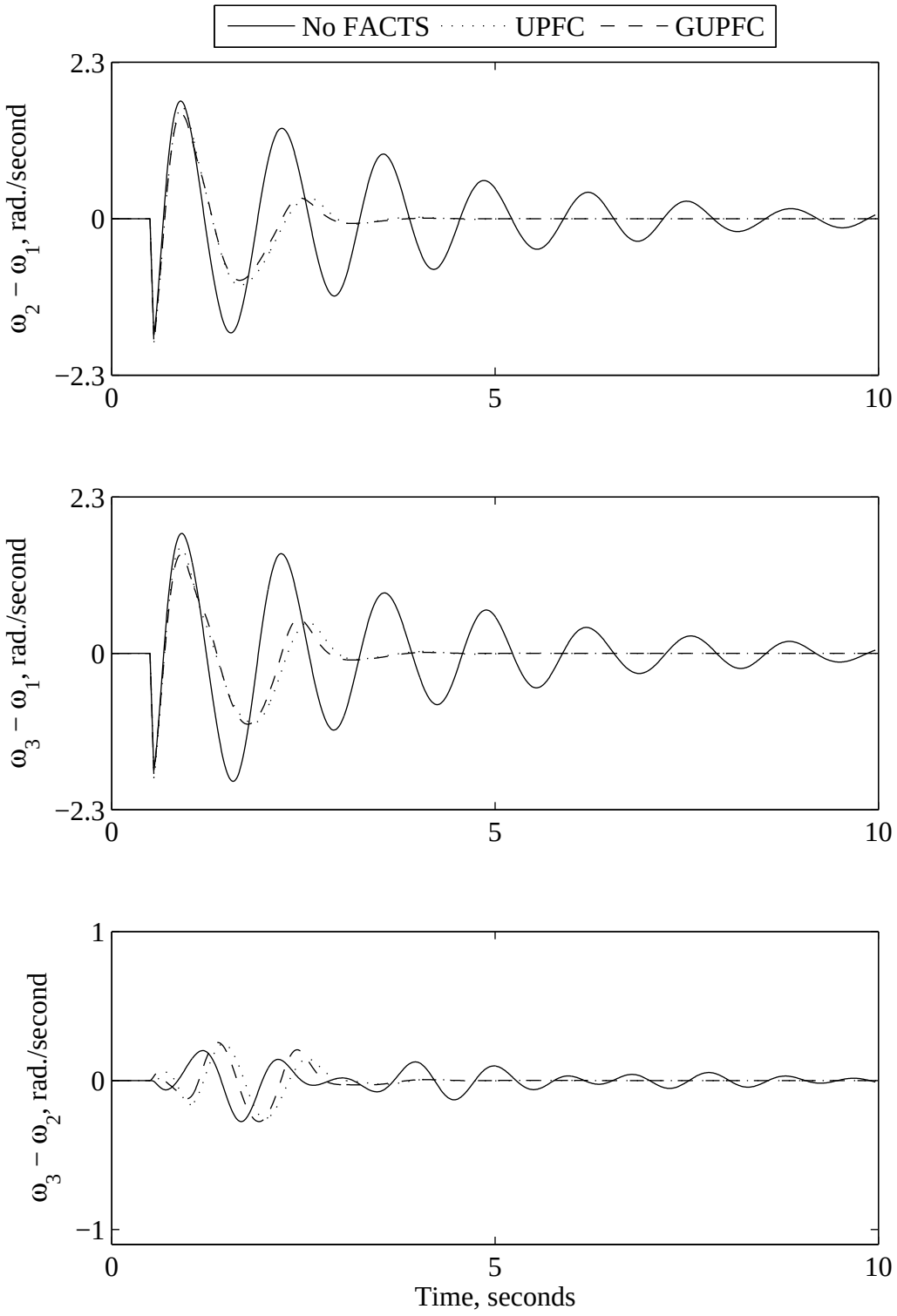

Figure 5.21 Relative generator speeds due to a 3-cycle three-phase fault at bus 1 (a GUPFC is installed at LOC4).

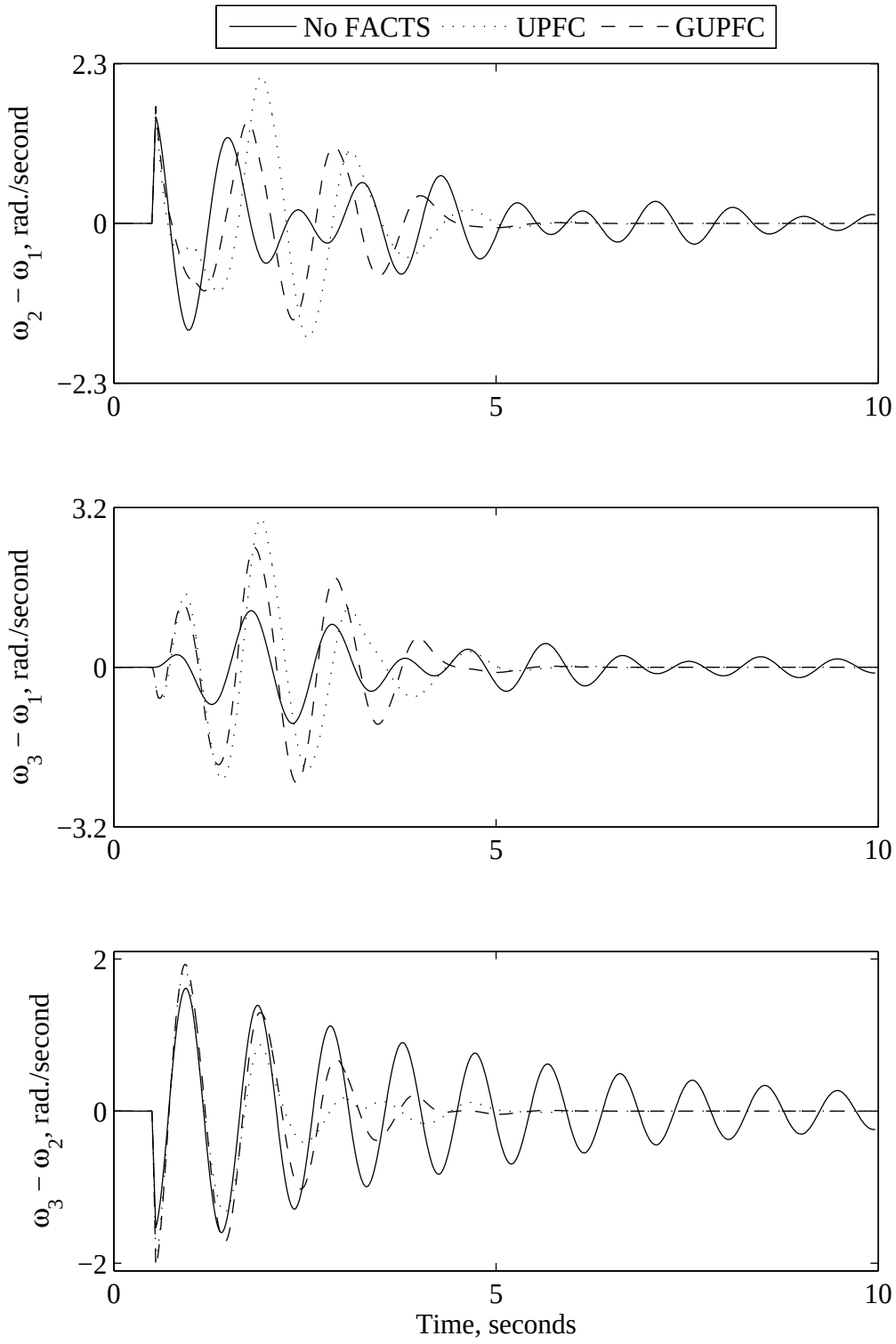

Figure 5.22 Relative generator speeds due to a 3-cycle three-phase fault at bus 2 (a GUPFC is installed at LOC4).

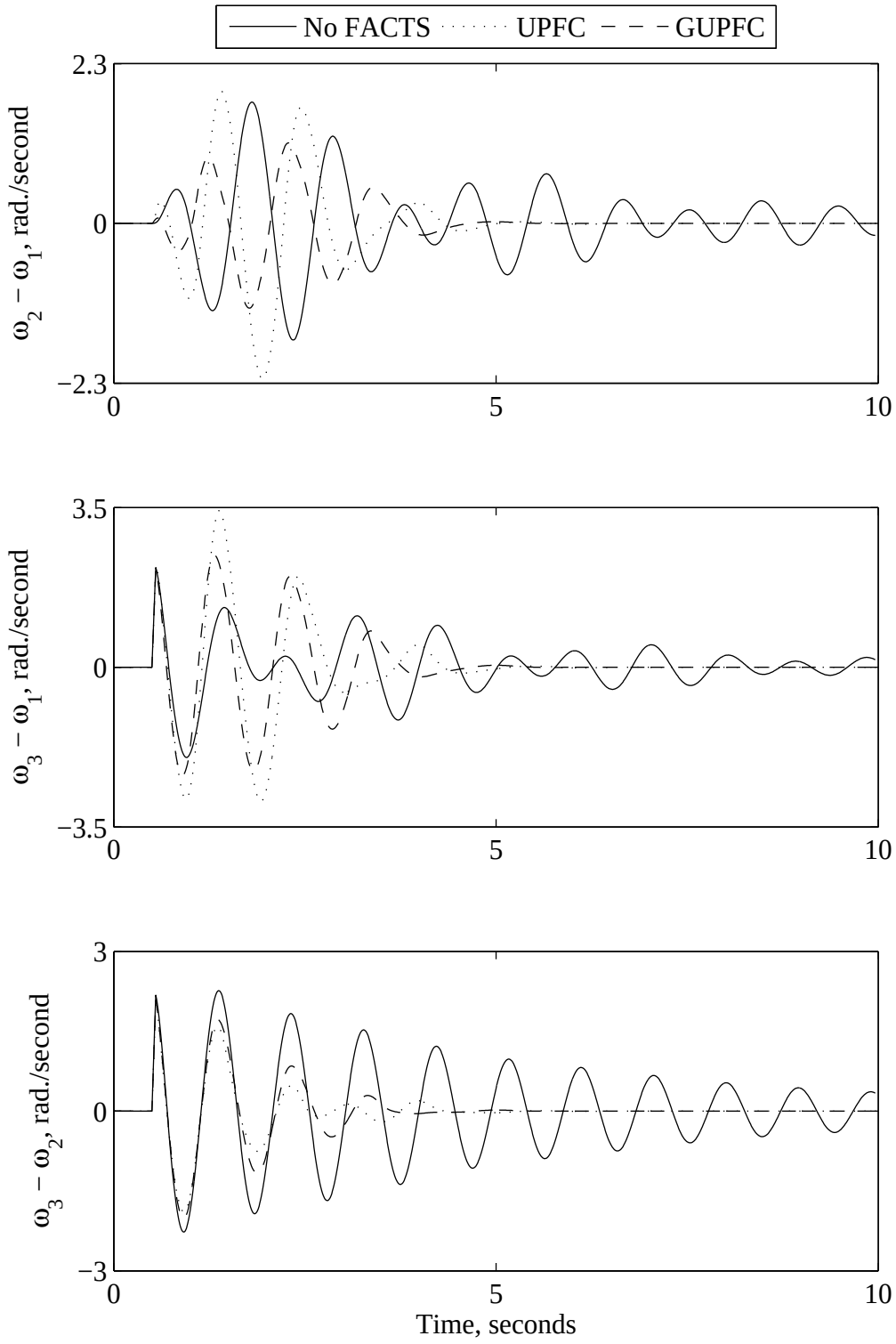

Figure 5.23 Relative generator speeds due to a 3-cycle three-phase fault at bus 3 (a GUPFC is installed at LOC4).

FACTS devices as well as the fault location affect the performance of such devices. Examining these figures yields the same conclusions of Section 3.5.2.

5.4.3. Effect of Adding another GUPFC

The effect of adding another GUPFC in the system to enhance its performance is studied in this section. The two GUPFCs are installed again at LOC1 and LOC3. The controller design in this case is based on a linearized model of a power system incorporating two FACTS controllers. A PI controller is considered again in these investigations. Figures 5.24 to 5.26 illustrate the time responses of the generators relative speeds due to 3-cycle three-phase faults at buses 1, 2 and 3 with two GUPFCs installed at LOC1 and LOC3. It can be seen from these figures that the system responses are relatively improved. Examining these figures shows again that GUPFCs relatively perform better than UPFCs.

5.5. GA Based VSC BtB Controller Performance during System Faults

The effectiveness of the VSC BtB controller in damping interarea oscillations is examined using several system disturbances. Studies similar to these conducted in Section 5.4 are considered in this section. Figures 5.27 to 5.29 illustrate the time responses of the relative generator speeds due to 3-cycle three-phase faults at buses 1, 2 and 3 with the VSC BtB installed at LOC1. The time responses of the generator terminal voltages and real powers are shown respectively in Figures 5.30 and 5.31. The dc link capacitor voltage and the dc power of the VSC BtB are illustrated respectively in Figures 5.32 and 5.33. Different locations for the VSC BtB controller are also investigated. Figures 5.34 to 5.42 show system responses due to 3-cycle three-phase faults at buses 1, 2 and 3 with the VSC BtB installed at LOC2, LOC3 and LOC4. It can be concluded, again, that the best location for the VSC BtB controller is at the middle of the tie-line that transfers the highest amount of power. The effect of adding another VSC BtB controller is also investigated. The system responses due to 3-cycle three-phase faults at buses 1, 2 and 3 with two VSC BtB devices installed at LOC1 and LOC3 are given in Figures 5.43 to 5.45. It can be seen again that adding another FACTS controller enhances the damping of interarea oscillations.

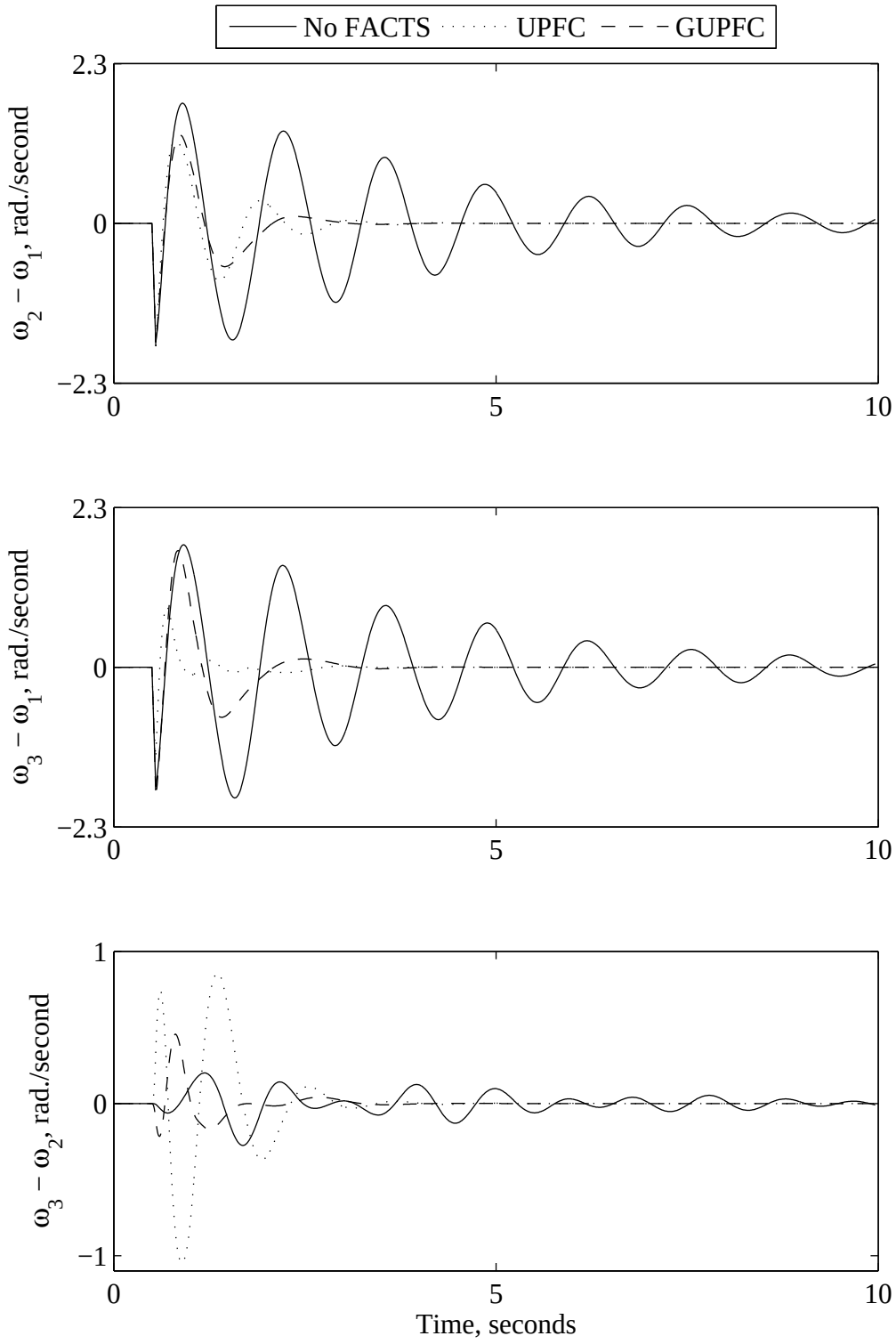

Figure 5.24 Relative generator speeds due to a 3-cycle three-phase fault at bus 1 (two GUPFCs are installed at LOC1 and LOC3).

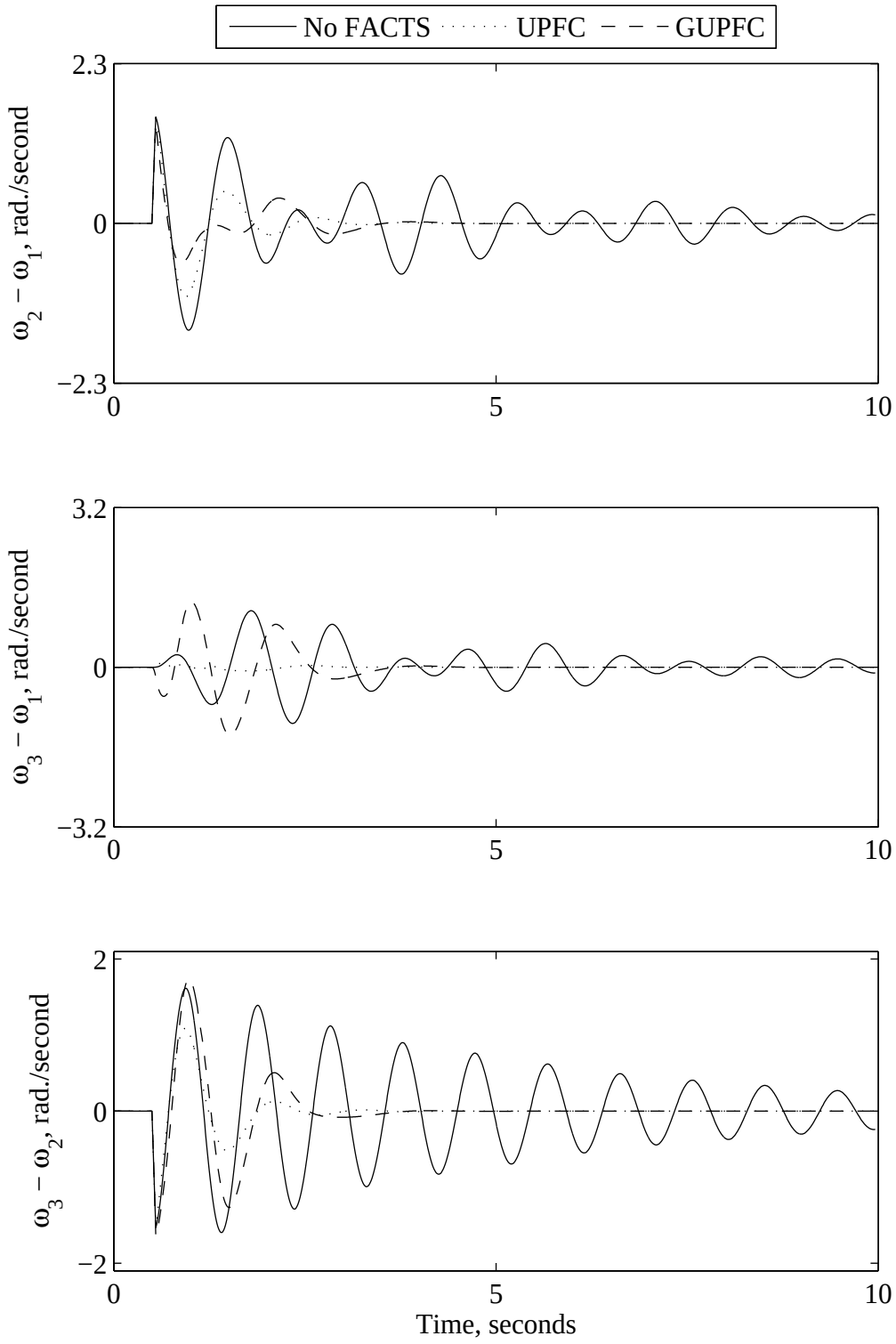

Figure 5.25 Relative generator speeds due to a 3-cycle three-phase fault at bus 2 (two GUPFCs are installed at LOC1 and LOC3).

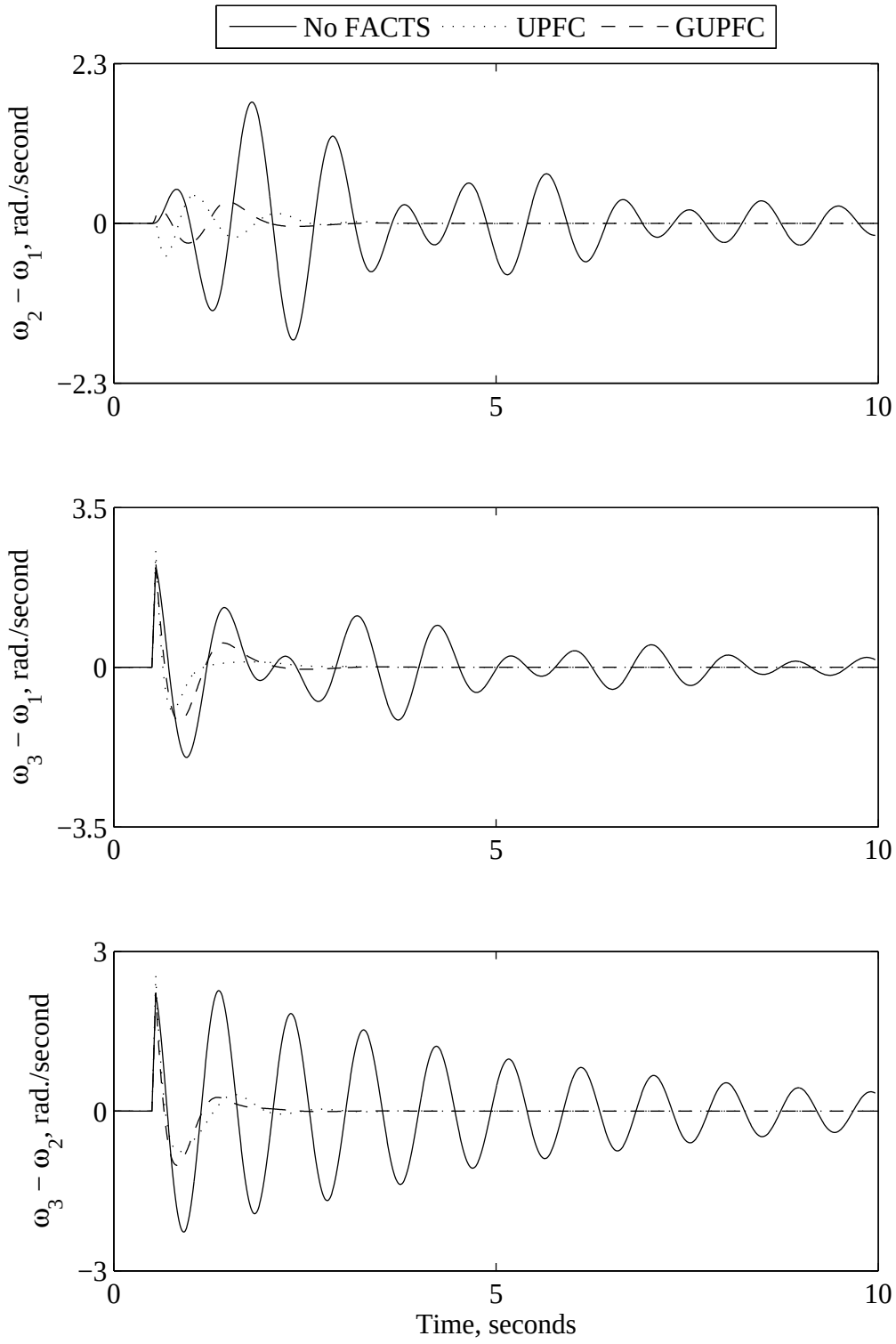

Figure 5.26 Relative generator speeds due to a 3-cycle three-phase fault at bus 3 (two GUPFCs are installed at LOC1 and LOC3).

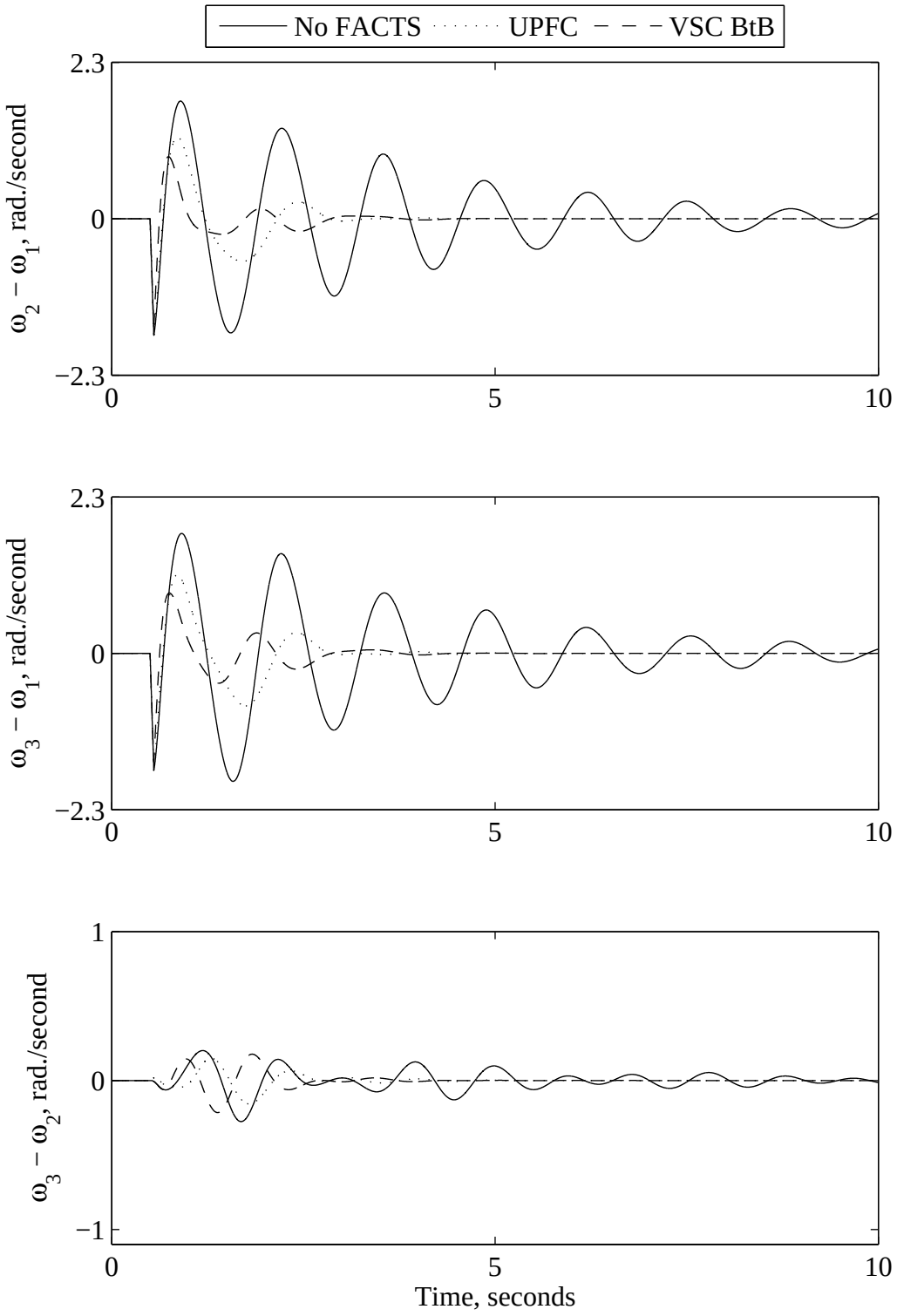

Figure 5.27 Relative generator speeds due to a 3-cycle three-phase fault at bus 1 (a VSC BtB is installed at LOC1).

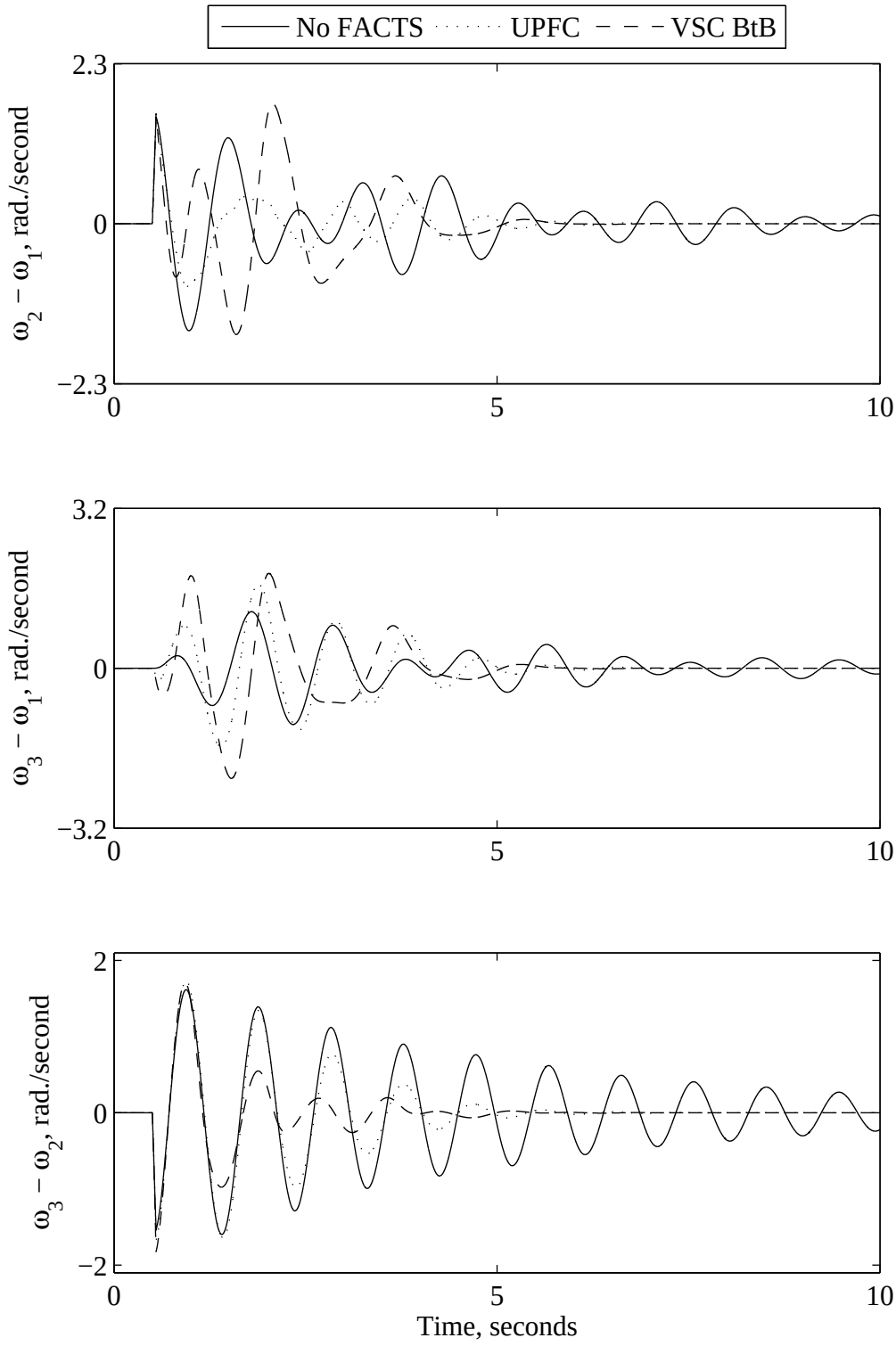

Figure 5.28 Relative generator speeds due to a 3-cycle three-phase fault at bus 2 (a VSC BtB is installed at LOC1).

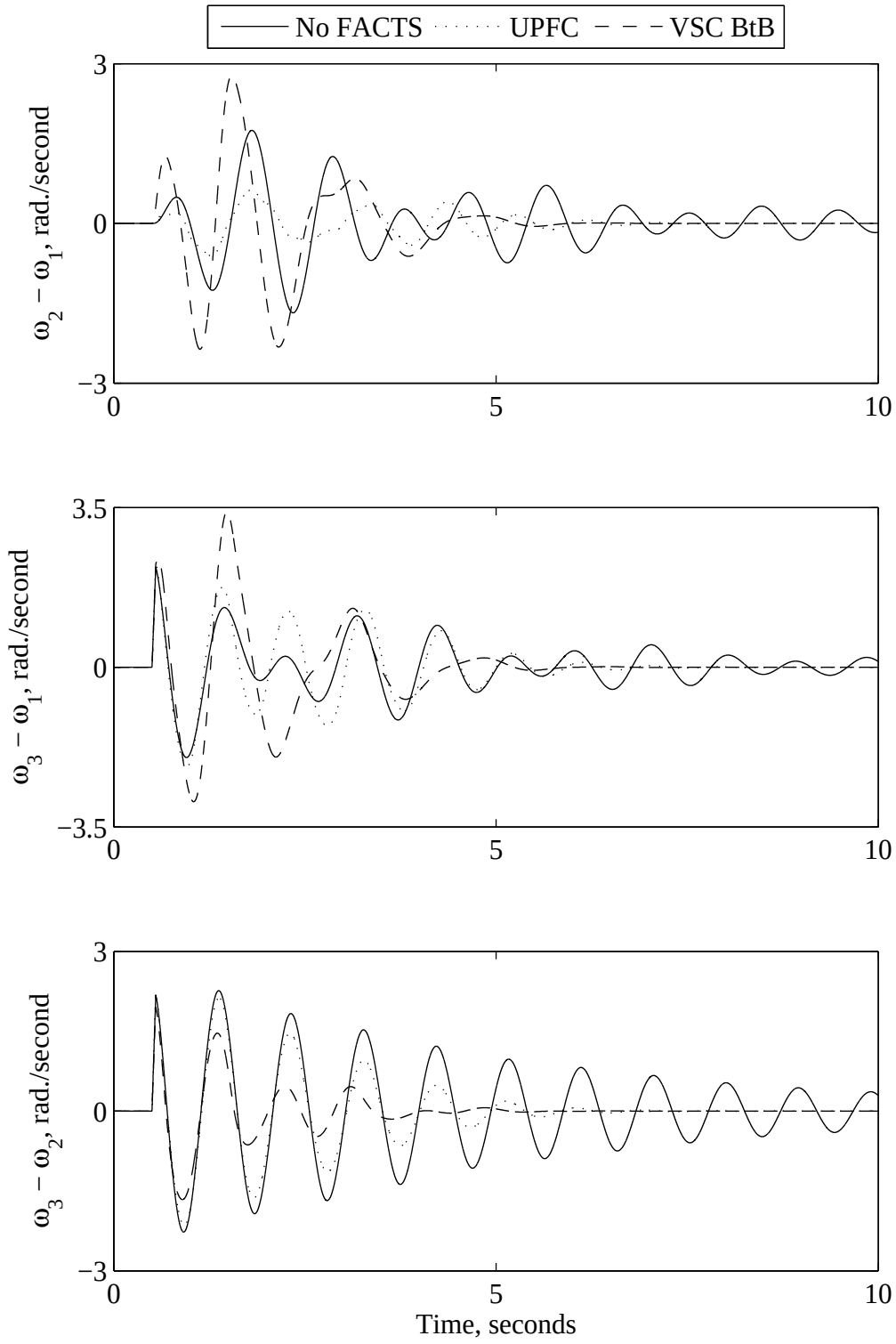

Figure 5.29 Relative generator speeds due to a 3-cycle three-phase fault at bus 3 (a VSC BtB is installed at LOC1).

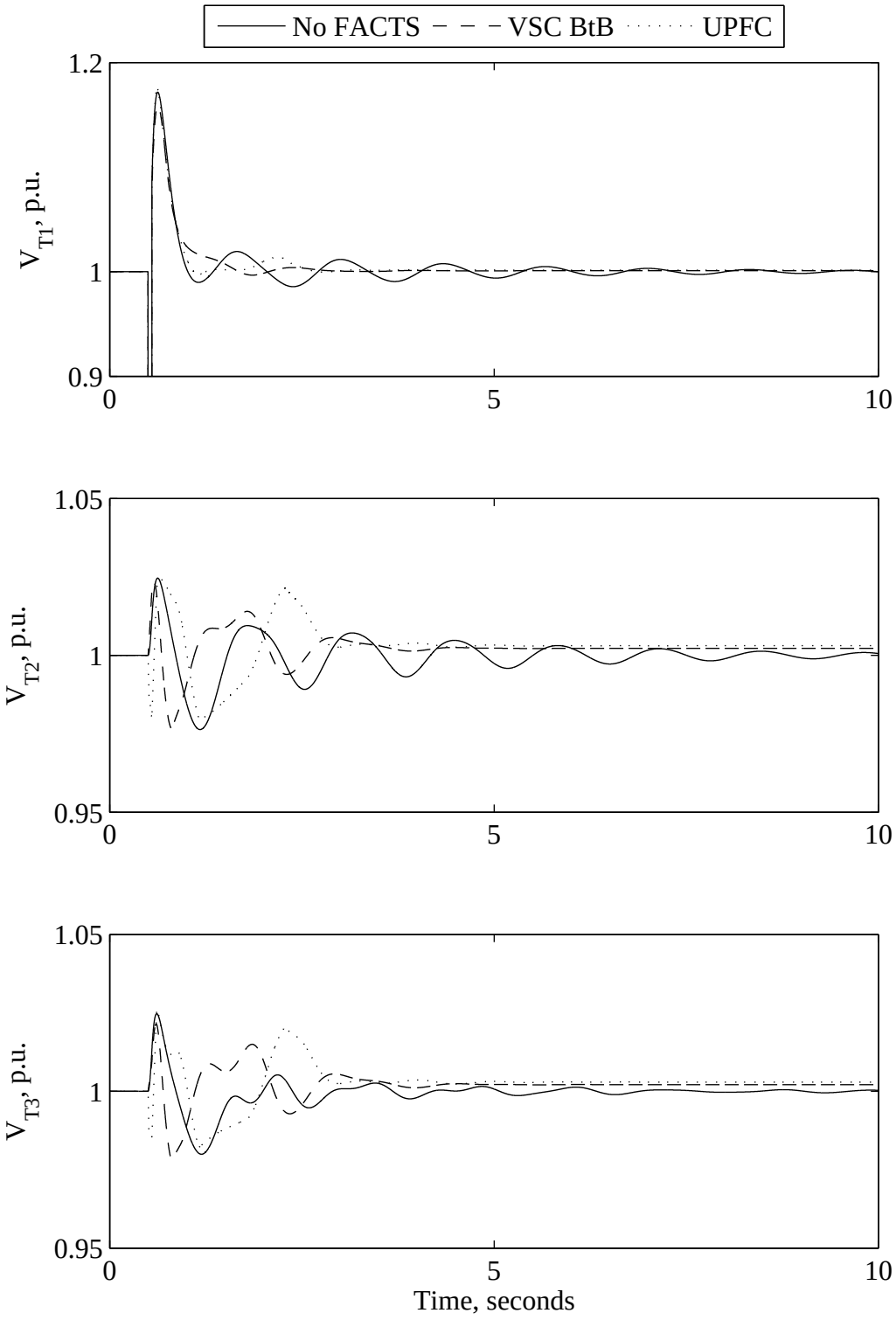

Figure 5.30 Generator terminal voltages due to a 3-cycle three-phase fault at bus 1 (a VSC BtB is installed at LOC1).

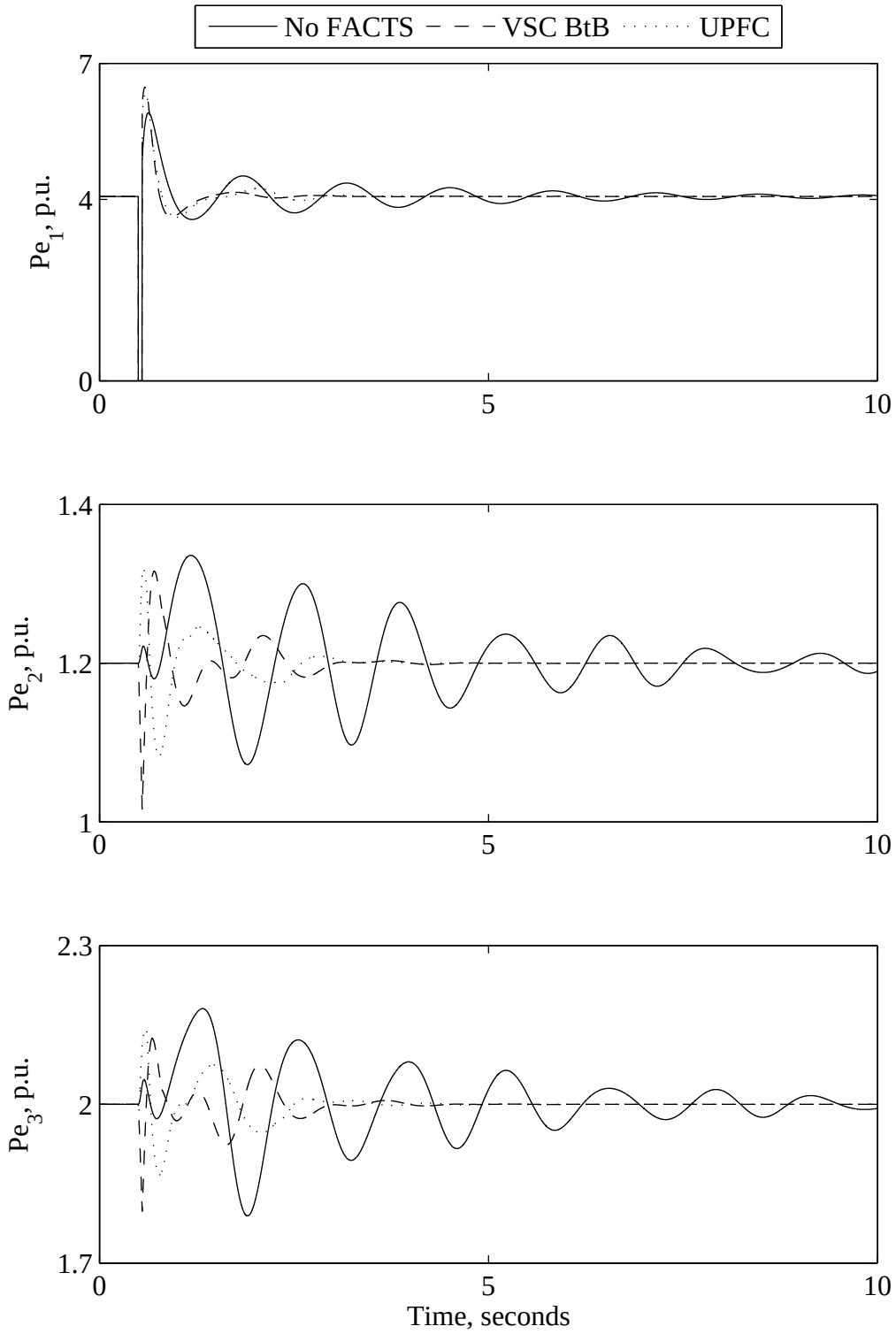

Figure 5.31 Generator real powers due to a 3-cycle three-phase fault at bus 1 (a VSC BtB is installed at LOC1).

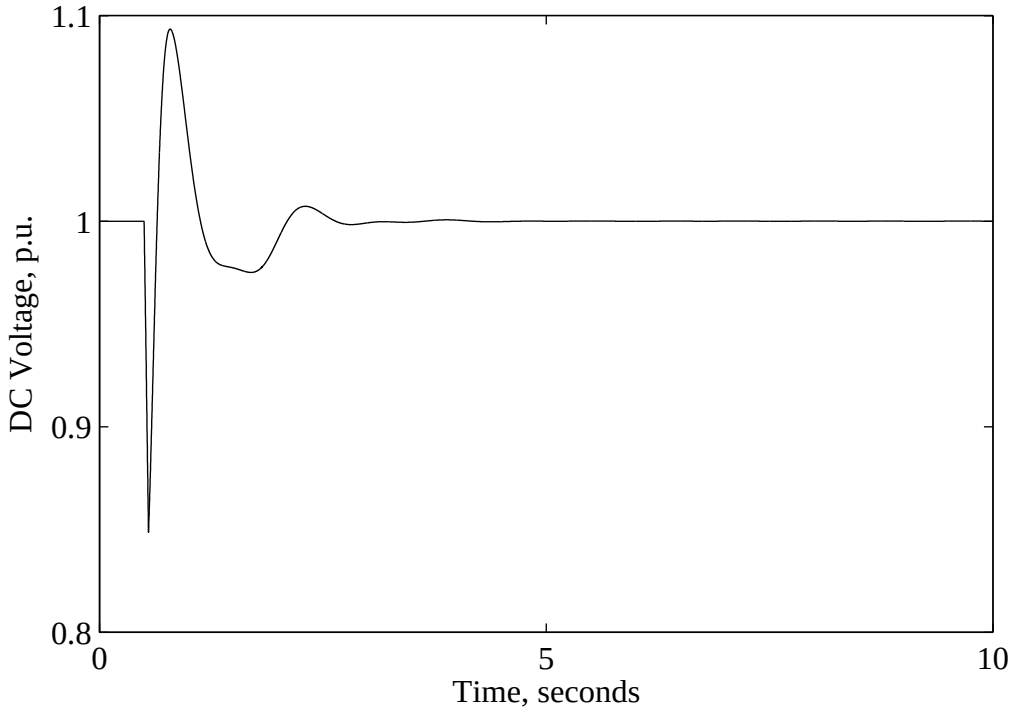

Figure 5.32 VSC BtB dc-link capacitor voltage due to a 3-cycle three-phase fault at bus 1 (a VSC BtB is installed at LOC1).

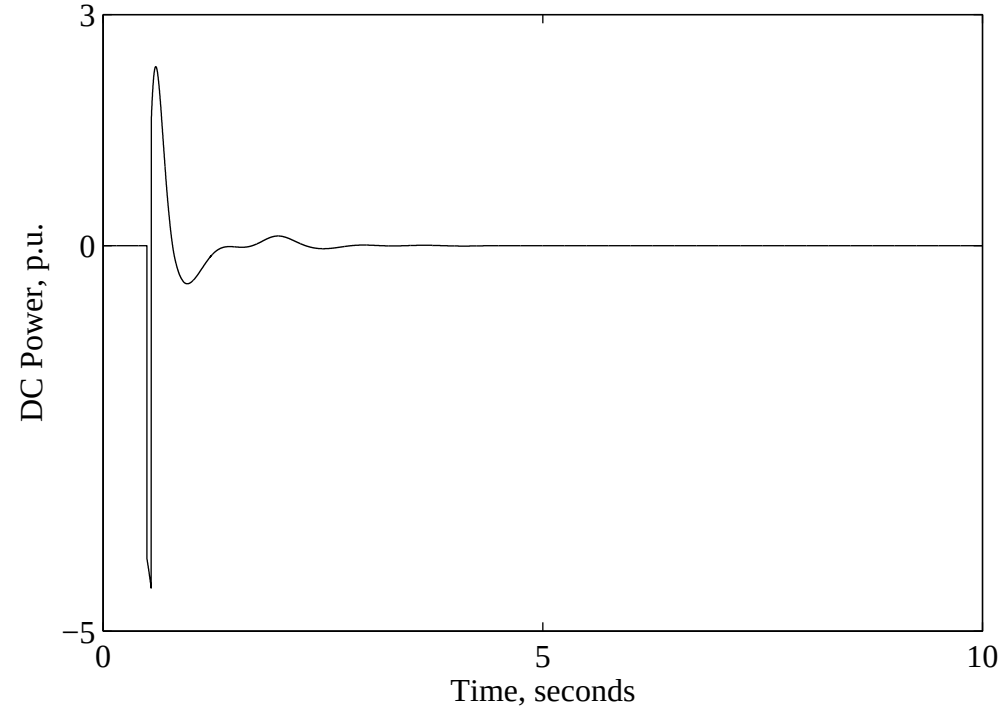

Figure 5.33 VSC BtB dc power due to a 3-cycle three-phase fault at bus 1 (a VSC BtB is installed at LOC1).

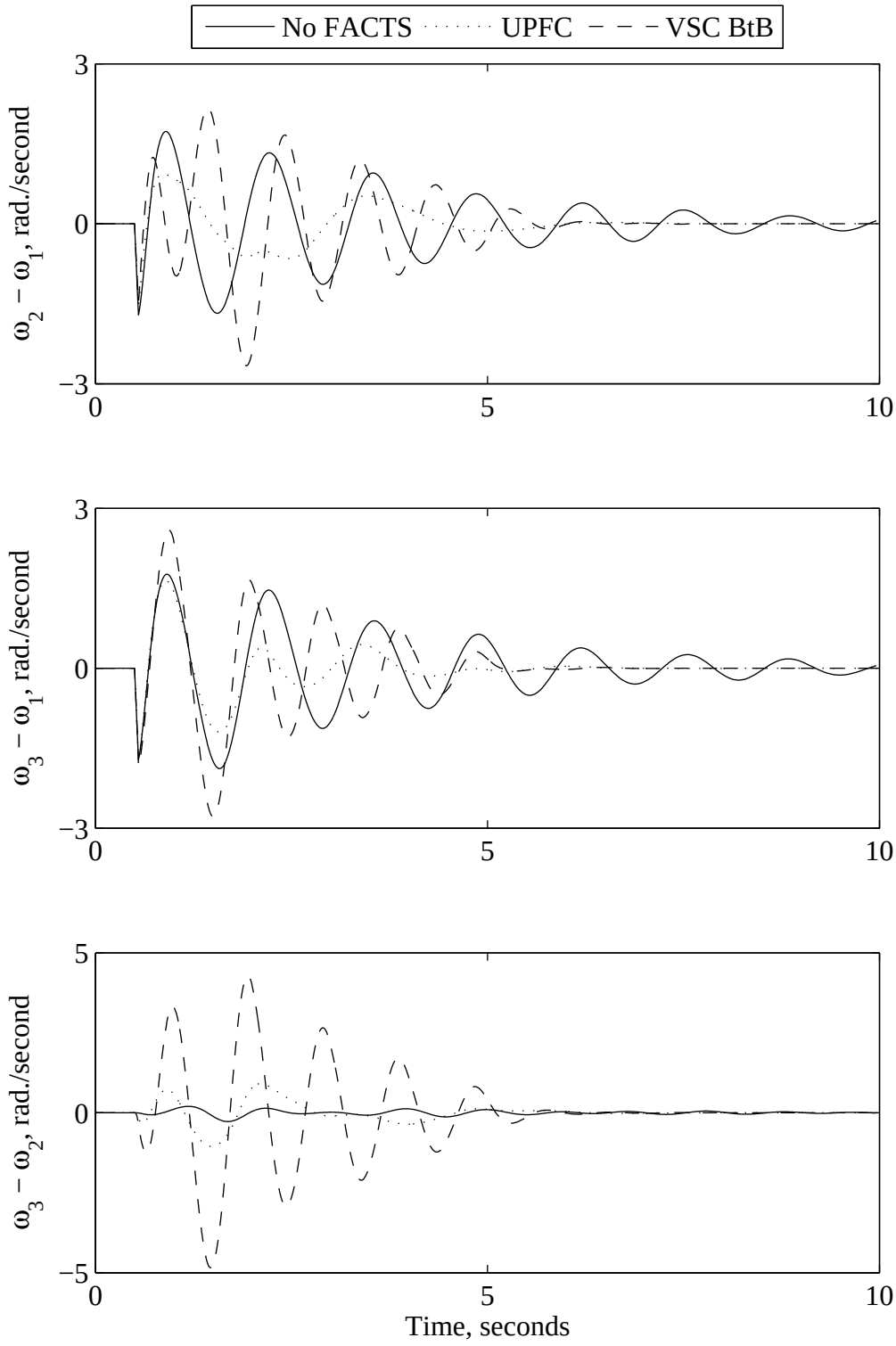

Figure 5.34 Relative generator speeds due to a 3-cycle three-phase fault at bus 1 (a VSC BtB is installed at LOC2).

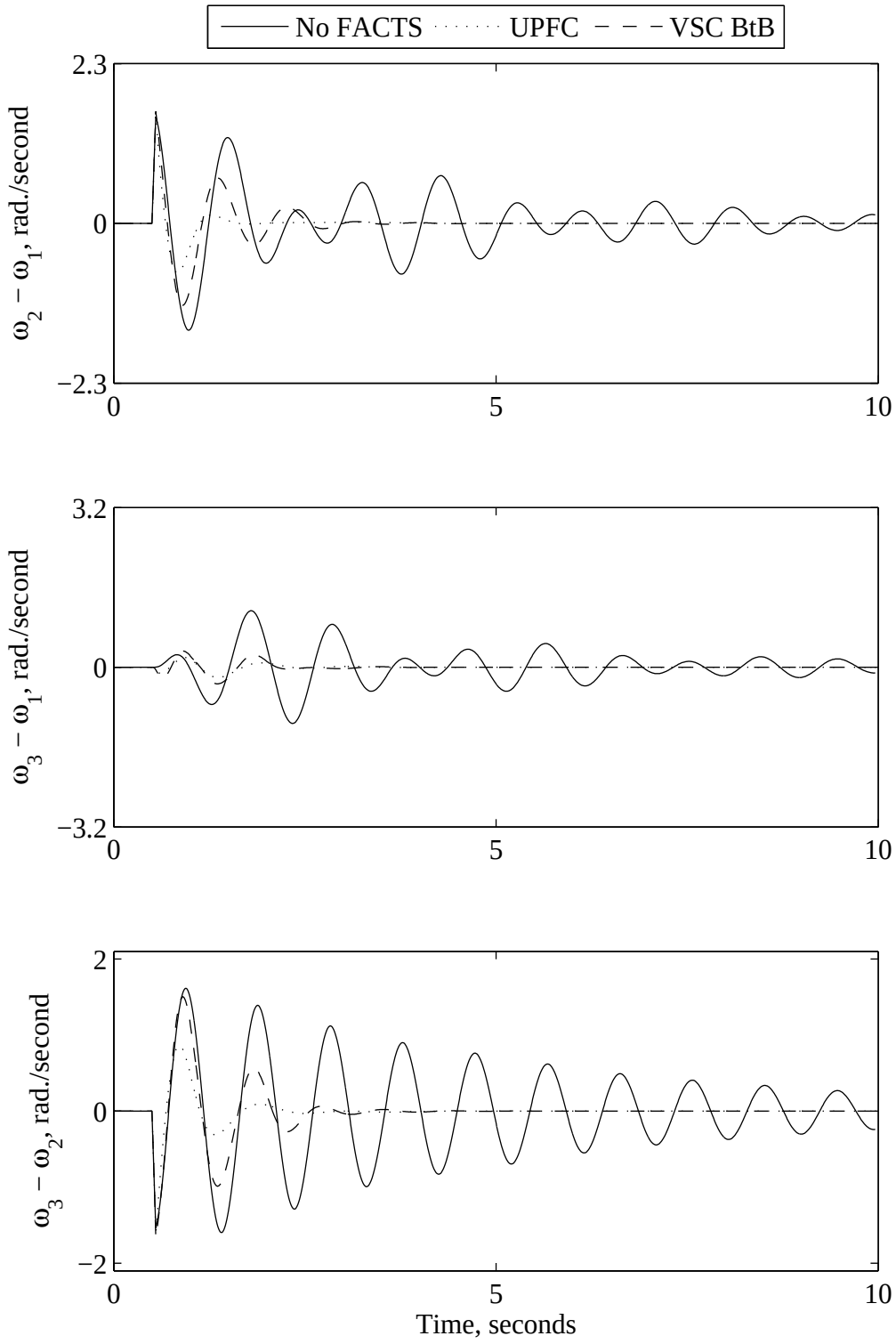

Figure 5.35 Relative generator speeds due to a 3-cycle three-phase fault at bus 2 (a VSC BtB is installed at LOC2).

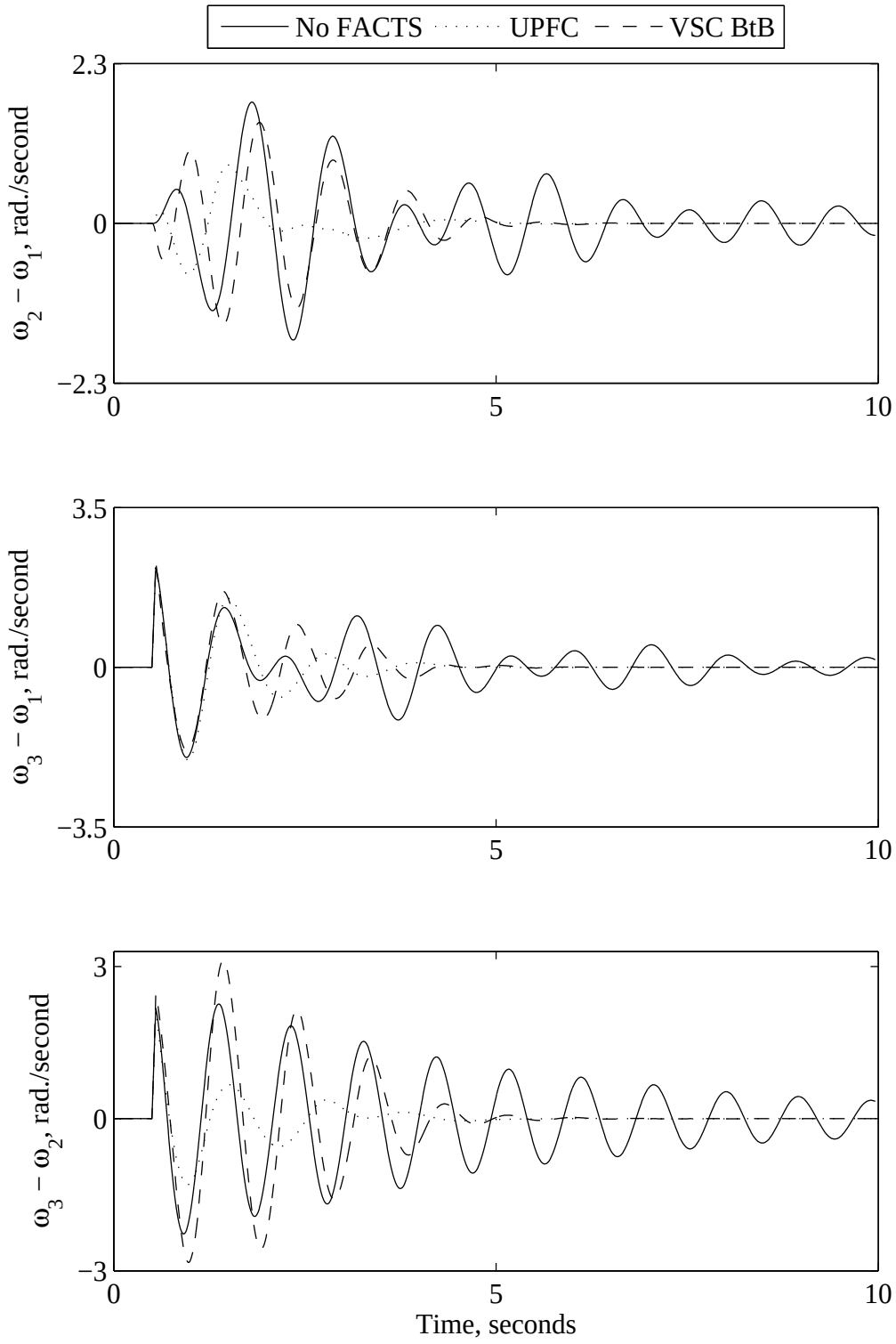

Figure 5.36 Relative generator speeds due to a 3-cycle three-phase fault at bus 3 (a VSC BtB is installed at LOC2).

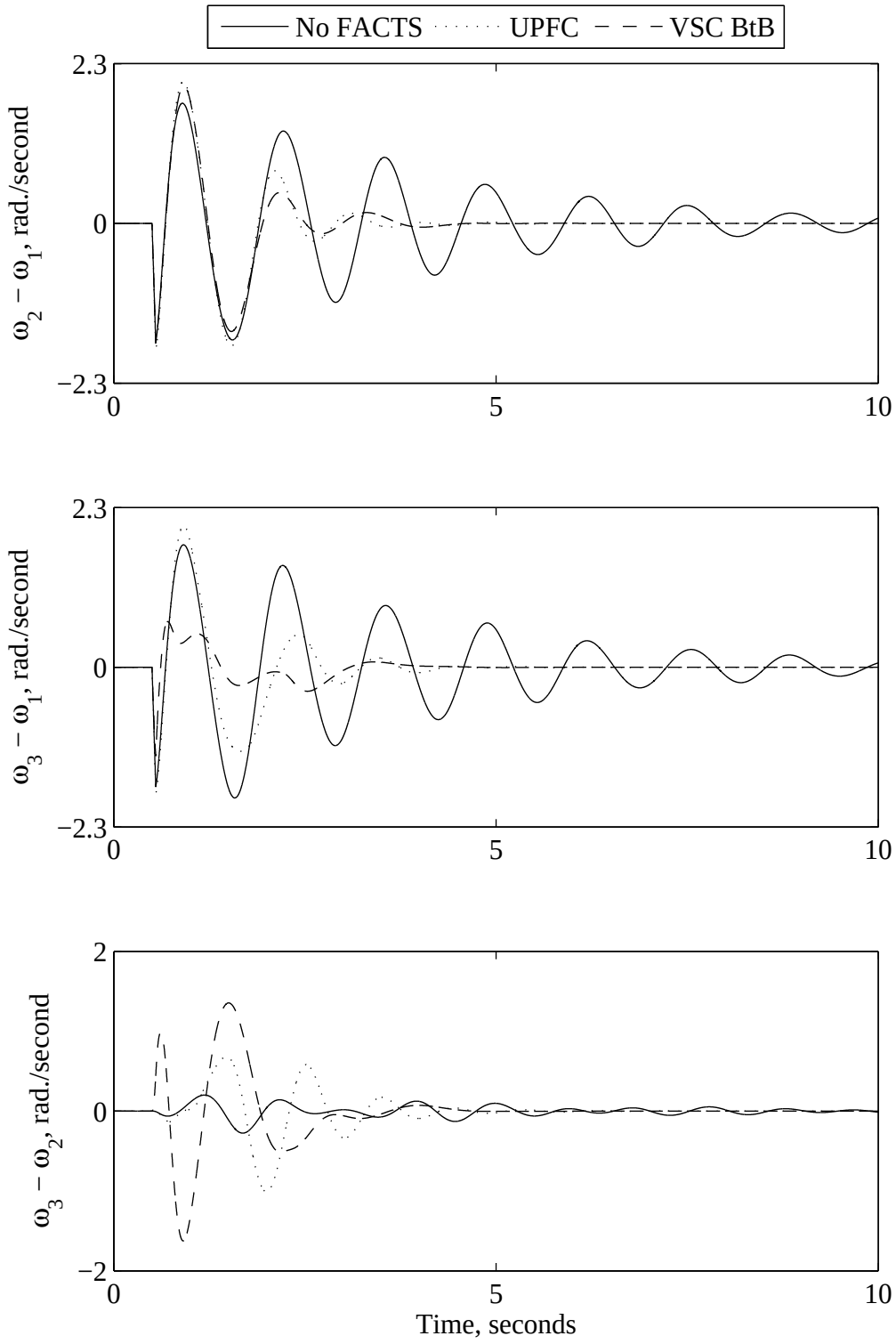

Figure 5.37 Relative generator speeds due to a 3-cycle three-phase fault at bus 1 (a VSC BtB is installed at LOC3).

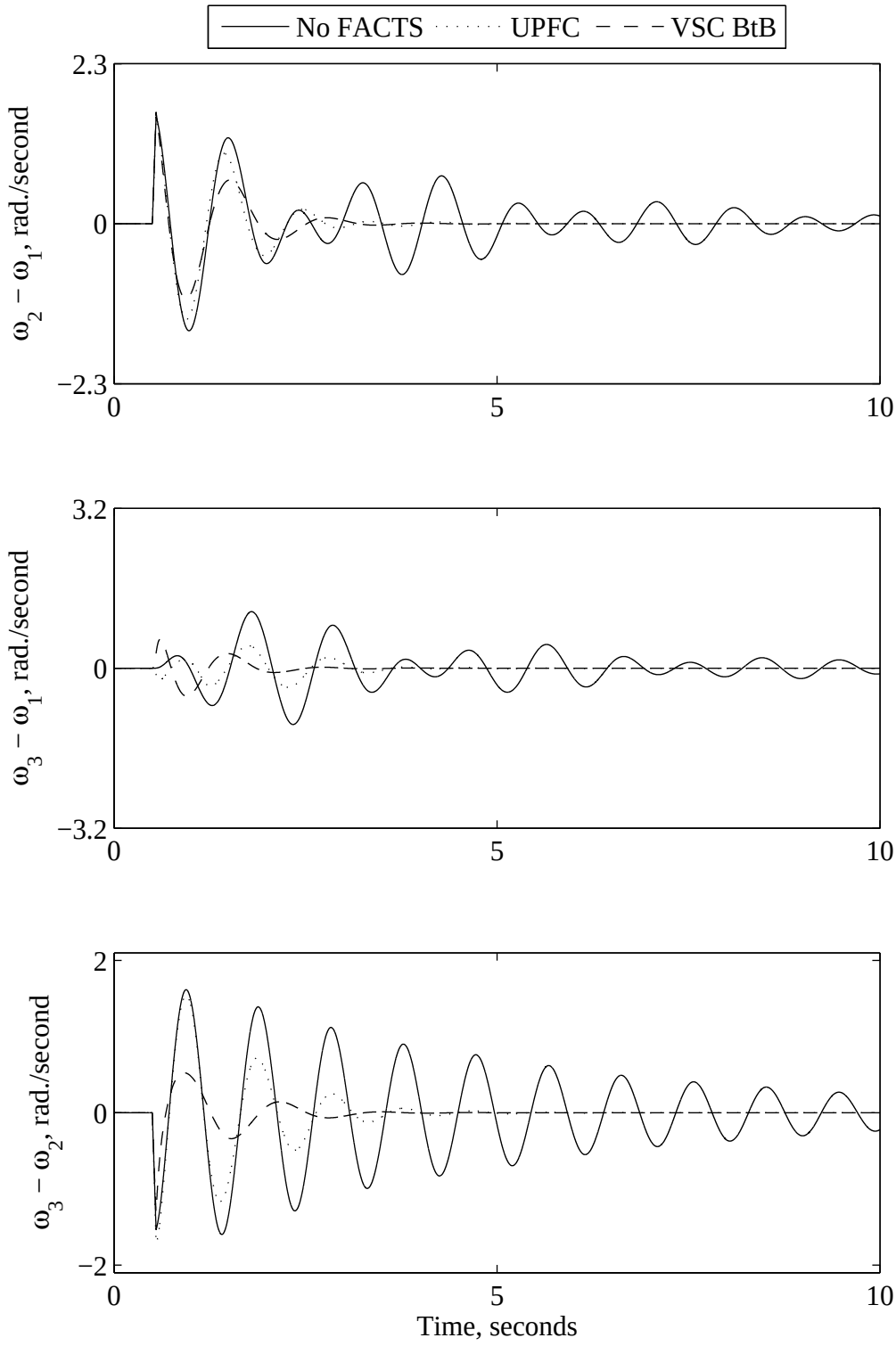

Figure 5.38 Relative generator speeds due to a 3-cycle three-phase fault at bus 2 (a VSC BtB is installed at LOC3).

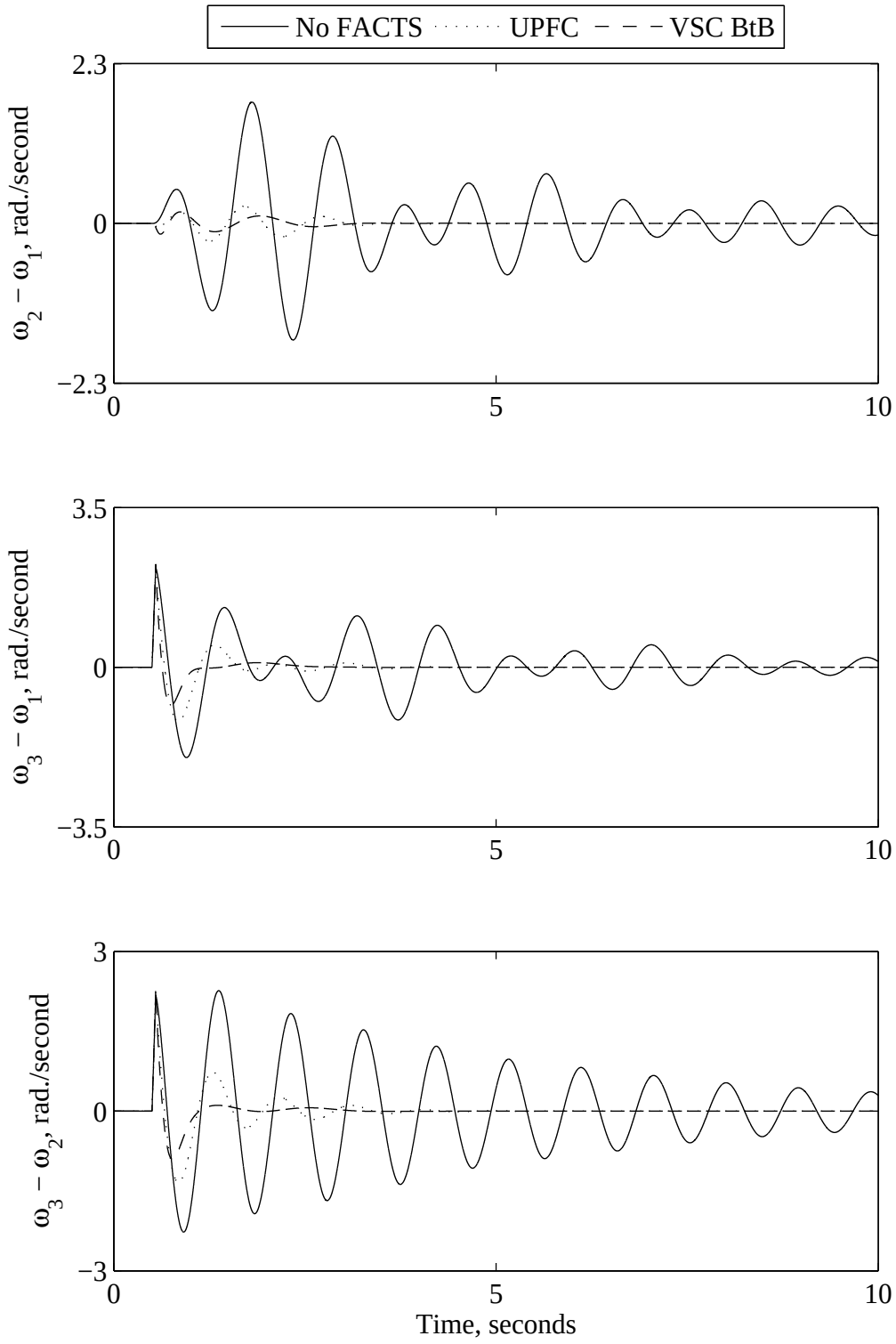

Figure 5.39 Relative generator speeds due to a 3-cycle three-phase fault at bus 3 (a VSC BtB is installed at LOC3).

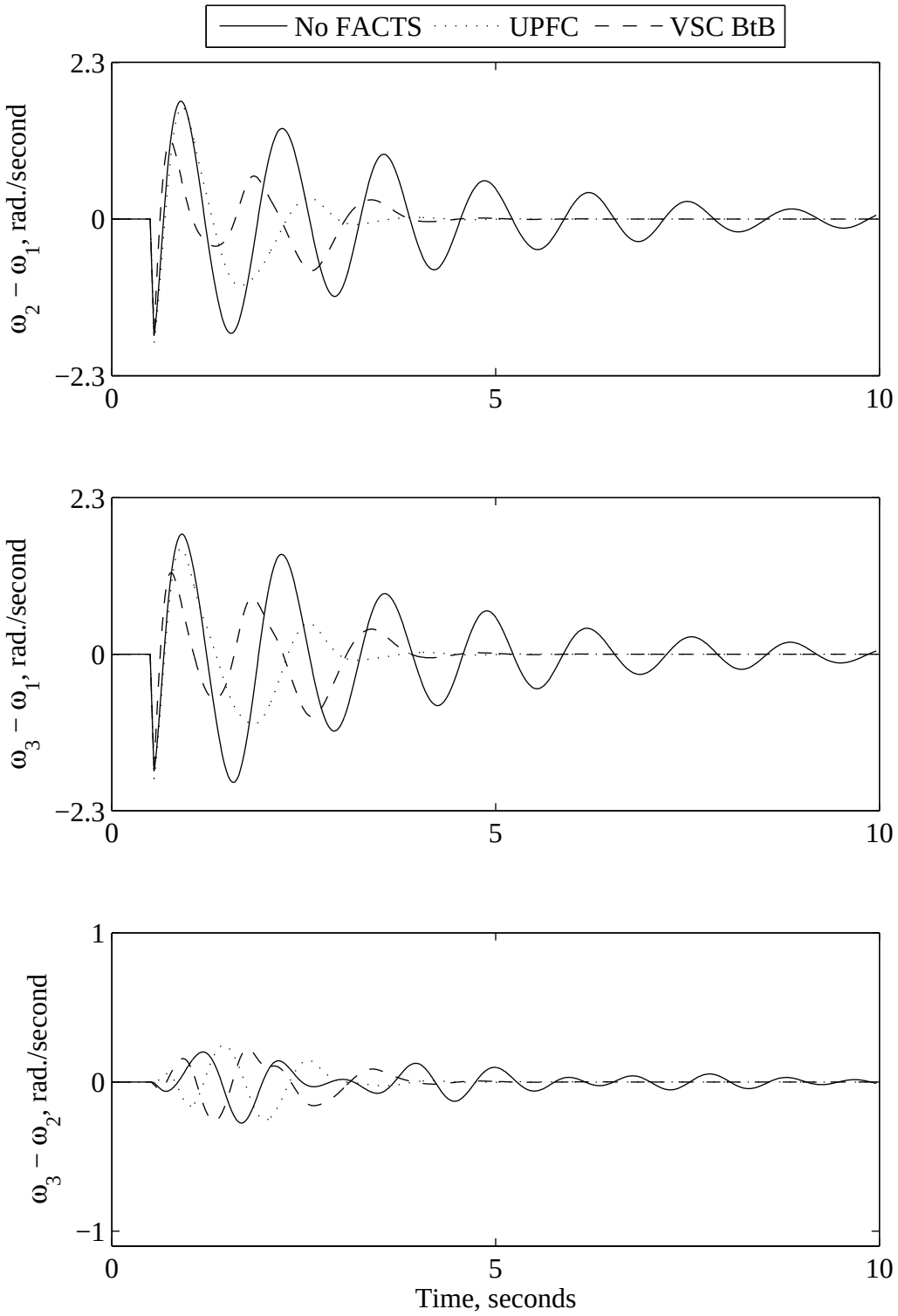

Figure 5.40 Relative generator speeds due to a 3-cycle three-phase fault at bus 1 (a VSC BtB is installed at LOC4).

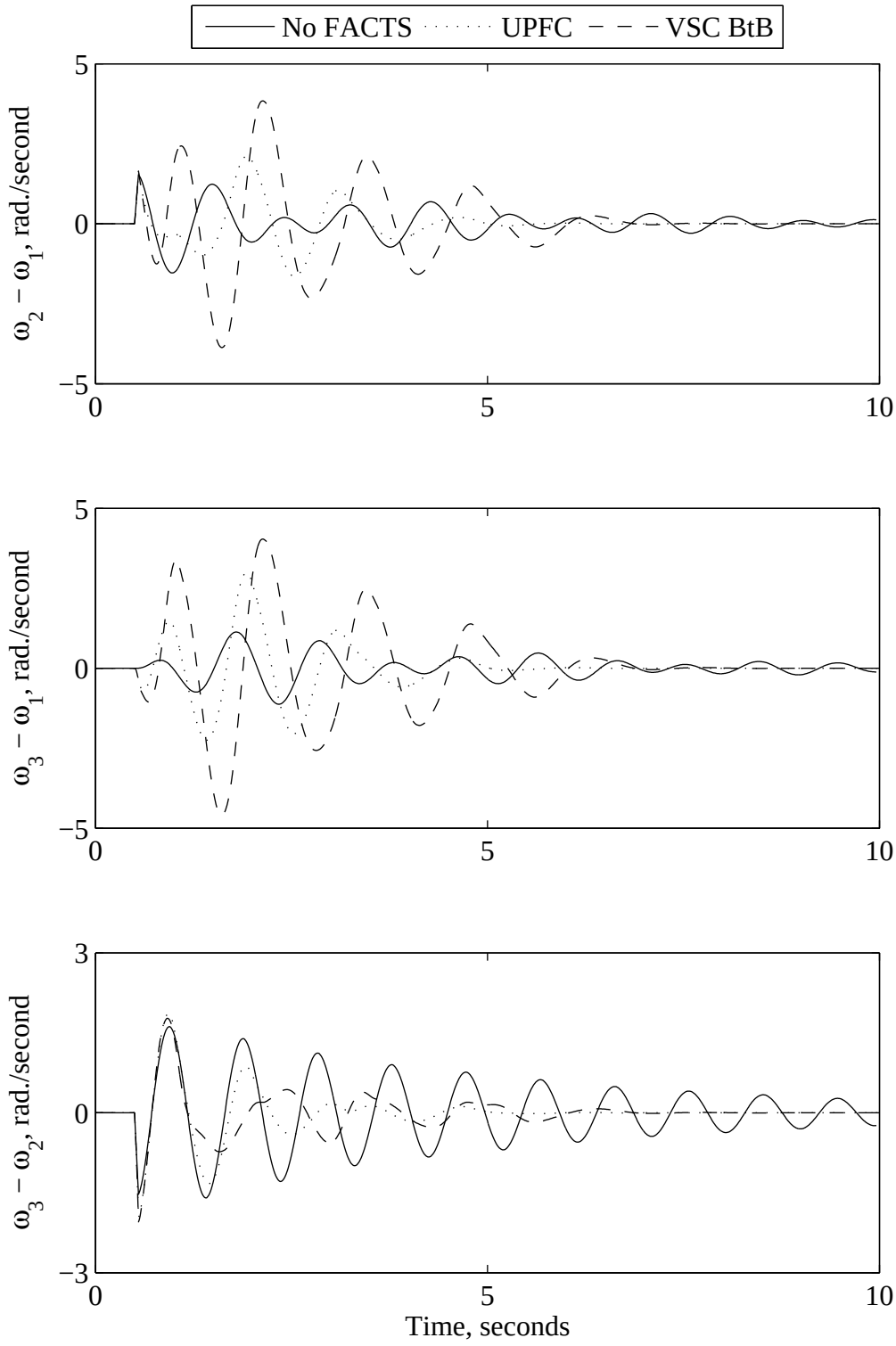

Figure 5.41 Relative generator speeds due to a 3-cycle three-phase fault at bus 2 (a VSC BtB is installed at LOC4).

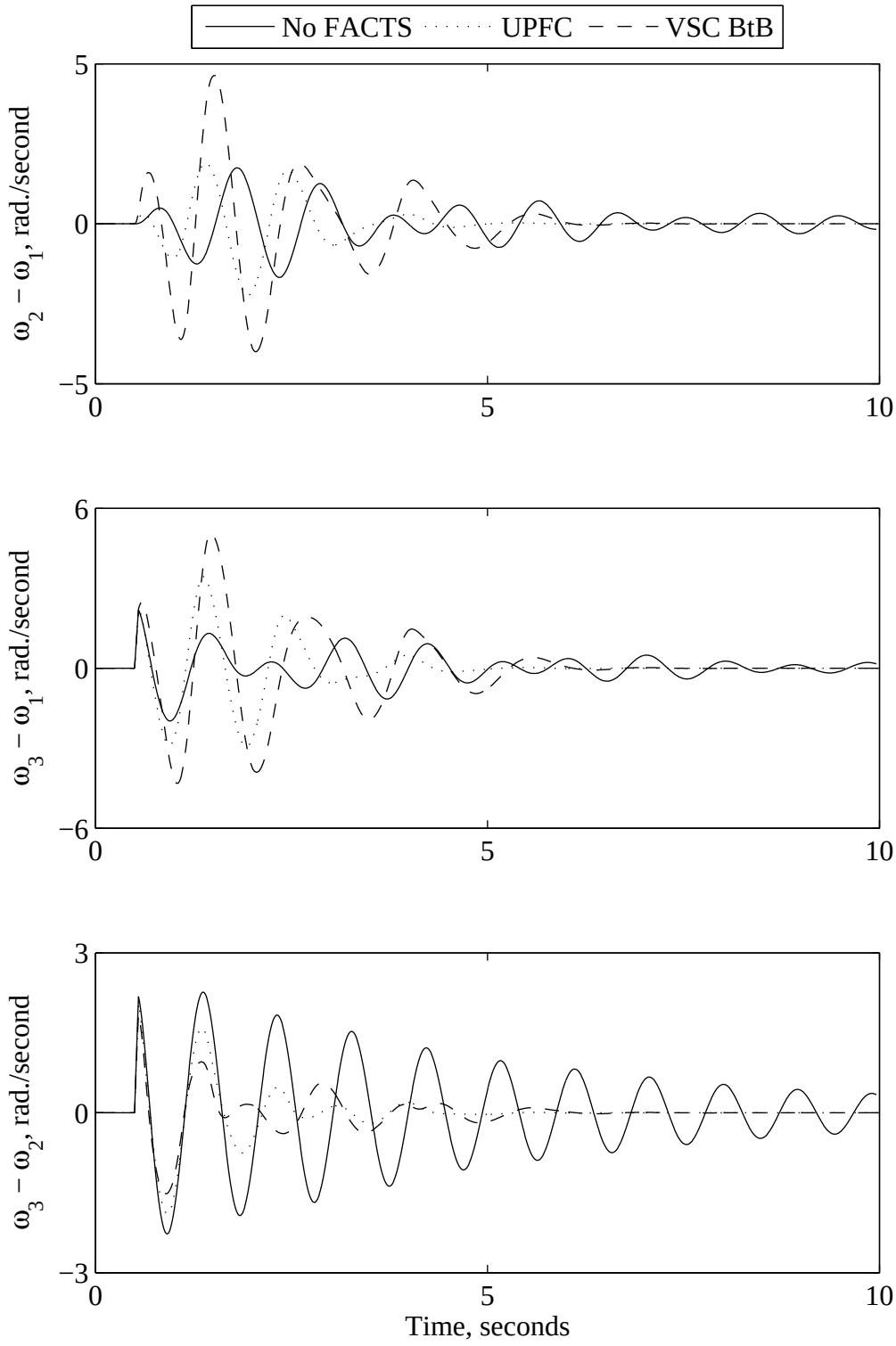

Figure 5.42 Relative generator speeds due to a 3-cycle three-phase fault at bus 3 (a VSC BtB is installed at LOC4).

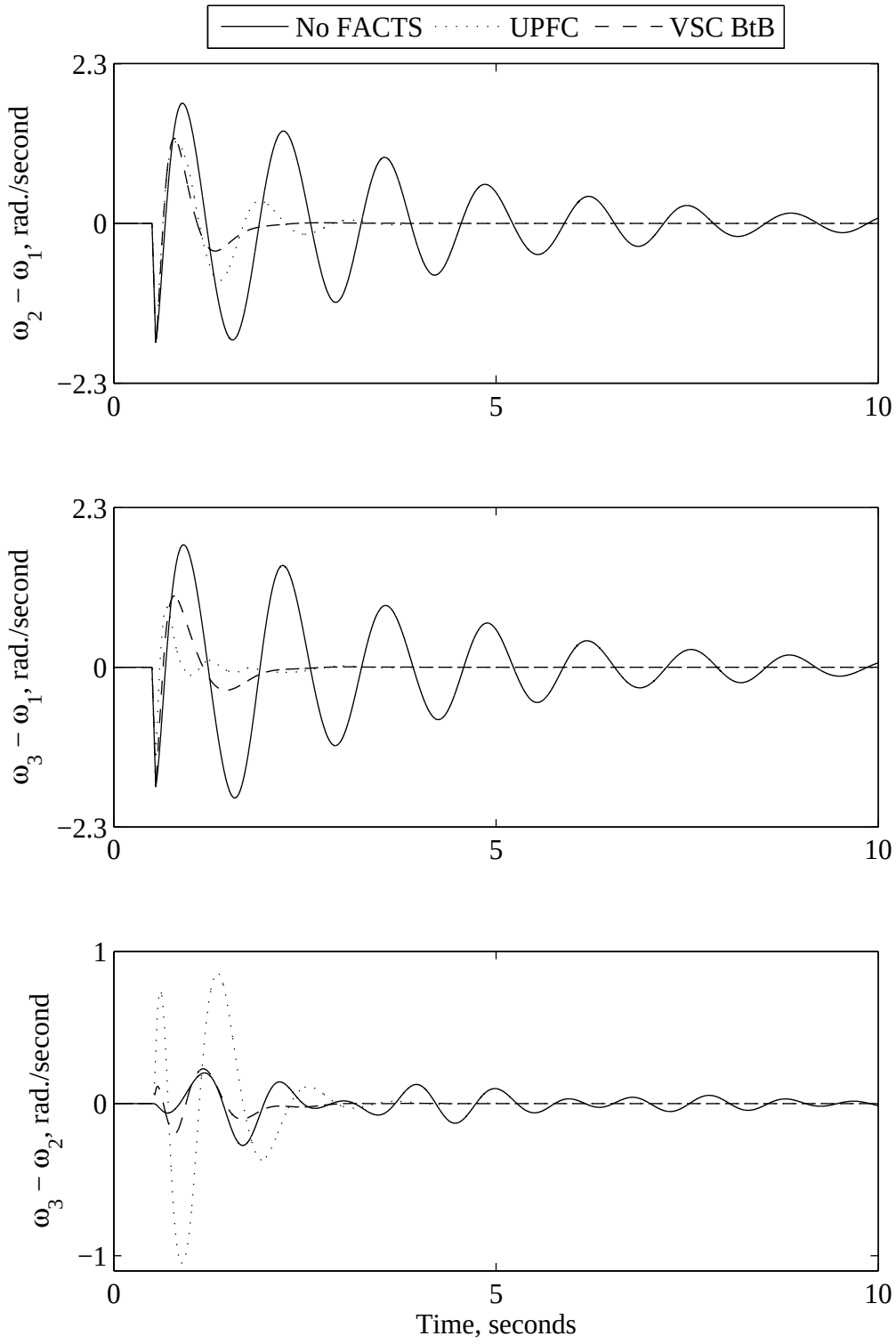

Figure 5.43 Relative generator speeds due to a 3-cycle three-phase fault at bus 1 (two VSC BtBs are installed at LOC1 and LOC3).

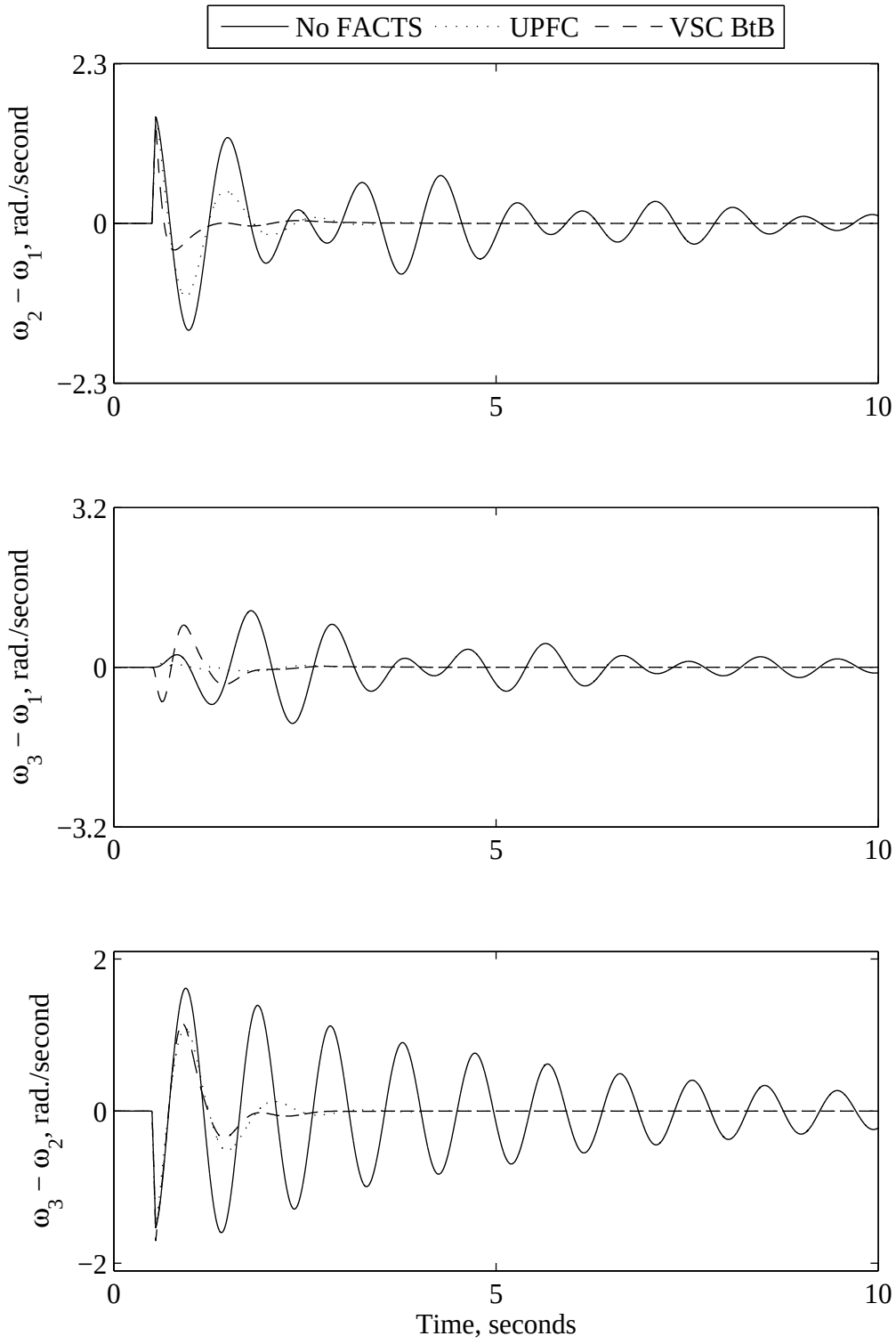

Figure 5.44 Relative generator speeds due to a 3-cycle three-phase fault at bus 2 (two VSC BtBs are installed at LOC1 and LOC3).

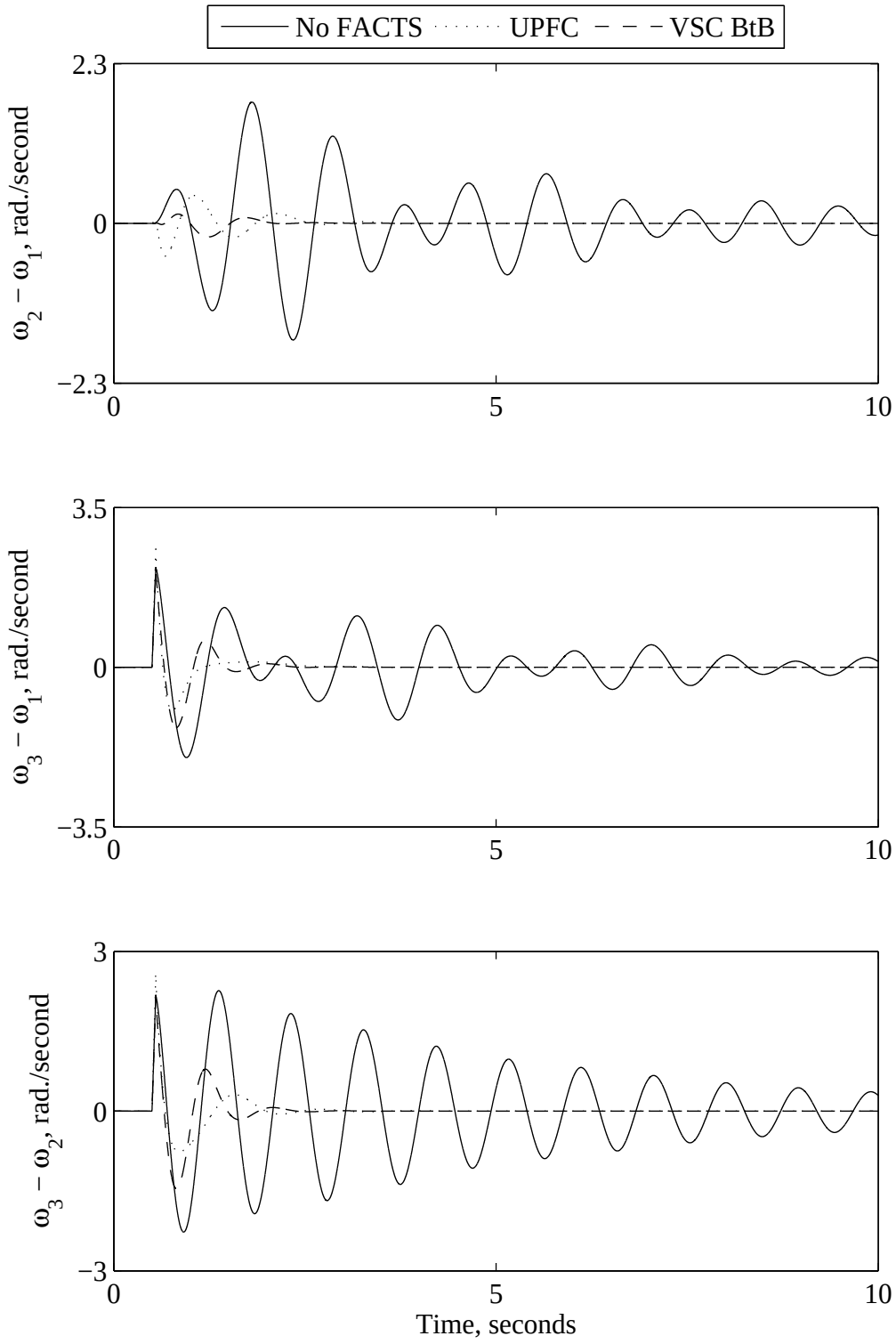

Figure 5.45 Relative generator speeds due to a 3-cycle three-phase fault at bus 3 (two VSC BtBs are installed at LOC1 and LOC3).

5.6. GUPFC Performance during Other Disturbances

The effectiveness of the GUPFC in damping system oscillations during severe disturbances such as three-phase faults is examined in Section 5.4. Its effectiveness in damping system oscillations during two large and small system disturbances is examined in this section. In this context, a sudden load decrease of 95% is considered as the simulated large disturbance while a 20% decrease in the input reference mechanical power is considered as the simulated small disturbance.

Figures 5.46 and 5.47 show the power system time response following a 20% sudden decrease in the input reference mechanical power of generator G_1 with the GUPFC installed at LOC1 and with two GUPFCs installed at LOC1 and LOC3 respectively. It can be seen from these figures that the designed controller for the GUPFC is capable of damping small disturbances. It can also be seen from Figures 5.46 and 5.47 that more damping in the interarea oscillations is achieved with two GUPFCs.

Figures 5.48 and 5.49 respectively show the system response due to a 95%, 3-cycle sudden decrease in loads S_1 and S_2 with the GUPFC installed at LOC1. System responses due to the same disturbance with two GUPFCs installed at LOC1 and LOC3 are shown in Figures 5.50 and 5.51. It can be seen from these figures that, the GUPFCs exhibit excellent performance in damping the system oscillations. Examining these figures shows again that the GUPFC performance is relatively better than the UPFC.

5.7. VSC BtB Performance during Different Disturbances

In this section, the VSC BtB performance is examined during the same disturbances considered in the previous section. Figures 5.52 and 5.53 show the power system time response following a 20% sudden decrease in the input reference mechanical power of generator G_1 with the VSC BtB installed at LOC1 and with two VSC BtB devices installed at LOC1 and LOC3 respectively. It can be seen from these figures that the designed controller for the VSC BtB is capable of damping small disturbances. It can also be seen from Figures 5.52 and 5.53 that more damping in the interarea oscillations is achieved with two VSC BtB devices.

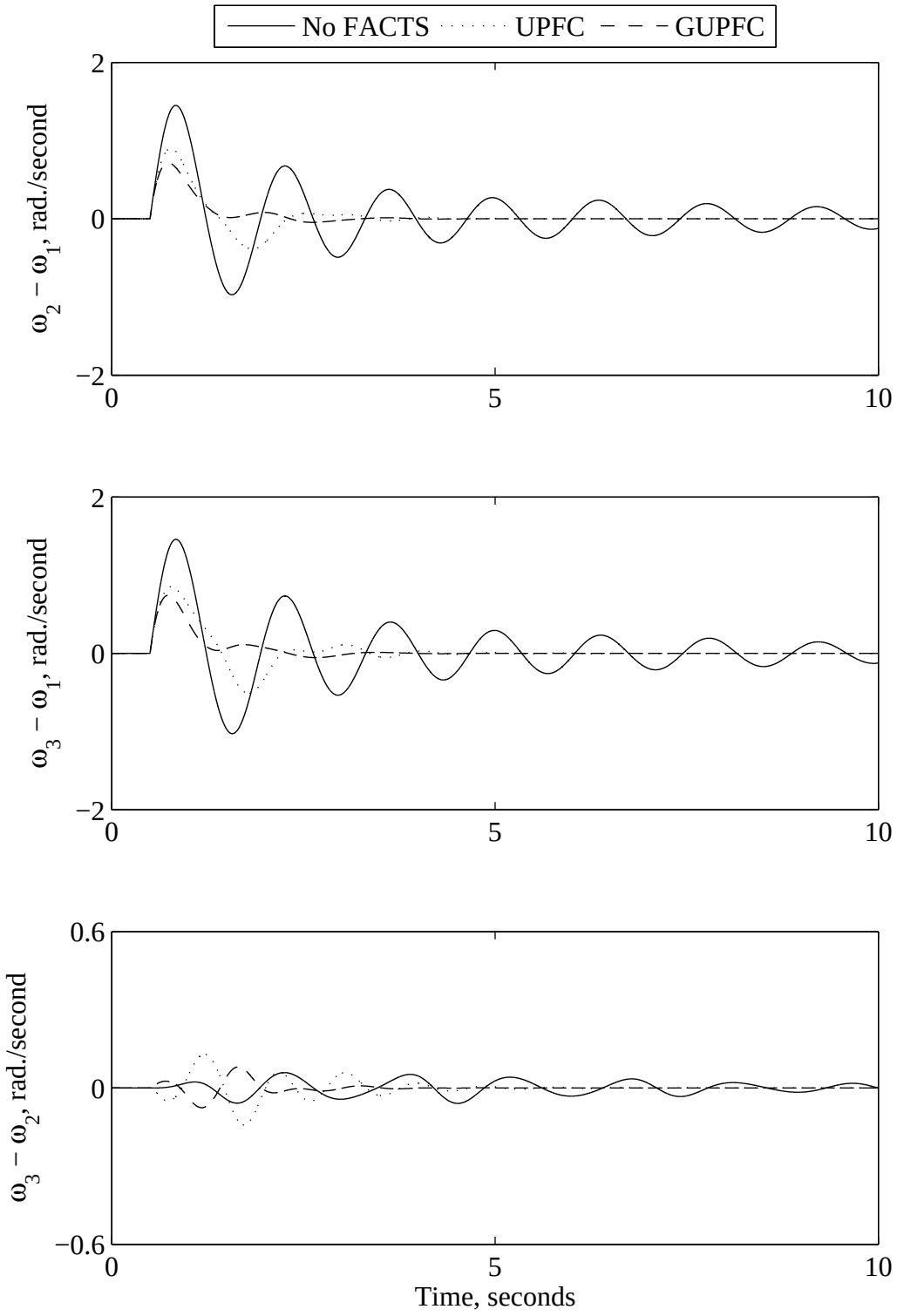

Figure 5.46 Relative generator speed responses for a 20% sudden decrease in the reference power of generator G_1 (a GUPFC is installed at LOC1).

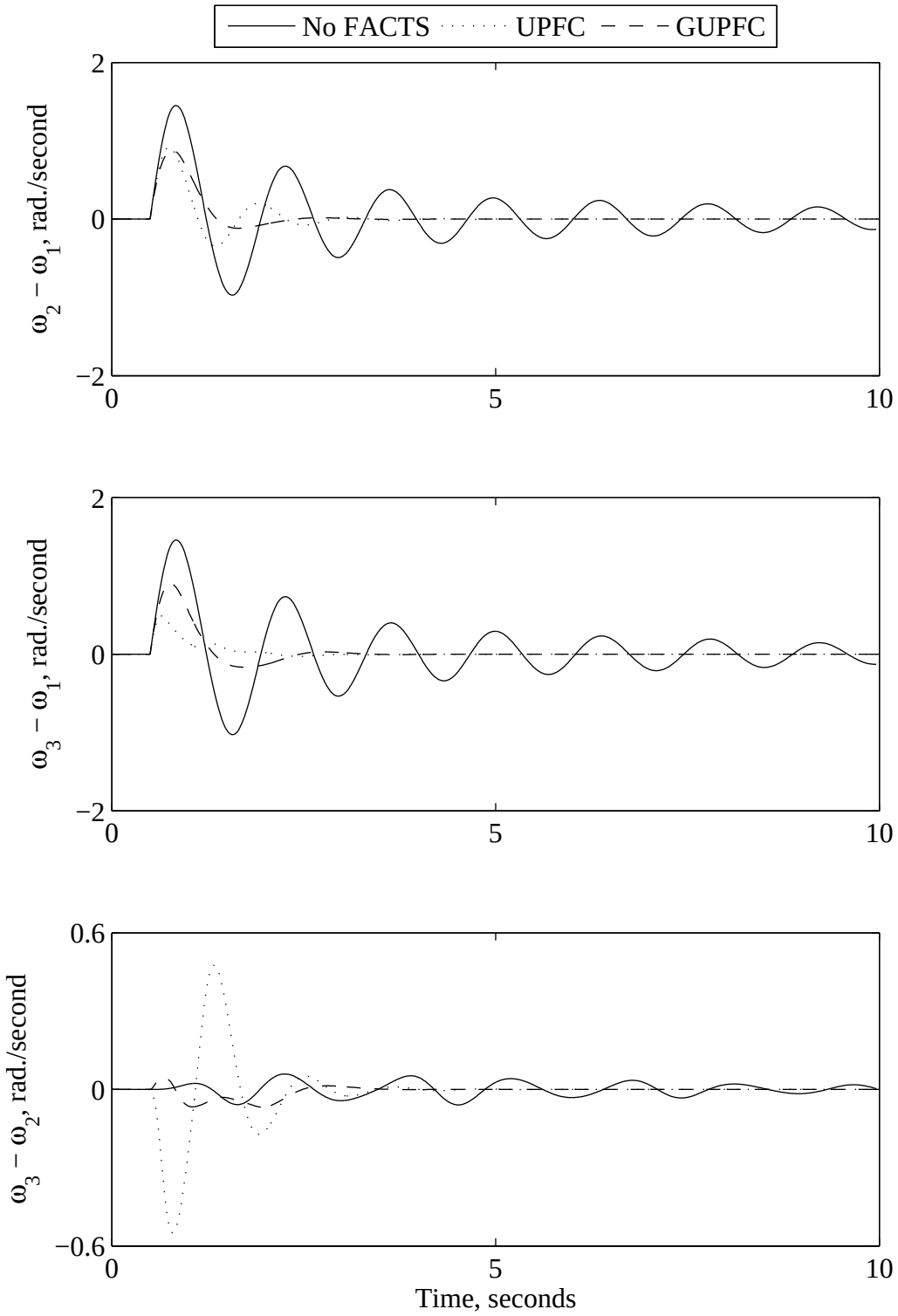

Figure 5.47 Relative generator speed responses for a 20% sudden decrease in the reference power of generator G_1 (two GUPFCs are installed at LOC1 and LOC3).

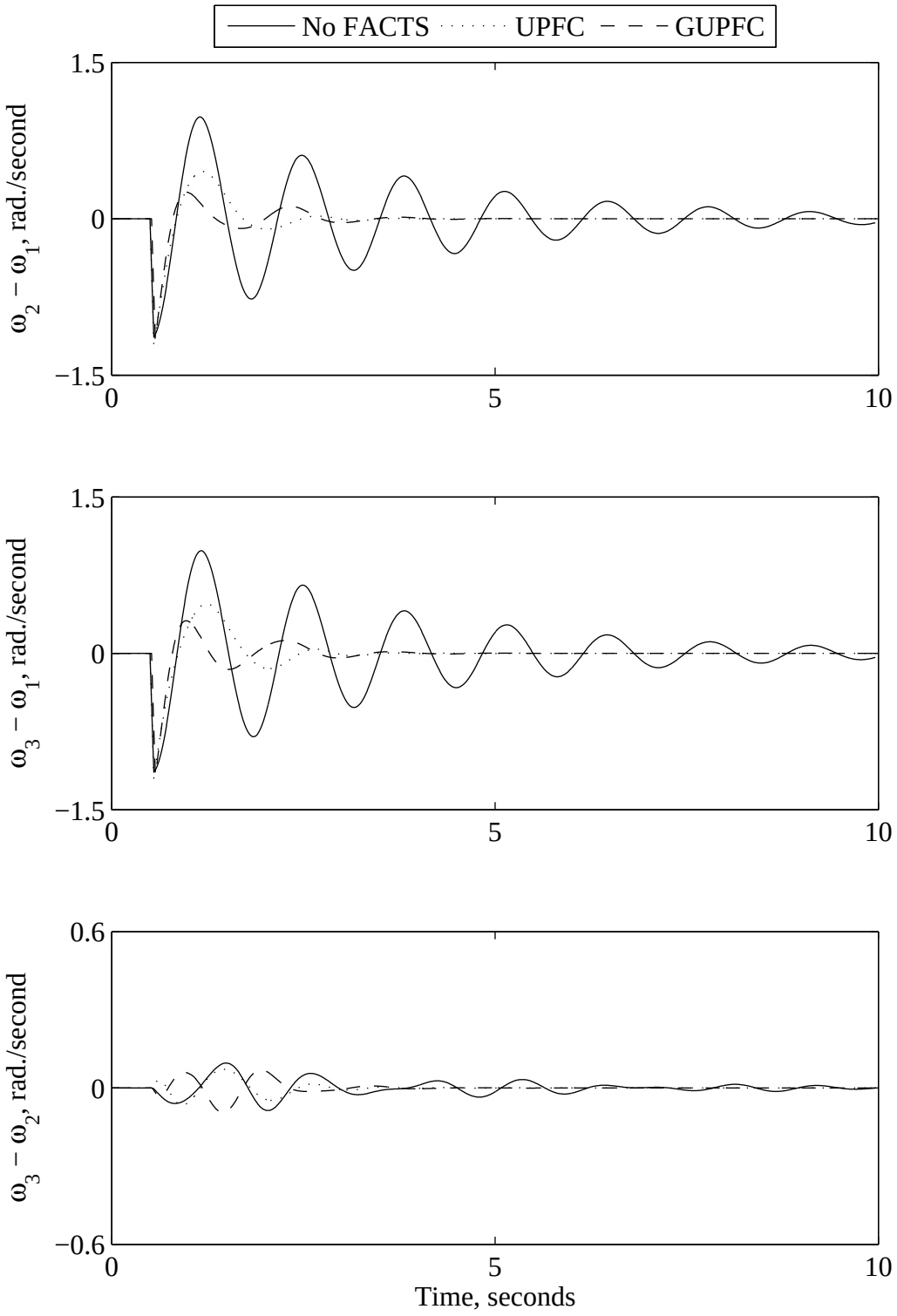

Figure 5.48 Relative generator speed responses due to a 3-cycle 95% sudden load decrease at bus 1 (a GUPFC is installed at LOC1).

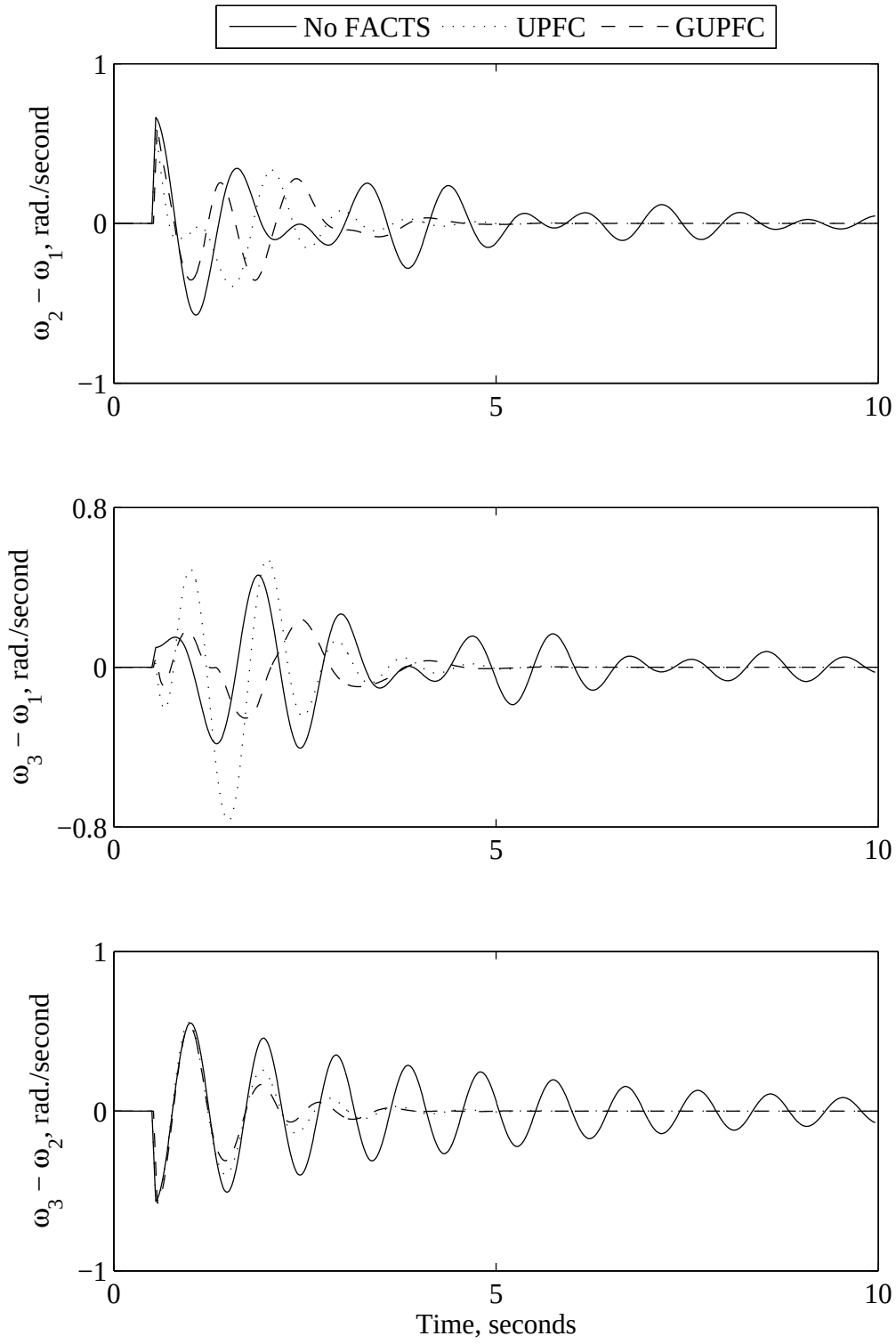

Figure 5.49 Relative generator speed responses due to a 3-cycle 95% sudden load decrease at bus 2 (a GUPFC is installed at LOC1).

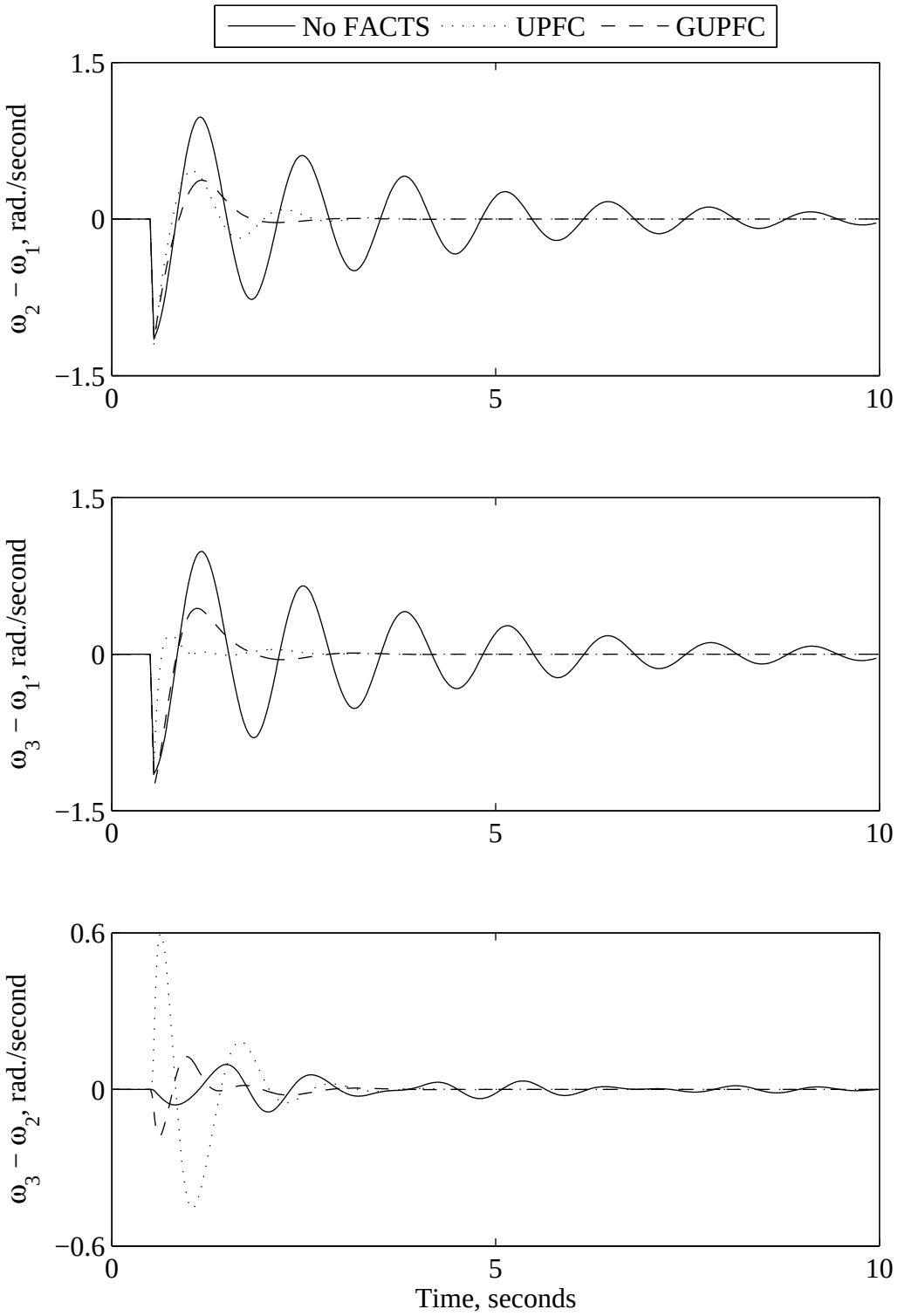

Figure 5.50 Relative generator speed responses due to a 3-cycle 95% sudden load decrease at bus 1 (two GUPFCs are installed at LOC1 and LOC3).

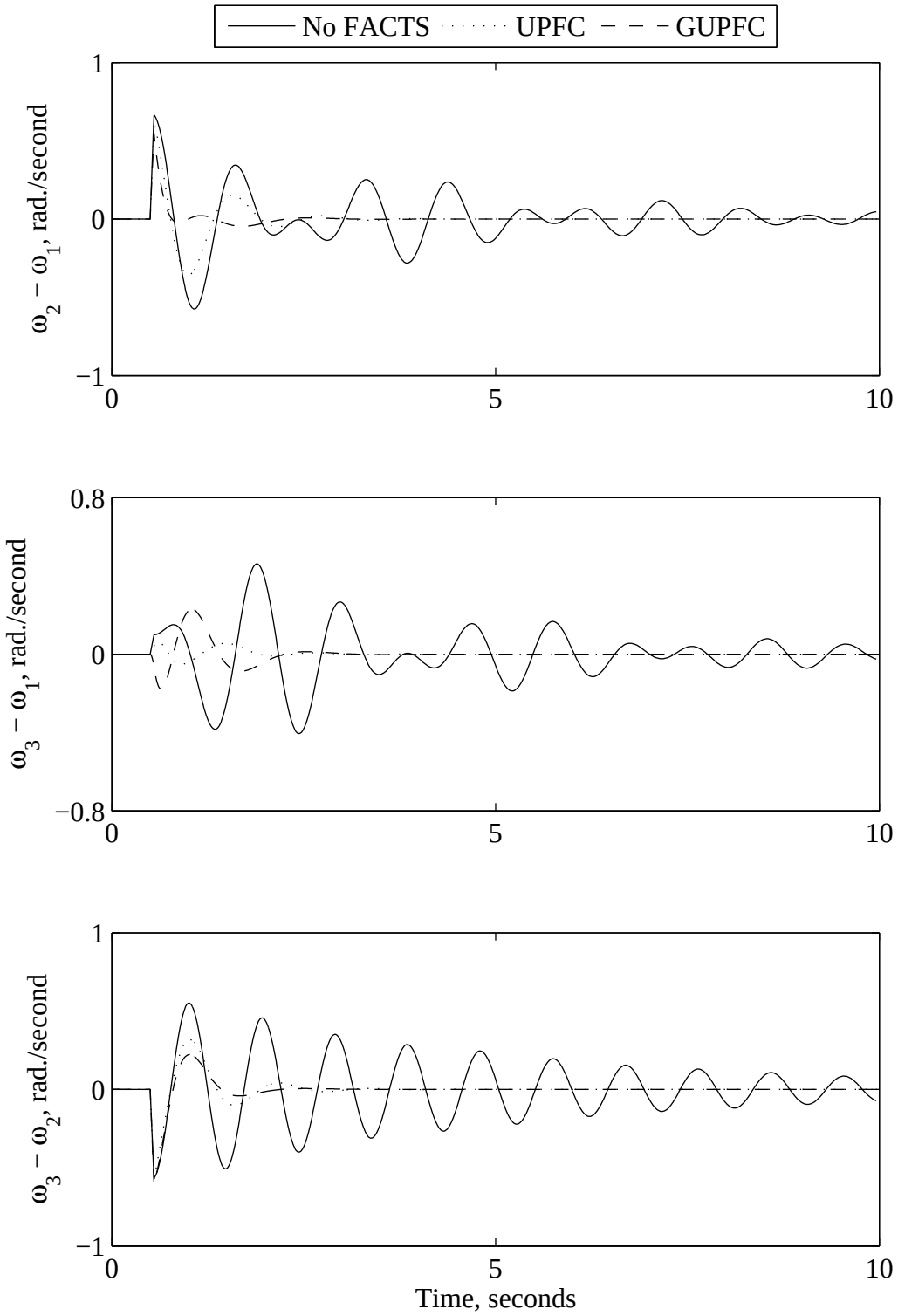

Figure 5.51 Relative generator speed responses due to a 3-cycle 95% sudden load decrease at bus 2 (two GUPFCs are installed at LOC1 and LOC3).

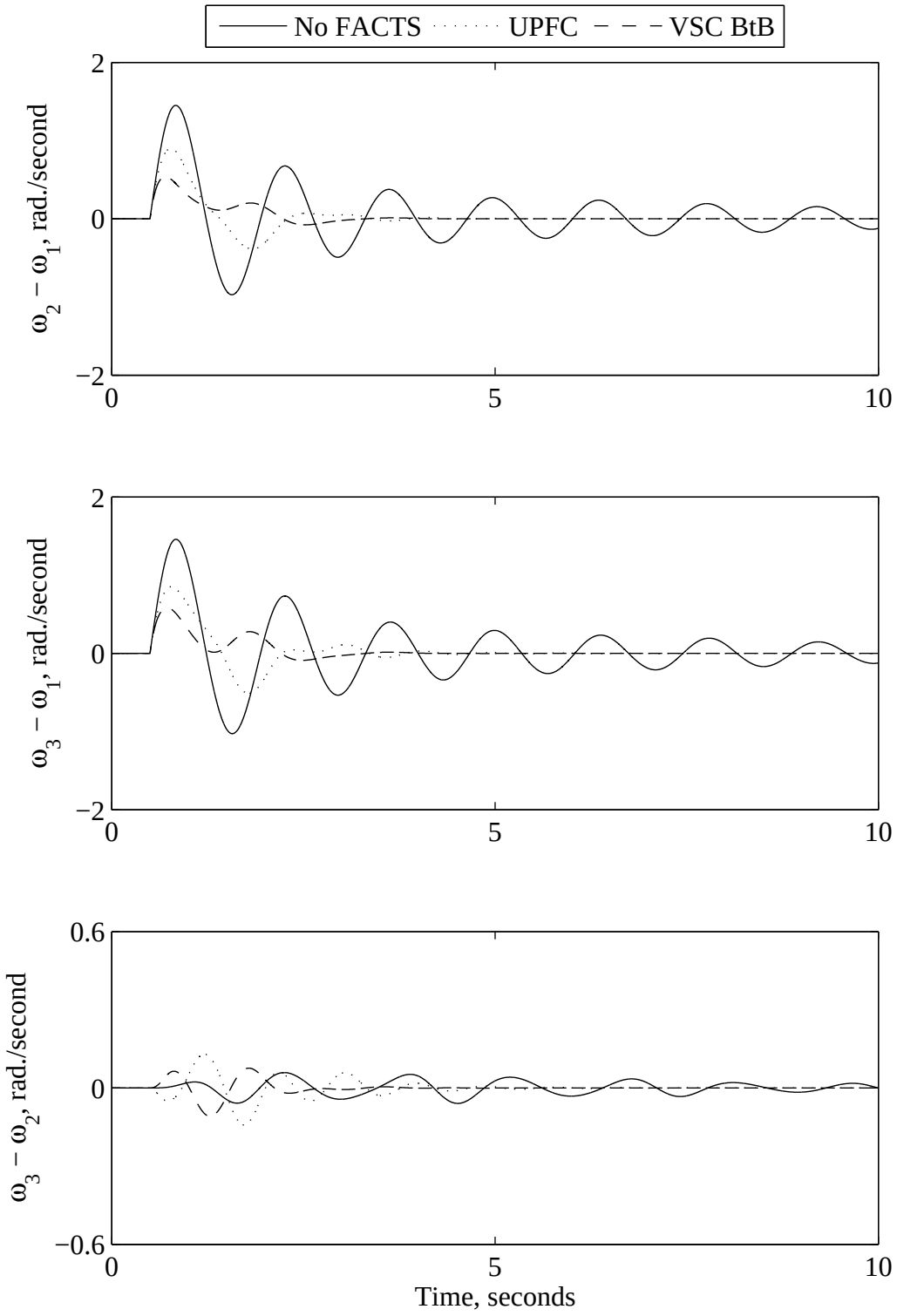

Figure 5.52 Relative generator speed responses for a 20% sudden decrease in the reference power of generator G_1 (a VSC BtB is installed in LOC1).

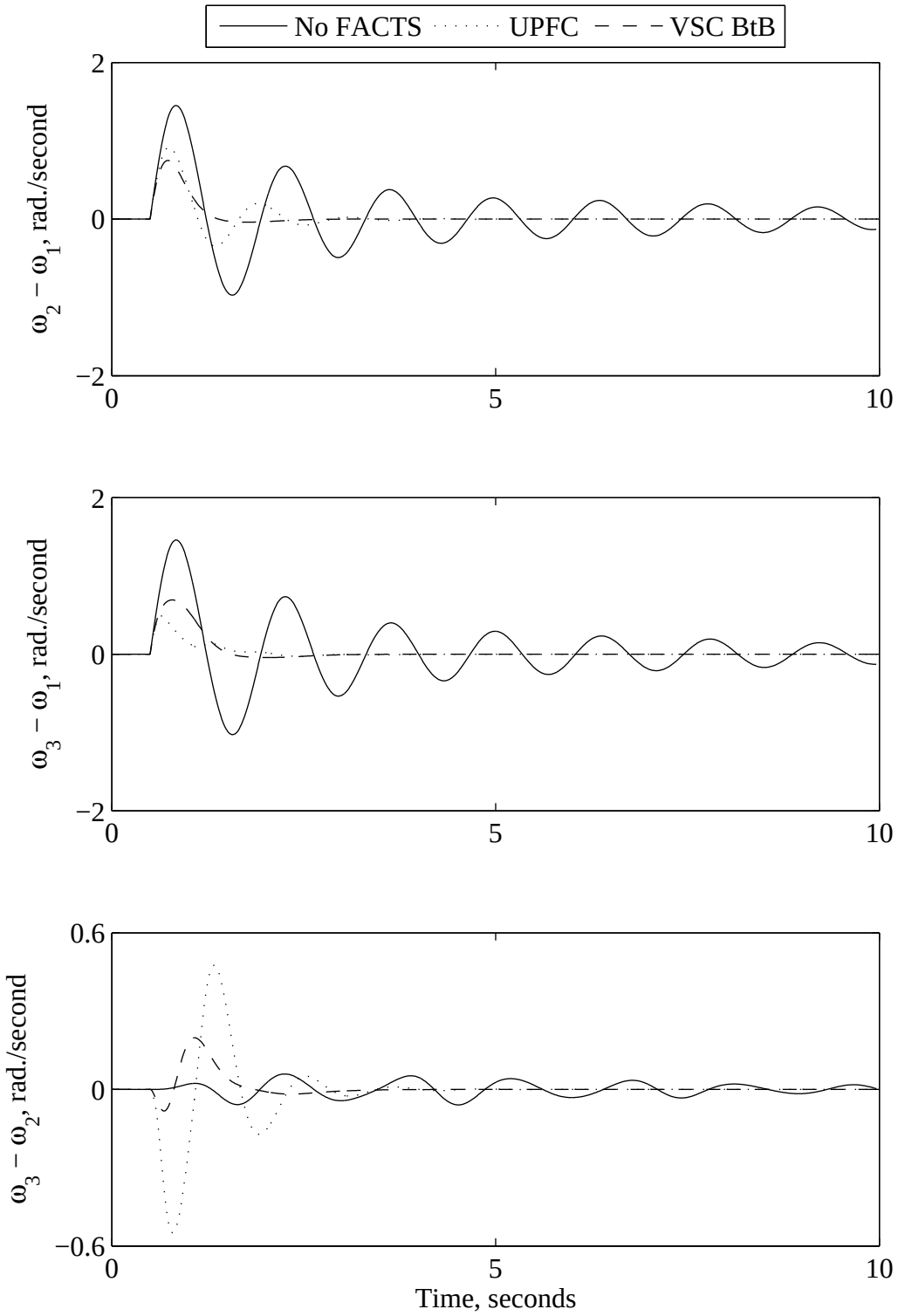

Figure 5.53 Relative generator speed responses for a 20% sudden decrease in the reference power of generator G_1 (two VSC BtB devices are installed at LOC1 and LOC3).

Figures 5.54 and 5.55 show the system response due to a 95%, 3-cycle sudden decrease in loads S_1 and S_2 with the VSC BtB installed at LOC1. The system responses due to the same disturbance with two VSC BtB devices installed at LOC1 and LOC3 are shown in Figures 5.56 and 5.57. It can be seen from these figures that, the VSC BtB exhibits excellent performance in damping the system oscillations. Examining these figures shows again that the VSC BtB performance is relatively better than the UPFC.

5.8. Summary

In this chapter, the steady-state and dynamic models for a proposed three-converter Generalized Unified Power Flow Controller and a Voltage-Source Converter Back-to-Back HVdc link were developed. The GA optimization technique developed in this thesis was applied to design PI controllers for the GUPFC and the VSC BtB. The results of the investigations conducted in this chapter have shown that these two FACTS devices are effective in damping both large and small disturbances and are robust with respect to the fault location. It has been also shown that the GUPFC and VSC BtB provide, in most of the cases, better damping than the UPFC.

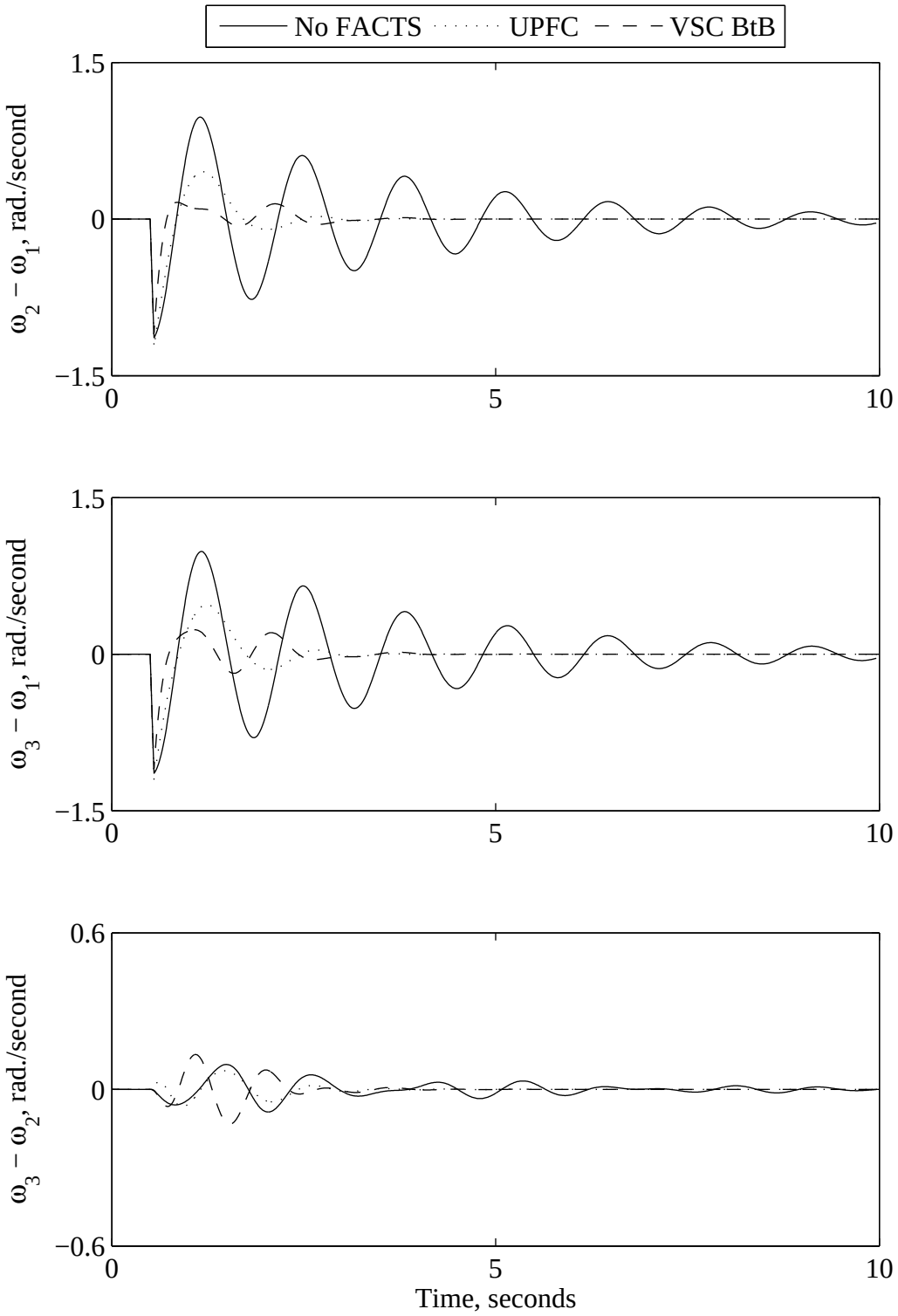

Figure 5.54 Relative generator speed responses due to a 3-cycle 95% sudden load decrease at bus 1 (a VSC BtB is installed at LOC1).

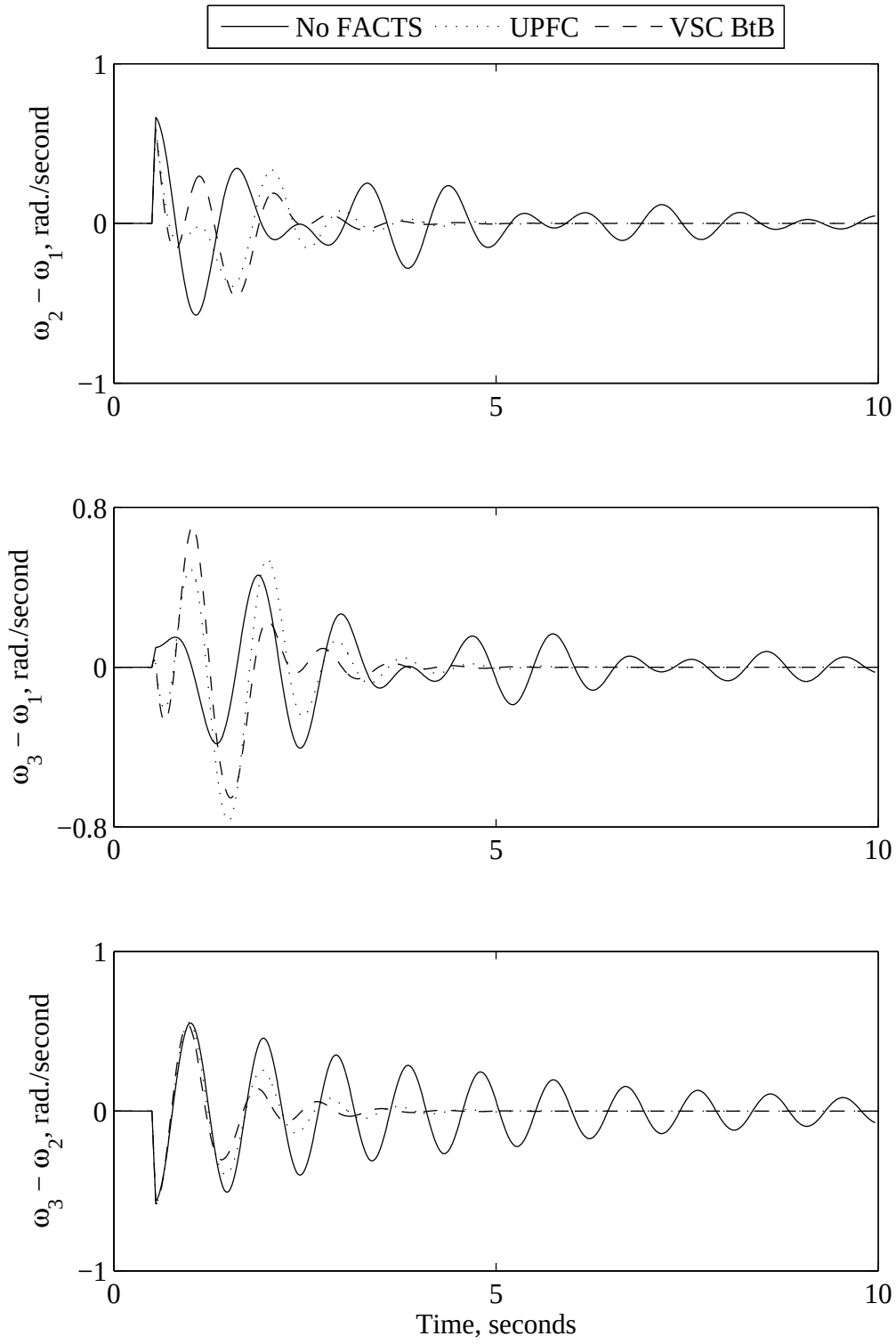

Figure 5.55 Relative generator speed responses due to a 3-cycle 95% sudden load decrease at bus 2 (a VSC BtB is installed at LOC1).

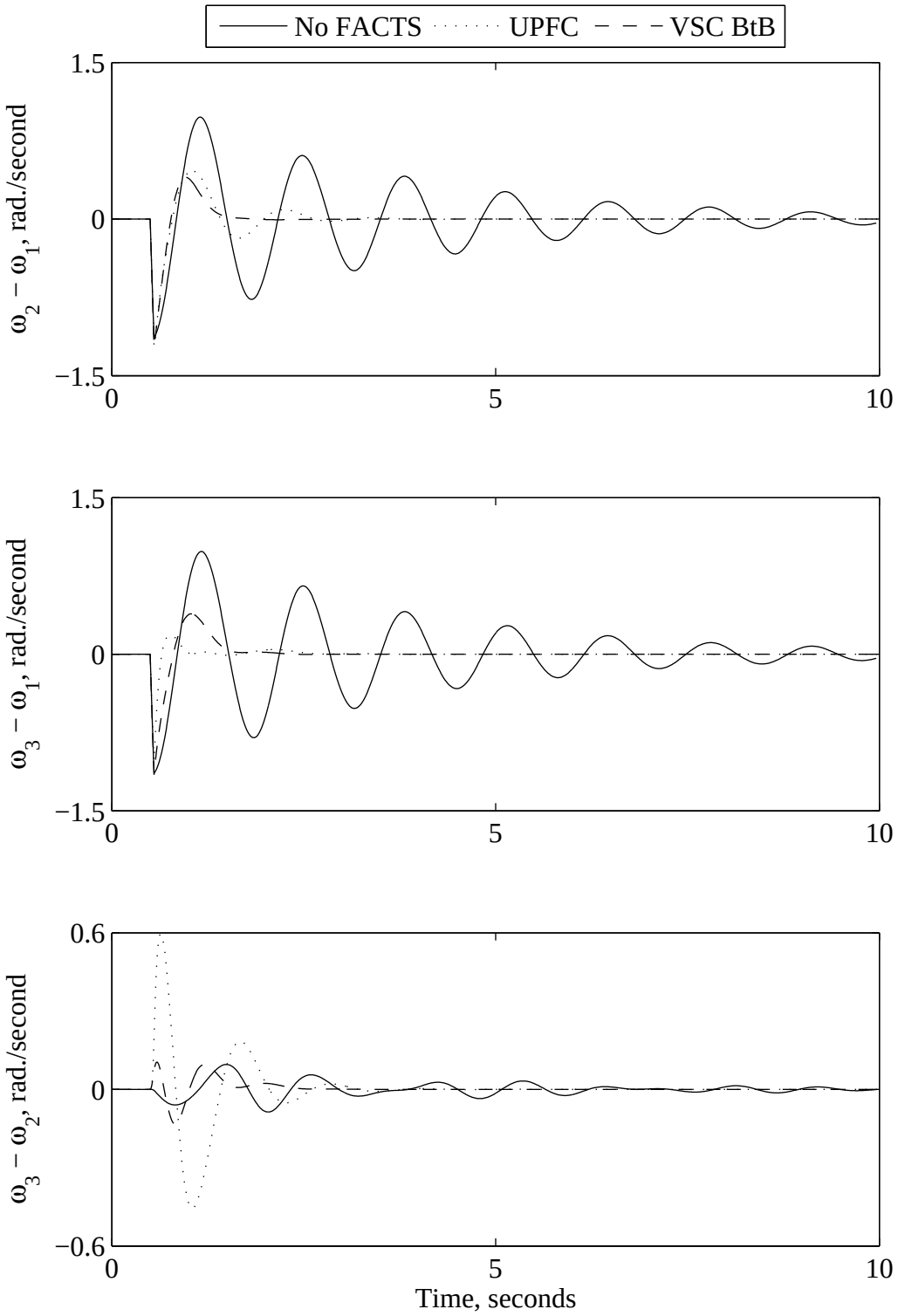

Figure 5.56 Relative generator speed responses due to a 3-cycle 95% sudden load decrease at bus 1 (two VSC BtBa are installed at LOC1 and LOC3).

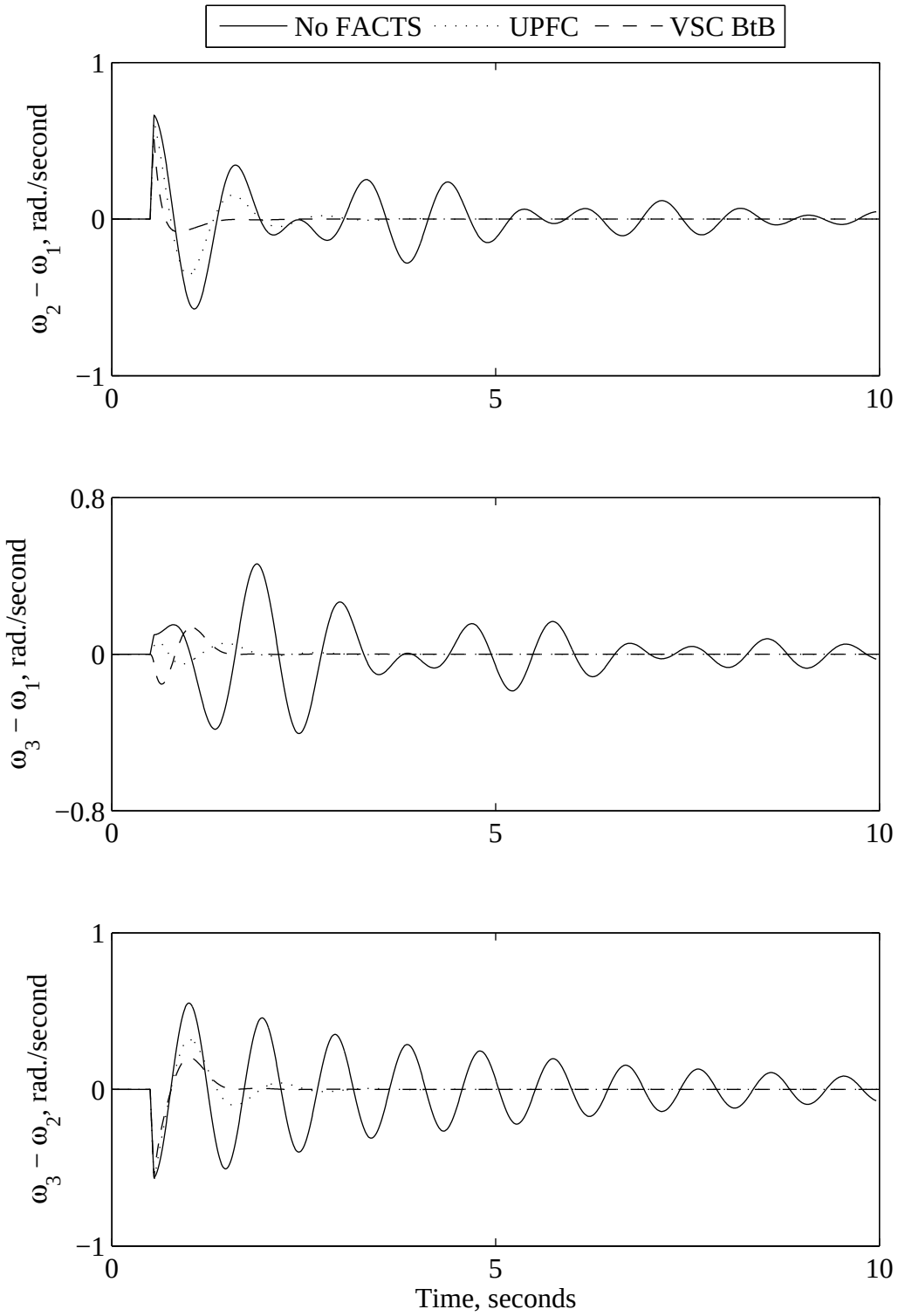

Figure 5.57 Relative generator speed responses due to a 3-cycle 95% sudden load decrease at bus 2 (two VSC BtBa are installed at LOC1 and LOC3).

6. DAMPING TURBINE-GENERATOR SHAFT TORSIONAL TORQUES USING A VOLTAGE SOURCE CONVERTER BACK-TO-BACK HVDC LINK

6.1. Introduction

As it has been mentioned in Chapter 1, FACTS controllers can play a major role in the mitigation of the subsynchronous torsional oscillations resulting from the interaction between turbine-generator shaft systems and the electrical network disturbances. The high torsional stresses induced during some of these disturbances reduce the life expectancy of the turbine-generators and, in severe cases, can cause shaft damage [83]-[87]. In most of the reported studies on the mitigation of the torsional oscillations using FACTS devices, attention has been focused on the TCSC, the STATCOM and the SSSC [88]-[93]. Relatively few studies, however, have been published on the application of the Voltage Source Converter (VSC) Back-to-Back (BtB) HVdc link in damping subsynchronous torsional oscillations [94].

This chapter presents a Genetic Algorithms (GAs) based optimization scheme for designing a PI controller for a VSC BtB HVdc link. This controller is aimed at damping the high torsional torques induced in turbine-generator shafts during clearing and high-speed reclosing of transmission system faults. In this context, investigations have been conducted on a large turbine-generator unit connected to an infinite bus system through a VSC BtB HVdc link. The chapter also presents the same optimization scheme applied to a Unified Power Flow Controller that is able to provide series compensation to the transmission system as well as to damp the torsional oscillations. The effectiveness of the proposed GA FACTS controllers in damping turbine-generator shaft torsional torques is demonstrated through simulation results of typical time responses for different system faults.

6.2. System under Study

The system used in the investigation of this chapter is shown in Figure 6.1. It consists of a turbine-generator connected via a transformer to an infinite bus through a VSC BtB HVdc system. In order to explore the generality of the proposed scheme, investigations have been conducted on two turbine-generator sets of different designs, namely turbine-generator A (600 MVA) and turbine-generator B (892.4 MVA).

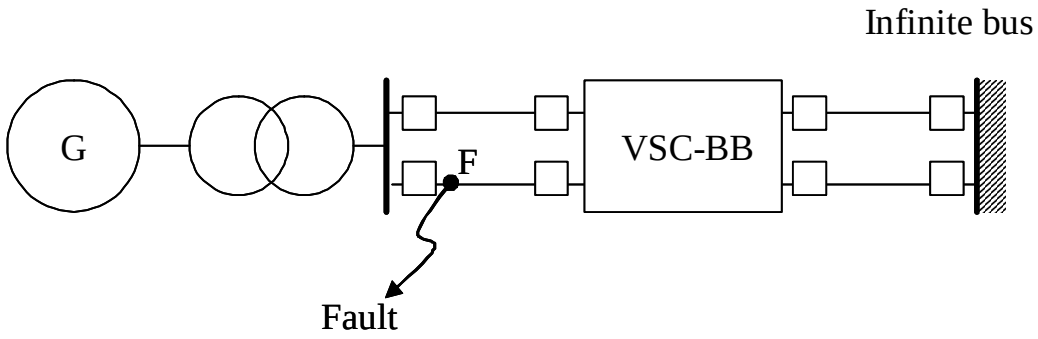

Figure 6.1 System under study.

The shaft system of turbine-generator A, Figure 6.2, consists of a high-pressure turbine (HP), a low-pressure turbine (LP), the generator rotor (GEN) and a rotating exciter (EXC). The shaft system of turbine-generator B, Figure 6.3, consists of high-pressure turbine (HP), an intermediate-pressure turbine (IP), two low-pressure turbines (LPA and LPB), the generator rotor (GEN) and a rotating exciter (EXC). The data of generators A and B and their associated turbines are taken from the IEEE first and second benchmark model established for the purpose of studying subsynchronous resonance [95], [96]. Faults are assumed to occur at the beginning of one of the transmission line circuits (point F, Figure 6.1) and to be cleared by the circuit breaker operations at both ends of the line. The system data are given in Table 6-1.

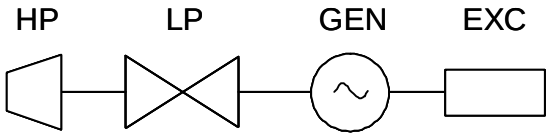

Figure 6.2 Turbine-generator A shaft system.

Table 6-1 System data

Electrical data of the transmission system			
Transformer (600, 892.4 MVA, 22, 26/500 kV)			
x_T = 0.1 p.u.		r_T = 0.001 *p.u.*	
Transmission Line (500 kV)			
x_L = 0.48 *p.u.*		r_L = 0.04 *p.u.*	
Mechanical data of the turbine-generator A			
Mass	Inertia (p.u.)	Damping (p.u./p.u. speed)	Spring Constant (p.u./rad.)
EXC	5.195	0.0013	3.741
GEN	661.918	0.1761	83.497
LP	1167.267	0.3105	42.715
HP	187.496	0.0498	
Electrical data of the turbine-generator A			
Generator (600 MVA, 22kV, 60 Hz)			
$x_l = 0.14$ *p.u.*	$x_d = 1.65$ *p.u.*	$x'_d = 0.25$ *p.u.*	$x''_d = 0.2$ *p.u.*
$r_a = 0.0045$ *p.u.*	$x_q = 1.59$ *p.u.*	$x'_q = 0.46$ *p.u.*	$x''_q = 0.2$ *p.u.*
$T'_{do} = 4.5s$	$T''_{do} = 0.04s$	$T'_{qo} = 0.55s$	$T''_{qo} = 0.09s$
Mechanical data of the turbine-generator B			
Mass	Inertia (p.u.)	Damping (p.u./p.u. speed)	Spring Constant (p.u./rad.)
EXC	25.798	0.068	2.822
GEN	654.829	0.099	70.858
LPB	666.682	0.1	52.038
LPA	647.421	0.1	34.929
IP	117.311	0.025	19.303
HP	70.042	0.008	
Electrical data of the turbine-generator B			
Generator (692.4 MVA, 26kV, 60 Hz)			
$x_l = 0.13$ *p.u.*	$x_d = 1.79$ *p.u.*	$x'_d = 0.169$ *p.u.*	$x''_d = 0.135$ *p.u.*
$r_a = 0$ *p.u.*	$x_q = 1.71$ *p.u.*	$x'_q = 0.228$ *p.u.*	$x''_q = 0.2$ *p.u.*
$T'_{do} = 4.3s$	$T''_{do} = 0.032s$	$T'_{qo} = 0.85s$	$T''_{qo} = 0.05s$

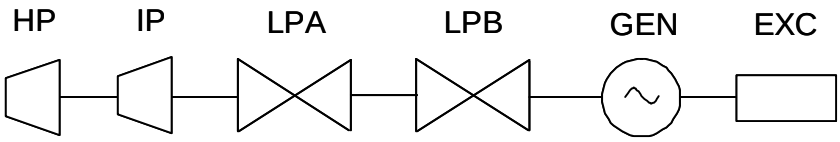

Figure 6.3 Turbine-generator B shaft system.

6.3. Modeling of the Turbine-Generator Shaft System

The turbine-generator mechanical system is modeled using a lumped-mass model [97]. In such a model, Figure 6.4, each major rotating element (generator, turbine stage, etc.) is modeled as a lumped mass and each shaft segment is modeled as a massless rotational spring with its spring constant representing the shaft stiffness. The values of the various inertias M incorporated in such a model are functions of the rotor-dimensions and are usually provided by the manufacturer. The stiffness K of the various parts of the shaft are functions of the shaft diameters and the elasticity of its material and are also provided by the manufacturer.

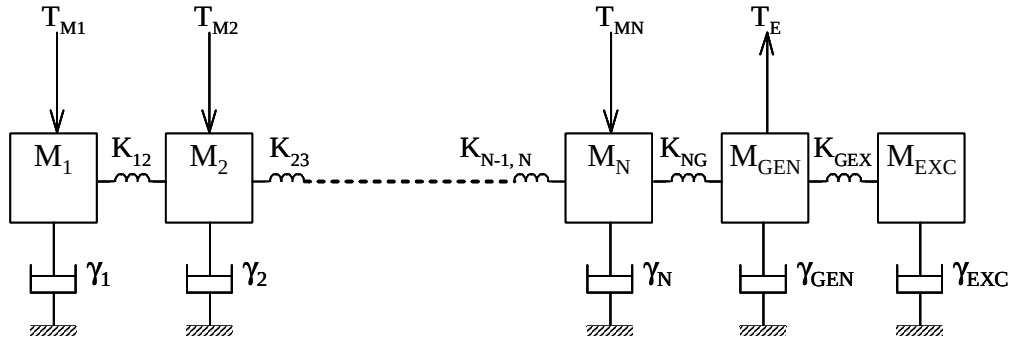

Figure 6.4 Lumped-mass model of a turbine-generator mechanical system.

On the other hand, the mechanical damping is made of various components (steam damping, windage damping of rotors, bearing oil film damping and shaft material hysteresis damping) which are different in nature [98].

In the analysis conducted in this chapter, the mechanical damping is represented by constant damping coefficients γ_i located at each inertia.

6.3.1. The mathematical representation of the turbine-generator mechanical system

The mathematical treatment of the lumped-mass model is usually expressed as a set of first-order differential equations. For a mechanical system of a turbine-generator with a

rotating exciter and an N-stage turbine (Figure 6.4), these equations can be expressed in a normalized form as follows [99], [100]:

$$
\begin{aligned}
&M_1\dot{\omega}_1 = T_{M1} - \gamma_1\dot{\delta}_1 - K_{12}(\delta_1 - \delta_2)\\
&\dot{\delta}_1 = \omega_1 - \omega_o\\
&M_2\dot{\omega}_2 = T_{M2} - \gamma_2\dot{\delta}_2 + K_{12}(\delta_1 - \delta_2) - K_{23}(\delta_2 - \delta_3)\\
&\dot{\delta}_2 = \omega_2 - \omega_o\\
&\cdots\\
&\cdots\\
&M_N\dot{\omega}_N = T_{MN} - \gamma_N\dot{\delta}_N + K_{N-1,N}(\delta_{N-1} - \delta_N) - K_{NG}(\delta_N - \delta)\\
&\dot{\delta}_N = \omega_N - \omega_o\\
&M_{GEN}\dot{\omega} = -T_E - \gamma_{GEN}\dot{\delta} + K_{NG}(\delta_N - \delta) - K_{GEX}(\delta - \delta_{EXC})\\
&\dot{\delta} = \omega - \omega_o\\
&M_{EXC}\dot{\omega}_{EXC} = -\gamma_{EXC}\dot{\delta}_{EXC} + K_{GEX}(\delta - \delta_{EXC})\\
&\dot{\delta}_{EXC} = \omega_{EXC} - \omega_o
\end{aligned}
\tag{6-1}
$$

The mechanical torque T_{Mi}, ($i = 1, N$) can be written as follows:

$$T_{Mi} = T_{Mo} - T_{Mio}\frac{\Delta\omega}{\omega_o} \tag{6-2}$$

As it has been assumed that no governor action is represented, $T_{Mio} = \frac{P_{Mi}}{\omega_o}$, where P_{Mi} is the turbine power which is constant and equal to its initial value. The second term of Equation (6-2), namely $T_{Mio}\frac{\Delta\omega}{\omega_o}$, represents the steam damping of the turbine-stage.

6.3.2. The complete mathematical representation of the turbine-generator system connected to the infinite bus system

Development of the complete mathematical model is based on combining Equations (6-1) and (6-2) with the power system and BtB controller dynamic equations. A PI controller is then designed using the same technique used in Section 2.5 with the stabilizing signal chosen to be either the generator speed or the generator and exciter speeds.

6.4. VSC BtB Controller Performance during Fault Clearing

To demonstrate the effectiveness of the designed PI controller in damping turbine-generator shaft torsional torques, several time domain studies are carried out on the system under investigations. The system pre-disturbance operating condition is such that the turbine-generator is delivering its rated power to the infinite bus system.

6.4.1. Case study I: a three-phase fault with $\Delta\omega$ as the stabilizing signal

The shaft torsional torque responses of turbine-generator A during a 4-cycle three-phase fault are illustrated in Figure 6.5 with the BtB HVdc controller out of service and in Figure 6.6 with the BtB HVdc controller in service with the generator speed deviation as the stabilizing signal. Figures 6.7 and 6.8 show the shaft speed responses with the BtB HVdc controller out of service and with the BtB HVdc controller in service.

System short circuits impress slightly offset pulsating torsional torques on the shaft sections, the magnitude and behavior of which are governed by the sudden loss of load and by the pulsating electromagnetic torque. As it can be seen from Figure 6.5, the turbine-generator torsional torques are, most often, not sinusoidal with a single frequency component, but contain contributions from all the torsional modes. Moreover, it can be noticed that the shaft section between the generator and the low-pressure stage is subjected to the highest stresses.

Comparing Figures 6.5 and 6.7 with Figures 6.6 and 6.8 reveals that the BtB HVdc controller is effective in damping all the shaft torsional torques. It can be also noticed from Figure 6.6 that the (GEN-EXC) shaft torsional torque is less damped than the other two shaft torsional torques. It is worth noting here that the eigenvectors analysis of the turbine-generator shaft system reveals that torsional Mode 3 (51.1 Hz) is more dominant in the (GEN-EXC) shaft section (Appendix G) [96].

Figures 6.9 to 6.11 illustrate the shaft torsional torque responses of turbine-generator B. As can be seen from these figures, the designed controller significantly damps the torsional torques in all the shaft sections. Figures 6.12 to 6.15 show the turbine-generator speed responses of turbine-generator B due to a 4-cycle three-phase fault with and without employing the BtB HVdc controller.

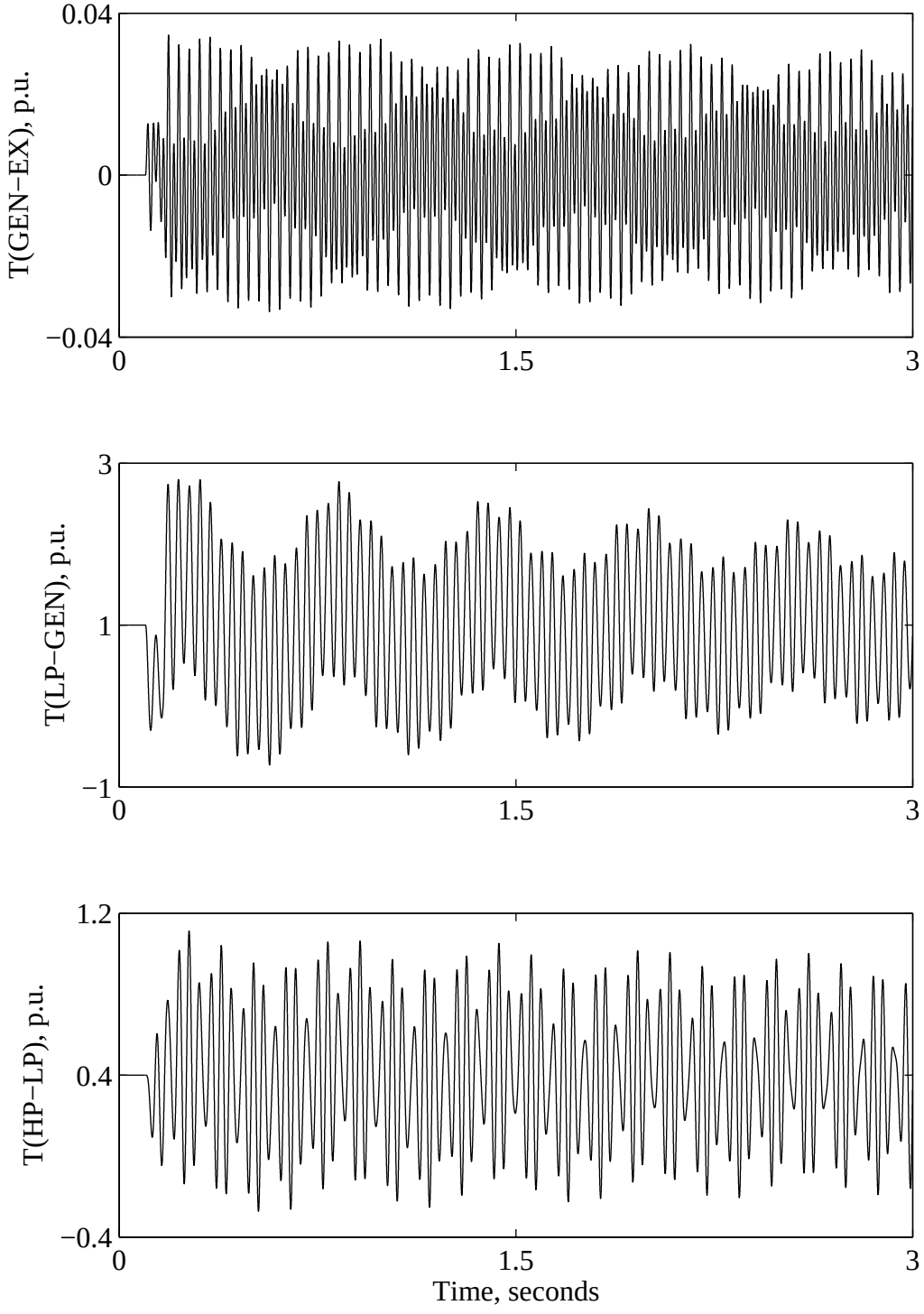

Figure 6.5 Torsional torque responses of turbine-generator A due to a 4-cycle three-phase fault, BtB controller is not employed.

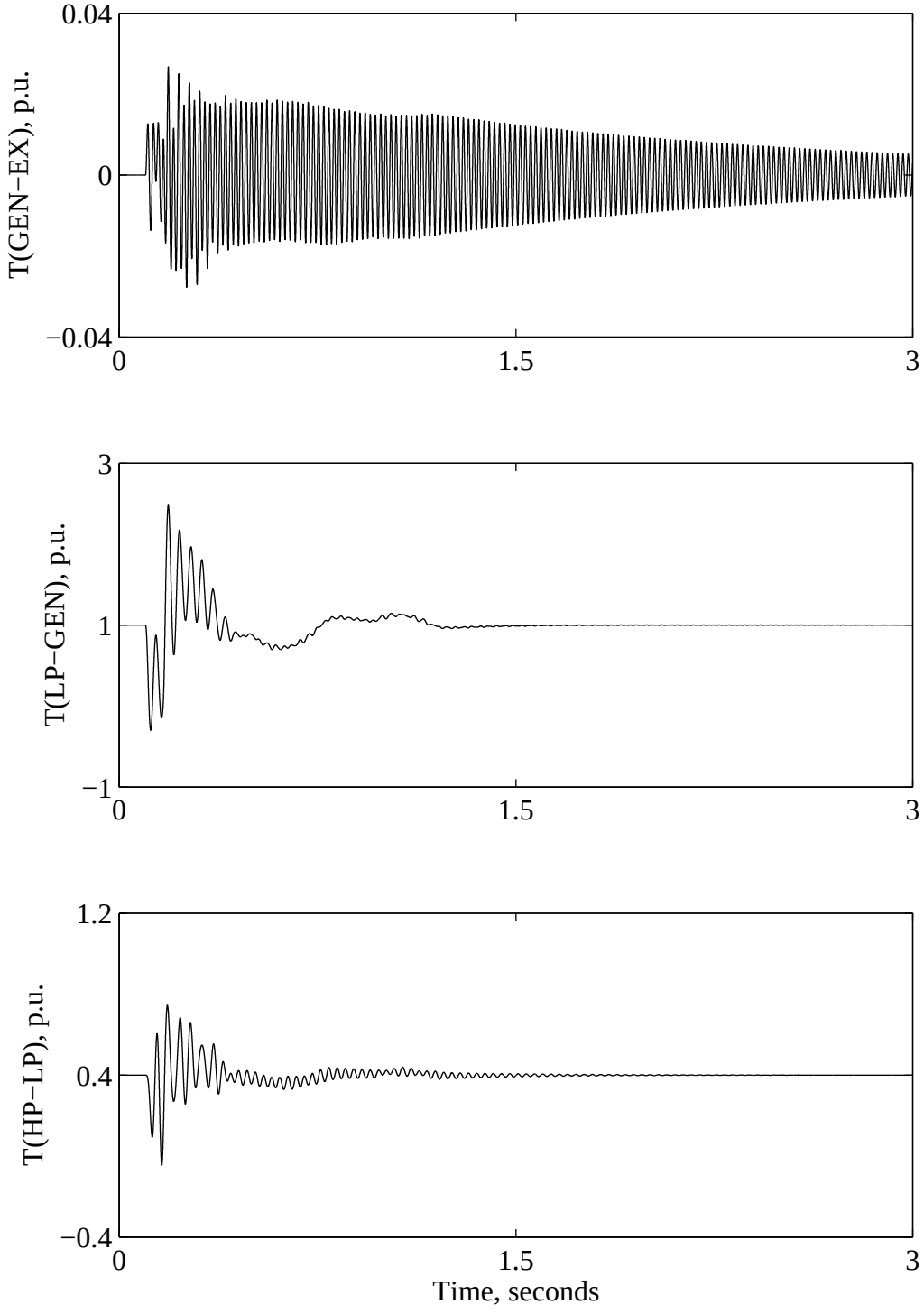

Figure 6.6 Torsional torque responses of turbine-generator A due to a 4-cycle three-phase fault, BtB controller is employed with the generator speed as the stabilizing signal.

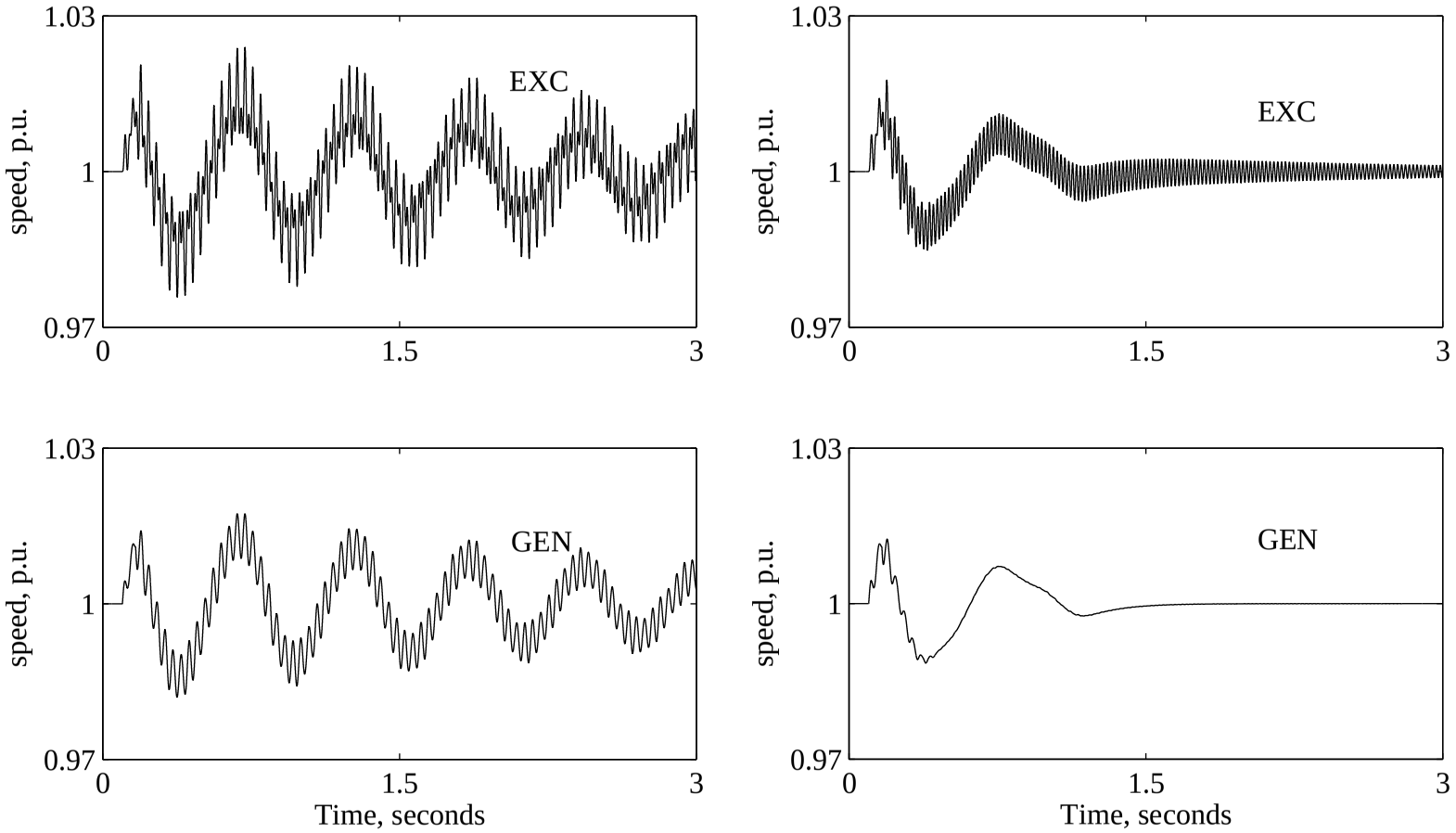

Figure 6.7 Speed responses of turbine-generator A due to a 4-cycle three-phase fault: (a) BtB controller is not employed, (b) BtB controller is employed with the generator speed as the stabilizing signal.

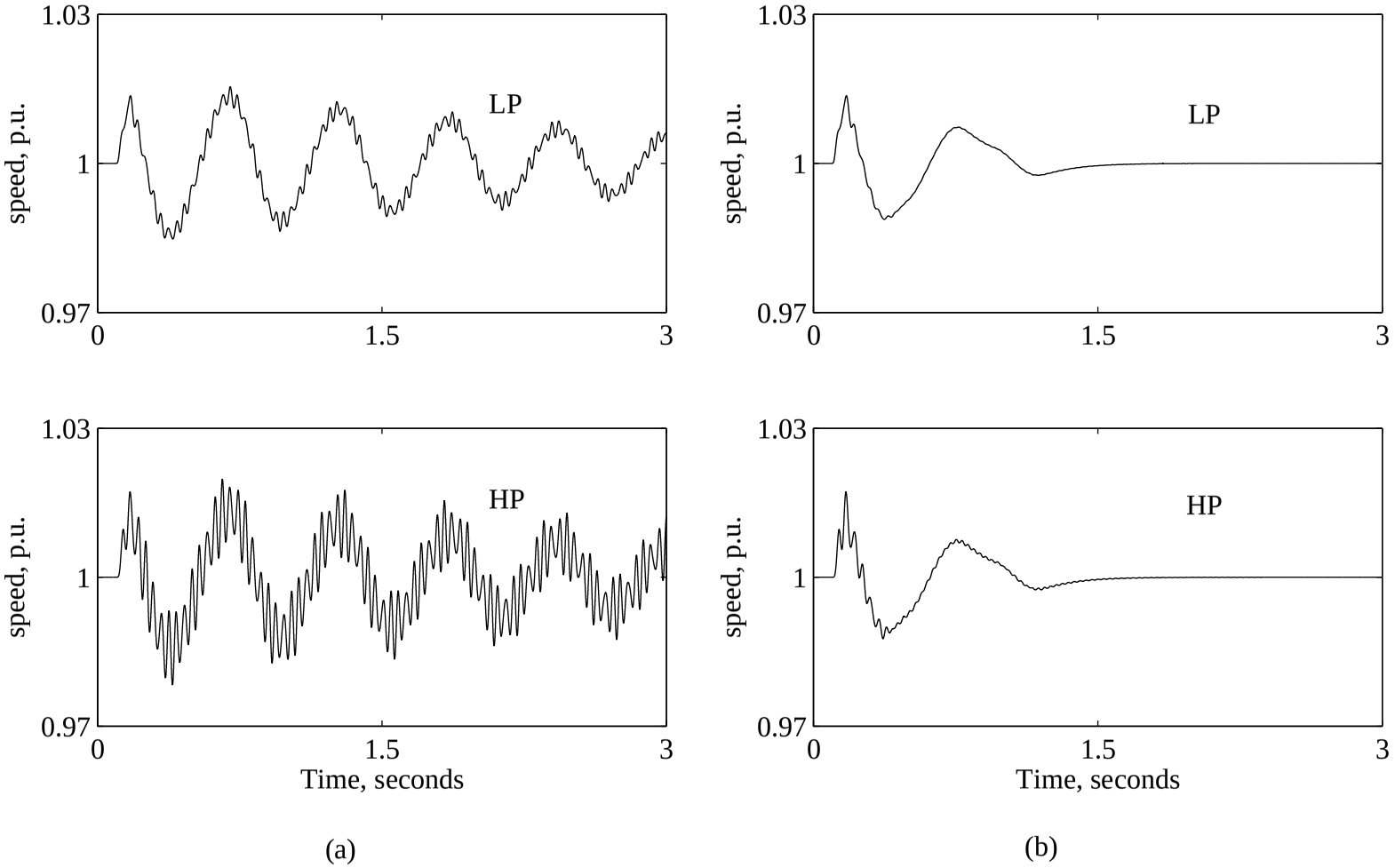

Figure 6.8 Speed responses of turbine-generator A due to a 4-cycle three-phase fault: (a) BtB controller is not employed, (b) BtB controller is employed with the generator speed as the stabilizing signal.

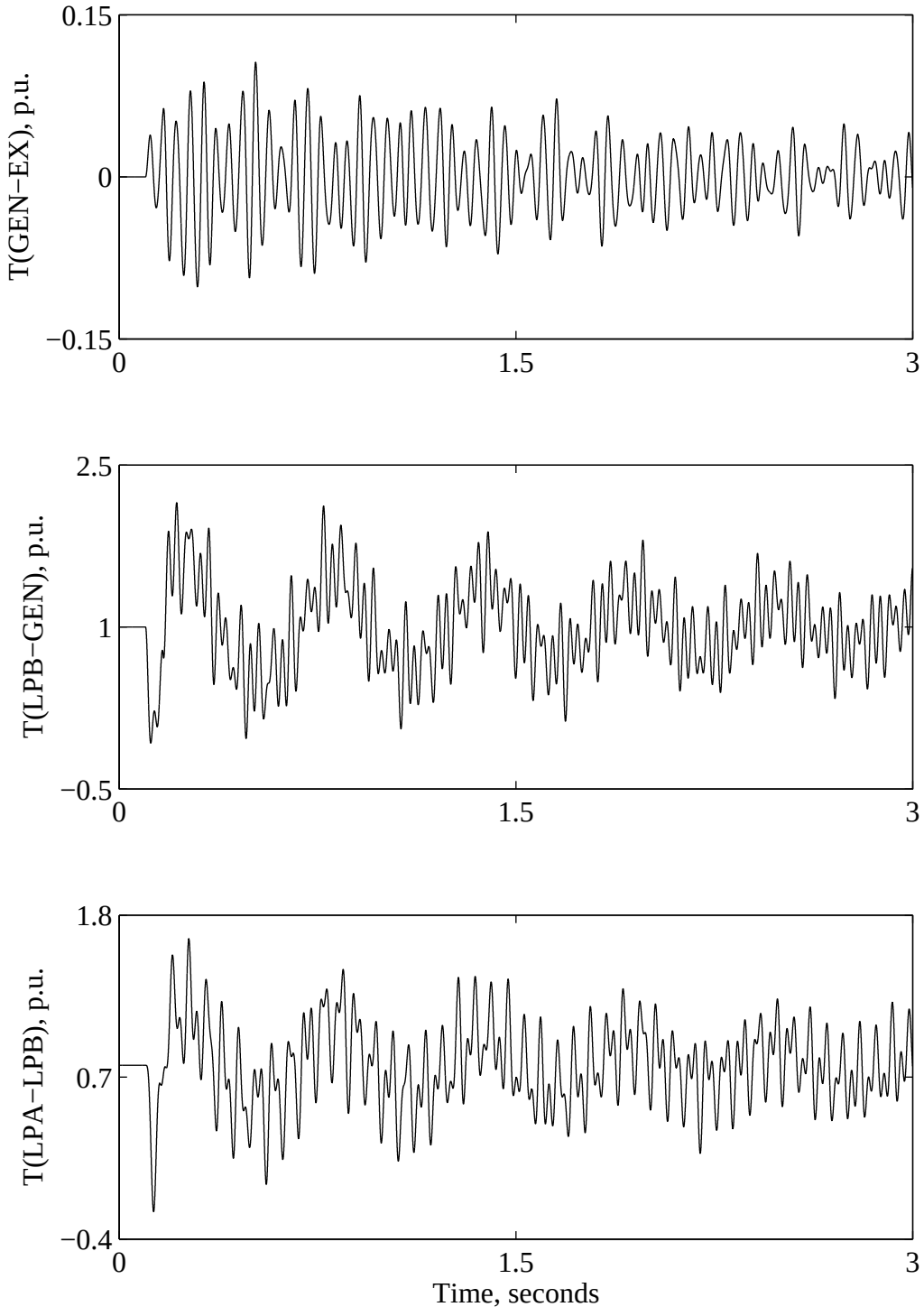

Figure 6.9 Torsional torque responses of turbine-generator B due to a 4-cycle three-phase fault, BtB controller is not employed.

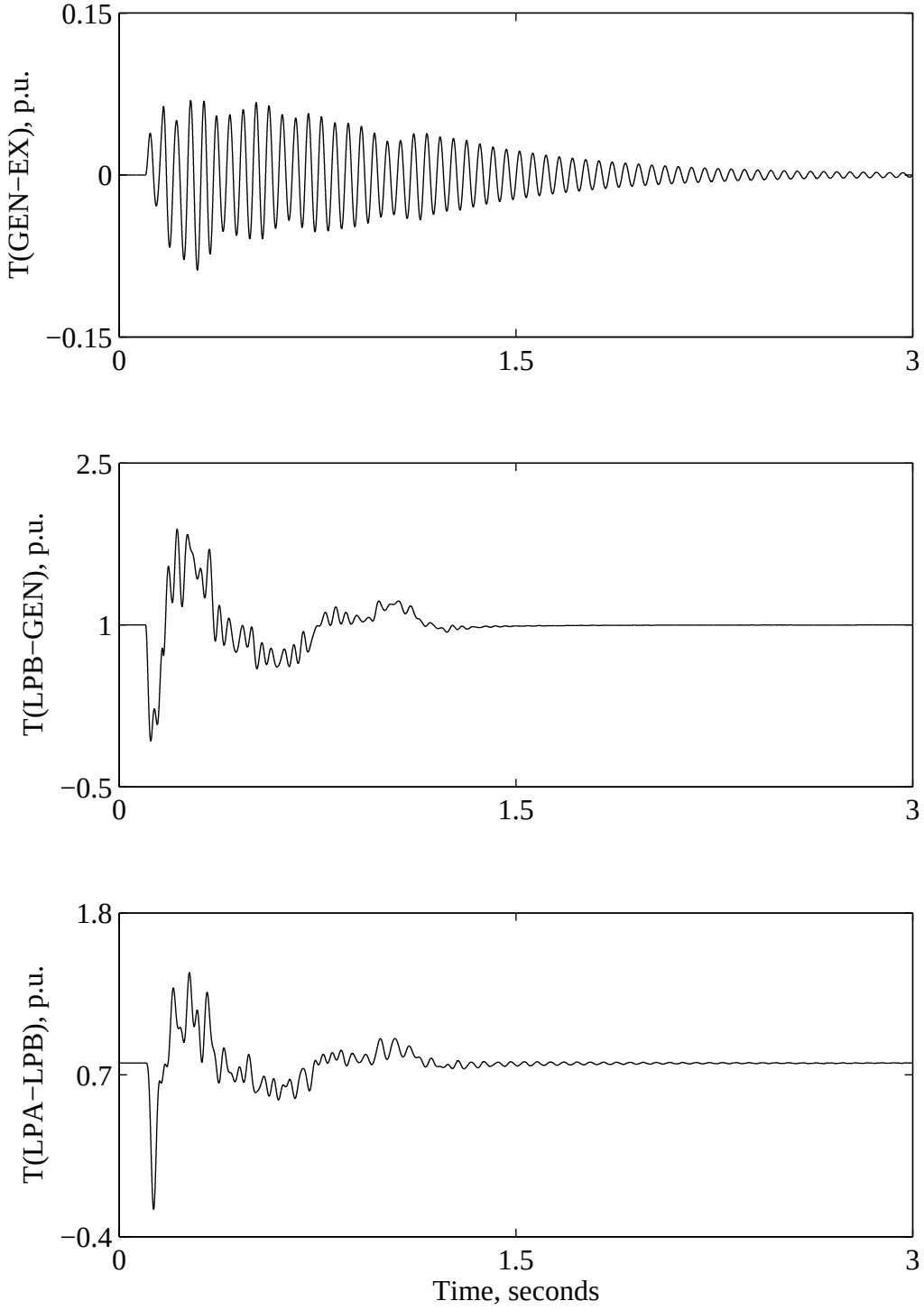

Figure 6.10 Torsional torque responses of turbine-generator B due to a 4-cycle three-phase fault, BtB controller is employed with the generator speed as the stabilizing signal.

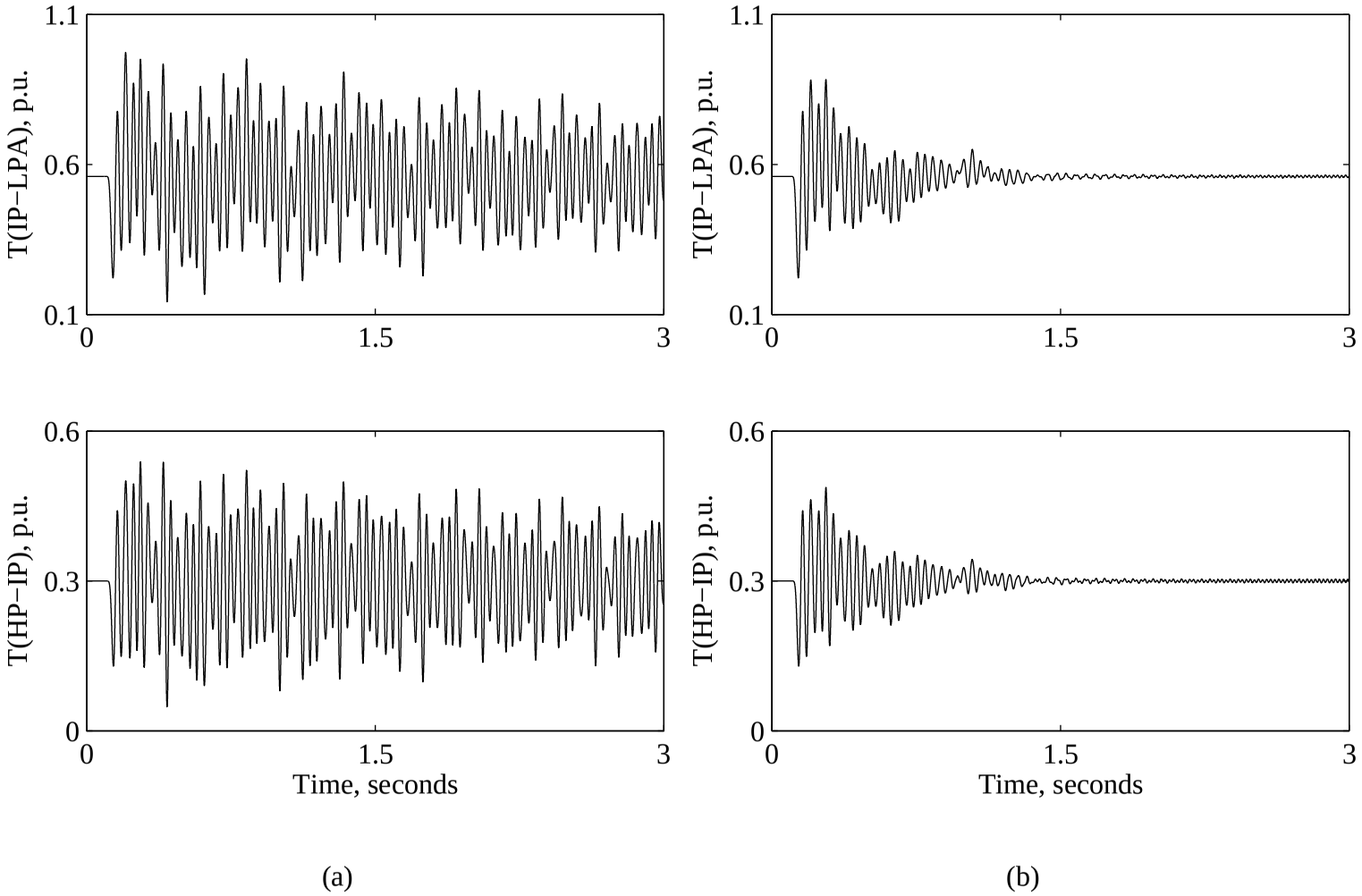

Figure 6.11 Torsional torque responses of turbine-generator B due to a 4-cycle three-phase fault: (a) BtB controller is not employed, (b) BtB controller is employed with the generator speed as the stabilizing signal.

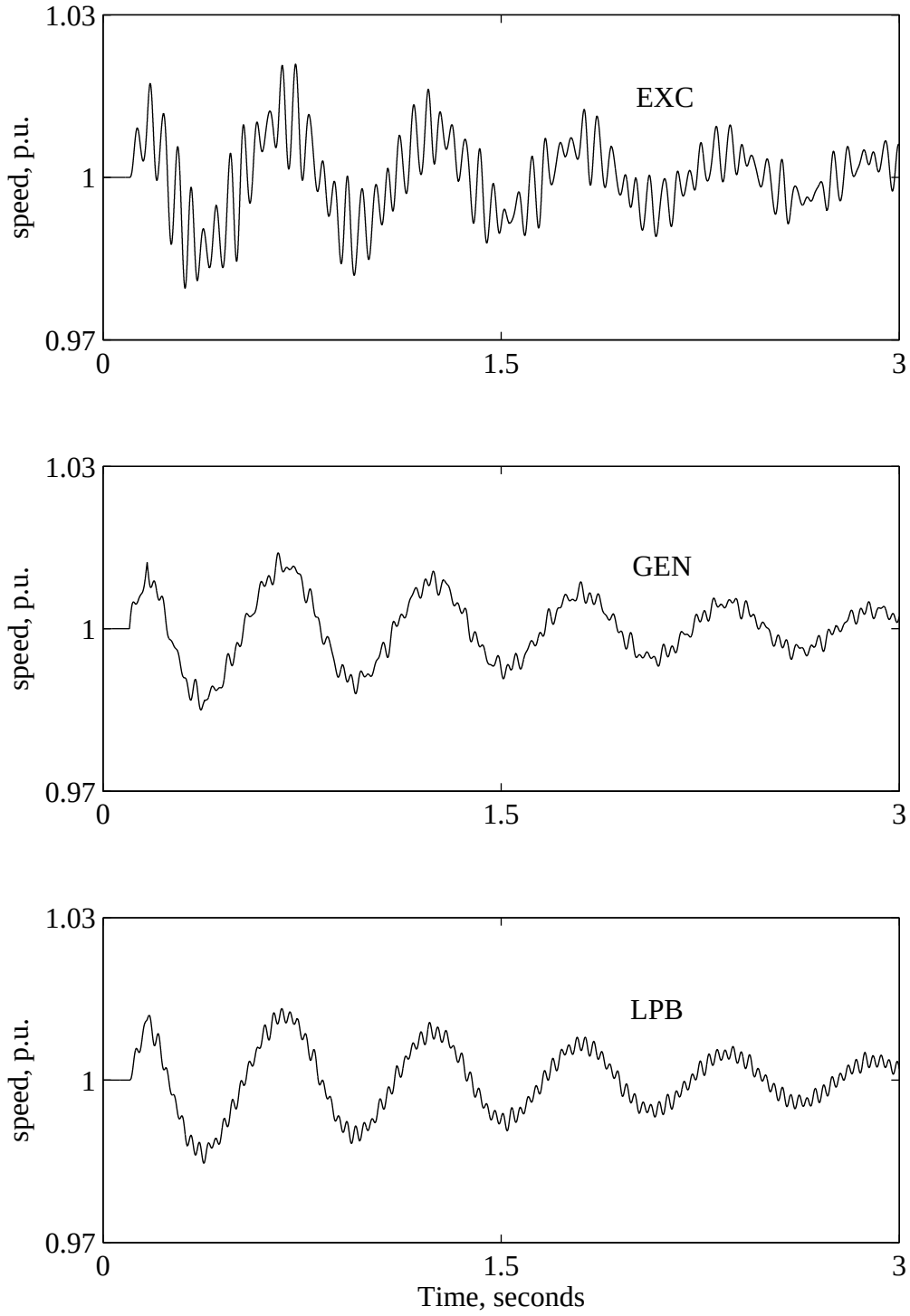

Figure 6.12 Speed responses of turbine-generator B due to a 4-cycle three-phase fault, BtB controller is not employed.

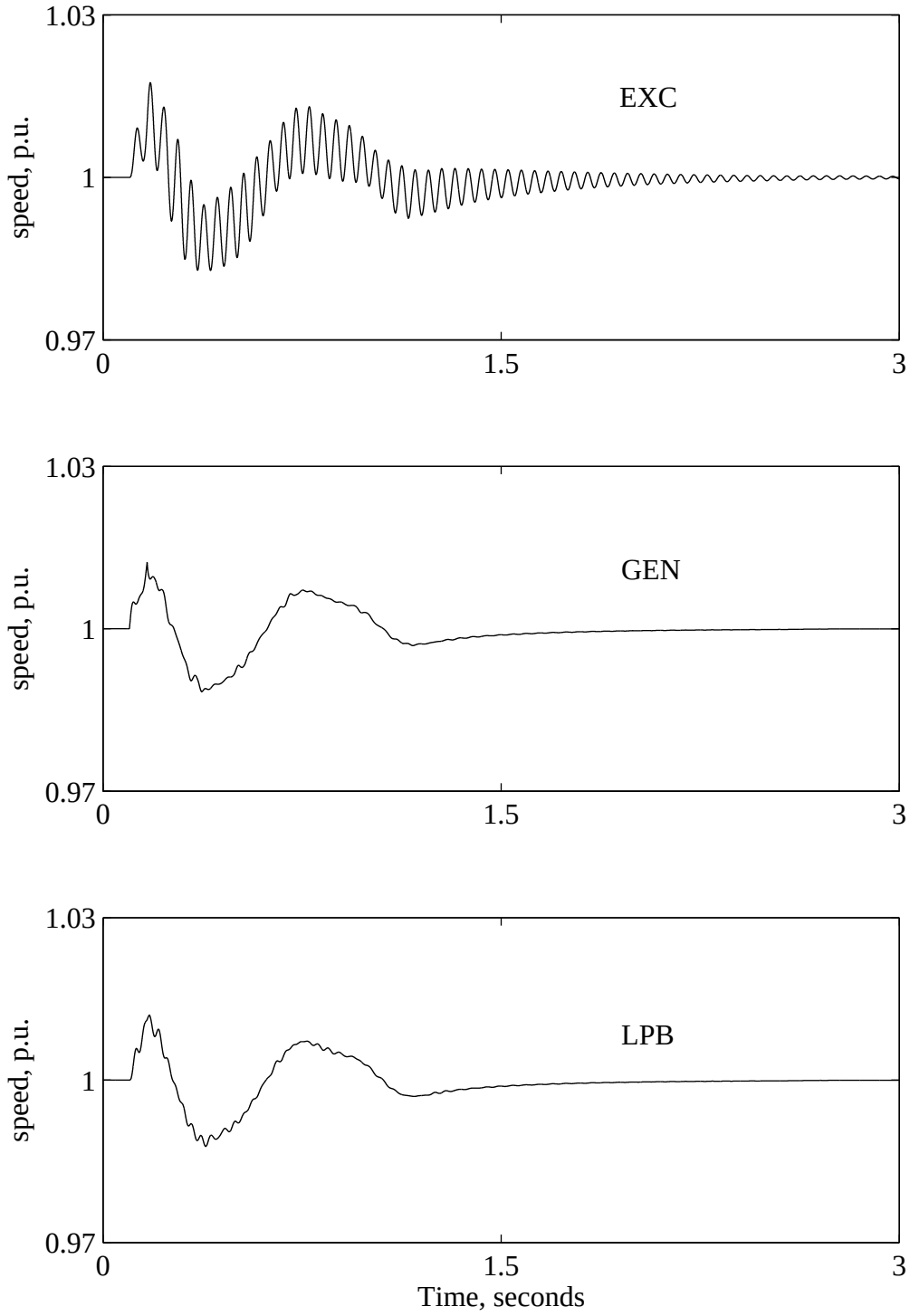

Figure 6.13 Speed responses of turbine-generator B due to a 4-cycle three-phase fault, BtB controller is employed with the generator speed as the stabilizing signal.

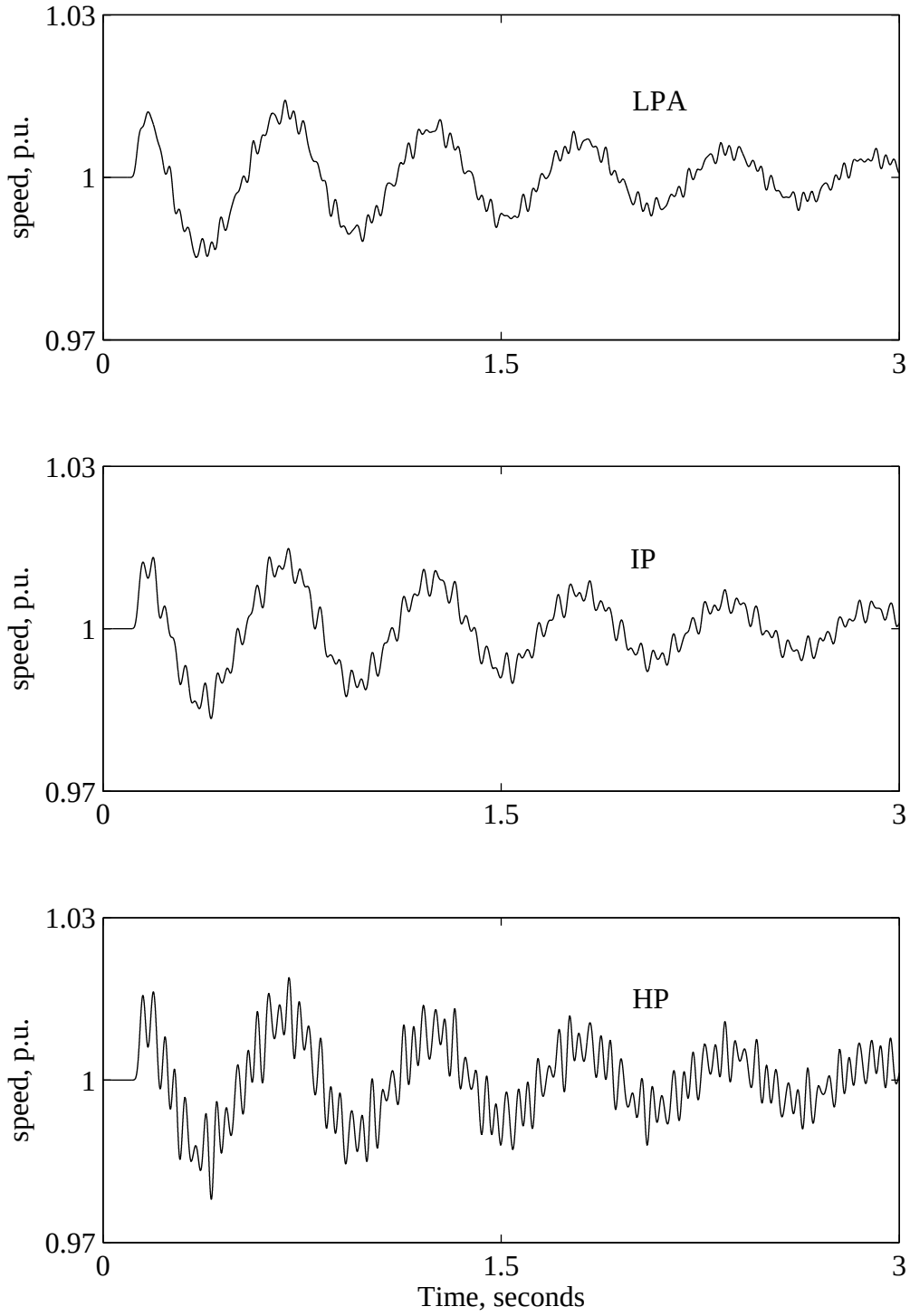

Figure 6.14 Speed responses of turbine-generator B due to a 4-cycle three-phase fault, BtB controller is not employed.

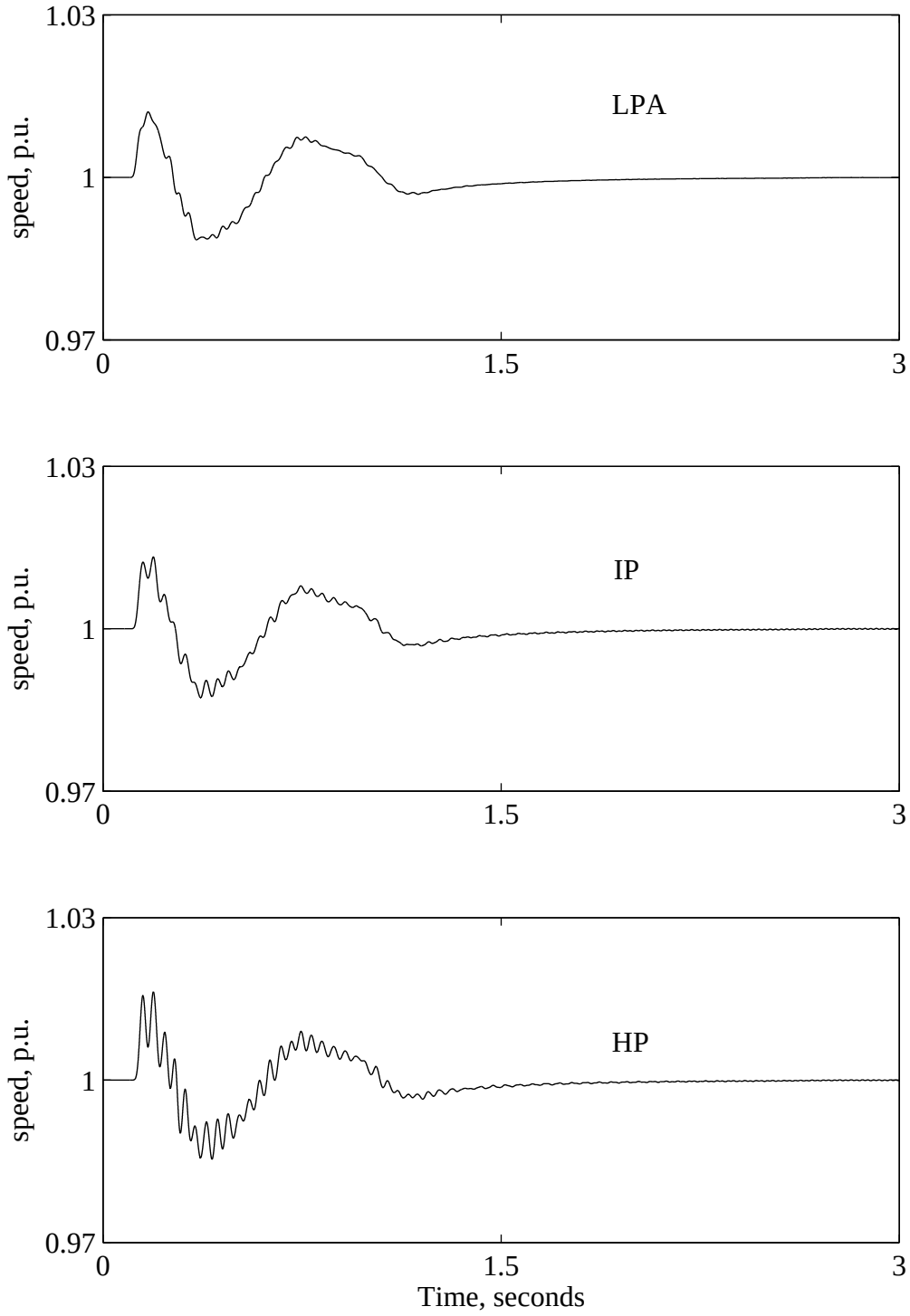

Figure 6.15 Speed responses of turbine-generator B due to a 4-cycle three-phase fault, BtB controller is employed with the generator speed as the stabilizing signal.

6.4.2. Case study II: a three-phase fault with $\Delta\omega$ and $\Delta\omega_{EXC}$ as the stabilizing signals

In order to further damp the (GEN-EXC) shaft torsional torque of turbine-generator A, both the generator and exciter speed deviations are used as auxiliary signals to the BtB HVdc controller. Figure 6.16 illustrates the shaft torsional torque responses of turbine-generator A for the same fault in case study I. Figure 6.17 shows the turbine-generator speed responses of turbine-generator A for the same case. Comparing Figures 6.6 and 6.16 shows that the BtB HVdc controller provides better damping with the choice of $\Delta\omega$ and $\Delta\omega_{EXC}$ as stabilizing signals.

6.5. VSC BtB Controller Performance during High-Speed Reclosing

It is well known that automatic high-speed reclosure of multi-phase faults, especially unsuccessful reclosure, aggravates the potential impact on the turbine-generator shaft due to the large number of rapidly succeeding electrical transients to which the turbine-generator shaft system responds [42], [44].

The shaft torsional torque responses of turbine-generator A during unsuccessful reclosing of a 4-30-4 cycle three-phase fault are illustrated in Figure 6.18 with the BtB HVdc controller out of service and in Figure 6.19 with the BtB HVdc controller in service with the generator and exciter speeds as the stabilizing signals. As it can be seen from Figures 6.18 and 6.19 the BtB HVdc controller again provides good performance in damping the torsional torques in all the shaft sections.

6.5.1. Effect of the reclosing time on the VSC BtB controller performance

As far as power system stability is concerned, high-speed reclosing on a permanent fault may not always result in negative effects. In the 1960s, studies of various stability-control methods for a transmission system conducted by BC Hydro [101], showed that faster reclosures are not necessarily better. For unsuccessful reclosures (permanent faults) in the studied transmission systems, the 45-cycle reclosure was the best, followed by the 35-cycle. The 25-cycle reclosure was the worst and caused the system to lose stability [102]. In this section, the effect of the above three reclosing times on the performance of the VSC BtB controllers is investigated. Figures 6.18 to 6.25 show the

Shaft torsional torque responses of turbine-generator A during unsuccessful reclosing of 4-25-4, 4-35-4 and 4-45-4 cycles three-phase fault respectively. The VSC BtB

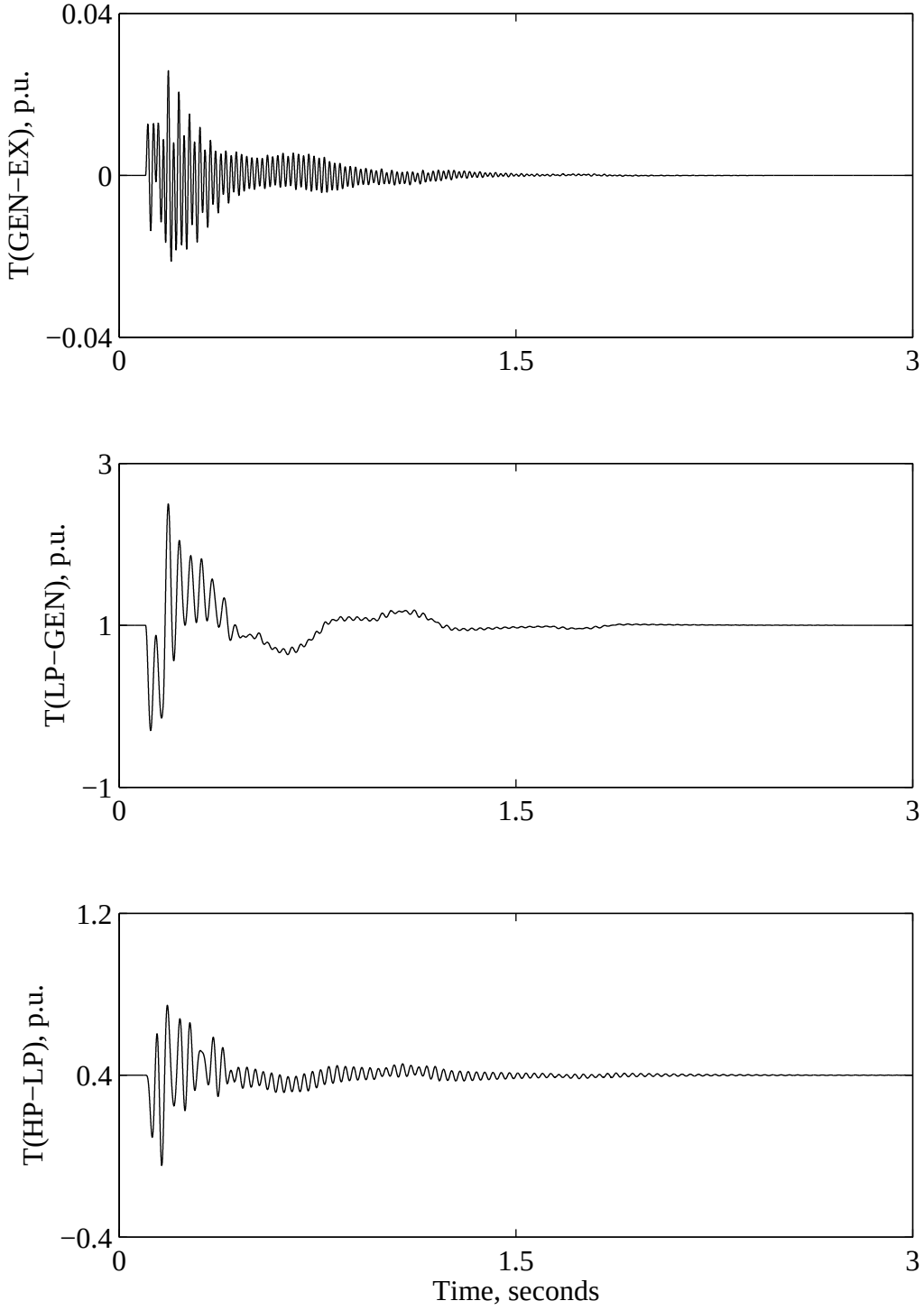

Figure 6.16 Torsional torque responses of turbine-generator A due to a 4-cycle three-phase fault, BtB controller is employed with the generator and exciter speeds as stabilizing signals.

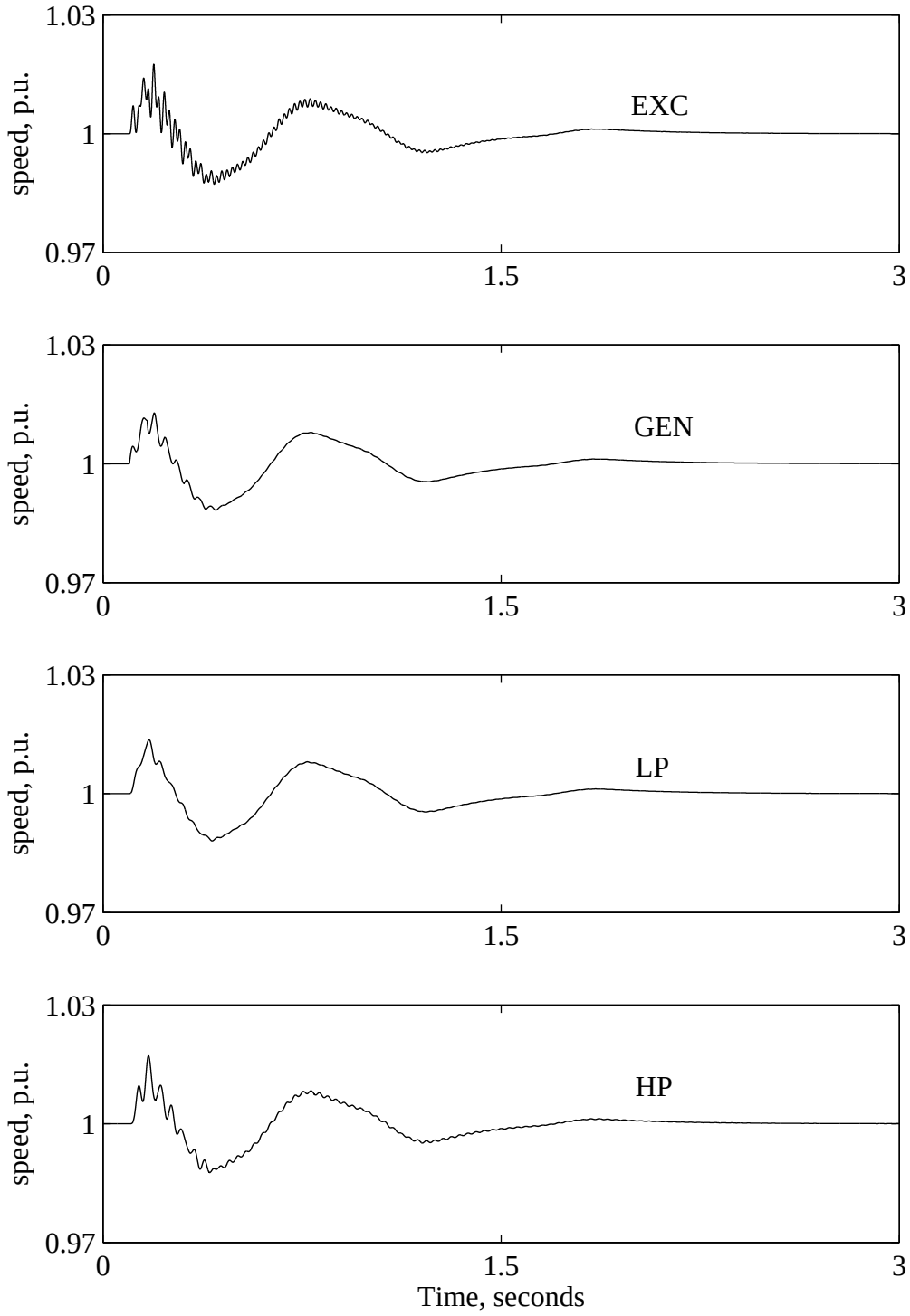

Figure 6.17 Speed responses of turbine-generator A due to a 4-cycle three-phase fault, BtB controller is employed with the generator and exciter speeds as stabilizing signals.

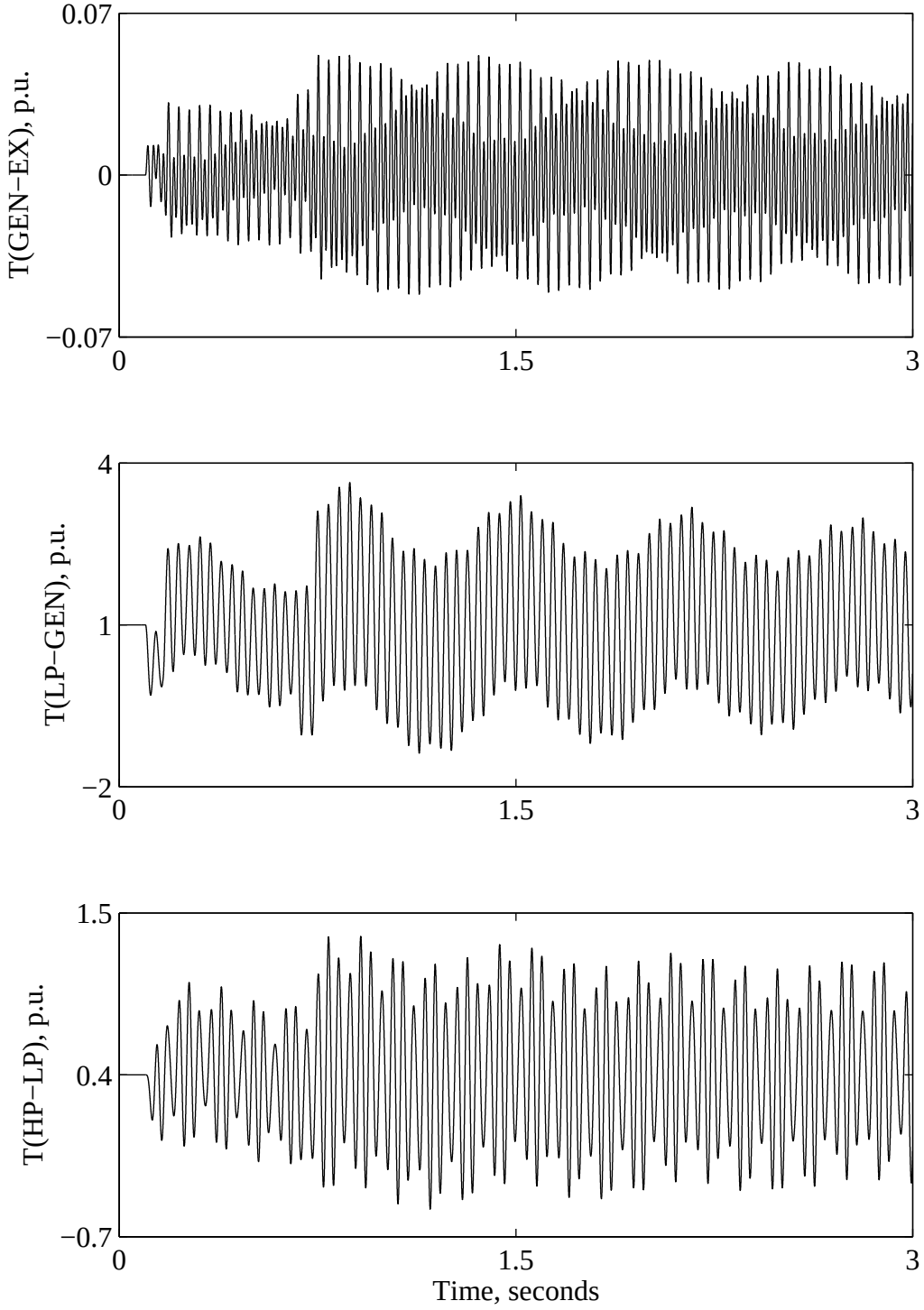

Figure 6.18 Shaft torsional torque responses of turbine-generator A due to unsuccessful reclosing of a 4-30-4 cycles three-phase fault, BtB controller is not employed.

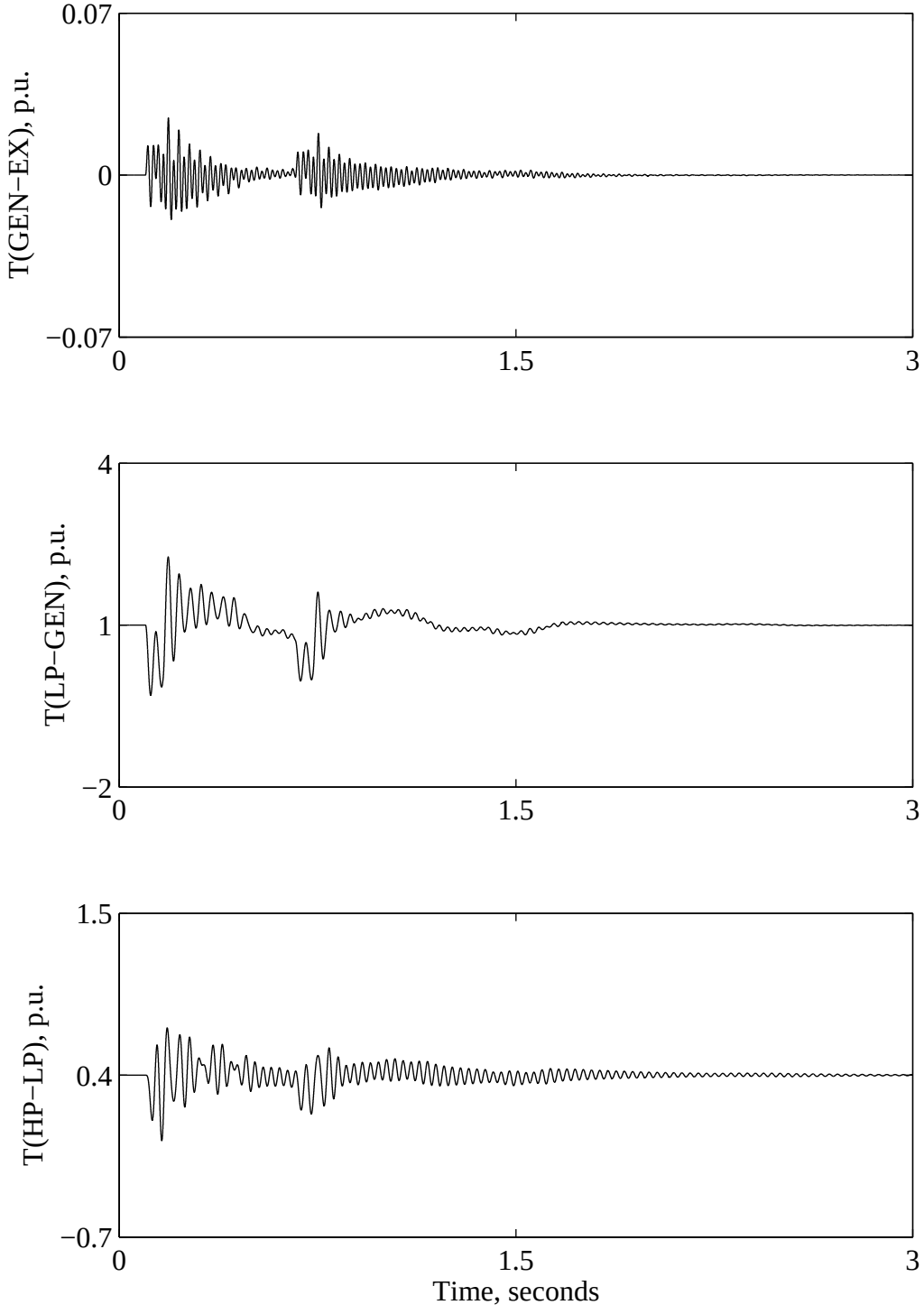

Figure 6.19 Shaft torsional torque responses of turbine-generator A due to unsuccessful reclosing of a 4-30-4 cycles three-phase fault, BtB controller is employed with the generator and exciter speeds as stabilizing signals.

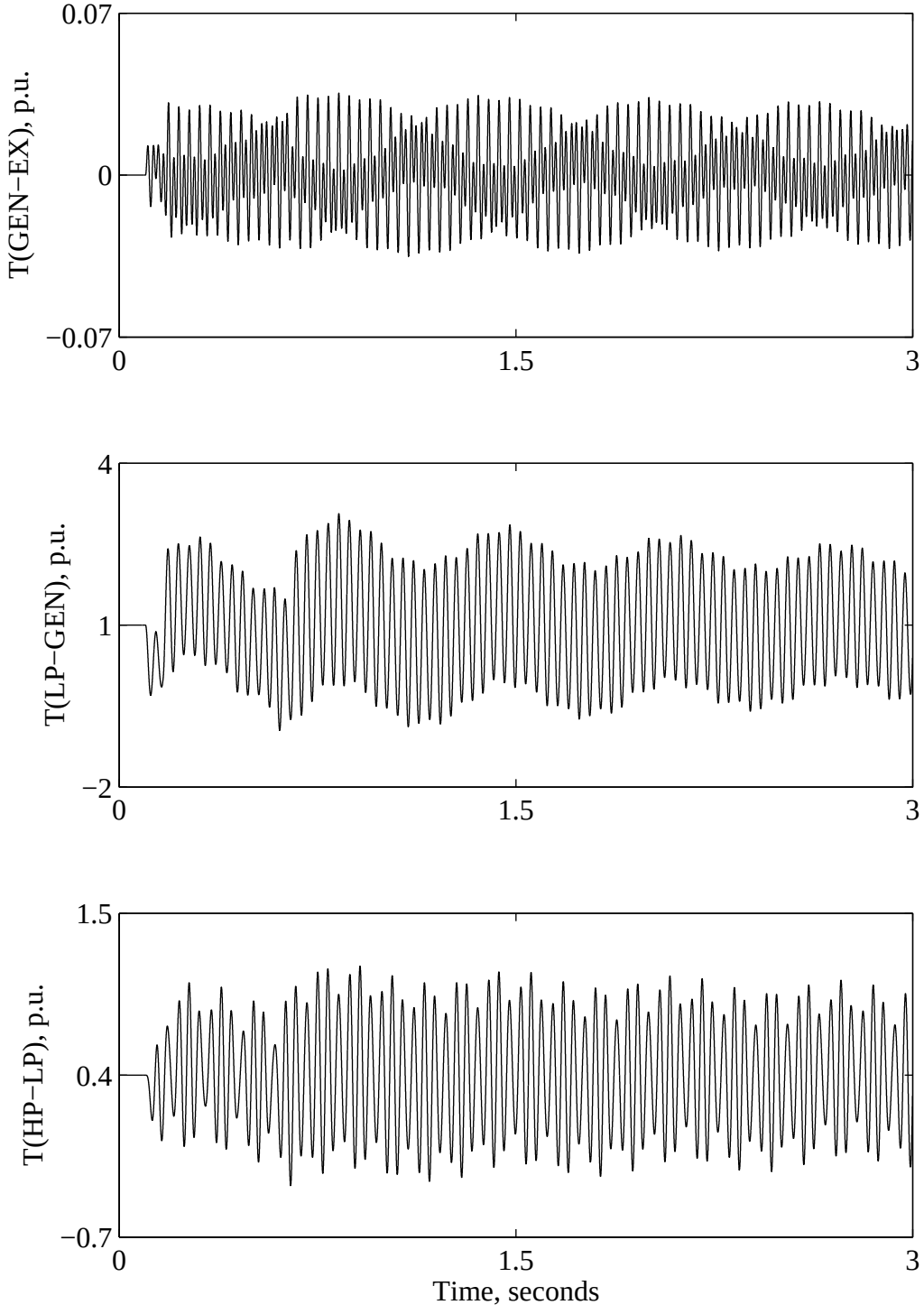

Figure 6.20 Shaft torsional torque responses of turbine-generator A due to unsuccessful reclosing of a 4-25-4 cycles three-phase fault, BtB controller is not employed.

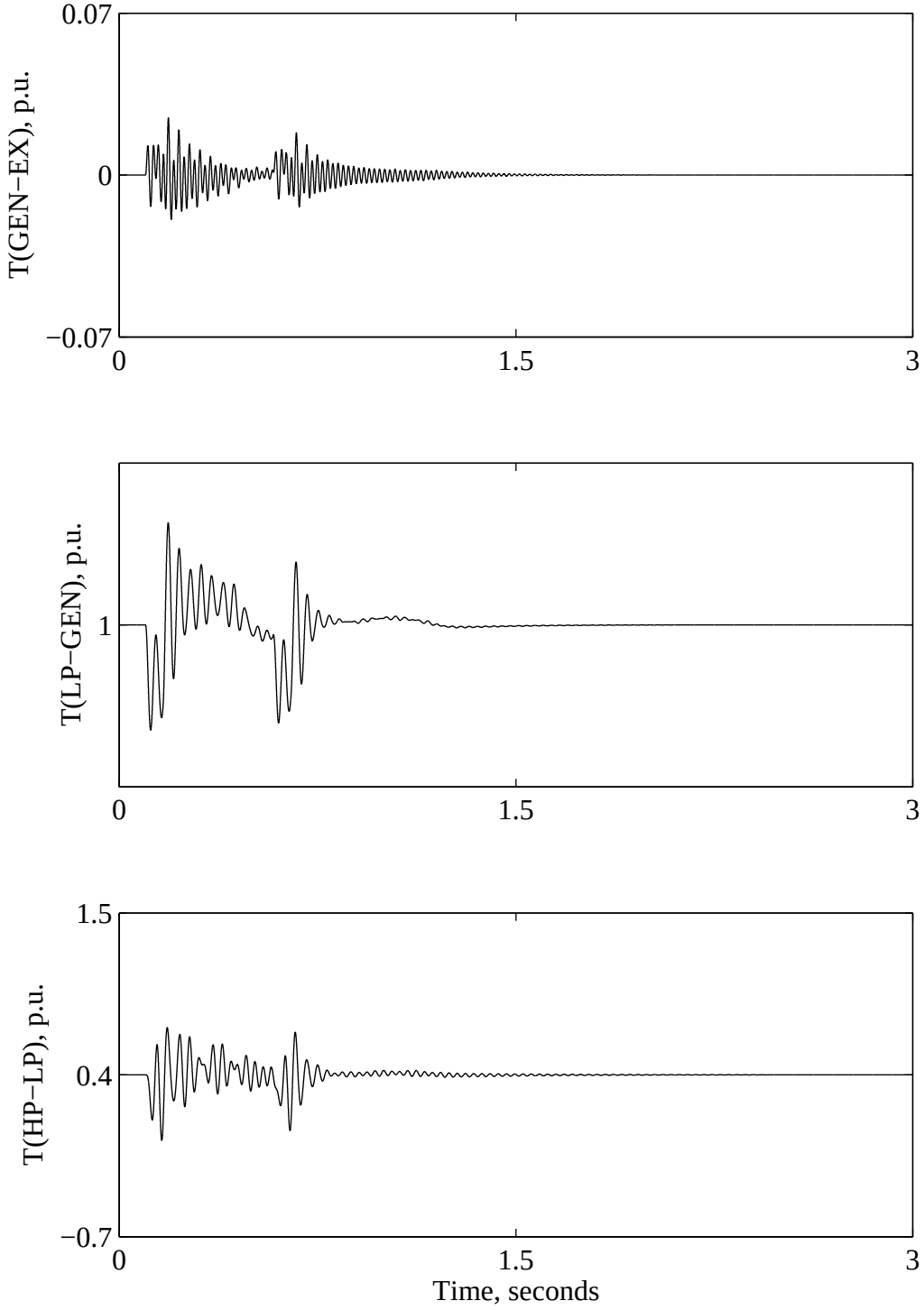

Figure 6.21 Shaft torsional torque responses of turbine-generator A due to unsuccessful reclosing of a 4-25-4 cycles three-phase fault, BtB controller is employed with the generator and exciter speeds as stabilizing signals.

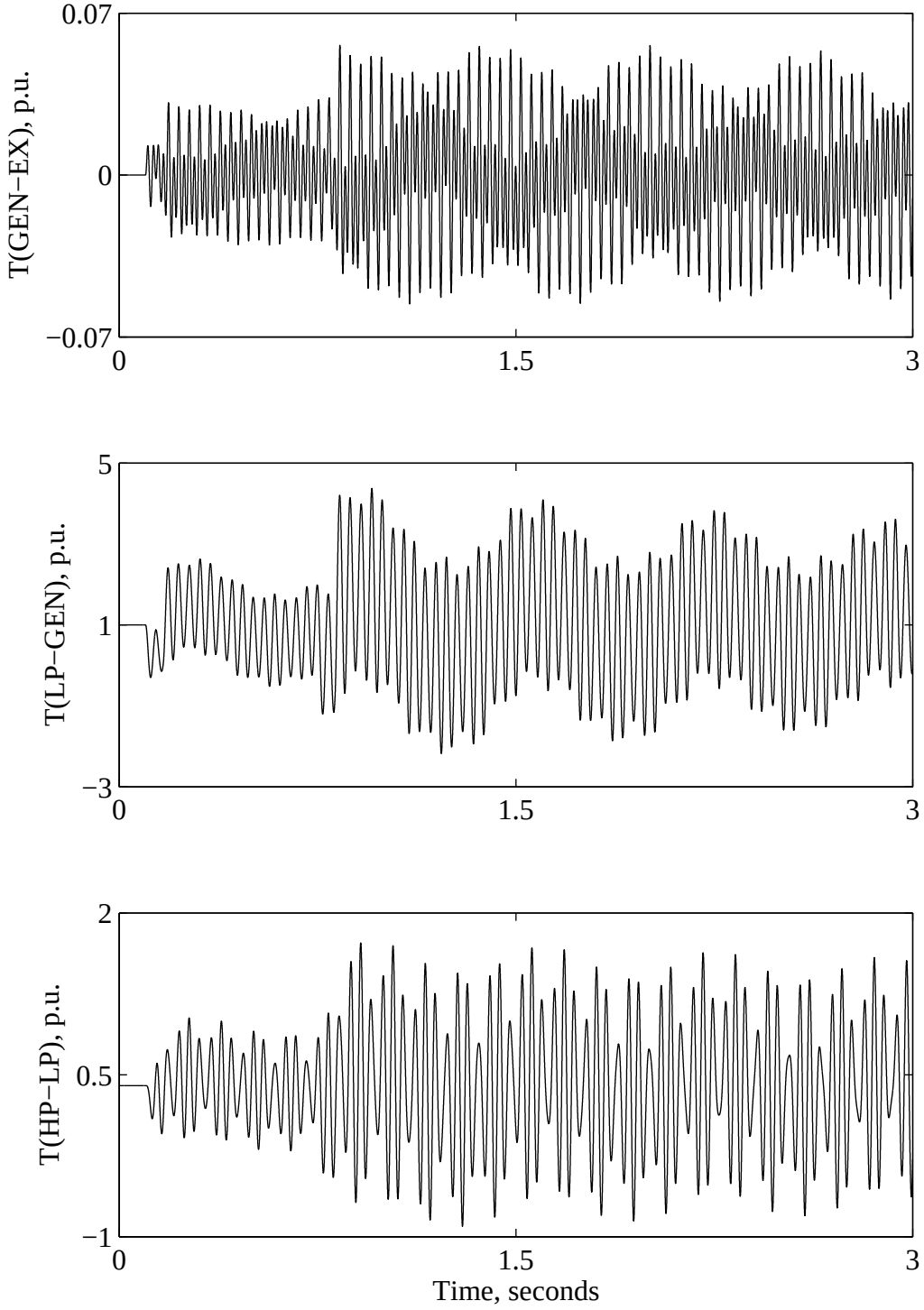

Figure 6.22 Shaft torsional torque responses of turbine-generator A due to unsuccessful reclosing of a 4-35-4 cycles three-phase fault, BtB controller is not employed.

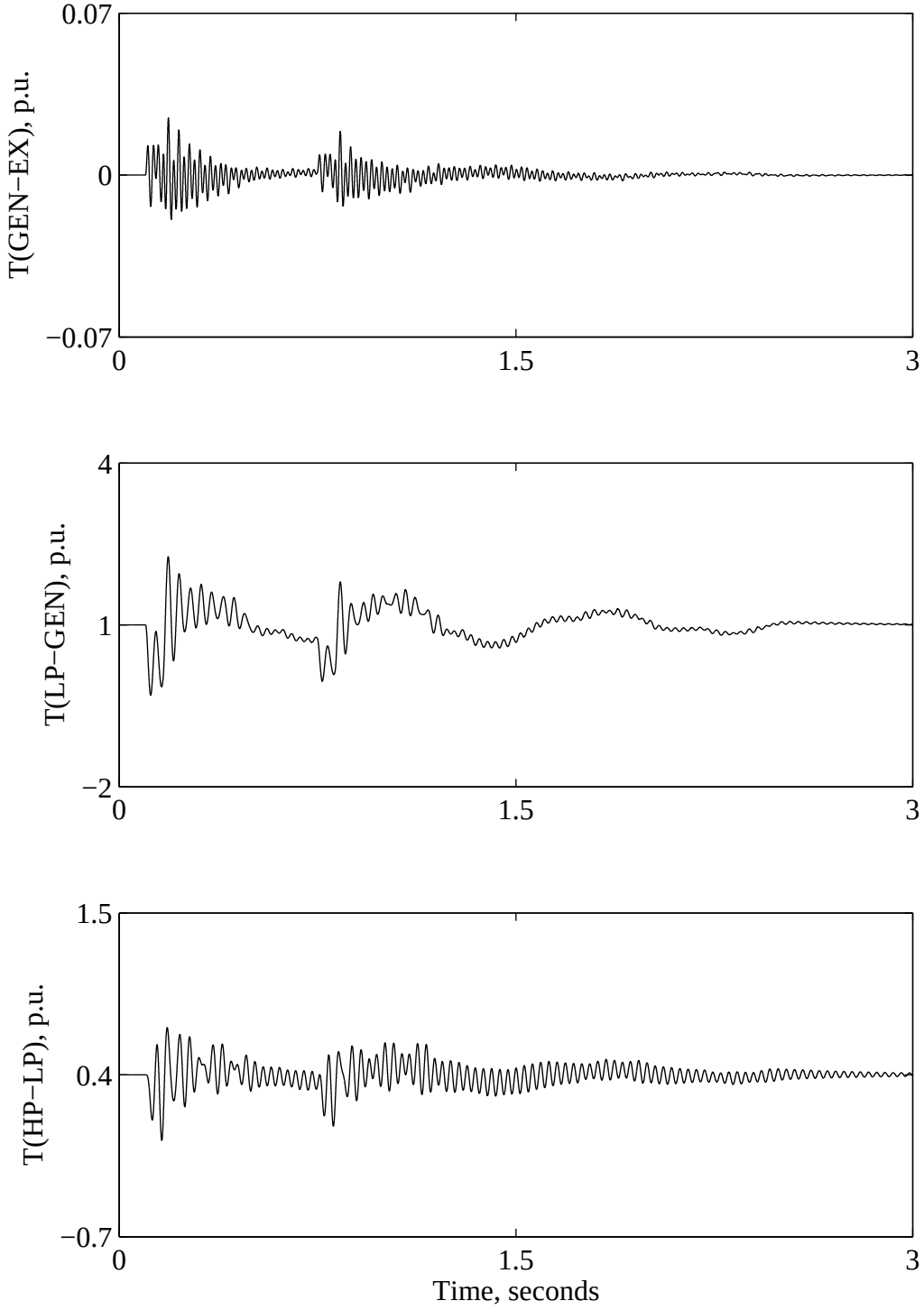

Figure 6.23 Shaft torsional torque responses of turbine-generator A due to unsuccessful reclosing of a 4-35-4 cycles three-phase fault, BtB controller is employed with the generator and exciter speeds as stabilizing signals.

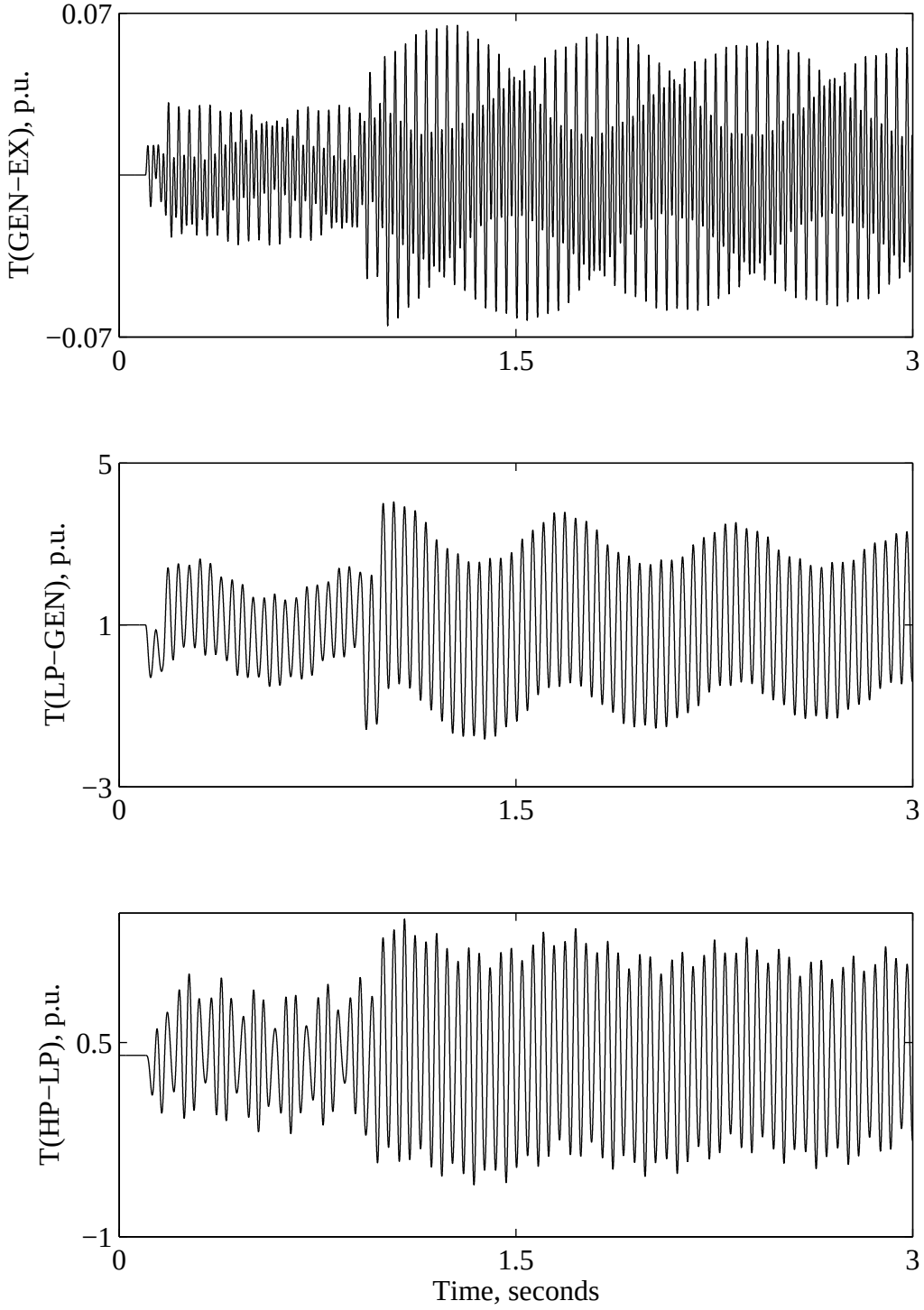

Figure 6.24 Shaft torsional torque responses of turbine-generator A due to unsuccessful reclosing of a 4-45-4 cycles three-phase fault, BtB controller is not employed.

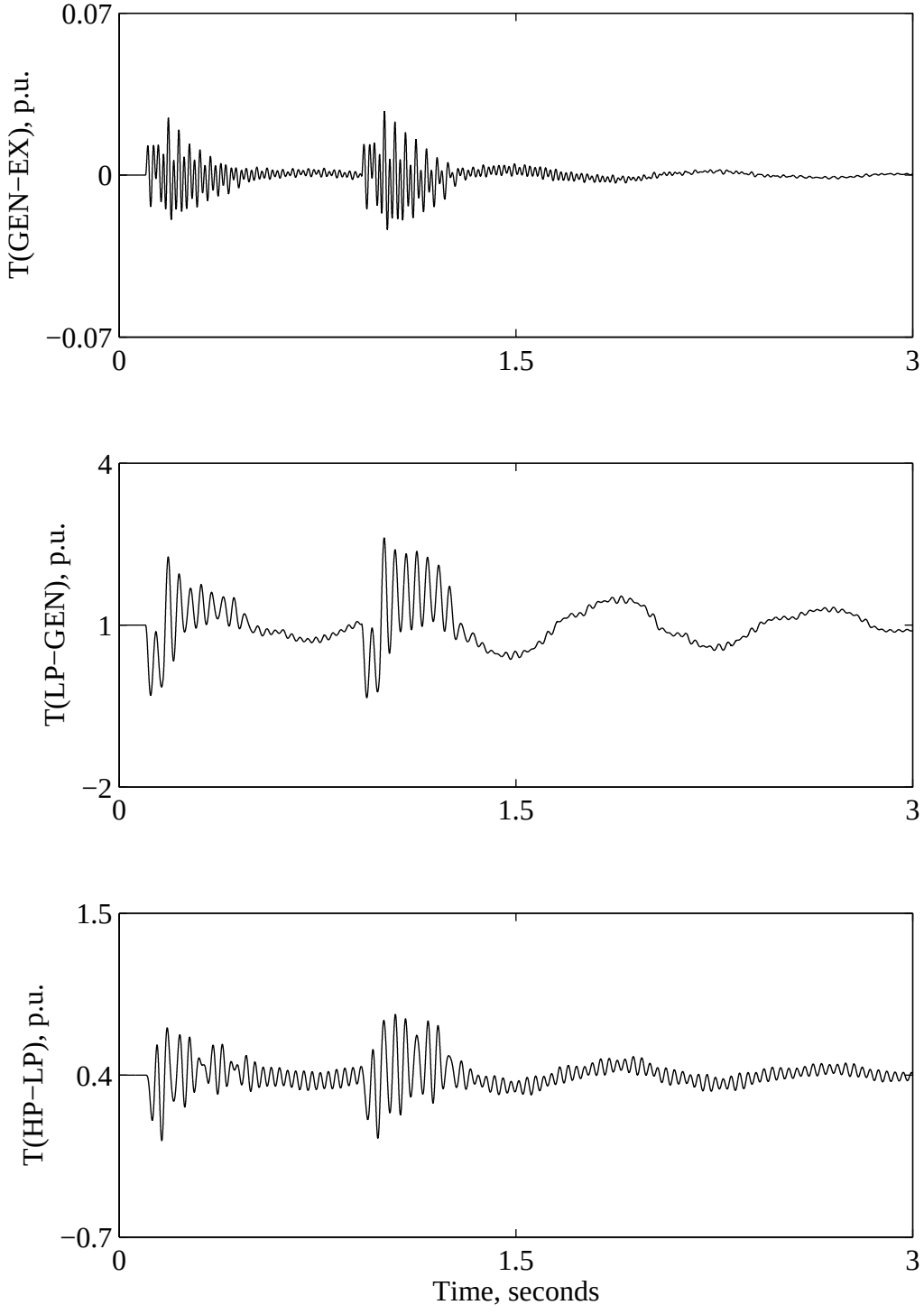

Figure 6.25 Shaft torsional torque responses of turbine-generator A due to unsuccessful reclosing of a 4-45-4 cycles three-phase fault, BtB controller is employed with the generator and exciter speeds as stabilizing signals.

controller is employed with the generator and exciter speeds as stabilizing signals. As can be seen from these figures, increase in the reclosing time does not necessarily improve the shaft torsional torque responses. The figures also show the effectiveness of the VSC BtB controller in damping all the turbine-generator shaft torsional torques.

6.6. Design of a UPFC Controller for Damping Turbine-Generator Shaft Torsional Torques

The series converter of the UPFC can insert a synchronous voltage component in series with the line in phase-quadrature with the line current, thereby allowing the power flow on the line to be regulated. This feature eliminates the need for using a capacitor for series compensation and, therefore, avoids the occurrence of subsynchronous resonance. The GAs optimization scheme developed in this thesis is used to design a PI controller for a UPFC installed in the middle of the transmission system of Figure 6.1. Figure 6.26 shows the shaft torsional torque responses of turbine-generator A due to the same three-phase fault considered in Section 6.4.1. The series converter of the UPFC is assumed to provide 50% capacitive compensation for the transmission line. As it can be seen from Figure 6.26, the UPFC controller provides good performance in damping the torsional torques in all the shaft sections.

Figure 6.27 shows the system eigenvalues with and without employing the FACTS devices. It can be seen that the dominant eigenvalues of the system are improved to provide a good damping for the system oscillations. It can also be seen from Figure 6.27 that when both generator and exciter speeds are used as stabilizing signals, more system damping is obtained.

6.7. Summary

In this chapter, a GA based optimization scheme for designing VSC BtB HVdc link and UPFC controllers capable of damping the torsional torques induced in turbine-generator shafts due to clearing and high-speed reclosing of system faults is presented. The results of the investigations conducted in this chapter show that the achieved control laws are effective for damping the induced torsional torques in all the shaft sections. It is also shown that, in general, the use of the generator speed deviation in the controller as a stabilizing signal is effective in damping all the torsional torques. It is also shown that

the use of two stabilizing signals namely, the generator and exciter speed deviations provides more damping to the turbine-generator shaft system. The controller design procedure is very general and can be applied to power system damping control design employing other FACTS devices such as the IPFC.

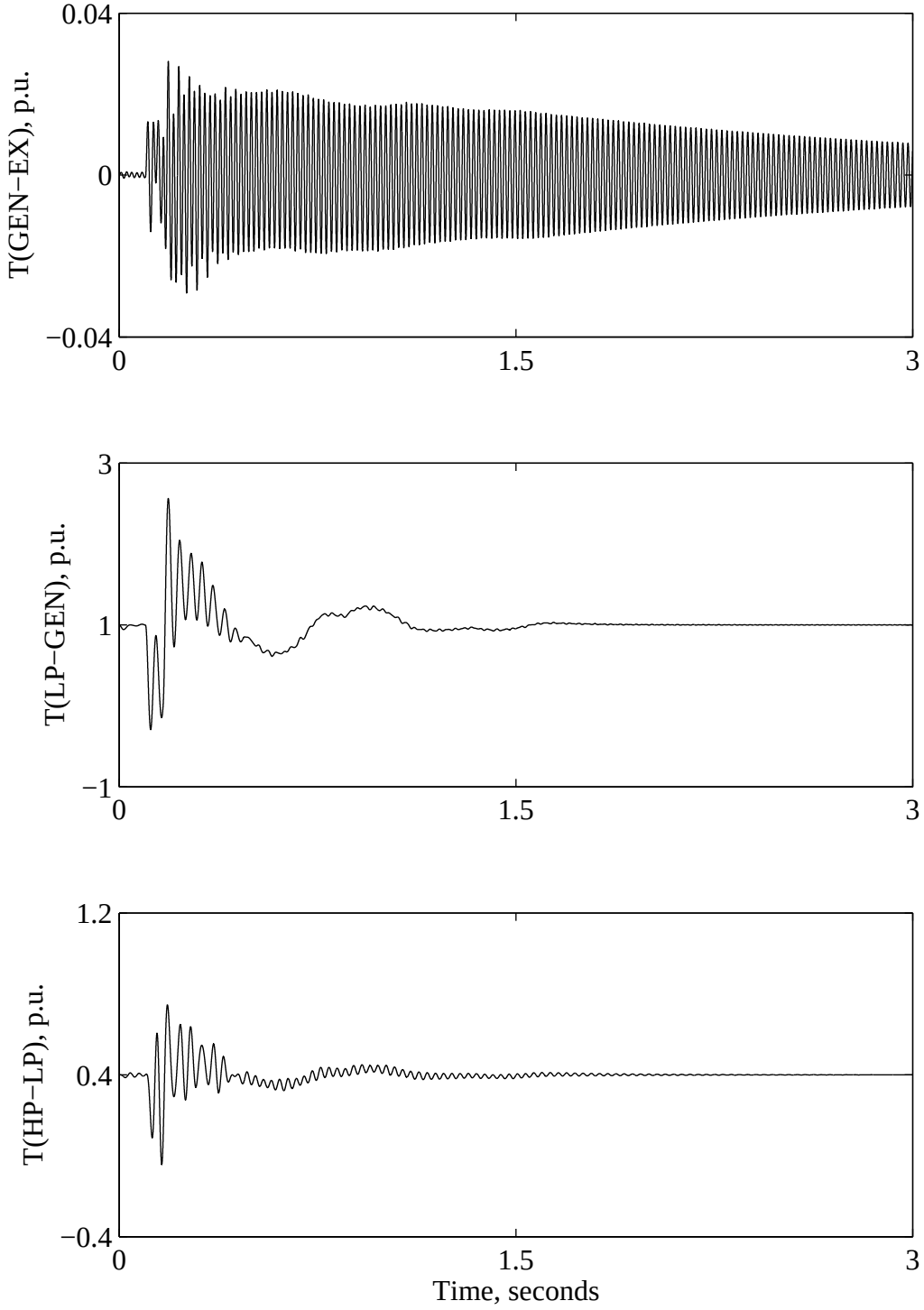

Figure 6.26 Torsional torque responses of turbine-generator A due to a 4-cycle three-phase fault (UPFC controller is employed with the generator speed as the stabilizing signal).

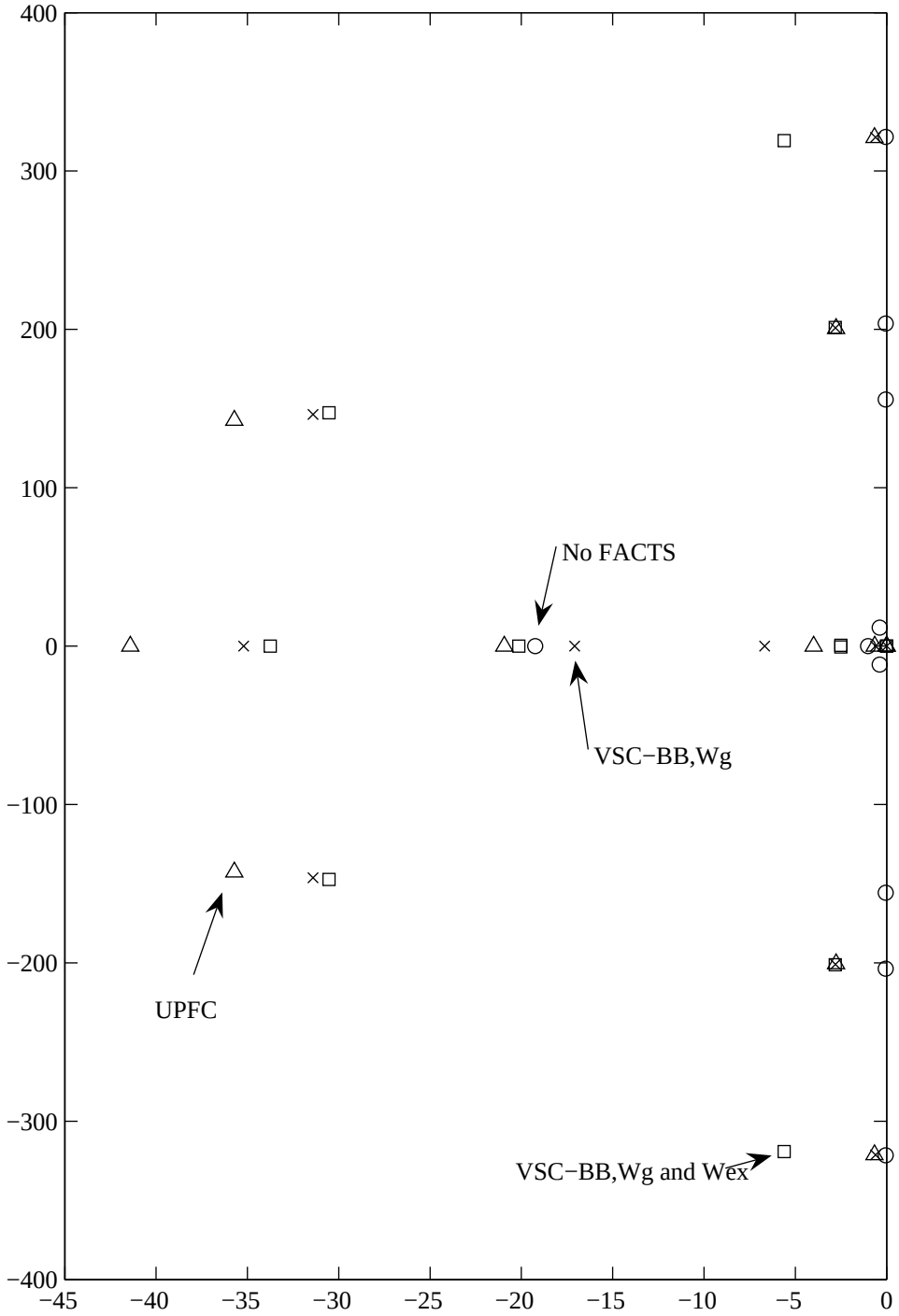

Figure 6.27 System eigenvalues.

7. SUMMARY AND CONCLUSIONS

7.1. Summary

In the evolving utility environment, financial and market forces are, and will continue to, demand an optimal and a profitable operation of the power system with respect to generation, transmission and distribution. Now, more than ever, advanced technologies are paramount for the reliable and secure operation of power systems. To achieve both operational reliability and financial profitability, it has become clear that more efficient utilization and control of the existing transmission system infrastructure is required.

Improved utilization of the existing power system can be provided through the application of advanced control technologies. Power electronics based equipment, or Flexible AC Transmission Systems (FACTS), provide proven technical solutions to address these new operating challenges being presented today. FACTS technologies allow for improved transmission system operation with minimal infrastructure investment, environmental impact and implementation time compared to the construction of new transmission lines.

Low frequency oscillations in some parts or between parts of the interconnected power systems are commonly experienced in modern power systems. These oscillations take place as the synchronous generators swing against each other. The frequency range of these oscillations is from 0.1 to 2.5 Hz and is related to the dynamic power transfer between areas. These oscillations can severely restrict system operations by requiring the curtailment of electric power transfers as an operational measure. These oscillations can also lead to widespread system disturbances if cascading outages of transmission lines occur due to oscillatory swings.

Another problem of concern in the power industry is the interaction between turbine-generator shaft systems and the electrical network disturbances. Some of these disturbances can inflict severe torsional stress on the shafts of the turbine-generators.

The induced high stresses reduce the life expectancy of the turbine-generators and, in severe cases, may cause shaft damage.

An introduction to the phenomena of interarea oscillations and turbine-generator torsional oscillations is presented in Chapter 1. A brief review of the various FACTS devices that can improve the security of a power system by enhancing its steady-state and transient stability is also presented in this chapter. The primary focus in this research work is on employing the Unified Power Flow Controller (UPFC) to damp interarea and torsional oscillations. Two other FACTS devices have been also investigated.

In Chapter 2, the steady-state and dynamic models for the UPFC and various power system components are presented. For power flow studies, the UPFC is modeled by a series reactance together with a set of active and reactive nodal power injections at each end of the series reactance. These powers are expressed as functions of the terminal, nodal voltages and the voltages of the series and shunt sources which represent the UPFC series and shunt converters respectively. The UPFC injection model is implemented into a full Newton-Raphson power flow program by adding the UPFC power injections and their derivatives with respect to the AC network state variables, i.e. nodal voltage magnitude and angles, at the appropriate locations of the mismatch vector and Jacobian matrix. The original dimensions of the mismatch vector and Jacobian matrix are not altered. The attraction of this formulation is that it can be implemented easily in existing power flow programs. To formulate the overall dynamic system equations, state equations of each dynamic device and the network are developed separately. The overall state matrices are then formed by augmented dynamic device models and interfacing the results with the network equations. To construct the state-space model of each dynamic device, either its terminal voltage or its current injected into the network, whichever is more convenient, is assumed as the input, and the other as the output. Using this approach, the overall system model for a single-machine infinite-bus power system incorporating UPFC is developed to study power system oscillations.

The Genetic Algorithms (GA) and fuzzy logic techniques which are used in designing controllers for the different FACTS devices considered in this thesis are presented. In

the GA technique, the objective function used for the optimization is set to shift the dominant system eigenvalues to the left side of the wedge shape sector in the complex plane. Novel controllers based on these two techniques are developed and examined through eigenvalue analysis as well as time domain simulations of small system disturbances. Eigenvalue analysis describes the small signal behavior of the system, i.e. the behavior around one operating point, and does not take into account the nonlinear behavior of some system components, at large system perturbations. Therefore, time domain simulations and eigenvalue analysis complement each other.

In Chapter 3, a complete dynamic model of a multi-area power system incorporated with UPFCs is developed to study interarea oscillations. A three-area power system is considered in these investigations. Centralized Proportional Integral (PI) controllers with global signals are designed to control the UPFCs based on the GA technique. Several investigations are conducted in this chapter to select the appropriate GA parameters used in designing such controllers. The robustness of the designed controllers is examined with respect to the fault location, the location of the FACTS device and the operating conditions. Simplified centralized PI controllers for the UPFC to damp interarea oscillations are also investigated.

In Chapter 4, a fuzzy logic controller for UPFC is designed and its potential in damping interarea oscillations in the three-area power system is examined. The effectiveness of the fuzzy logic controller for the UPFC is examined for both large and small system disturbances. The potential of tuning the fuzzy logic controller using GA techniques is also studied in this chapter.

In Chapter 5, the GA based optimization technique used previously for designing controllers for the UPFC is utilized to design PI controllers for two FACTS devices. These controllers are also aimed at enhancing the damping of interarea oscillations. The two FACTS devices considered are, a proposed three-converter Generalized Unified Power Flow Controller (GUPFC) and a Voltage-Source Converter Back-to-Back HVdc link (VSC BtB). The effectiveness of the proposed GA FACTS controllers in damping interarea oscillations is demonstrated through eigenvalue analysis as well as simulation results of typical time responses of different system disturbances.

In Chapter 6, the potential of using the UPFC and VSC BtB in damping turbine-generator shaft torsional torques is investigated. The complete mathematical representation of a turbine-generator connected to an infinite bus through a VSC BtB is presented. VSC BtB controller performance due to fault clearing and high-speed reclosing are examined. The effect of the selection of the input signal on the VSC BtB controller performance is also investigated.

7.2. General conclusions

The studies conducted in this thesis yield the following conclusions:

1. The designed controllers for the FACTS devices do not need state observers since they have an output feedback form using the deviation in generator angular speeds. Nevertheless, several dynamic modes, that may enrich the control signals, can be generated from the measured signals using the integral action.
2. The designed controllers for the FACTS devices considered in this thesis are robust with respect to the fault location and the operating conditions.
3. The GA based controller design procedure is very general and can be applied to power system damping control design employing other FACTS devices (e.g. TCSC, SSSC and IPFC). Moreover, it allows the simultaneous tuning of multiple FACTS controllers.
4. For the GA parameter selection, increasing the population size over 100 strings does not significantly affect the controller design as the differences among the final values of the fitness function are relatively small. Moreover, the value of the fitness function converges to its optimum value within 40 to 60 generations when using a population size greater than 100 strings. Furthermore, a crossover probability in the range of 0.7 to 0.77 results in a good system response.
5. Selecting a mutation probability between 0.03 and 0.07 results in a desirable convergence for the fitness function and, consequently, in a better design for the UPFC controller. Moreover, the value of the angle β does not significantly affect the system response.

6. A simplified centralized UPFC controller using a reduced number of stabilizing signals can also be effective in damping interarea oscillations.

7. The designed fuzzy logic controllers for the UPFC are capable of damping power system oscillations during large and small disturbances. Moreover, fuzzy logic controllers for the UPFC tuned with a GA technique exhibit enhanced performance due to different system disturbances.

8. The decision on where to install a FACTS device is largely dependent on the desired effect and the characteristics of the specific system. It can be concluded from the simulation results that the best location for the FACTS devices is at the middle of the tie-line that transfers the highest amount of power. It is also shown that the closeness of the FACTS device to the fault location improves the performance of such a device in damping interarea oscillations.

9. The designed controllers for the proposed GUPFC and the VSC BtB provide, in most cases, better interarea oscillations damping than the UPFC.

10. Unsuccessful high-speed reclosing of a system fault results in high torsional torques induced in the turbine-generator shafts. The magnitudes of these torques depend highly on the timing of the reclosing switching sequence (the combination of the fault clearing and reclosing time). Moreover, the shaft section between the generator and the low-pressure stage turbine is subjected to the highest stresses.

11. The designed GA based controllers for the VSC BtB HVdc link and the UPFC are effective in damping the torsional torques induced in turbine-generator shafts due to clearing and high-speed reclosing of system faults.

12. In general, the use of the generator speed deviation in the controller as a stabilizing signal is effective in damping all the torsional torques. However, the use of two stabilizing signals namely, the generator and exciter speed deviations provides more damping to the turbine-generator shaft system.

8. REFERENCES

[1] IEEE FACTS Working Group, IEEE Transmission and Distribution Committee, "FACTS Applications", IEEE Publication No. 96TP 116-0.

[2] Yong Hua Song and Allan T Johns, *Flexible AC Transmission Systems (FACTS)*, The Institution of Electrical Engineers, Michael Faraday House, 1999.

[3] Narain G. Hingorani and Laszlo Gyugyi, *Understanding FACTS, Concepts and Technology of Flexible AC Transmission Systems*, IEEE Press, 2000.

[4] Pranesh Rao, M. L. Crow and Zhiping yang, "STATCOM Control for Power System Voltage Control Applications," IEEE Transactions on Power Delivery, vol. 15, No. 4, October 2000, pp. 1311-1317.

[5] K. V. Patil, J. Senthil, J. Jiang and R. M. Mathur, "Application of STATCOM for Damping Torsional Oscillations in Series Compensated AC Systems," IEEE Transactions on Energy Conversion, vol. 13, No. 3, September 1998, pp. 237-243.

[6] P. Aree and E. Acha, "Block Diagram Model for Fundamental Studies of a Synchronous Generator-Static Var Compensator System," IEE Proc.-Gener. Transm. Distrib., vol. 146, No. 5, September 1999, pp. 507-514.

[7] X. R. Chen, N. C. Pahalawaththa, U. D. Annakkage and C. S. Kumble, "Design of Decentralised output Feedback TCSC Damping Controllers by Using Simulated Annealing," IEE Proc.-Gener. Transm. Distrib., vol. 145, No. 5, September 1998, pp. 553-558.

[8] A. A. El-Emary, "Formula for the Effect of a Static Var Compensator on Synchronising Torque Coefficient," IEE Proc.-Gener. Transm. Distrib., vol. 143, No. 6, November 1996, pp. 582-586.

[9] C. S. Chang and J. S. Huang, "Optimal Multiobjective SVC Planning for Voltage Stability Enhancement," IEE Proc.-Gener. Transm. Distrib., vol. 145, No. 2, March 1998, pp. 203-209.

[10] M. Parniani and M. R. Iravani, "Optimal Robust Control Design of Static Var Compensators," IEE Proc.-Gener. Transm. Distrib., vol. 145, No. 3, May 1998, pp. 301-307.

[11] B. Changaroon, S. C. Srivastava, D. Thukaram and S. Chirarattananon, "Neural network Based Power System Damping Controller for SVC," IEE Proc.-Gener. Transm. Distrib., vol. 146, No. 4, July 1999, pp. 370-376.

[12] H. F. Wang and F. J. Swift, "Capability of the Static Var Compensator in Damping Power System Oscillations," IEE Proc.-Gener. Transm. Distrib., vol. 143, No. 4, July 1996, pp. 353-358.

[13] Y. Y. Hsu and T. S. Luor, “Damping of Power System Oscillations Using Adaptive Thyristor-Controlled Series Compensators Tuned by Artificial Neural Networks,” IEE Proc.-Gener. Transm. Distrib., vol. 146, No. 2, March 1999, pp. 137-142.

[14] X. Zhou and J. Liang, “Overview of Control Schemes for TCSC to Enhance the Stability of Power Systems,” IEE Proc.-Gener. Transm. Distrib., vol. 146, No. 2, March 1999, pp. 125-130.

[15] K. L. Lo and Y. J. Lin, “Strategy for the Control of Multiple Series Compensators in the Enhancement of Interconnected Power system Stability,” IEE Proc.-Gener. Transm. Distrib., vol. 146, No. 2, March 1999, pp. 149-158.

[16] X. R. Chen, N. C. Pahalawaththa, U. D. Annakkage and C. S. Kumble, “Output Feedback TCSC Controllers to Improve Damping of Meshed Multi-Machine Power Systems,” IEE Proc.-Gener. Transm. Distrib., vol. 144, No. 3, May 1997, pp. 243-248.

[17] X. X. Zhou and J. Liang, “Nonlinear Adaptive Control of TCSC to Improve the Performance of Power Systems,” IEE Proc.-Gener. Transm. Distrib., vol. 146, No. 3, May 1999, pp. 301-305.

[18] Gyugyi, L., “A Unified Power Flow Concept for Flexible AC Transmission Systems,” IEE Fifth International Conference on AC and DC Power Transmission, London, Publication No. 345, pp. 19-26. Reprinted in IEE Proceedings, Part C, vol. 139, No. 4, July 1992.

[19] A. Elices, L. Rouco, H. Bourles and T. Margotin, “Design of Robust Controllers for Damping Interarea Oscillations: Application to the European Power System,” IEEE Transactions on Power Systems, vol. 19, No. 2, May 2004, pp. 1058-1067.

[20] H.F.Wang and F.J.Swift, “A Unified Model for the Analysis of FACTS Devices in Damping Power System Oscillations Part I: Single-Machine Infinite-bus Power System,” IEEE Transactions on Power Delivery, vol. 12, No. 2, April 1997, pp. 941-946.

[21] H.F.Wang and F.J.Swift, “A Unified Model for the Analysis of FACTS Devices in Damping Power System Oscillations Part II: Multi-Machine Power Systems,” IEEE Transactions on Power Delivery, vol. 13, No. 4, October 1998, pp. 1355-1362.

[22] L. Fan and A. Feliachi, “Robust TCSC Control Design for Damping Inter-Area Oscillations,” Proceedings of 2001 IEEE PES Summer Meeting, Vancouver, British Columbia, Canada, July 15-19, 2001.

[23] P.K. Dash, S. Mishra and G. Panda, “Damping Multimodal Power System Oscillation Using a Hybrid Fuzzy Controller for Series Connected FACTS Devices,” IEEE Transactions on Power Systems, vol. 15, No. 4, November 2000, pp. 1360-1366.

[24] G.N. Taranto and D.M. Falcao, “Robust Decenteralized Control Design Using Genetic Algorithm in Power System Damping Control,” IEE Proc.-Gener. Transm. Distrib., vol. 145, No. 1, January 1998, pp. 1-6.

[25] G.Li, T.T. Lie, G.B. Shrestha and K.L. Lo, “Design and Application of Co-ordinated Multiple FACTS Controllers,” IEE Proc.-Gener. Transm. Distrib., vol. 147, No. 2, March 2000, pp. 112-120.

[26] G.N. Taranto, J.-K. Shiau, J.H. Chow and H.A. Othman, “Robust Decenterlized Design for Multiple FACTS Damping Controllers,” IEE Proc.-Gener. Transm. Distrib., vol. 144, No. 1, January 1997, pp. 61-67.

[27] N. Yang, Q. Liu, J.D. McCalley, “TCSC Controller Design for Damping Inter-Area Oscillations,” IEEE Transaction on Power Systems, vol. 13, No. 4, November 1998, pp. 1304-1310.

[28] M.M. Farsangi, Y.H. Song and Kwang Y. Lee, “Choice of FACTS Device Control Inputs for Damping Interarea Oscillations,” IEEE Transactions on Power Systems, vol. 19, No. 2, May 2004, pp. 1135-1143.

[29] M. Klein, G.J. Rogers and P. Kundur, “A Fundamental Study of Inter-Area Oscillations in Power Systems,” IEEE Transactions on Power Systems, vol. 6, No. 3, August 1991, pp. 914-921.

[30] Graham Rogers, *Power System Oscillations*, Kluwer Academic Publishers, 2000.

[31] X. Yang, A. Feliachi, “Stabilization of Inter-Area Oscillation Modes through Excitation Systems,” IEEE Transactions on Power Systems, vol. 9, No.1, February 1994, pp. 494–502.

[32] M. E. Aboul-Ela, A. A. Sallam, J. D. McCalley and A. A. Fouad, “Damping Controller Design for Power System Oscillations using Global Signals,” IEEE Transactions on Power Systems, vol. 11, No. 2, May 1996, pp. 767-773.

[33] J. F. Hauer, D. J. Trudinowski, G. J. Rogers, W. A. Mittelstadt, W. H. Litzenburger and J. M. Johnston, “Keeping an Eye on Power System Dynamics,” IEEE Computer Applications in Power, October 1997, pp. 50-54.

[34] Carson W. Taylor, “Improving grid Behavior,” IEEE Spectrum, June 1999, pp. 40-45.

[35] ANIS. C50.13-1977, American National Standard, “Requirements of Cylindrical Rotor Synchronous Generator”.

[36] D. N. Walker, C. E. J. Bowler, R. L. Jackson and D. A. Hodgers, “Results of the Subsynchronous Resonance Tests at Mohave,” IEEE Transaction on Power Apparatus and Systems, vol. PAS-94, 1975, pp. 1878-1889.

[37] M. C. Hall and D. A. Hodge, “Experience with 500 kV Subsynchronous Resonance and Resulting Turbine-Generator Shaft Damage at Mohave Generating Station,” IEEE Publication No. CH1066-0-PWR, Symposium on Analysis and Control of Subsynchronous Resonance, 1976, pp. 22-29.

[38] J. W. Ballance and S. Goldberg, “Subsynchronous Resonance in Series Compensated Transmission Lines,” IEEE Transaction on Power Apparatus and Systems, vol. PAS-92, 1973, pp. 1649-1658.

[39] J. Stein and H. Fick, “The Torsional Stress Analysis for Continuously Monitoring Turbine-Generators,” IEEE Transaction on Power Apparatus and Systems, vol. PAS-99, 1980, pp. 703-710.

[40] T. J. Hammons, “Accumulative Fatigue Life Expenditure of Turbine-Generator Shafts following Worst-Case System Disturbances,” IEEE Transactions on Power Apparatus and Systems, vol. PAS-101, 1982, pp. 2364-2374.

[41] D. Lambrecht, T. S. Kulig, W. Berchtold, J. Van Hoorn and H. Fick, “Evaluation of the Torsional Impact of Accumulated Failure Combinations on Turbine-Generator Shafts as a Basis of Design Guidelines,” CIGRE Report No. 11-06, 1984.

[42] T. Watanabe, T. Kawamura, M. Goto and K. Okuda, “Influence of High-Speed Reclosing on Turbine-Generators and the Shaft System,” Hitachi Review, vol. 27, 1978, pp. 33-38.

[43] H. E. Lokay, R. G. Ramey and W. R. Brose, “Turbine-Generator Shaft Loss-of-Life Concepts for Power System Disturbances,” Proceeding of the American Power Conference, vol. 40, 1978, pp. 1106-1115.

[44] A. Abolins, D. Lambrecht, J. S. Joyce and L.T. Rosenberg, “Effect of Clearing Short Circuits and Automatic Reclosing on Torsional Stress and Life Expenditure of Turbine-Generator Shafts,” IEEE Transaction on Power Apparatus and Systems, vol. PAS-95, 1976, pp. 14-25.

[45] J. S. Joyce, T. Kulig and D. Lambrecht, “The Impact of High-Speed Reclosure of Single and Multi-Phase System Faults on Turbine-Generator Shaft Torsional Fatigue,” IEEE Transaction on Power Apparatus and Systems, vol. PAS-99, 1980, pp. 279-291.

[46] Chambers, Lance, *Practical Handbook of Genetic Algorithms*, Boca Raton, CRC Press, 1995.

[47] Michael D. Vose, *The Simple Genetic Algorithm: Foundations and Theory*, Cambridge, Mass. MIT Press, 1999.

[48] David E. Goldberg, *Genetic Algorithm In Search, Optimization and Machine Learning*, The University of Alabama, Addison-Wesley Publishing company, 1989.

[49] M. Srinivas and L. M. Patnaik, “Genetic Algorithms: a survey,” IEEE Transaction on Computer, vol. 27, no. 6, June 1994, pp. 17-26.

[50] J. L. Ribeiro Filho, P. C. Treleaven and C. Alippi, “Genetic-Algorithm programming environments,” IEEE Transaction on Computer, vol. 27, no. 6, June 1994, pp. 28-43.

[51] Cornelius T. Leondes, *Fuzzy Therory Systems: Techniques and Applications*, San Diago, Calif. Academic Press, London, 1999.

[52] Michio Sugeno, Hung T. Nguyen and Nadipuram R. Prasad, *Fuzzy Modeling and Control: Selected Works of M. Sugeno*, CRC Press, Boca Raton, 1999.

[53] Kalyan K. Sen and Eric J. Stacey, "UPFC – Unified Power Flow Controller: Theory, Modeling, and Applications," IEEE Transactions on Power Delivery, vol. 13, No. 4, October 1998, pp. 1453-1460.

[54] C. R. Fuerte-Esquivel and E. Acha, "Unified Power Flow Controller: A Critical Comparison of Newton-Raphson UPFC Algorithms in Power Flow Studies," IEE Proc.-Gener. Transm. Distrib., vol. 144, No. 5, September 1997, pp. 437-444.

[55] H. F. Wang, "Applications of Modeling UPFC into Multi-Machine Power Systems," IEE Proc.-Gener. Transm. Distrib., vol. 146, No. 3, May 1999, pp. 306-312.

[56] K. S. Smith, L. Ran and J. Penman, "Dynamic Modeling of a Unified Power Flow Controller," IEE Proc.-Gener. Transm. Distrib., vol. 144, No. 1, January 1997, pp. 7-12.

[57] Ogata, Katsuhiko, *Modern Control Engineering*, Uper Saddle River, N.J., Prentice Hall, 2002.

[58] Hao Ying, *Fuzzy Control and Modeling: Analytical Foundations and Applications*, IEEE Press Series on Biomedical Engineering, Series Editor: Metin Akay, New York, 2000.

[59] Kevin M. Passino and Stephen Yurkovich, *Fuzzy Control*, Addison Wesley Longman, Menlo Park, CA, 1998.

[60] T. Takagi and M. Sugeno, "Fuzzy Identification of System and Its Applications to Modeling and Control," IEEE Transactions on Systems, Man and Cybernetics, vol. 15, 1985, No. 1, pp. 116-132.

[61] Joe H. Chow, J. J. Sanchez-Gasca, Haoxing Ren and Shaopeng Wang, "Power System Damping Controller Design Using Multiple Input Signals," IEEE Control Systems Magazine, vol. 20, No 4, August 2000, pp. 82-90.

[62] Amer Hasanovic and Ali Feliachi, "Genetic Algorithm Based Inter-Area Oscillation Damping Controller Design Using MATLAB," IEEE Power Engineering Society Summer Meeting, vol. 3, July 2002, pp. 1136-1141.

[63] A. Elices, L. Rouco, H. Bourlès and T. Margotin, "Physical Interpretation of State Feedback Controllers to Damp Power System Oscillations," IEEE Transactions on Power Systems, vol. 19, No. 1, February 2004, pp. 436-443.

[64] H. F. Wang, "Selection of Robust installing Locations and Feedback Signals of FACTS-Based Stabilizers in Multi-Machine Power Systems," IEEE Transactions on Power Systems, vol. 14, No. 2, May 1999, pp. 569-574.

[65] Balarko Chaudhuri, Bilash C. Pal, Argyrios C. Zolotas, Imad M. Jaimoukha and Tim C. Green, "Mixed-Sensitivity Approach to H_∞ Control of Power System Oscillations Employing Multiple FACTS Devices," IEEE Transactions on Power Systems, vol. 18, No. 3, August 2003, pp. 1149-1156.

[66] Y. L. Kang, G. B. Shrestha and T. T. Lie, "Application of an NLPID Controller on a UPFC to Improve Transient Stability of a Power System," IEE Proc.-Gener. Transm. Distrib., vol. 148, No. 6, November 2001, pp. 523-529.

[67] H. F. Wang, F. J. Swift and M. Li, “Indices for Selecting the Best Location of PSSs or FACTS-Based Stabilisers in Multimachine Power Systems: A Comparative Study,” IEE Proc.-Gener. Transm. Distrib., vol. 144, No. 2, March 1997, pp. 155-159.

[68] Farzad Pourboghrat, Farshad Farid, Constantine J. Hatziadoniu, Morteza Daneshdoost, Fred Mehdian and Mohsen Lotfalian, “Local Sliding Control for Damping Interarea Power Oscillations,” IEEE Transactions on Power Systems, vol. 19, No. 2, May 2004, pp. 1123-1134.

[69] F. J. Swift and H. F. Wang, “Application of the Controllable Series Compensator in Damping Power System Oscillations,” IEE Proc.-Gener. Transm. Distrib., vol. 143, No. 4, July 1996, pp. 359-364.

[70] Lingling Fan and Ali Feliachi, “Robust TCSC Control Design for Damping Inter-Area Oscillations,” Proceeding of the IEEE Society Transmission and Distribution Conference, vol. 2, No. Summer, 2001, pp. 784-789.

[71] IEEE Working Group H-7 of the Relaying Channels Subcommittee of the IEEE Power System Relaying Committee, “Synchronized Sampling and Phasor Measurements for Relaying and Control,” IEEE Trans. on Power Delivery, vol. 9, no. 1, 1994, pp. 442-452.

[72] B. T. Ooi, M. Kazerani, R. Marceau, Z. Wolanki, F. D. Galiana, D. McGillis and G. Joos, “Mid-Point Sitting of FACTS Devices in Transmission Lines,” IEEE Transactions on Power Delivery, vol. 12, No. 4, October 1997, pp. 1717-1722.

[73] B. A. Renz, A. Keri, A. S. Mehraban, C. Schauder, E. Stacey, L. Kovalsky, L. Gyugyi, A. Edris, “AEP Unified Power Flow Controller Performance,” IEEE Transactions on Power Delivery, vol. 14, No. 4, October 1999, pp. 1374-1381.

[74] Pirjo Heine and Matti Lehtonen, “Voltage Sag Distributions Caused by Power System Faults,” IEEE Transactions on Power Systems, vol. 18, No. 4, November 2003, pp. 1367-1373.

[75] Ying Jiang-Häfner, Hugo Duchén, Kerstin Lindén, Mats Hyttinen, Paulo Fischer de Toledo, Tomas Tulkiewicz, Anna-Karin Skytt and Hans Björklund, “Improvement of Subsynchronous Torsional Damping using VSC HVDC,” Power Conference 2002, Kunming, China, October 13-17, 2002.

[76] Y. Jiang- Häfner, Mats Hyttinen and B. Pääjärvi, “On the Short Circuit Current Contribution of HVDC Light,” IEEE PES T&D 2002 Asia Pacific Conference, Yokohama, Japan, October 6-10, 2002.

[77] K. Eriksson, “HVDC Light™ and Development of Voltage Source Converter,” IEEE PES T&D 2002 Latin American Conference, Sao Paulo, Brazil, March 18-22, 2002.

[78] Gunnar Asplund, “Sustainable Energy Systems with HVDC transmission,” Global Power Systems for Sustainable Energy Development at IEEE PES 2004 General Meeting, Denvor, June 6-12, 2004.

[79] Kjell Eriksson, Christer Liljegren and Kent Sobrink, “HVDC Light Experiences Applicable for Power Transmission from Offshore Wind Power Parks,” ASME/AIAA Wind Energy Symposium, Reno NV, USA, January 5-8, 2004.

[80] Stefan G. Johansson, Gunnar Asplund, Erik Jansson and Roberto Rudervall, “Power System Stability Benefits with VSC DC-Transmission Systems,” Cigré Conference, Paris, France, Aug. 29-Sept. 3, 2004.

[81] Mike Wyckmans, “Innovation in the Market: HVDC Light, the New Technology,” 7th International Transmission and Distribution Conference, Adelaide, Australia, November 16-19, 2003.

[82] J. Arrillaga, *High Voltage Direct Current Transmission*, Peter Peregrinus Ltd: IEE Power Engineering Series 6, London, UK, 1998.

[83] IEEE Working Group on the Effect of Switching on Turbine-Generators, “Effect of Switching Network Disturbances on Turbine-Generator Shaft Systems,” IEEE Transactions on Power Apparatus and Systems, vol. PAS-101, 1982, pp. 3151-3157.

[84] IEEE Torsional Issues Working Group, “Fourth Supplement to a Bibliography for the Study of Subsynchronous Resonance between Rotating Machines and Power Systems,” IEEE Transactions on Power Systems, vol. 12, 1997, pp. 1276.1282.

[85] ANSI C50.13 - 1977, American National Standard, "Requirements of Cylindrical Rotor Synchronous Generators".

[86] C.E.J. Bowler, P.G. Brown and D.N. Walker, "Evaluation of the Effect of Power Circuit Breaker Reclosing Practices on Turbine-Generator Shafts," IEEE Transactions on Power Apparatus and Systems, vol. PAS-99, 1980, pp. 1764-1779.

[87] J.S. Joyce, T. Kulig and D. Lambrecht, "Torsional Fatigue of Turbine-Generator Shafts Caused by Different Electrical System Faults and Switching Operations," IEEE Transactions on Power Apparatus and Systems, vol. PAS-97, 1978, pp. 1965-1977.

[88] K.V. Patil, J. Senthil, J. Jiang and R.M. Mathur, “Application of STATCOM for Damping Torsional Oscillations in Series Compensated AC Systems,” IEEE Transactions on Energy Conversion, vol. 13, No. 3, September 1998, pp. 237-243.

[89] A.H.M.A. Rahim, A.M. Mohammad and M.R. Khan, “Control of Subsynchronous Resonant Modes in a Series Compensated System Through Superconducting Magnetic Energy Storage Units,” IEEE Transactions on Energy Conversion, vol. 11, No. 1, March 1996, pp. 175-180.

[90] H. A. Othman and L. Angquist, “Analytical Modeling of Thyristor-Controlled Series Capacitors for SSR Studies,” IEEE Transactions on Power Systems, Vol. 11, No. 1, February 1996, pp. 119-127.

[91] B.K. Perkins and M.R. Iravani, “Dynamic Modeling of a TCSC with Application to SSR Analysis,” IEEE Transactions on Power Systems, vol. 12, No. 4, November 1997, pp. 1619-1625.

[92] R.J. Piwko, C.W. Wegner, S.J. Kinney and J.D. Eden, “Subsynchronous Resonance Performance Tests of the Slatt Thyristor-Controlled Series Capacitor,” IEEE Transactions on Power Delivery, vol. 11, No. 2, April 1996, pp. 1112-1119.

[93] W. Zhu, R. Spee, R.R. Mohler, G.C. Alexander, W.A. Mittelstadt and D. Maratukulam, “An EMTP Study of SSR Mitigation Using the Thyristor-Controlled Series Capacitor,” IEEE Transactions on Power Delivery, vol. 10, No. 3, July 1995, pp. 1479-1485.

[94] Y. Jiang-Hafner, H. Duchen, K. Linden, M. Hyttinen, P.F. de Toledo, T. Tulkiewicz, A.K Skytt and H. Bjorklund, “Improvement of Subsynchronous Torsional Damping Using VSC HVDC,” Proceedings of Power Con 2002, Kunming, China, October 13-17, 2002.

[95] IEEE Task Force on SSR, “First Benchmark Model for Computer Simulation of Subsynchronous Resonance,” IEEE Transaction on Power Apparatus and Systems, vol. PAS-96, 1977, pp. 1565-1573.

[96] IEEE Subsynchronous Resonance Working Group of the Dynamic System Performance Subcommittee, Power System Engineering Committee, “Second Benchmark Model for Computer Simulation of Subsynchronous Resonance,” IEEE Transaction on Power Apparatus and Systems, vol. PAS-104, 1985, pp. 1057-1066.

[97] T.J. Hammons, M. Istin and A. Crocquevieile, “Analysis of Continuum and Reduced Shaft Models in Evaluating Turbine-Generator Shaft Torsional Response Following Severe Disturbances on the System Supply,” Electric Machines and Power Systems, vol. 13, 1987, pp. 387-408.

[98] A. Shaltout, “Subsynchronous Resonance in Large Turbo-Generators Connected to Series Capacitor Compensated Power Systems,” Ph.D. Thesis, University of Saskatchewan, 1981.

[99] K. Murotani and M, Asano, “Subsynchronous Resonance Oscillations of Series Compensated Transmission System and their Suppressions” Electrical Engineering in Japan, vol. 96, 1976, pp. 113-121.

[100] S. Goldberg and W. R. Schmus, “Subsynchronous Resonance and Torsional Stresses in Turbine-Generator Shafts,” IEEE Transactions on Power Apparatus and Systems, vol. PAS-98, 1979, pp. 1233-1237.

[101] Y. Mansour, E. Vaahedi, A. Y. Chang, B. R. Corns, B. W. Garrett, K. Demaree, T. Athay and K. Cheung, “B. C. Hydro’s On-line Transient Stability Assessment (TSA) Model Development, Analysis, and Post-Processing,” IEEE Transaction on Power Systems, vol. 10, Feb. 1995, pp. 241-253.

[102] M. B. Djuri and V. V. Terzija, “A New Approach to the Arcing Faults Detection for Fast Autoreclosure in Transmission systems,” IEEE Transaction on Power Delivery, vol. 10, October 1995, pp. 1793-1798.

APPENDIX A - PHILLIPS-HEFFRON MODEL OF A SINGLE-MACHINE INFINITE-BUS POWER SYSTEM EQUIPPED WITH UPFC

The dynamic differential equations of the UPFC can be written as:

$$\begin{bmatrix} i_{Eq} \\ i_{Bq} \end{bmatrix} = \begin{bmatrix} x_q + x_{1E} + x_E & x_q + x_{1E} \\ x_E & -x_B - x_{E2} \end{bmatrix}^{-1} \begin{bmatrix} \dfrac{m_E \cos\delta_E v_{dc}}{2} \\ \dfrac{m_E \cos\delta_E v_{dc}}{2} - \dfrac{m_B \cos\delta_B v_{dc}}{2} - V_b \sin\delta \end{bmatrix}$$

$$\begin{bmatrix} i_{Ed} \\ i_{Bd} \end{bmatrix} = \begin{bmatrix} x_d' + x_{1E} + x_E & x_d' + x_{1E} \\ x_E & -x_B - x_{E2} \end{bmatrix}^{-1} \begin{bmatrix} E_q' - \dfrac{m_E \sin\delta_E v_{dc}}{2} \\ \dfrac{m_B \sin\delta_B v_{dc}}{2} + V_b \cos\delta - \dfrac{m_E \sin\delta_E v_{dc}}{2} \end{bmatrix}$$

The linear model of a single-machine infinite-bus power system is:

$$\dot{\delta} = \omega_o \Delta\omega$$
$$\Delta\dot{\omega} = \left(P_m - P_e - D\Delta\omega\right)/2H$$
$$\dot{E}_q' = \left(-E_q + E_{qe}\right)/T_{do}'$$
$$\dot{E}_{qe} = reg(s)\left(v_{to} - v_t\right)$$

where

$$P_e = v_{qt} i_{qt} + v_{dt} i_{dt}, \qquad E_q = E_q' + \left(x_d - x_d'\right) i_{dt},$$

$$v_{qt} = E_q' - x_d' i_{dt}, \qquad v_t = \sqrt{v_{dt}^2 + v_{qt}^2}, \qquad i_{dt} = i_{Ed} + i_{Bd}$$
$$v_{dt} = x_q i_{qt} \qquad\qquad\qquad\qquad i_{qt} = i_{Eq} + i_{Bq}$$

$$E_q = v_{qt} + x_d i_{dt}, \qquad reg(s) = \frac{K_A}{1 + sT_A}$$

Let

$$\begin{bmatrix} x_q + x_{1E} + x_E & x_q + x_{1E} \\ x_E & -x_B - x_{E2} \end{bmatrix}^{-1} = \begin{bmatrix} x_{11q} & x_{12q} \\ x_{21q} & x_{22q} \end{bmatrix}$$

and $$\begin{bmatrix} x_d' + x_{1E} + x_E & x_d' + x_{1E} \\ x_E & -x_B - x_{E2} \end{bmatrix}^{-1} = \begin{bmatrix} x_{11d} & x_{12d} \\ x_{21d} & x_{22d} \end{bmatrix}$$

Therefore,

$$\begin{bmatrix} i_{Eq} \\ i_{Bq} \end{bmatrix} = \begin{bmatrix} x_{11q} & x_{12q} \\ x_{21q} & x_{22q} \end{bmatrix} \begin{bmatrix} \dfrac{m_E \cos\delta_E v_{dc}}{2} \\ \dfrac{m_E \cos\delta_E v_{dc}}{2} - \dfrac{m_B \cos\delta_B v_{dc}}{2} - V_b \sin\delta \end{bmatrix}$$

$$\begin{bmatrix} i_{Ed} \\ i_{Bd} \end{bmatrix} = \begin{bmatrix} x_{11d} & x_{12d} \\ x_{21d} & x_{22d} \end{bmatrix} \begin{bmatrix} E_q' - \dfrac{m_E \sin\delta_E v_{dc}}{2} \\ \dfrac{m_B \sin\delta_B v_{dc}}{2} + V_b \cos\delta - \dfrac{m_E \sin\delta_E v_{dc}}{2} \end{bmatrix}$$

$$i_{Eq} = \frac{x_{11q} m_E \cos\delta_E v_{dc}}{2} + \frac{x_{12q} m_E \cos\delta_E v_{dc}}{2} - \frac{x_{12q} m_B \cos\delta_B v_{dc}}{2} - x_{12q} V_b \sin\delta$$

$$i_{Bq} = \frac{x_{21q} m_E \cos\delta_E v_{dc}}{2} + \frac{x_{22q} m_E \cos\delta_E v_{dc}}{2} - \frac{x_{22q} m_B \cos\delta_B v_{dc}}{2} - x_{22q} V_b \sin\delta$$

$$i_{qt} = \frac{(x_{11q} + x_{21q}) m_E \cos\delta_E v_{dc}}{2} + \frac{(x_{12q} + x_{22q}) m_E \cos\delta_E v_{dc}}{2} - \frac{(x_{12q} + x_{22q}) m_B \cos\delta_B v_{dc}}{2} - (x_{12q} + x_{22q}) V_b \sin\delta$$

$$i_{qt} = \frac{(x_{11q} + x_{21q} + x_{12q} + x_{22q}) m_E \cos\delta_E v_{dc}}{2} - \frac{(x_{12q} + x_{22q}) m_B \cos\delta_B v_{dc}}{2} - (x_{12q} + x_{22q}) V_b \sin\delta$$

$$i_{qt} = \frac{x_{1b} m_E \cos\delta_E v_{dc}}{2} - \frac{x_{2b} m_B \cos\delta_B v_{dc}}{2} - x_{3b} V_b \sin\delta$$

$$i_{Ed} = x_{11d} E_q' - \frac{x_{11d} m_E \sin\delta_E v_{dc}}{2} + \frac{x_{12d} m_B \sin\delta_B v_{dc}}{2} + x_{12d} V_b \cos\delta - \frac{x_{12d} m_E \sin\delta_E v_{dc}}{2}$$

$$i_{Bd} = x_{21d} E_q' - \frac{x_{21d} m_E \sin\delta_E v_{dc}}{2} + \frac{x_{22d} m_B \sin\delta_B v_{dc}}{2} + x_{22d} V_b \cos\delta - \frac{x_{22d} m_E \sin\delta_E v_{dc}}{2}$$

$$i_{dt} = (x_{11d} + x_{21d}) E_q' - \frac{(x_{11d} + x_{12d} + x_{21d} + x_{22d}) m_E \sin\delta_E v_{dc}}{2} + \frac{(x_{12d} + x_{22d}) m_B \sin\delta_B v_{dc}}{2} + (x_{12d} + x_{22d}) V_b \cos\delta$$

$$i_{dt} = x_{1a} E_q' - \frac{x_{2a} m_E \sin\delta_E v_{dc}}{2} + \frac{x_{3a} m_B \sin\delta_B v_{dc}}{2} + x_{4a} V_b \cos\delta$$

The state-space equation of the power system can be represented as:

$$\begin{bmatrix} \Delta\dot{\delta} \\ \Delta\dot{\omega}_{,} \\ \Delta\dot{E}_q \\ \Delta\dot{E}_{fd} \end{bmatrix} = \begin{bmatrix} 0 & \omega_o & 0 & 0 \\ -\frac{K1}{2H} & -\frac{D}{2H} & -\frac{K2}{2H} & 0 \\ -\frac{K4}{T_{do}^{,}} & 0 & -\frac{K3}{T_{do}^{,}} & \frac{1}{T_{do}^{,}} \\ -\frac{K_A K_5}{T_A} & 0 & -\frac{K_A K_6}{T_A} & -\frac{1}{T_A} \end{bmatrix} \begin{bmatrix} \Delta\delta \\ \Delta\omega_{,} \\ \Delta E_q \\ \Delta E_{fd} \end{bmatrix} + \begin{bmatrix} 0 \\ -\frac{K_{pd}}{2H} \\ -\frac{K_{qd}}{T_{do}^{,}} \\ -\frac{K_A K_{vd}}{T_A} \end{bmatrix} \Delta v_{dc}$$
$$+ \begin{bmatrix} 0 & 0 & 0 & 0 \\ -\frac{K_{pe}}{2H} & -\frac{K_{p\delta e}}{2H} & -\frac{K_{pb}}{2H} & -\frac{K_{p\delta b}}{2H} \\ -\frac{K_{qe}}{T_{do}^{,}} & -\frac{K_{q\delta e}}{T_{do}^{,}} & -\frac{K_{qb}}{T_{do}^{,}} & -\frac{K_{q\delta b}}{T_{do}^{,}} \\ -\frac{K_A K_{ve}}{T_A} & -\frac{K_A K_{v\delta e}}{T_A} & -\frac{K_A K_{vb}}{T_A} & -\frac{K_A K_{v\delta b}}{T_A} \end{bmatrix} \begin{bmatrix} \Delta m_E \\ \Delta\delta_E \\ \Delta m_B \\ \Delta\delta_B \end{bmatrix}$$

Where:

$$K_1 = -\left(1 - x_d^{,} x_{1a}\right) E_q^{,} x_{3b} V_b \cos\delta + \frac{x_d^{,} x_{2a} x_{3b} m_E \sin\delta_E v_{dc} V_b \cos\delta}{2}$$
$$- \frac{x_d^{,} x_{3a} x_{3b} m_B \sin\delta_B v_{dc} V_b \cos\delta}{2} - \frac{x_d^{,} x_{4a} x_{1b} m_E V_b \sin\delta \cos\delta_E v_{dc}}{2}$$
$$+ \frac{x_d^{,} x_{4a} x_{2b} m_B V_b \sin\delta \cos\delta_B v_{dc}}{2} + x_d^{,} x_{4a} x_{3b} V_b^{\,2} \sin^2\delta - x_d^{,} x_{4a} x_{3b} V_b^{\,2} \cos^2\delta$$
$$- \frac{x_q x_{1b} x_{4a} m_E \cos\delta_E v_{dc} V_b \sin\delta}{2} + \frac{x_q x_{2b} x_{4a} m_B \cos\delta_B v_{dc} V_b \sin\delta}{2}$$
$$- x_q x_{3b} x_{1a} E_q^{,} V_b \cos\delta + \frac{x_q x_{3b} x_{2a} m_E V_b \sin\delta_E v_{dc} \cos\delta}{2}$$
$$- \frac{x_q x_{3b} x_{3a} m_B V_b \sin\delta_B v_{dc} \cos\delta}{2} - x_q x_{3b} x_{4a} V_b^{\,2} \cos^2\delta + x_q x_{3b} x_{4a} V_b^{\,2} \sin^2\delta$$

$$K_2 = \frac{\left(1 - x_d^{,} x_{1a}\right) x_{1b} m_E \cos\delta_E v_{dc}}{2} - \frac{\left(1 - x_d^{,} x_{1a}\right) x_{2b} m_B \cos\delta_B v_{dc}}{2} - \left(1 - x_d^{,} x_{1a}\right) x_{3b} V_b \sin\delta$$
$$+ \frac{x_q x_{1b} x_{1a} m_E \cos\delta_E v_{dc}}{2} - \frac{x_q x_{2b} x_{1a} m_B \cos\delta_B v_{dc}}{2} - x_q x_{3b} x_{1a} V_b \sin\delta$$

$$K_{pd} = \frac{\left(1 - x_d' x_{1a}\right) E_q' x_{1b} m_E \cos\delta_E}{2} - \frac{\left(1 - x_d' x_{1a}\right) E_q' x_{2b} m_B \cos\delta_B}{2}$$
$$- \frac{x_d' x_{2a} x_{1b} m_E^2 \sin\delta_E \cos\delta_E v_{dc}}{2} + \frac{x_d' x_{2a} x_{2b} m_E m_B \sin\delta_E \cos\delta_B v_{dc}}{2}$$
$$+ \frac{x_d' x_{2a} x_{3b} m_E \sin\delta_E V_b \sin\delta}{2} + \frac{x_d' x_{3a} x_{1b} m_B m_E \sin\delta_B \cos\delta_E v_{dc}}{2}$$
$$- \frac{x_d' x_{3a} x_{2b} m_B^2 \sin\delta_B \cos\delta_B v_{dc}}{2} - \frac{x_d' x_{3a} x_{3b} m_B \sin\delta_B V_b \sin\delta}{2}$$
$$+ \frac{x_d' x_{4a} x_{1b} m_E V_b \cos\delta \cos\delta_E}{2} - \frac{x_d' x_{4a} x_{2b} m_B V_b \cos\delta \cos\delta_B}{2}$$
$$+ \frac{x_q x_{1b} x_{1a} m_E E_q' \cos\delta_E}{2} - \frac{x_q x_{1b} x_{2a} m_E^2 \cos\delta_E \sin\delta_E v_{dc}}{2}$$
$$+ \frac{x_q x_{1b} x_{3a} m_E m_B \cos\delta_E \sin\delta_B v_{dc}}{2} + \frac{x_q x_{1b} x_{4a} m_E \cos\delta_E V_b \cos\delta}{2}$$
$$- \frac{x_q x_{2b} x_{1a} E_q' m_B \cos\delta_B}{2} + \frac{x_q x_{2b} x_{2a} m_B m_E \cos\delta_B \sin\delta_E v_{dc}}{2}$$
$$- \frac{x_q x_{2b} x_{3a} m_B m_B \cos\delta_B \sin\delta_B v_{dc}}{2} - \frac{x_q x_{2b} x_{4a} m_B \cos\delta_B V_b \cos\delta}{2}$$
$$+ \frac{x_q x_{3b} x_{2a} m_E V_b \sin\delta_E \sin\delta}{2} - \frac{x_q x_{3b} x_{3a} m_B V_b \sin\delta_B \sin\delta}{2}$$

$$K_{pe} = \frac{\left(1 - x_d' x_{1a}\right) E_q' x_{1b} \cos\delta_E v_{dc}}{2} - \frac{x_d' x_{2a} x_{1b} m_E \sin\delta_E \cos\delta_E v_{dc}^2}{2}$$
$$+ \frac{x_d' x_{2a} x_{2b} m_B \sin\delta_E \cos\delta_B v_{dc}^2}{4} + \frac{x_d' x_{2a} x_{3b} \sin\delta_E v_{dc} V_b \sin\delta}{2}$$
$$+ \frac{x_d' x_{3a} x_{1b} m_B \sin\delta_B \cos\delta_E v_{dc}^2}{4} + \frac{x_d' x_{4a} x_{1b} V_b \cos\delta \cos\delta_E v_{dc}}{2}$$
$$+ \frac{x_q x_{1b} x_{1a} E_q' \cos\delta_E v_{dc}}{2} - \frac{x_q x_{1b} x_{2a} m_E \cos\delta_E \sin\delta_E v_{dc}^2}{2}$$
$$+ \frac{x_q x_{1b} x_{3a} m_B \cos\delta_E \sin\delta_B v_{dc}^2}{4} + \frac{x_q x_{1b} x_{4a} \cos\delta_E v_{dc} V_b \cos\delta}{2}$$
$$+ \frac{x_q x_{2b} x_{2a} m_B \cos\delta_B \sin\delta_E v_{dc}^2}{4} + \frac{x_q x_{3b} x_{2a} V_b \sin\delta_E v_{dc} \sin\delta}{2}$$

$$K_{p\delta e} = -\frac{\left(1 - x_d' x_{1a}\right) E_q' x_{1b} m_E \sin\delta_E v_{dc}}{2} - \frac{x_d' x_{2a} x_{1b} m_E^{\,2} \cos^2\delta_E v_{dc}^{\,2}}{4}$$
$$+ \frac{x_d' x_{2a} x_{1b} m_E^{\,2} \sin^2\delta_E v_{dc}^{\,2}}{4} + \frac{x_d' x_{2a} x_{2b} m_E m_B \cos\delta_E \cos\delta_B v_{dc}^{\,2}}{4}$$
$$+ \frac{x_d' x_{2a} x_{3b} m_E \cos\delta_E v_{dc} V_b \sin\delta}{2} - \frac{x_d' x_{3a} x_{1b} m_B m_E \sin\delta_B \sin\delta_E v_{dc}^{\,2}}{4}$$
$$- \frac{x_d' x_{4a} x_{1b} m_E V_b \cos\delta \sin\delta_E v_{dc}}{2} - \frac{x_q x_{1b} x_{1a} m_E E_q' \sin\delta_E v_{dc}}{2}$$
$$- \frac{x_q x_{1b} x_{2a} m_E^{\,2} \cos^2\delta_E v_{dc}^{\,2}}{4} + \frac{x_q x_{1b} x_{2a} m_E^{\,2} \sin^2\delta_E v_{dc}^{\,2}}{4}$$
$$- \frac{x_q x_{1b} x_{3a} m_E m_B \sin\delta_E \sin\delta_B v_{dc}^{\,2}}{4} - \frac{x_q x_{1b} x_{4a} m_E \sin\delta_E v_{dc} V_b \cos\delta}{2}$$
$$+ \frac{x_q x_{2b} x_{2a} m_B m_E \cos\delta_B \cos\delta_E v_{dc}^{\,2}}{4} + \frac{x_q x_{3b} x_{2a} m_E V_b \cos\delta_E v_{dc} \sin\delta}{2}$$

$$K_{pb} = -\frac{\left(1 - x_d' x_{1a}\right) E_q' x_{2b} \cos\delta_B v_{dc}}{2} + \frac{x_d' x_{2a} x_{2b} m_E \sin\delta_E \cos\delta_B v_{dc}^{\,2}}{4}$$
$$+ \frac{x_d' x_{3a} x_{1b} m_E \sin\delta_B \cos\delta_E v_{dc}^{\,2}}{4} - \frac{x_d' x_{3a} x_{2b} m_B \sin\delta_B \cos\delta_B v_{dc}^{\,2}}{2}$$
$$- \frac{x_d' x_{3a} x_{3b} \sin\delta_B v_{dc} V_b \sin\delta}{2} - \frac{x_d' x_{4a} x_{2b} V_b \cos\delta \cos\delta_B v_{dc}}{2}$$
$$+ \frac{x_q x_{1b} x_{3a} m_E \cos\delta_E \sin\delta_B v_{dc}^{\,2}}{4} - \frac{x_q x_{2b} x_{1a} E_q' \cos\delta_B v_{dc}}{2}$$
$$+ \frac{x_q x_{2b} x_{2a} m_E \cos\delta_B \sin\delta_E v_{dc}^{\,2}}{4} - \frac{x_q x_{2b} x_{3a} m_B \cos\delta_B \sin\delta_B v_{dc}^{\,2}}{2}$$
$$- \frac{x_q x_{2b} x_{4a} \cos\delta_B v_{dc} V_b \cos\delta}{2} - \frac{x_q x_{3b} x_{3a} V_b \sin\delta_B v_{dc} \sin\delta}{2}$$

$$K_{p\delta b} = \frac{\left(1 - x_d' x_{1a}\right) E_q' x_{2b} m_B \sin\delta_B v_{dc}}{2} - \frac{x_d' x_{2a} x_{2b} m_E m_B \sin\delta_E \sin\delta_B v_{dc}^2}{4}$$
$$+ \frac{x_d' x_{3a} x_{1b} m_B m_E \cos\delta_B \cos\delta_E v_{dc}^2}{4} - \frac{x_d' x_{3a} x_{2b} m_B^2 \cos^2\delta_B v_{dc}^2}{4}$$
$$+ \frac{x_d' x_{3a} x_{2b} m_B^2 \sin^2\delta_B v_{dc}^2}{4} - \frac{x_d' x_{3a} x_{3b} m_B \cos\delta_B v_{dc} V_b \sin\delta}{2}$$
$$+ \frac{x_d' x_{4a} x_{2b} m_B V_b \cos\delta \sin\delta_B v_{dc}}{2} + \frac{x_q x_{1b} x_{3a} m_E m_B \cos\delta_E \cos\delta_B v_{dc}^2}{4}$$
$$+ \frac{x_q x_{2b} x_{1a} E_q' m_B \sin\delta_B v_{dc}}{2} - \frac{x_q x_{2b} x_{2a} m_B m_E \sin\delta_B \sin\delta_E v_{dc}^2}{4}$$
$$+ \frac{x_q x_{2b} x_{3a} m_B m_B \sin^2\delta_B v_{dc}^2}{4} - \frac{x_q x_{2b} x_{3a} m_B m_B \cos^2\delta_B v_{dc}^2}{4}$$
$$+ \frac{x_q x_{2b} x_{4a} m_B \sin\delta_B v_{dc} V_b \cos\delta}{2} - \frac{x_q x_{3b} x_{3a} m_B V_b \cos\delta_B v_{dc} \sin\delta}{2}$$

$$K_3 = \left(1 - x_d' x_{1a}\right) x_d x_{1a}$$

$$K_4 = -\left(x_d' + x_d\right) x_{4a} V_b \sin\delta$$

$$K_{pd} = -\frac{\left(x_d' + x_d\right) x_{2a} m_E \sin\delta_E}{2} + \frac{\left(x_d' + x_d\right) x_{3a} m_B \sin\delta_B}{2}$$

$$K_{qe} = -\frac{\left(x_d' + x_d\right) x_{2a} \sin\delta_E v_{dc}}{2}$$

$$K_{q\delta e} = -\frac{\left(x_d' + x_d\right) x_{2a} m_E \cos\delta_E v_{dc}}{2}$$

$$K_{qb} = \frac{\left(x_d' + x_d\right) x_{3a} \sin\delta_B v_{dc}}{2}$$

$$K_{q\delta b} = \frac{\left(x_d' + x_d\right) x_{3a} m_B \cos\delta_B v_{dc}}{2}$$

$$K_5 = \frac{1}{2}\left[\begin{array}{l}
\dfrac{x_q^{\,2} x_{1b}^{\,2} m_E^{\,2} \cos^2\delta_E v_{dc}^{\,2}}{4} - \dfrac{x_q^{\,2} x_{1b} x_{2b} m_E m_B \cos\delta_E \cos\delta_B v_{dc}^{\,2}}{2} \\
- x_q^{\,2} x_{1b} x_{3b} m_E \cos\delta_E v_{dc} V_b \sin\delta + \dfrac{x_q^{\,2} x_{2b}^{\,2} m_B^{\,2} \cos^2\delta_B v_{dc}^{\,2}}{4} \\
+ x_q^{\,2} x_{2b} x_{3b} m_B \cos\delta_B v_{dc} V_b \sin\delta + x_q^{\,2} x_{3b}^{\,2} V_b^{\,2} \sin^2\delta \\
+ \left(1 - x_d^{\,\prime} x_{1a}\right)^2 E_q^{\,\prime 2} - \left(1 - x_d^{\,\prime} x_{1a}\right) E_q^{\,\prime} x_d^{\,\prime} x_{2a} m_E \sin\delta_E v_{dc} \\
+ \left(1 - x_d^{\,\prime} x_{1a}\right) E_q^{\,\prime} x_d^{\,\prime} x_{3a} m_B \sin\delta_B v_{dc} + 2\left(1 - x_d^{\,\prime} x_{1a}\right) E_q^{\,\prime} x_d^{\,\prime} x_{4a} V_b \cos\delta \\
+ \dfrac{x_d^{\,\prime 2} x_{2a}^{\,2} m_E^{\,2} \sin^2\delta_E v_{dc}^{\,2}}{4} - \dfrac{x_d^{\,\prime 2} x_{2a} x_{3a} m_E m_B \sin\delta_E \sin\delta_B v_{dc}^{\,2}}{2} \\
- x_d^{\,\prime 2} x_{2a} x_{4a} m_E \sin\delta_E v_{dc} V_b \cos\delta + \dfrac{x_d^{\,\prime 2} x_{3a}^{\,2} m_B^{\,2} \sin^2\delta_B v_{dc}^{\,2}}{4} \\
+ x_d^{\,\prime 2} x_{3a} x_{4a} m_B \sin\delta_B v_{dc} V_b \cos\delta + x_d^{\,\prime 2} x_{4a}^{\,2} V_b^{\,2} \cos^2\delta
\end{array}\right]^{-1/2} \times$$

$$\left[\begin{array}{l}
- x_q^{\,2} x_{1b} x_{3b} m_E \cos\delta_E v_{dc} V_b \cos\delta + x_q^{\,2} x_{2b} x_{3b} m_B \cos\delta_B v_{dc} V_b \cos\delta \\
+ 2 x_q^{\,2} x_{3b}^{\,2} V_b^{\,2} \sin\delta\cos\delta - 2\left(1 - x_d^{\,\prime} x_{1a}\right) E_q^{\,\prime} x_d^{\,\prime} x_{4a} V_b \sin\delta \\
+ x_d^{\,\prime 2} x_{2a} x_{4a} m_E \sin\delta_E v_{dc} V_b \sin\delta - x_d^{\,\prime 2} x_{3a} x_{4a} m_B \sin\delta_B v_{dc} V_b \sin\delta \\
- 2 x_d^{\,\prime 2} x_{4a}^{\,2} V_b^{\,2} \cos\delta\sin\delta
\end{array}\right]$$

$$K_6 = \frac{1}{2}\left[\begin{array}{l}
\dfrac{x_q^{\,2} x_{1b}^{\,2} m_E^{\,2} \cos^2\delta_E v_{dc}^{\,2}}{4} - \dfrac{x_q^{\,2} x_{1b} x_{2b} m_E m_B \cos\delta_E \cos\delta_B v_{dc}^{\,2}}{2} \\
- x_q^{\,2} x_{1b} x_{3b} m_E \cos\delta_E v_{dc} V_b \sin\delta + \dfrac{x_q^{\,2} x_{2b}^{\,2} m_B^{\,2} \cos^2\delta_B v_{dc}^{\,2}}{4} \\
+ x_q^{\,2} x_{2b} x_{3b} m_B \cos\delta_B v_{dc} V_b \sin\delta + x_q^{\,2} x_{3b}^{\,2} V_b^{\,2} \sin^2\delta + \left(1 - x_d^{\,\prime} x_{1a}\right)^2 E_q^{\,\prime 2} \\
- \left(1 - x_d^{\,\prime} x_{1a}\right) E_q^{\,\prime} x_d^{\,\prime} x_{2a} m_E \sin\delta_E v_{dc} + \left(1 - x_d^{\,\prime} x_{1a}\right) E_q^{\,\prime} x_d^{\,\prime} x_{3a} m_B \sin\delta_B v_{dc} \\
+ 2\left(1 - x_d^{\,\prime} x_{1a}\right) E_q^{\,\prime} x_d^{\,\prime} x_{4a} V_b \cos\delta + \dfrac{x_d^{\,\prime 2} x_{2a}^{\,2} m_E^{\,2} \sin^2\delta_E v_{dc}^{\,2}}{4} \\
- \dfrac{x_d^{\,\prime 2} x_{2a} x_{3a} m_E m_B \sin\delta_E \sin\delta_B v_{dc}^{\,2}}{2} - x_d^{\,\prime 2} x_{2a} x_{4a} m_E \sin\delta_E v_{dc} V_b \cos\delta \\
+ \dfrac{x_d^{\,\prime 2} x_{3a}^{\,2} m_B^{\,2} \sin^2\delta_B v_{dc}^{\,2}}{4} + x_d^{\,\prime 2} x_{3a} x_{4a} m_B \sin\delta_B v_{dc} V_b \cos\delta \\
+ x_d^{\,\prime 2} x_{4a}^{\,2} V_b^{\,2} \cos^2\delta
\end{array}\right]^{-1/2} \times$$

$$\left[\begin{array}{l} 2\left(1-x_d^{'}x_{1a}\right)^2 E_q^{'}-\left(1-x_d^{'}x_{1a}\right)x_d^{'}x_{2a}m_E\sin\delta_E v_{dc} \\ +\left(1-x_d^{'}x_{1a}\right)x_d^{'}x_{3a}m_B\sin\delta_B v_{dc}+2\left(1-x_d^{'}x_{1a}\right)x_d^{'}x_{4a}V_b\cos\delta \end{array}\right]$$

$$K_{vd}=\frac{1}{2}\left[\begin{array}{l} \dfrac{x_q^{\,2}x_{1b}^{\,2}m_E^{\,2}\cos^2\delta_E v_{dc}^{\,2}}{4}-\dfrac{x_q^{\,2}x_{1b}x_{2b}m_E m_B\cos\delta_E\cos\delta_B v_{dc}^{\,2}}{2} \\ -x_q^{\,2}x_{1b}x_{3b}m_E\cos\delta_E v_{dc}V_b\sin\delta+\dfrac{x_q^{\,2}x_{2b}^{\,2}m_B^{\,2}\cos^2\delta_B v_{dc}^{\,2}}{4} \\ +x_q^{\,2}x_{2b}x_{3b}m_B\cos\delta_B v_{dc}V_b\sin\delta+x_q^{\,2}x_{3b}^{\,2}V_b^{\,2}\sin^2\delta \\ +\left(1-x_d^{'}x_{1a}\right)^2 E_q^{'2}-\left(1-x_d^{'}x_{1a}\right)E_q^{'}x_d^{'}x_{2a}m_E\sin\delta_E v_{dc} \\ +\left(1-x_d^{'}x_{1a}\right)E_q^{'}x_d^{'}x_{3a}m_B\sin\delta_B v_{dc}+2\left(1-x_d^{'}x_{1a}\right)E_q^{'}x_d^{'}x_{4a}V_b\cos\delta \\ +\dfrac{x_d^{'2}x_{2a}^{\,2}m_E^{\,2}\sin^2\delta_E v_{dc}^{\,2}}{4}-\dfrac{x_d^{'2}x_{2a}x_{3a}m_E m_B\sin\delta_E\sin\delta_B v_{dc}^{\,2}}{2} \\ -x_d^{'2}x_{2a}x_{4a}m_E\sin\delta_E v_{dc}V_b\cos\delta+\dfrac{x_d^{'2}x_{3a}^{\,2}m_B^{\,2}\sin^2\delta_B v_{dc}^{\,2}}{4} \\ +x_d^{'2}x_{3a}x_{4a}m_B\sin\delta_B v_{dc}V_b\cos\delta+x_d^{'2}x_{4a}^{\,2}V_b^{\,2}\cos^2\delta \end{array}\right]^{-1/2} \times$$

$$\left[\begin{array}{l} \dfrac{x_q^{\,2}x_{1b}^{\,2}m_E^{\,2}\cos^2\delta_E v_{dc}}{2}-x_q^{\,2}x_{1b}x_{2b}m_E m_B\cos\delta_E\cos\delta_B v_{dc} \\ -x_q^{\,2}x_{1b}x_{3b}m_E\cos\delta_E V_b\sin\delta+\dfrac{x_q^{\,2}x_{2b}^{\,2}m_B^{\,2}\cos^2\delta_B v_{dc}}{2} \\ +x_q^{\,2}x_{2b}x_{3b}m_B\cos\delta_B V_b\sin\delta-\left(1-x_d^{'}x_{1a}\right)E_q^{'}x_d^{'}x_{2a}m_E\sin\delta_E \\ +\left(1-x_d^{'}x_{1a}\right)E_q^{'}x_d^{'}x_{3a}m_B\sin\delta_B+\dfrac{x_d^{'2}x_{2a}^{\,2}m_E^{\,2}\sin^2\delta_E v_{dc}}{2} \\ -x_d^{'2}x_{2a}x_{3a}m_E m_B\sin\delta_E\sin\delta_B v_{dc}-x_d^{'2}x_{2a}x_{4a}m_E\sin\delta_E V_b\cos\delta \\ +\dfrac{x_d^{'2}x_{3a}^{\,2}m_B^{\,2}\sin^2\delta_B v_{dc}}{2}+x_d^{'2}x_{3a}x_{4a}m_B\sin\delta_B V_b\cos\delta \end{array}\right]$$

$$K_{ve} = \frac{1}{2}\left[\begin{array}{l}
\dfrac{x_q^{\,2} x_{1b}^{\,2} m_E^{\,2} \cos^2\delta_E v_{dc}^{\,2}}{4} - \dfrac{x_q^{\,2} x_{1b} x_{2b} m_E m_B \cos\delta_E \cos\delta_B v_{dc}^{\,2}}{2} \\
- x_q^{\,2} x_{1b} x_{3b} m_E \cos\delta_E v_{dc} V_b \sin\delta + \dfrac{x_q^{\,2} x_{2b}^{\,2} m_B^{\,2} \cos^2\delta_B v_{dc}^{\,2}}{4} \\
+ x_q^{\,2} x_{2b} x_{3b} m_B \cos\delta_B v_{dc} V_b \sin\delta + x_q^{\,2} x_{3b}^{\,2} V_b^{\,2} \sin^2\delta + \left(1 - x_d^{\,\prime} x_{1a}\right)^2 E_q^{\,\prime 2} \\
- \left(1 - x_d^{\,\prime} x_{1a}\right) E_q^{\,\prime} x_d^{\,\prime} x_{2a} m_E \sin\delta_E v_{dc} + \left(1 - x_d^{\,\prime} x_{1a}\right) E_q^{\,\prime} x_d^{\,\prime} x_{3a} m_B \sin\delta_B v_{dc} \\
+ 2\left(1 - x_d^{\,\prime} x_{1a}\right) E_q^{\,\prime} x_d^{\,\prime} x_{4a} V_b \cos\delta + \dfrac{x_d^{\,\prime 2} x_{2a}^{\,2} m_E^{\,2} \sin^2\delta_E v_{dc}^{\,2}}{4} \\
- \dfrac{x_d^{\,\prime 2} x_{2a} x_{3a} m_E m_B \sin\delta_E \sin\delta_B v_{dc}^{\,2}}{2} - x_d^{\,\prime 2} x_{2a} x_{4a} m_E \sin\delta_E v_{dc} V_b \cos\delta \\
+ \dfrac{x_d^{\,\prime 2} x_{3a}^{\,2} m_B^{\,2} \sin^2\delta_B v_{dc}^{\,2}}{4} + x_d^{\,\prime 2} x_{3a} x_{4a} m_B \sin\delta_B v_{dc} V_b \cos\delta \\
+ x_d^{\,\prime 2} x_{4a}^{\,2} V_b^{\,2} \cos^2\delta
\end{array}\right]^{-1/2} \times$$

$$\left[\begin{array}{l}
\dfrac{x_q^{\,2} x_{1b}^{\,2} m_E \cos^2\delta_E v_{dc}^{\,2}}{2} - \dfrac{x_q^{\,2} x_{1b} x_{2b} m_B \cos\delta_E \cos\delta_B v_{dc}^{\,2}}{2} \\
- x_q^{\,2} x_{1b} x_{3b} \cos\delta_E v_{dc} V_b \sin\delta - \left(1 - x_d^{\,\prime} x_{1a}\right) E_q^{\,\prime} x_d^{\,\prime} x_{2a} \sin\delta_E v_{dc} \\
+ \dfrac{x_d^{\,\prime 2} x_{2a}^{\,2} m_E \sin^2\delta_E v_{dc}^{\,2}}{2} - \dfrac{x_d^{\,\prime 2} x_{2a} x_{3a} m_B \sin\delta_E \sin\delta_B v_{dc}^{\,2}}{2} \\
- x_d^{\,\prime 2} x_{2a} x_{4a} \sin\delta_E v_{dc} V_b \cos\delta
\end{array}\right]$$

$$K_{v\delta e} = \frac{1}{2}\left[\begin{array}{l}
\dfrac{x_q^{\,2} x_{1b}^{\,2} m_E^{\,2} \cos^2\delta_E v_{dc}^{\,2}}{4} - \dfrac{x_q^{\,2} x_{1b} x_{2b} m_E m_B \cos\delta_E \cos\delta_B v_{dc}^{\,2}}{2} \\
- x_q^{\,2} x_{1b} x_{3b} m_E \cos\delta_E v_{dc} V_b \sin\delta + \dfrac{x_q^{\,2} x_{2b}^{\,2} m_B^{\,2} \cos^2\delta_B v_{dc}^{\,2}}{4} \\
+ x_q^{\,2} x_{2b} x_{3b} m_B \cos\delta_B v_{dc} V_b \sin\delta + x_q^{\,2} x_{3b}^{\,2} V_b^{\,2} \sin^2\delta + \left(1 - x_d^{'} x_{1a}\right)^2 E_q^{'2} \\
- \left(1 - x_d^{'} x_{1a}\right) E_q^{'} x_d^{'} x_{2a} m_E \sin\delta_E v_{dc} + \left(1 - x_d^{'} x_{1a}\right) E_q^{'} x_d^{'} x_{3a} m_B \sin\delta_B v_{dc} \\
+ 2\left(1 - x_d^{'} x_{1a}\right) E_q^{'} x_d^{'} x_{4a} V_b \cos\delta + \dfrac{x_d^{'2} x_{2a}^{\,2} m_E^{\,2} \sin^2\delta_E v_{dc}^{\,2}}{4} \\
- \dfrac{x_d^{'2} x_{2a} x_{3a} m_E m_B \sin\delta_E \sin\delta_B v_{dc}^{\,2}}{2} - x_d^{'2} x_{2a} x_{4a} m_E \sin\delta_E v_{dc} V_b \cos\delta \\
+ \dfrac{x_d^{'2} x_{3a}^{\,2} m_B^{\,2} \sin^2\delta_B v_{dc}^{\,2}}{4} + x_d^{'2} x_{3a} x_{4a} m_B \sin\delta_B v_{dc} V_b \cos\delta \\
+ x_d^{'2} x_{4a}^{\,2} V_b^{\,2} \cos^2\delta
\end{array}\right]^{-1/2} \times$$

$$\left[\begin{array}{l}
- \dfrac{x_q^{\,2} x_{1b}^{\,2} m_E^{\,2} \cos\delta_E \sin\delta_E v_{dc}^{\,2}}{4} + \dfrac{x_q^{\,2} x_{1b} x_{2b} m_E m_B \sin\delta_E \cos\delta_B v_{dc}^{\,2}}{2} \\
+ x_q^{\,2} x_{1b} x_{3b} m_E \sin\delta_E v_{dc} V_b \sin\delta - \left(1 - x_d^{'} x_{1a}\right) E_q^{'} x_d^{'} x_{2a} m_E \cos\delta_E v_{dc} \\
+ \dfrac{x_d^{'2} x_{2a}^{\,2} m_E^{\,2} \sin\delta_E \cos\delta_E v_{dc}^{\,2}}{2} - \dfrac{x_d^{'2} x_{2a} x_{3a} m_E m_B \cos\delta_E \sin\delta_B v_{dc}^{\,2}}{2} \\
- x_d^{'2} x_{2a} x_{4a} m_E \cos\delta_E v_{dc} V_b \cos\delta
\end{array}\right]$$

$$K_{vb} = \frac{1}{2}\left[\begin{array}{l}
\dfrac{x_q^{\,2} x_{1b}^{\,2} m_E^{\,2} \cos^2\delta_E v_{dc}^{\,2}}{4} - \dfrac{x_q^{\,2} x_{1b} x_{2b} m_E m_B \cos\delta_E \cos\delta_B v_{dc}^{\,2}}{2} \\
- x_q^{\,2} x_{1b} x_{3b} m_E \cos\delta_E v_{dc} V_b \sin\delta + \dfrac{x_q^{\,2} x_{2b}^{\,2} m_B^{\,2} \cos^2\delta_B v_{dc}^{\,2}}{4} \\
+ x_q^{\,2} x_{2b} x_{3b} m_B \cos\delta_B v_{dc} V_b \sin\delta + x_q^{\,2} x_{3b}^{\,2} V_b^{\,2} \sin^2\delta + \left(1 - x_d^{\,\prime} x_{1a}\right)^2 E_q^{\,\prime 2} \\
- \left(1 - x_d^{\,\prime} x_{1a}\right) E_q^{\,\prime} x_d^{\,\prime} x_{2a} m_E \sin\delta_E v_{dc} + \left(1 - x_d^{\,\prime} x_{1a}\right) E_q^{\,\prime} x_d^{\,\prime} x_{3a} m_B \sin\delta_B v_{dc} \\
+ 2\left(1 - x_d^{\,\prime} x_{1a}\right) E_q^{\,\prime} x_d^{\,\prime} x_{4a} V_b \cos\delta + \dfrac{x_d^{\,\prime 2} x_{2a}^{\,2} m_E^{\,2} \sin^2\delta_E v_{dc}^{\,2}}{4} \\
- \dfrac{x_d^{\,\prime 2} x_{2a} x_{3a} m_E m_B \sin\delta_E \sin\delta_B v_{dc}^{\,2}}{2} - x_d^{\,\prime 2} x_{2a} x_{4a} m_E \sin\delta_E v_{dc} V_b \cos\delta \\
+ \dfrac{x_d^{\,\prime 2} x_{3a}^{\,2} m_B^{\,2} \sin^2\delta_B v_{dc}^{\,2}}{4} + x_d^{\,\prime 2} x_{3a} x_{4a} m_B \sin\delta_B v_{dc} V_b \cos\delta \\
+ x_d^{\,\prime 2} x_{4a}^{\,2} V_b^{\,2} \cos^2\delta
\end{array}\right]^{-1/2} \times$$

$$\left[\begin{array}{l}
- \dfrac{x_q^{\,2} x_{1b} x_{2b} m_E \cos\delta_E \cos\delta_B v_{dc}^{\,2}}{2} + \dfrac{x_q^{\,2} x_{2b}^{\,2} m_B \cos^2\delta_B v_{dc}^{\,2}}{2} \\
+ x_q^{\,2} x_{2b} x_{3b} \cos\delta_B v_{dc} V_b \sin\delta + \left(1 - x_d^{\,\prime} x_{1a}\right) E_q^{\,\prime} x_d^{\,\prime} x_{3a} \sin\delta_B v_{dc} \\
- \dfrac{x_d^{\,\prime 2} x_{2a} x_{3a} m_E \sin\delta_E \sin\delta_B v_{dc}^{\,2}}{2} + \dfrac{x_d^{\,\prime 2} x_{3a}^{\,2} m_B \sin^2\delta_B v_{dc}^{\,2}}{2} \\
+ x_d^{\,\prime 2} x_{3a} x_{4a} \sin\delta_B v_{dc} V_b \cos\delta
\end{array}\right]$$

$$K_{v\delta b} = \frac{1}{2}\left[\begin{array}{l}
\frac{x_q^{\,2} x_{1b}^{\,2} m_E^{\,2} \cos^2\delta_E v_{dc}^{\,2}}{4} - \frac{x_q^{\,2} x_{1b} x_{2b} m_E m_B \cos\delta_E \cos\delta_B v_{dc}^{\,2}}{2} \\
- x_q^{\,2} x_{1b} x_{3b} m_E \cos\delta_E v_{dc} V_b \sin\delta + \frac{x_q^{\,2} x_{2b}^{\,2} m_B^{\,2} \cos^2\delta_B v_{dc}^{\,2}}{4} \\
+ x_q^{\,2} x_{2b} x_{3b} m_B \cos\delta_B v_{dc} V_b \sin\delta + x_q^{\,2} x_{3b}^{\,2} V_b^{\,2} \sin^2\delta + \left(1 - x_d^{'} x_{1a}\right)^2 E_q^{'2} \\
- \left(1 - x_d^{'} x_{1a}\right) E_q^{'} x_d^{'} x_{2a} m_E \sin\delta_E v_{dc} + \left(1 - x_d^{'} x_{1a}\right) E_q^{'} x_d^{'} x_{3a} m_B \sin\delta_B v_{dc} \\
+ 2\left(1 - x_d^{'} x_{1a}\right) E_q^{'} x_d^{'} x_{4a} V_b \cos\delta + \frac{x_d^{'2} x_{2a}^{\,2} m_E^{\,2} \sin^2\delta_E v_{dc}^{\,2}}{4} \\
- \frac{x_d^{'2} x_{2a} x_{3a} m_E m_B \sin\delta_E \sin\delta_B v_{dc}^{\,2}}{2} - x_d^{'2} x_{2a} x_{4a} m_E \sin\delta_E v_{dc} V_b \cos\delta \\
+ \frac{x_d^{'2} x_{3a}^{\,2} m_B^{\,2} \sin^2\delta_B v_{dc}^{\,2}}{4} + x_d^{'2} x_{3a} x_{4a} m_B \sin\delta_B v_{dc} V_b \cos\delta \\
+ x_d^{'2} x_{4a}^{\,2} V_b^{\,2} \cos^2\delta
\end{array}\right]^{-1/2} \times$$

$$\left[\begin{array}{l}
+ \frac{x_q^{\,2} x_{2b}^{\,2} m_B^{\,2} \cos\delta_B \sin\delta_B v_{dc}^{\,2}}{2} - x_q^{\,2} x_{2b} x_{3b} m_B \sin\delta_B v_{dc} V_b \sin\delta \\
+ \left(1 - x_d^{'} x_{1a}\right) E_q^{'} x_d^{'} x_{3a} m_B \cos\delta_B v_{dc} - \frac{x_d^{'2} x_{2a} x_{3a} m_E m_B \sin\delta_E \cos\delta_B v_{dc}^{\,2}}{2} \\
+ \frac{x_d^{'2} x_{3a}^{\,2} m_B^{\,2} \sin\delta_B \cos\delta_B v_{dc}^{\,2}}{2} + x_d^{'2} x_{3a} x_{4a} m_B \cos\delta_B v_{dc} V_b \cos\delta
\end{array}\right]$$

APPENDIX B - GENETIC ALGORITHMS: AN OVERVIEW

Genetic Algorithms (GA) is a technique that mimics natural evolution to solve problems in wide variety of domains. This appendix presents the basic definitions and principles of GA.

B.1 Fundamentals of Genetic Algorithms

In nature, individuals best suited to competition for scanty resources survive. Adapting to changing environment is essential for the survival of individuals of each species. While the various features that uniquely characterize an individual determine its survival capacity, the features in turn are determined by the individual's genetic content. A basic unit called *gene* controls each feature. The sets of genes controlling features form the *chromosomes*, the "keys" to the survival of the individual in a competitive environment. In nature, competition among individuals for scant resources such as food and space and for mates, results in the fittest individuals dominating over weaker ones. Only the fittest individuals survive and reproduce a natural phenomenon called "the survival of the fittest". Hence, the genes of the fittest survive, while the genes of weaker individuals die out. Natural *selection* leads to the survival of the fittest individuals, but it also implicitly leads to the survival of the fittest genes. The reproduction process generates diversity in the *gene pool*. Evolution is initiated when the genetic material (*chromosomes*) from two parents recombines during reproduction. New combinations of genes are generated from previous ones; a new gene pool is created. The exchange of genetic material among chromosomes is called *crossover*. Segments of the two parents' chromosomes are exchanged during *crossover*, creating the possibility of the "right" combination of genes for better individuals. Repeated *selection* and *crossover* cause the continuous evolution of the gene pool and the generation of individuals that survive better in a competitive environment.

Holland proposed genetic algorithms in the early 1970s as computer programs that mimic the evolutionary processes in nature [48]. Table B-1 presents the analogy between genetic terminology and the corresponding GA terminology.

Table B-1 GA terminology

Genetics Terminology	GA Equivalent
Individual, String or Chromosome	A coded parametric set
Population	A Collection of search points
Generation	Next iteration
Gene	Feature or character
Allele	Feature value
Fitness function or objective Function or Performance index	Function to be optimized
Schemata or similarity templates	Building blocks

B.2 Simple Genetic Algorithms

Genetic algorithms are different from normal search methods encountered in engineering optimization in the following ways:

1- GA work with a coding of the parameter set not the parameters themselves.

2- GA search from a population of points, not a single point.

3- GA use probabilistic transition rules, not deterministic transition rules.

A typical GA search starts with a random population of individuals. Each individual (a string) is a coded set of parameters that we want to optimize. An objective (fitness) function is used to determine how fit these individuals are. A suitable selection strategy is employed to select the individuals that will reproduce. Reproduction (or a new set of individuals) is achieved by using crossover and mutation operators. The GA then manipulates the most promising strings in its search for improved solutions. A GA operates through a simple cycle of stages as follows:

1- Creation of a “population” of strings (using a random generator).

2- Evaluation of each string (using a fitness function).

3- Selection of best strings (using a suitable selection method).

4- Genetic manipulation to create the new population of strings.

Figure B.1 shows these four stages using the biologically inspired GA terminology.

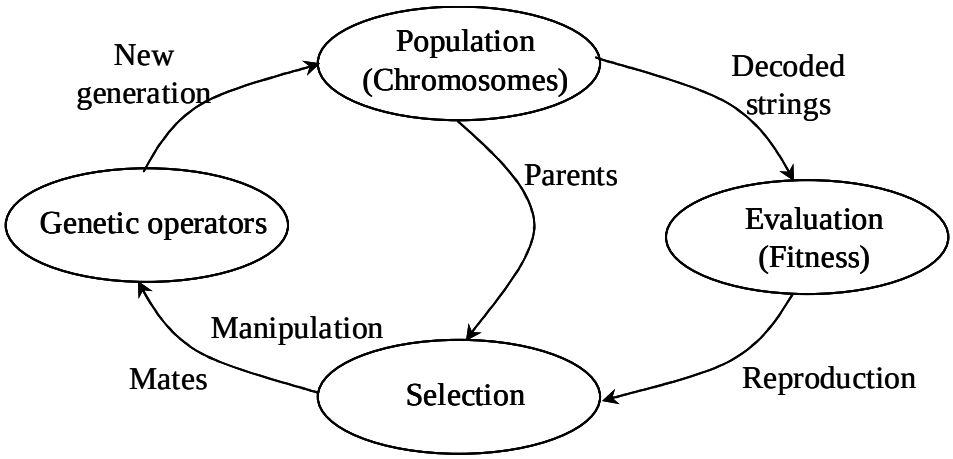

Figure B.1 The GA cycle.

B.3 Coding of parameters

Genetic Algorithms require the natural parameter set of the optimization problem to be coded as a finite-length string. As an example, consider the linear optimal control problem shown in Figure B.2. For this optimization problem, the two parameters (K_1 and K_2) are discretized by mapping from a smallest possible parametric set K_{min} to a largest possible parametric set K_{max}. This mapping uses a 10-bit binary unsigned integer for both K_1 and K_2. In this coding string code 0000000000 maps to K_{min} and an 1111111111 maps to K_{max} with a linear mapping in between. Next, the two 10-bit sets are chained together to form a 20-bit string representing a particular controller design. A single 20-bit string represents one of the 2^{20} = 1,048,576 alternative solutions. Table B-2 presents a coding example and a sample random initial population.

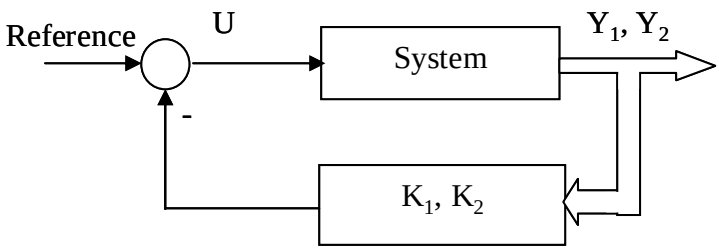

Evaluate K_1 and K_2 for min $J = \int_0^T f(Y_1, Y_2, U)dt$

Figure B.2 An example of linear optimal control.

Table B-2 Coding example

String Number	K1	Coding (Population Size = 5) K1 K2	K2
1	-25.00 (K_{min})	0000000000 0000000000	-25.00 (K_{min})
2	8.3	1010101010 1010111101	9.23
3	19.43	1110001110 0001101101	-19.67
4	15.57	1100111111 0000110111	-22.31
5	25.00 (K_{max})	1111111111 1111111111	25.00 (K_{max})

Example of coding

Range of parameter K (-25 to 25)

Number of states for 10 bits string = 2^{10} = 1024 state

Q (Quantitization) = 50 / 1024 = 0.048828

For string # 2 $K_1 = 682 \times 0.048828 - 25 = 8.3$

where $(1010101010)_2 = (682)_{10}$

For string # 3 $K_2 = 109 \times 0.048828 - 25 = -19.67$

where $(0001101101)_2 = (109)_{10}$

B.4 GA Operators

A simple genetic algorithm is composed of three operators: *selection*, *crossover*, and *mutation*.

1- Selection is a process where an old string is carried through into a new population depending on the value of fitness function. Due to this move, strings with better fitness values get larger numbers of copies in the next generation. Selecting good strings for this operation can be implemented in many different ways. A simple way is to let strings with higher fitness values "F" get a proportionally higher probability of selection (roulette wheel selection, Figure B.3) based on P(select) = $F_i / \sum_i F_i$; where i = string index.

This strategy, in which good strings get more copies in the next generation, emphasizes the survival-of-the-fittest concept of Genetic Algorithms.

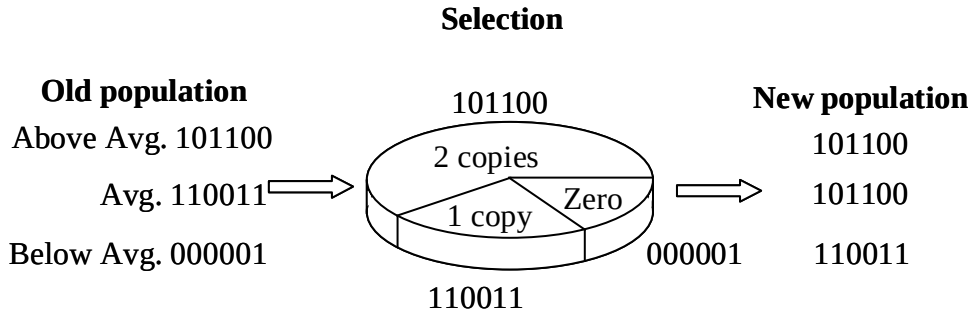

Figure B.3 Roulette wheel selection.

2- A simple crossover follows the selection is made in three steps. First, the newly selected strings are paired together at random. Second, an integer position "n" along every pair of strings is selected uniformly at random. Finally, based on a probability of crossover (ρ_c), the paired strings undergo crossing over at the integer position "n" along the string. This results in new pairs of strings that are created by swapping all the characters between characters 1 and "n" inclusively. As an example, consider two strings X and Y of length 5 mated at random from the mating pool of the new generation (numbers in brackets show a binary coded representation of a possible combination):

X = X1 X2 X3 X4 X5 [0 0 0 | 1 1]

Y = Y1 Y2 Y3 Y4 Y5 [1 1 1 | 0 0]

If the random draw chooses position 3, the resulting crossover yields two new strings X*, Y* after the crossover.

X* = Y1 Y2 Y3 X4 X5 [0 0 0 0 0]

Y* = X1 X2 X3 Y4 Y5 [1 1 1 1 1]

Although the crossover operation is a randomized event, when combined with selection it becomes an effective means of exchanging information and

combining portions of good quality solutions. Selection and crossover give GA most of their search power.

3- Mutation is simply an occasional random alteration of a string position based on probability of mutation (ρ_m). In a binary code, this involves changing a 1 to a 0 and vice versa. The mutation operator helps in avoiding the possibility of mistaking a local minimum for a global minimum. When mutation is used with selection and crossover, it improves the global nature of the genetic algorithm search. Figure B.4 presents crossover and mutation examples. Note that a crossover can occur at many random locations. Thus in a GA, every new generation consists of selected individuals from the previous generation who have gone through crossover and mutation based on the probability rates chosen.

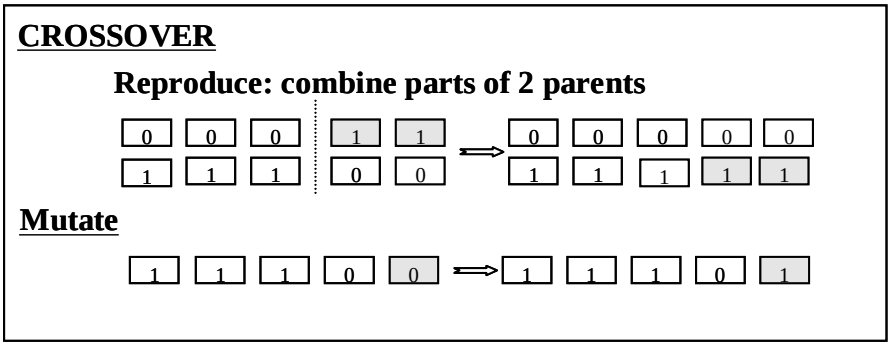

Figure B.4 Crossover and mutation.

Figure B.5 presents a computational flow chart of a simple genetic algorithm. One of the benefits of the genetic algorithm is the problem-independent characteristic of the search scheme. This enables a black-box treatment of the GA code. That is, the GA supplies the parameters to the optimization problem at hand and in return, the specific problem-dependent software provides the fitness function. This fitness function is then used by the GA to develop the next generation.

Several practical means of deciding when to stop regeneration are used. These are:

1- Stop after a period of time (Maximum number of generations).

2- Stop when the average fitness is close to the minimum (or the maximum) of the fitness.

3- Stop when there is no improvement in the maximum (or minimum) value of the fitness.

4- Stop after finding a better solution than the one proposed by other means or criterion.

5- Stop after finding the desired maximum (or minimum).

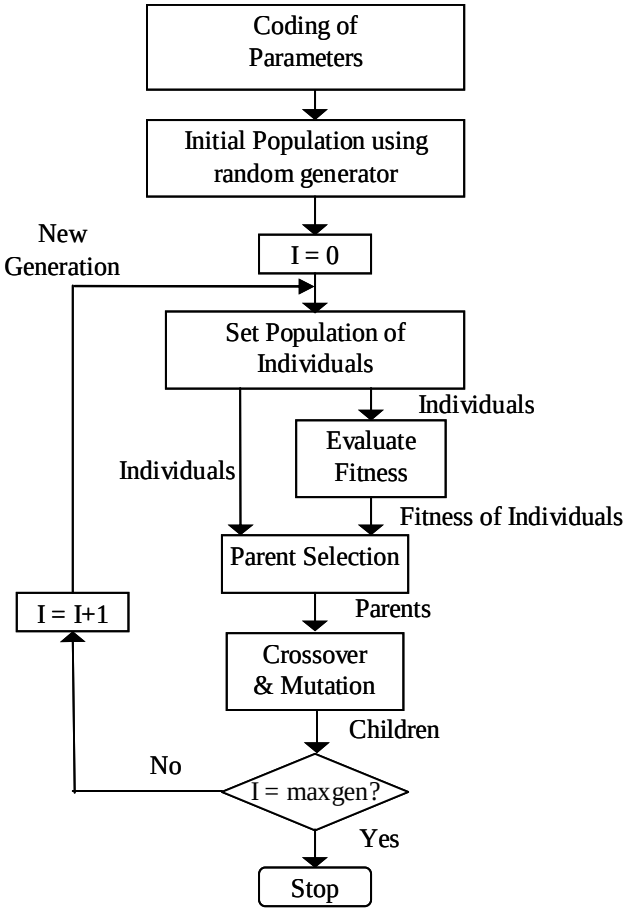

Figure B.5 GA flowchart.

B.5 Tournament Selection Method

Roulette wheel selection defined earlier suffers from two problems: (1) it can handle only maximization problems, and (2) scaling of the fitness becomes very important near convergence. Essentially, members with very poor fitness die out very early causing

premature convergence. To overcome these problems, few other selection techniques are available. The most used of all of these techniques is *tournament selection*. This method of selection is used for the work of this thesis.

In tournament selection, the population members are randomly divided into subgroups and members with the best fitness among the subgroups get selected for reproduction. The subgroups can be of any size. The usual choices are two and three. Figure B.6 shows the flow chart of a tournament selection with the subgroup size of two.

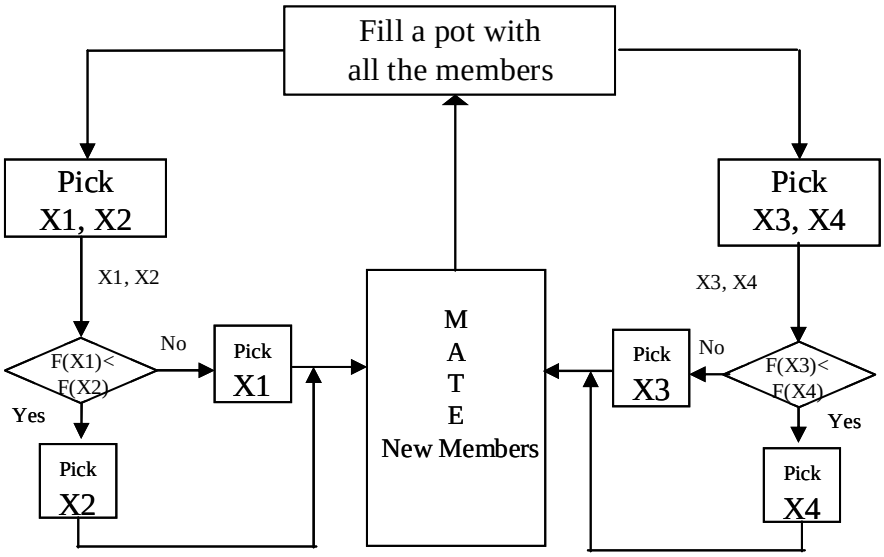

Figure B.6 Tournament selection.

APPENDIX C - THE THREE-AREA POWER SYSTEM DATA

C.1 The Three-Area Power System Data

Generators data

Generator	G_1	G_2	G_3
Rating, MVA	5500	1800	2400
Inertia constant, sec	4	4	3.5
x_d , p.u.	2	1	1.79
x_q , p.u.	1.9	0.6	1.71
$x_d^{'}$, p.u.	0.25	0.3	0.169
$T_{do}^{'}$, sec	6	6	4.3
K_A	30	10	10
T_A	0.05	0.05	0.05

Transmission lines, 500 kV

Line	L_1	L_2	L_3
Length, km	300	200	250
Z, Ω/km	0.01864 + j 0.3728		

System loads (1000 MVA, 500 kV base)

Load	S_1	S_2	S_3	S_4
S, p.u.	4.5 + j 2.7	0.9 + j 0.24	1.32 + j 0.36	0.6 + j 0.36

C.2 State Matrix Constants of the Three-Area Power System Equipped with UPFCs

$$K_1 = \begin{bmatrix} K_1(1,1) & K_1(1,2) & K_1(1,3) \\ K_1(2,1) & K_1(2,2) & K_1(2,3) \\ K_1(3,1) & K_1(3,2) & K_1(3,3) \end{bmatrix}$$

$$K_1(1,1) = \left[(x_{q1} - x'_{d1}) \frac{\partial I_{q1}}{\partial \delta_1} I_{d10} + (x_{q1} - x'_{d1}) \frac{\partial I_{d1}}{\partial \delta_1} I_{q10} + \frac{\partial I_{q1}}{\partial \delta_1} E'_{q10} \right]$$

$$K_1(1,2)=\left[\left(x_{q1}-x'_{d1}\right)\frac{\partial I_{q1}}{\partial \delta_2}I_{d10}+\left(x_{q1}-x'_{d1}\right)\frac{\partial I_{d1}}{\partial \delta_2}I_{q10}+\frac{\partial I_{q1}}{\partial \delta_2}E'_{q10}\right]$$

$$K_1(1,3)=\left[\left(x_{q1}-x'_{d1}\right)\frac{\partial I_{q1}}{\partial \delta_3}I_{d10}+\left(x_{q1}-x'_{d1}\right)\frac{\partial I_{d1}}{\partial \delta_3}I_{q10}+\frac{\partial I_{q1}}{\partial \delta_3}E'_{q10}\right]$$

$$K_1(2,1)=\left[\left(x_{q2}-x'_{d2}\right)\frac{\partial I_{q2}}{\partial \delta_1}I_{d20}+\left(x_{q2}-x'_{d2}\right)\frac{\partial I_{d2}}{\partial \delta_1}I_{q20}+\frac{\partial I_{q2}}{\partial \delta_1}E'_{q20}\right]$$

$$K_1(2,2)=\left[\left(x_{q2}-x'_{d2}\right)\frac{\partial I_{q2}}{\partial \delta_2}I_{d20}+\left(x_{q2}-x'_{d2}\right)\frac{\partial I_{d2}}{\partial \delta_2}I_{q20}+\frac{\partial I_{q2}}{\partial \delta_2}E'_{q20}\right]$$

$$K_1(2,3)=\left[\left(x_{q2}-x'_{d2}\right)\frac{\partial I_{q2}}{\partial \delta_3}I_{d20}+\left(x_{q2}-x'_{d2}\right)\frac{\partial I_{d2}}{\partial \delta_3}I_{q20}+\frac{\partial I_{q2}}{\partial \delta_3}E'_{q20}\right]$$

$$K_1(3,1)=\left[\left(x_{q3}-x'_{d3}\right)\frac{\partial I_{q3}}{\partial \delta_1}I_{d30}+\left(x_{q3}-x'_{d3}\right)\frac{\partial I_{d3}}{\partial \delta_1}I_{q30}+\frac{\partial I_{q3}}{\partial \delta_1}E'_{q30}\right]$$

$$K_1(3,2)=\left[\left(x_{q3}-x'_{d3}\right)\frac{\partial I_{q3}}{\partial \delta_2}I_{d30}+\left(x_{q3}-x'_{d3}\right)\frac{\partial I_{d3}}{\partial \delta_2}I_{q30}+\frac{\partial I_{q3}}{\partial \delta_2}E'_{q30}\right]$$

$$K_1(3,3)=\left[\left(x_{q3}-x'_{d3}\right)\frac{\partial I_{q3}}{\partial \delta_3}I_{d30}+\left(x_{q3}-x'_{d3}\right)\frac{\partial I_{d3}}{\partial \delta_3}I_{q30}+\frac{\partial I_{q3}}{\partial \delta_3}E'_{q30}\right]$$

$$K_2=\begin{bmatrix}K_2(1,1) & K_2(1,2) & K_2(1,3)\\ K_2(2,1) & K_2(2,2) & K_2(2,3)\\ K_2(3,1) & K_2(3,2) & K_2(3,3)\end{bmatrix}$$

$$K_2(1,1)=\left[\left(x_{q1}-x'_{d1}\right)\frac{\partial I_{q1}}{\partial E'_{q1}}I_{d10}+\left(x_{q1}-x'_{d1}\right)\frac{\partial I_{d1}}{\partial E'_{q1}}I_{q10}+I_{q10}+\frac{\partial I_{q1}}{\partial E'_{q1}}E'_{q10}\right]$$

$$K_2(1,2)=\left[\left(x_{q1}-x'_{d1}\right)\frac{\partial I_{q1}}{\partial E'_{q2}}I_{d10}+\left(x_{q1}-x'_{d1}\right)\frac{\partial I_{d1}}{\partial E'_{q2}}I_{q10}+\frac{\partial I_{q1}}{\partial E'_{q2}}E'_{q10}\right]$$

$$K_2(1,3)=\left[\left(x_{q1}-x'_{d1}\right)\frac{\partial I_{q1}}{\partial E'_{q3}}I_{d10}+\left(x_{q1}-x'_{d1}\right)\frac{\partial I_{d1}}{\partial E'_{q3}}I_{q10}+\frac{\partial I_{q1}}{\partial E'_{q3}}E'_{q10}\right]$$

$$K_2(2,1)=\left[\left(x_{q2}-x'_{d2}\right)\frac{\partial I_{q2}}{\partial E'_{q1}}I_{d20}+\left(x_{q2}-x'_{d2}\right)\frac{\partial I_{d2}}{\partial E'_{q1}}I_{q20}+\frac{\partial I_{q2}}{\partial E'_{q1}}E'_{q20}\right]$$

$$K_2(2,2)=\left[\left(x_{q2}-x'_{d2}\right)\frac{\partial I_{q2}}{\partial E'_{q2}}I_{d20}+\left(x_{q2}-x'_{d2}\right)\frac{\partial I_{d2}}{\partial E'_{q2}}I_{q20}+I_{q20}+\frac{\partial I_{q2}}{\partial E'_{q2}}E'_{q20}\right]$$

$$K_2(2,3)=\left[\left(x_{q2}-x'_{d2}\right)\frac{\partial I_{q2}}{\partial E'_{q3}}I_{d20}+\left(x_{q2}-x'_{d2}\right)\frac{\partial I_{d2}}{\partial E'_{q3}}I_{q20}+\frac{\partial I_{q2}}{\partial E'_{q3}}E'_{q20}\right]$$

$$K_2(3,1)=\left[\left(x_{q3}-x'_{d3}\right)\frac{\partial I_{q3}}{\partial E'_{q1}}I_{d30}+\left(x_{q3}-x'_{d3}\right)\frac{\partial I_{d3}}{\partial E'_{q1}}I_{q30}+\frac{\partial I_{q3}}{\partial E'_{q1}}E'_{q30}\right]$$

$$K_2(3,2)=\left[\left(x_{q3}-x'_{d3}\right)\frac{\partial I_{q3}}{\partial E'_{q2}}I_{d30}+\left(x_{q3}-x'_{d3}\right)\frac{\partial I_{d3}}{\partial E'_{q2}}I_{q30}+\frac{\partial I_{q3}}{\partial E'_{q2}}E'_{q30}\right]$$

$$K_2(3,3)=\left[\left(x_{q3}-x'_{d3}\right)\frac{\partial I_{q3}}{\partial E'_{q3}}I_{d30}+\left(x_{q3}-x'_{d3}\right)\frac{\partial I_{d3}}{\partial E'_{q3}}I_{q30}+I_{q30}+\frac{\partial I_{q3}}{\partial E'_{q3}}E'_{q30}\right]$$

$$K_3=\begin{bmatrix}1+\left(x_{d1}-x'_{d1}\right)\frac{\partial I_{d1}}{\partial E'_{q1}} & \left(x_{d1}-x'_{d1}\right)\frac{\partial I_{d1}}{\partial E'_{q2}} & \left(x_{d1}-x'_{d1}\right)\frac{\partial I_{d1}}{\partial E'_{q3}}\\ \left(x_{d2}-x'_{d2}\right)\frac{\partial I_{d2}}{\partial E'_{q1}} & 1+\left(x_{d2}-x'_{d2}\right)\frac{\partial I_{d2}}{\partial E'_{q2}} & \left(x_{d2}-x'_{d2}\right)\frac{\partial I_{d2}}{\partial E'_{q3}}\\ \left(x_{d3}-x'_{d3}\right)\frac{\partial I_{d3}}{\partial E'_{q1}} & \left(x_{d3}-x'_{d3}\right)\frac{\partial I_{d3}}{\partial E'_{q2}} & 1+\left(x_{d3}-x'_{d3}\right)\frac{\partial I_{d3}}{\partial E'_{q3}}\end{bmatrix}$$

$$K_4=\begin{bmatrix}\left(x_{d1}-x'_{d1}\right)\frac{\partial I_{d1}}{\partial \delta_1} & \left(x_{d1}-x'_{d1}\right)\frac{\partial I_{d1}}{\partial \delta_2} & \left(x_{d1}-x'_{d1}\right)\frac{\partial I_{d1}}{\partial \delta_3}\\ \left(x_{d2}-x'_{d2}\right)\frac{\partial I_{d2}}{\partial \delta_1} & \left(x_{d2}-x'_{d2}\right)\frac{\partial I_{d2}}{\partial \delta_2} & \left(x_{d2}-x'_{d2}\right)\frac{\partial I_{d2}}{\partial \delta_3}\\ \left(x_{d3}-x'_{d3}\right)\frac{\partial I_{d3}}{\partial \delta_1} & \left(x_{d3}-x'_{d3}\right)\frac{\partial I_{d3}}{\partial \delta_2} & \left(x_{d3}-x'_{d3}\right)\frac{\partial I_{d3}}{\partial \delta_3}\end{bmatrix}$$

$$K_5 = \begin{bmatrix} \dfrac{V_{d1}\dfrac{\partial I_{d1}}{\partial \delta_1} + V_{q1}\dfrac{\partial V_{q1}}{\partial \delta_1}}{\sqrt{V_{d1}^2 + V_{q1}^2}} & \dfrac{V_{d1}\dfrac{\partial I_{d1}}{\partial \delta_2} + V_{q1}\dfrac{\partial V_{q1}}{\partial \delta_2}}{\sqrt{V_{d1}^2 + V_{q1}^2}} & \dfrac{V_{d1}\dfrac{\partial I_{d1}}{\partial \delta_3} + V_{q1}\dfrac{\partial V_{q1}}{\partial \delta_3}}{\sqrt{V_{d1}^2 + V_{q1}^2}} \\ \dfrac{V_{d2}\dfrac{\partial I_{d2}}{\partial \delta_1} + V_{q2}\dfrac{\partial V_{q2}}{\partial \delta_1}}{\sqrt{V_{d2}^2 + V_{q2}^2}} & \dfrac{V_{d2}\dfrac{\partial I_{d2}}{\partial \delta_2} + V_{q2}\dfrac{\partial V_{q2}}{\partial \delta_2}}{\sqrt{V_{d2}^2 + V_{q2}^2}} & \dfrac{V_{d2}\dfrac{\partial I_{d2}}{\partial \delta_3} + V_{q2}\dfrac{\partial V_{q2}}{\partial \delta_3}}{\sqrt{V_{d2}^2 + V_{q2}^2}} \\ \dfrac{V_{d3}\dfrac{\partial I_{d3}}{\partial \delta_1} + V_{q3}\dfrac{\partial V_{q3}}{\partial \delta_1}}{\sqrt{V_{d3}^2 + V_{q3}^2}} & \dfrac{V_{d3}\dfrac{\partial I_{d3}}{\partial \delta_2} + V_{q3}\dfrac{\partial V_{q3}}{\partial \delta_2}}{\sqrt{V_{d3}^2 + V_{q3}^2}} & \dfrac{V_{d3}\dfrac{\partial I_{d3}}{\partial \delta_3} + V_{q3}\dfrac{\partial V_{q3}}{\partial \delta_3}}{\sqrt{V_{d3}^2 + V_{q3}^2}} \end{bmatrix}$$

$$K_6 = \begin{bmatrix} \dfrac{V_{d1}\dfrac{\partial I_{d1}}{\partial E'_{q1}} + V_{q1}\dfrac{\partial V_{q1}}{\partial E'_{q1}}}{\sqrt{V_{d1}^2 + V_{q1}^2}} & \dfrac{V_{d1}\dfrac{\partial I_{d1}}{\partial E'_{q2}} + V_{q1}\dfrac{\partial V_{q1}}{\partial E'_{q2}}}{\sqrt{V_{d1}^2 + V_{q1}^2}} & \dfrac{V_{d1}\dfrac{\partial I_{d1}}{\partial E'_{q3}} + V_{q1}\dfrac{\partial V_{q1}}{\partial E'_{q3}}}{\sqrt{V_{d1}^2 + V_{q1}^2}} \\ \dfrac{V_{d2}\dfrac{\partial I_{d2}}{\partial E'_{q1}} + V_{q2}\dfrac{\partial V_{q2}}{\partial E'_{q1}}}{\sqrt{V_{d2}^2 + V_{q2}^2}} & \dfrac{V_{d2}\dfrac{\partial I_{d2}}{\partial E'_{q2}} + V_{q2}\dfrac{\partial V_{q2}}{\partial E'_{q2}}}{\sqrt{V_{d2}^2 + V_{q2}^2}} & \dfrac{V_{d2}\dfrac{\partial I_{d2}}{\partial E'_{q3}} + V_{q2}\dfrac{\partial V_{q2}}{\partial E'_{q3}}}{\sqrt{V_{d2}^2 + V_{q2}^2}} \\ \dfrac{V_{d3}\dfrac{\partial I_{d3}}{\partial E'_{q1}} + V_{q3}\dfrac{\partial V_{q3}}{\partial E'_{q1}}}{\sqrt{V_{d3}^2 + V_{q3}^2}} & \dfrac{V_{d3}\dfrac{\partial I_{d3}}{\partial E'_{q2}} + V_{q3}\dfrac{\partial V_{q3}}{\partial E'_{q2}}}{\sqrt{V_{d3}^2 + V_{q3}^2}} & \dfrac{V_{d3}\dfrac{\partial I_{d3}}{\partial E'_{q3}} + V_{q3}\dfrac{\partial V_{q3}}{\partial E'_{q3}}}{\sqrt{V_{d3}^2 + V_{q3}^2}} \end{bmatrix}$$

where

$I_{d1} =$

$$\begin{aligned}
&- C_{d11}E'_{q1}\sin(\beta_{d11}) - C_{d12}E'_{q2}\sin(\delta_2 - \delta_1 + \beta_{d12}) - C_{d13}E'_{q3}\sin(\delta_3 - \delta_1 + \beta_{d13}) \\
&+ C_{d11}(x_{q1} - x'_{d1})\cdot I_{q1}\cos(\beta_{d11}) + C_{d12}(x_{q2} - x'_{d2})\cdot I_{q2}\cos(\delta_2 - \delta_1 + \beta_{d12}) \\
&+ C_{d13}(x_{q3} - x'_{d3})\cdot I_{q3}\cos(\delta_3 - \delta_1 + \beta_{d13}) \\
&+ C_{d11}C_{E11}V_{E1}\cos(\delta_1 + \delta_{E1} + \beta_{d11} + \beta_{E11}) + C_{d11}C_{E12}V_{E2}\cos(\delta_1 + \delta_{E2} + \beta_{d11} + \beta_{E12}) \\
&+ C_{d12}C_{E21}V_{E1}\cos(\delta_1 + \delta_{E1} + \beta_{d12} + \beta_{E21}) + C_{d12}C_{E22}V_{E2}\cos(\delta_1 + \delta_{E2} + \beta_{d12} + \beta_{E22}) \\
&+ C_{d13}C_{E31}V_{E1}\cos(\delta_1 + \delta_{E1} + \beta_{d13} + \beta_{E31}) + C_{d13}C_{E32}V_{E2}\cos(\delta_1 + \delta_{E2} + \beta_{d13} + \beta_{E32}) \\
&+ C_{d11}C_{B11}V_{B1}\cos(\delta_1 + \delta_{B1} + \beta_{d11} + \beta_{B11}) + C_{d11}C_{B12}V_{B2}\cos(\delta_1 + \delta_{B2} + \beta_{d11} + \beta_{B12}) \\
&+ C_{d12}C_{B21}V_{B1}\cos(\delta_1 + \delta_{B1} + \beta_{d12} + \beta_{B21}) + C_{d12}C_{B22}V_{B2}\cos(\delta_1 + \delta_{B2} + \beta_{d12} + \beta_{B22}) \\
&+ C_{d13}C_{B31}V_{B1}\cos(\delta_1 + \delta_{B1} + \beta_{d13} + \beta_{B31}) + C_{d13}C_{B32}V_{B2}\cos(\delta_1 + \delta_{B2} + \beta_{d13} + \beta_{B32})
\end{aligned}$$

$$I_{q1} =$$

$$C_{d11}E'_{q1}\cos(\beta_{d11}) + C_{d12}E'_{q2}\cos(\delta_2 - \delta_1 + \beta_{d12}) + C_{d13}E'_{q3}\cos(\delta_3 - \delta_1 + \beta_{d13})$$
$$+ C_{d11}(x_{q1} - x'_{d1})\cdot I_{q1}\sin(\beta_{d11}) + C_{d12}(x_{q2} - x'_{d2})\cdot I_{q2}\sin(\delta_2 - \delta_1 + \beta_{d12})$$
$$+ C_{d13}(x_{q3} - x'_{d3})\cdot I_{q3}\sin(\delta_3 - \delta_1 + \beta_{d13})$$
$$+ C_{d11}C_{E11}V_{E1}\sin(\delta_1 + \delta_{E1} + \beta_{d11} + \beta_{E11}) + C_{d11}C_{E12}V_{E2}\sin(\delta_1 + \delta_{E2} + \beta_{d11} + \beta_{E12})$$
$$+ C_{d12}C_{E21}V_{E1}\sin(\delta_1 + \delta_{E1} + \beta_{d12} + \beta_{E21}) + C_{d12}C_{E22}V_{E2}\sin(\delta_1 + \delta_{E2} + \beta_{d12} + \beta_{E22})$$
$$+ C_{d13}C_{E31}V_{E1}\sin(\delta_1 + \delta_{E1} + \beta_{d13} + \beta_{E31}) + C_{d13}C_{E32}V_{E2}\sin(\delta_1 + \delta_{E2} + \beta_{d13} + \beta_{E32})$$
$$+ C_{d11}C_{B11}V_{B1}\sin(\delta_1 + \delta_{B1} + \beta_{d11} + \beta_{B11}) + C_{d11}C_{B12}V_{B2}\sin(\delta_1 + \delta_{B2} + \beta_{d11} + \beta_{B12})$$
$$+ C_{d12}C_{B21}V_{B1}\sin(\delta_1 + \delta_{B1} + \beta_{d12} + \beta_{B21}) + C_{d12}C_{B22}V_{B2}\sin(\delta_1 + \delta_{B2} + \beta_{d12} + \beta_{B22})$$
$$+ C_{d13}C_{B31}V_{B1}\sin(\delta_1 + \delta_{B1} + \beta_{d13} + \beta_{B31}) + C_{d13}C_{B32}V_{B2}\sin(\delta_1 + \delta_{B2} + \beta_{d13} + \beta_{B32})$$

$$I_{d2} =$$

$$-C_{d21}E'_{q1}\sin(\delta_1 - \delta_2 + \beta_{d21}) - C_{d22}E'_{q2}\sin(\beta_{d22}) - C_{d23}E'_{q3}\sin(\delta_3 - \delta_2 + \beta_{d23})$$
$$+ C_{d21}(x_{q1} - x'_{d1})\cdot I_{q1}\cos(\delta_1 - \delta_2 + \beta_{d21}) + C_{d22}(x_{q2} - x'_{d2})\cdot I_{q2}\cos(\beta_{d22})$$
$$+ C_{d23}(x_{q3} - x'_{d3})\cdot I_{q3}\cos(\delta_3 - \delta_2 + \beta_{d23})$$
$$+ C_{d21}C_{E11}V_{E1}\cos(\delta_2 + \delta_{E1} + \beta_{d21} + \beta_{E11}) + C_{d21}C_{E12}V_{E2}\cos(\delta_2 + \delta_{E2} + \beta_{d21} + \beta_{E12})$$
$$+ C_{d22}C_{E21}V_{E1}\cos(\delta_2 + \delta_{E1} + \beta_{d22} + \beta_{E21}) + C_{d22}C_{E22}V_{E2}\cos(\delta_2 + \delta_{E2} + \beta_{d22} + \beta_{E22})$$
$$+ C_{d23}C_{E31}V_{E1}\cos(\delta_2 + \delta_{E1} + \beta_{d23} + \beta_{E31}) + C_{d23}C_{E32}V_{E2}\cos(\delta_2 + \delta_{E2} + \beta_{d23} + \beta_{E32})$$
$$+ C_{d21}C_{B11}V_{B1}\cos(\delta_2 + \delta_{B1} + \beta_{d21} + \beta_{B11}) + C_{d21}C_{B12}V_{B2}\cos(\delta_2 + \delta_{B2} + \beta_{d21} + \beta_{B12})$$
$$+ C_{d22}C_{B21}V_{B1}\cos(\delta_2 + \delta_{B1} + \beta_{d22} + \beta_{B21}) + C_{d22}C_{B22}V_{B2}\cos(\delta_2 + \delta_{B2} + \beta_{d22} + \beta_{B22})$$
$$+ C_{d23}C_{B31}V_{B1}\cos(\delta_2 + \delta_{B1} + \beta_{d23} + \beta_{B31}) + C_{d23}C_{B32}V_{B2}\cos(\delta_2 + \delta_{B2} + \beta_{d23} + \beta_{B32})$$

$$I_{q2} =$$

$$C_{d21}E'_{q1}\cos(\delta_1 - \delta_2 + \beta_{d21}) + C_{d22}E'_{q2}\cos(\beta_{d22}) + C_{d23}E'_{q3}\cos(\delta_3 - \delta_2 + \beta_{d23})$$
$$+ C_{d21}(x_{q1} - x'_{d1})\cdot I_{q1}\sin(\delta_1 - \delta_2 + \beta_{d21}) + C_{d22}(x_{q2} - x'_{d2})\cdot I_{q2}\sin(\beta_{d22})$$
$$+ C_{d23}(x_{q3} - x'_{d3})\cdot I_{q3}\sin(\delta_3 - \delta_2 + \beta_{d23})$$
$$+ C_{d21}C_{E11}V_{E1}\sin(\delta_2 + \delta_{E1} + \beta_{d21} + \beta_{E11}) + C_{d21}C_{E12}V_{E2}\sin(\delta_2 + \delta_{E2} + \beta_{d21} + \beta_{E12})$$
$$+ C_{d22}C_{E21}V_{E1}\sin(\delta_2 + \delta_{E1} + \beta_{d22} + \beta_{E21}) + C_{d22}C_{E22}V_{E2}\sin(\delta_2 + \delta_{E2} + \beta_{d22} + \beta_{E22})$$
$$+ C_{d23}C_{E31}V_{E1}\sin(\delta_2 + \delta_{E1} + \beta_{d23} + \beta_{E31}) + C_{d23}C_{E32}V_{E2}\sin(\delta_2 + \delta_{E2} + \beta_{d23} + \beta_{E32})$$
$$+ C_{d21}C_{B11}V_{B1}\sin(\delta_2 + \delta_{B1} + \beta_{d21} + \beta_{B11}) + C_{d21}C_{B12}V_{B2}\sin(\delta_2 + \delta_{B2} + \beta_{d21} + \beta_{B12})$$
$$+ C_{d22}C_{B21}V_{B1}\sin(\delta_2 + \delta_{B1} + \beta_{d22} + \beta_{B21}) + C_{d22}C_{B22}V_{B2}\sin(\delta_2 + \delta_{B2} + \beta_{d22} + \beta_{B22})$$
$$+ C_{d23}C_{B31}V_{B1}\sin(\delta_2 + \delta_{B1} + \beta_{d23} + \beta_{B31}) + C_{d23}C_{B32}V_{B2}\sin(\delta_2 + \delta_{B2} + \beta_{d23} + \beta_{B32})$$

$$I_{d3} =$$

$$
\begin{aligned}
&- C_{d31}E'_{q1}\sin(\delta_1-\delta_3+\beta_{d31}) - C_{d32}E'_{q2}\sin(\delta_2-\delta_3+\beta_{d32}) - C_{d33}E'_{q3}\sin(\beta_{d33})\\
&+ C_{d31}(x_{q1}-x'_{d1})\cdot I_{q1}\cos(\delta_1-\delta_3+\beta_{d31}) + C_{d32}(x_{q2}-x'_{d2})\cdot I_{q2}\cos(\delta_2-\delta_3+\beta_{d32})\\
&+ C_{d33}(x_{q3}-x'_{d3})\cdot I_{q3}\cos(\beta_{d33})\\
&+ C_{d31}C_{E11}V_{E1}\cos(\delta_3+\delta_{E1}+\beta_{d31}+\beta_{E11}) + C_{d31}C_{E12}V_{E2}\cos(\delta_3+\delta_{E2}+\beta_{d31}+\beta_{E12})\\
&+ C_{d32}C_{E21}V_{E1}\cos(\delta_3+\delta_{E1}+\beta_{d32}+\beta_{E21}) + C_{d32}C_{E22}V_{E2}\cos(\delta_3+\delta_{E2}+\beta_{d32}+\beta_{E22})\\
&+ C_{d33}C_{E31}V_{E1}\cos(\delta_3+\delta_{E1}+\beta_{d33}+\beta_{E31}) + C_{d33}C_{E32}V_{E2}\cos(\delta_3+\delta_{E2}+\beta_{d33}+\beta_{E32})\\
&+ C_{d31}C_{B11}V_{B1}\cos(\delta_3+\delta_{B1}+\beta_{d31}+\beta_{B11}) + C_{d31}C_{B12}V_{B2}\cos(\delta_3+\delta_{B2}+\beta_{d31}+\beta_{B12})\\
&+ C_{d32}C_{B21}V_{B1}\cos(\delta_3+\delta_{B1}+\beta_{d32}+\beta_{B21}) + C_{d32}C_{B22}V_{B2}\cos(\delta_3+\delta_{B2}+\beta_{d32}+\beta_{B22})\\
&+ C_{d33}C_{B31}V_{B1}\cos(\delta_3+\delta_{B1}+\beta_{d33}+\beta_{B31}) + C_{d33}C_{B32}V_{B2}\cos(\delta_3+\delta_{B2}+\beta_{d33}+\beta_{B32})
\end{aligned}
$$

$$I_{q3} =$$

$$
\begin{aligned}
&+ C_{d31}E'_{q1}\cos(\delta_1-\delta_3+\beta_{d31}) + C_{d32}E'_{q2}\cos(\delta_2-\delta_3+\beta_{d32}) + C_{d33}E'_{q3}\cos(\beta_{d33})\\
&+ C_{d31}(x_{q1}-x'_{d1})\cdot I_{q1}\sin(\delta_1-\delta_3+\beta_{d31}) + C_{d32}(x_{q2}-x'_{d2})\cdot I_{q2}\sin(\delta_2-\delta_3+\beta_{d32})\\
&+ C_{d33}(x_{q3}-x'_{d3})\cdot I_{q3}\sin(\beta_{d33})\\
&+ C_{d31}C_{E11}V_{E1}\sin(\delta_3+\delta_{E1}+\beta_{d31}+\beta_{E11}) + C_{d31}C_{E12}V_{E2}\sin(\delta_3+\delta_{E2}+\beta_{d31}+\beta_{E12})\\
&+ C_{d32}C_{E21}V_{E1}\sin(\delta_3+\delta_{E1}+\beta_{d32}+\beta_{E21}) + C_{d32}C_{E22}V_{E2}\sin(\delta_3+\delta_{E2}+\beta_{d32}+\beta_{E22})\\
&+ C_{d33}C_{E31}V_{E1}\sin(\delta_3+\delta_{E1}+\beta_{d33}+\beta_{E31}) + C_{d33}C_{E32}V_{E2}\sin(\delta_3+\delta_{E2}+\beta_{d33}+\beta_{E32})\\
&+ C_{d31}C_{B11}V_{B1}\sin(\delta_3+\delta_{B1}+\beta_{d31}+\beta_{B11}) + C_{d31}C_{B12}V_{B2}\sin(\delta_3+\delta_{B2}+\beta_{d31}+\beta_{B12})\\
&+ C_{d32}C_{B21}V_{B1}\sin(\delta_3+\delta_{B1}+\beta_{d32}+\beta_{B21}) + C_{d32}C_{B22}V_{B2}\sin(\delta_3+\delta_{B2}+\beta_{d32}+\beta_{B22})\\
&+ C_{d33}C_{B31}V_{B1}\sin(\delta_3+\delta_{B1}+\beta_{d33}+\beta_{B31}) + C_{d33}C_{B32}V_{B2}\sin(\delta_3+\delta_{B2}+\beta_{d33}+\beta_{B32})
\end{aligned}
$$

$$V_{q1} = E'_{q1} - x'_{d1}I_{d1}, \quad V_{q2} = E'_{q2} - x'_{d2}I_{d2}, \quad V_{q3} = E'_{q3} - x'_{d3}I_{d3}$$

$$V_{d1} = x_{q1}I_{q1}, \quad V_{d2} = x_{q2}I_{q2}, \quad V_{d3} = x_{q3}I_{q3}$$

Considering two GUPFCs installed in the power system in tie-lines L_1 and L_3

$$K_{pd} = \begin{bmatrix} K_{pd}(1,1) & K_{pd}(1,2) \\ K_{pd}(2,1) & K_{pd}(2,2) \\ K_{pd}(3,1) & K_{pd}(3,2) \end{bmatrix}$$

$$K_{pd}(1,1) = \left[\left(x_{q1} - x'_{d1}\right)\frac{\partial I_{q1}}{\partial V_{dc1}} I_{d10} + \left(x_{q1} - x'_{d1}\right)\frac{\partial I_{d1}}{\partial V_{dc1}} I_{q10} + \frac{\partial I_{q1}}{\partial V_{dc1}} E'_{q10} \right]$$

$$K_{pd}(1,2)=\left[\left(x_{q1}-x'_{d1}\right)\frac{\partial I_{q1}}{\partial V_{dc2}}I_{d10}+\left(x_{q1}-x'_{d1}\right)\frac{\partial I_{d1}}{\partial V_{dc2}}I_{q10}+\frac{\partial I_{q1}}{\partial V_{dc2}}E'_{q10}\right]$$

$$K_{pd}(2,1)=\left[\left(x_{q2}-x'_{d2}\right)\frac{\partial I_{q2}}{\partial V_{dc1}}I_{d20}+\left(x_{q2}-x'_{d2}\right)\frac{\partial I_{d2}}{\partial V_{dc1}}I_{q20}+\frac{\partial I_{q2}}{\partial V_{dc1}}E'_{q20}\right]$$

$$K_{pd}(2,2)=\left[\left(x_{q2}-x'_{d2}\right)\frac{\partial I_{q2}}{\partial V_{dc2}}I_{d20}+\left(x_{q2}-x'_{d2}\right)\frac{\partial I_{d2}}{\partial V_{dc2}}I_{q20}+\frac{\partial I_{q2}}{\partial V_{dc2}}E'_{q20}\right]$$

$$K_{pd}(3,1)=\left[\left(x_{q3}-x'_{d3}\right)\frac{\partial I_{q3}}{\partial V_{dc1}}I_{d30}+\left(x_{q3}-x'_{d3}\right)\frac{\partial I_{d3}}{\partial V_{dc1}}I_{q30}+\frac{\partial I_{q3}}{\partial V_{dc1}}E'_{q30}\right]$$

$$K_{pd}(3,2)=\left[\left(x_{q3}-x'_{d3}\right)\frac{\partial I_{q3}}{\partial V_{dc2}}I_{d30}+\left(x_{q3}-x'_{d3}\right)\frac{\partial I_{d3}}{\partial V_{dc2}}I_{q30}+\frac{\partial I_{q3}}{\partial V_{dc2}}E'_{q30}\right]$$

$$\frac{\partial V_{q1}}{\partial v_{dc1}}=-x'_{d1}\cdot\frac{\partial I_{d1}}{\partial v_{dc1}},\qquad \frac{\partial V_{q1}}{\partial v_{dc2}}=-x'_{d1}\cdot\frac{\partial I_{d1}}{\partial v_{dc2}},\qquad \frac{\partial V_{q2}}{\partial v_{dc1}}=-x'_{d2}\cdot\frac{\partial I_{d2}}{\partial v_{dc1}}$$

$$\frac{\partial V_{q2}}{\partial v_{dc2}}=-x'_{d2}\cdot\frac{\partial I_{d2}}{\partial v_{dc2}},\qquad \frac{\partial V_{q3}}{\partial v_{dc1}}=-x'_{d3}\cdot\frac{\partial I_{d3}}{\partial v_{dc1}},\qquad \frac{\partial V_{q3}}{\partial v_{dc2}}=-x'_{d3}\cdot\frac{\partial I_{d3}}{\partial v_{dc2}}$$

$$\frac{\partial V_{d1}}{\partial v_{dc1}}=x_{q1}\cdot\frac{\partial I_{q1}}{\partial v_{dc1}}\qquad \frac{\partial V_{d1}}{\partial v_{dc2}}=x_{q1}\cdot\frac{\partial I_{q1}}{\partial v_{dc2}}$$

$$\frac{\partial V_{d2}}{\partial v_{dc1}}=x_{q2}\cdot\frac{\partial I_{q2}}{\partial v_{dc1}},\qquad \frac{\partial V_{d2}}{\partial v_{dc2}}=x_{q2}\cdot\frac{\partial I_{q2}}{\partial v_{dc2}}$$

$$\frac{\partial V_{d3}}{\partial v_{dc1}}=x_{q3}\cdot\frac{\partial I_{q3}}{\partial v_{dc1}}\qquad \frac{\partial V_{d3}}{\partial v_{dc2}}=x_{q3}\cdot\frac{\partial I_{q3}}{\partial v_{dc2}}$$

The constants K_{pe} to $K_{v\partial b}$ can be obtained similar to K_{pd}

APPENDIX D - THE PRE-DISTURBANCE OPERATING CONDITIONS OF THE THREE-AREA POWER SYSTEM

Case study used in Section 3.5

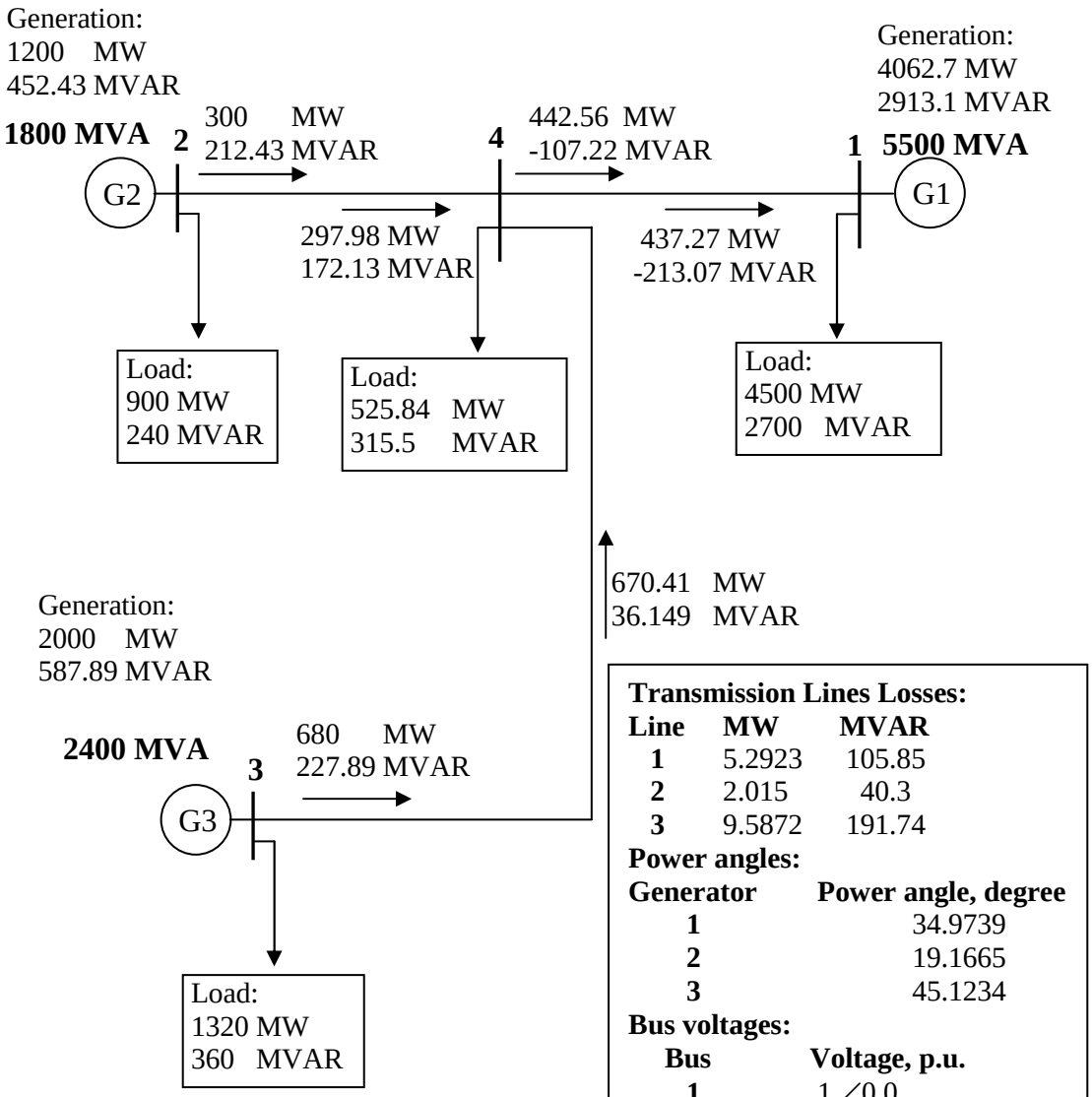

Transmission Lines Losses:

Line	MW	MVAR
1	5.2923	105.85
2	2.015	40.3
3	9.5872	191.74

Power angles:

Generator	Power angle, degree
1	34.9739
2	19.1665
3	45.1234

Bus voltages:

Bus	Voltage, p.u.
1	$1 \angle 0.0$
2	$1 \angle 17.65$
3	$1 \angle 27.8$
4	$0.9362 \angle 12.36$

Case 1, used in Section 3.8

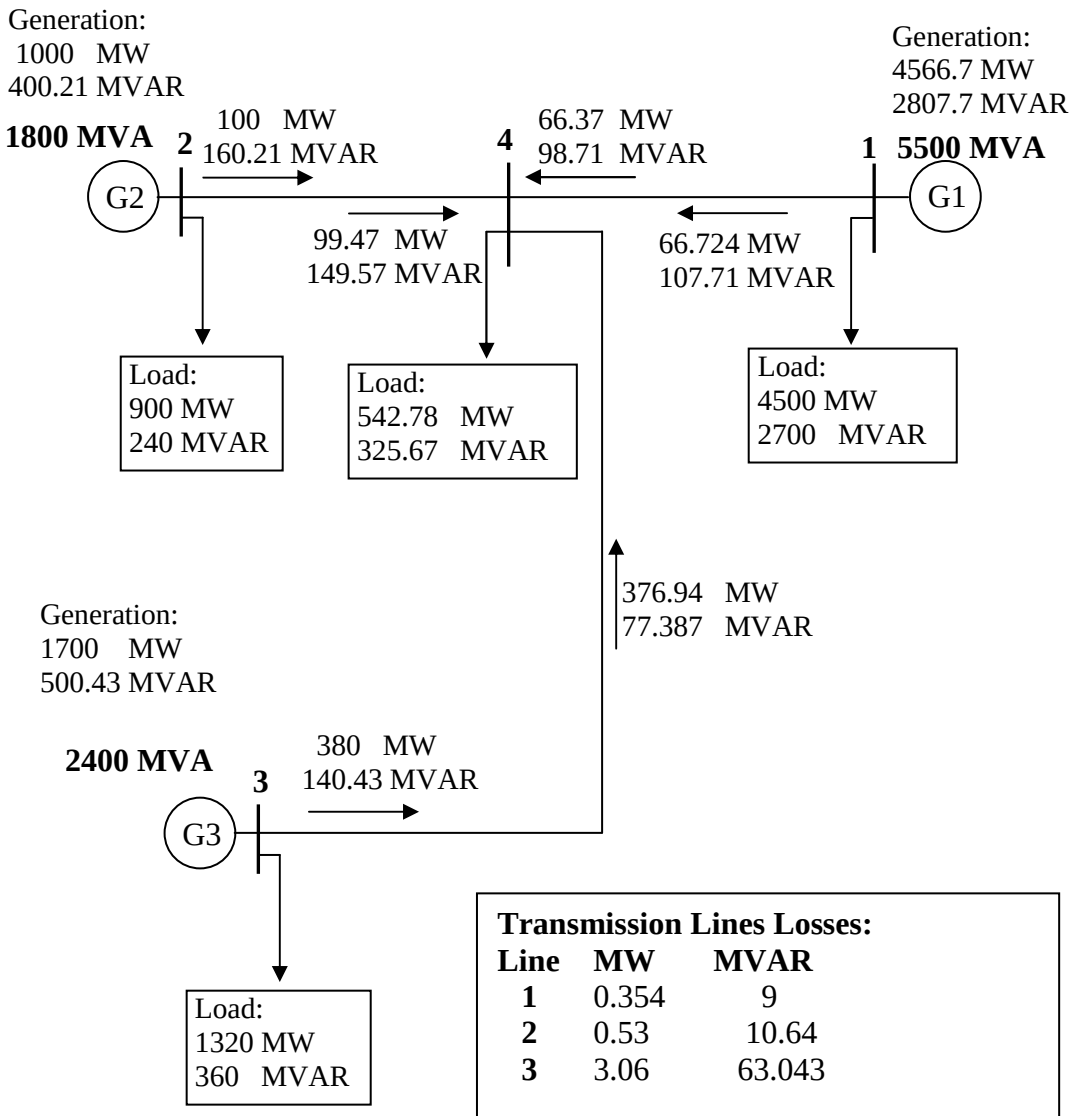

Transmission Lines Losses:

Line	MW	MVAR
1	0.354	9
2	0.53	10.64
3	3.06	63.043

Power angles:

Generator	Power angle, degree
1	38.689
2	16.3886
3	41.7612

Bus voltages:

Bus	Voltage, p.u.
1	$1 \angle 0.0$
2	$1 \angle 0$
3	$1 \angle 6.76$
4	$0.9511 \angle -1.66$

Case 2, used in Section 3.8

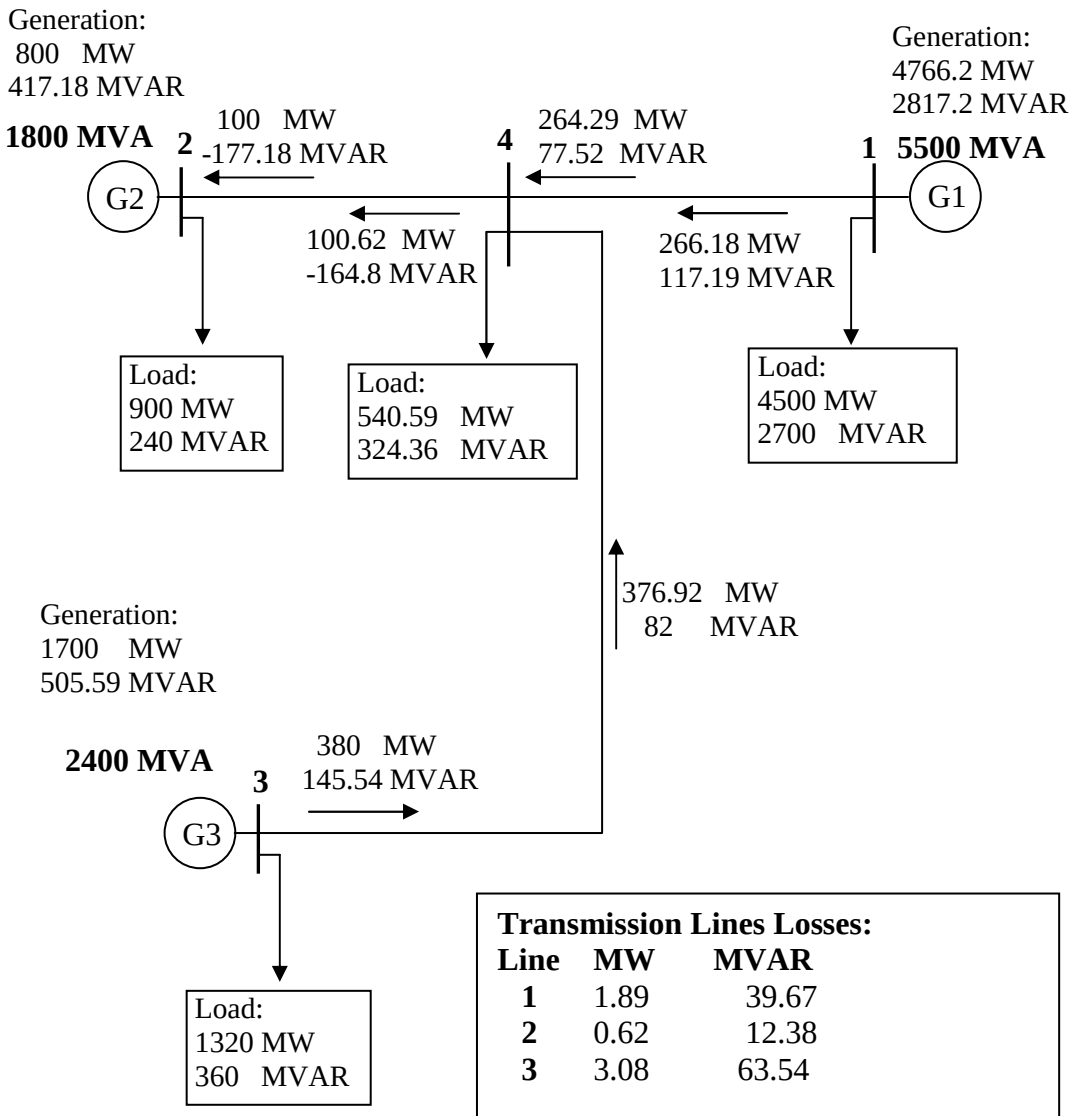

Transmission Lines Losses:

Line	MW	MVAR
1	1.89	39.67
2	0.62	12.38
3	3.08	63.54

Power angles:

Generator	Power angle, degree
1	39.84
2	13.17
3	41.68

Bus voltages:

Bus	Voltage, p.u.
1	1 ∠0.0
2	1 ∠-9.02
3	1 ∠1.37
4	0.9492 ∠-7.06

APPENDIX E - TIME DOMAIN SIMULATIONS FOR CASE 2

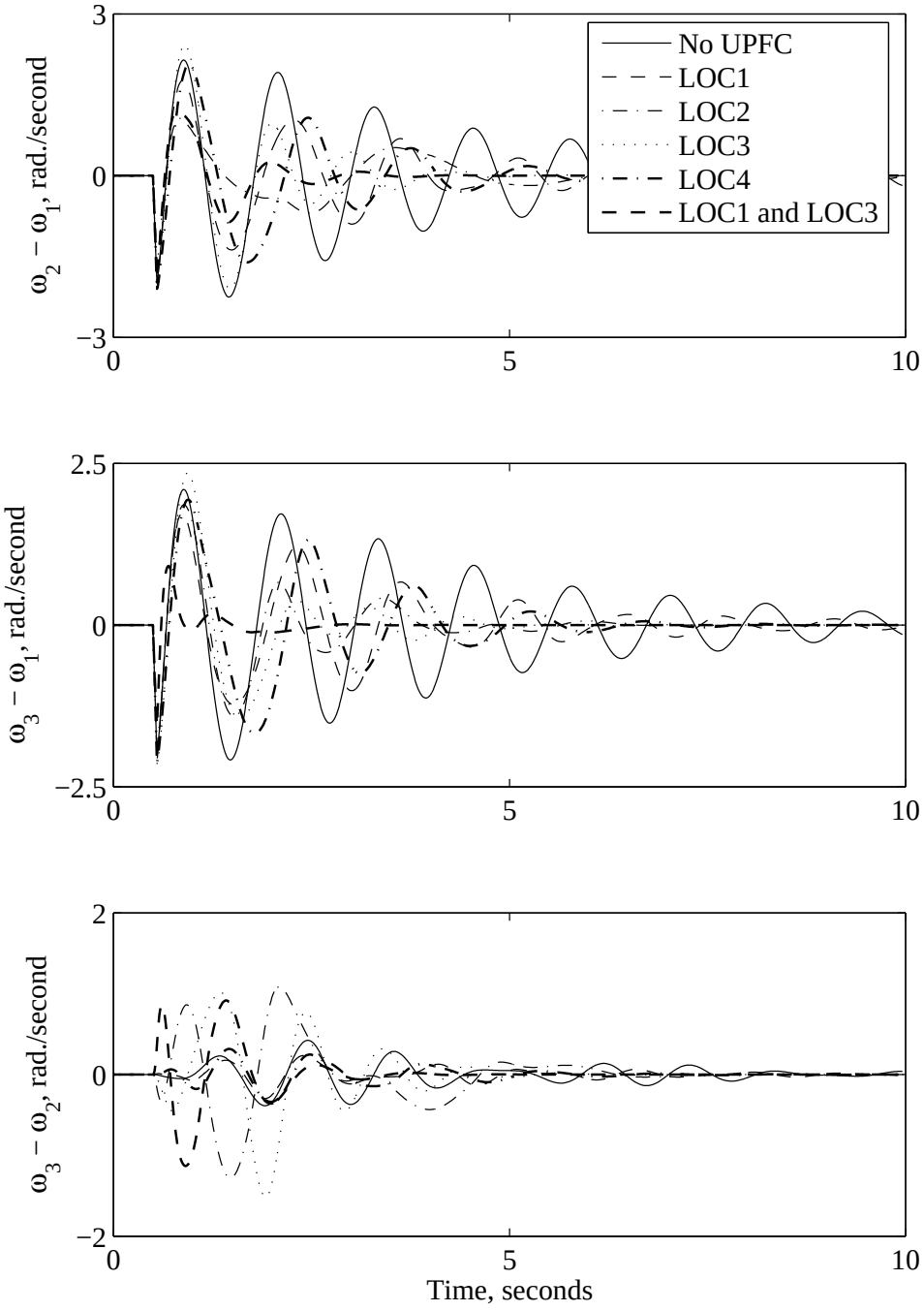

Figure E.1 Relative generator speeds due to a 3-cycle three-phase fault at bus 1 (operating conditions of case2).

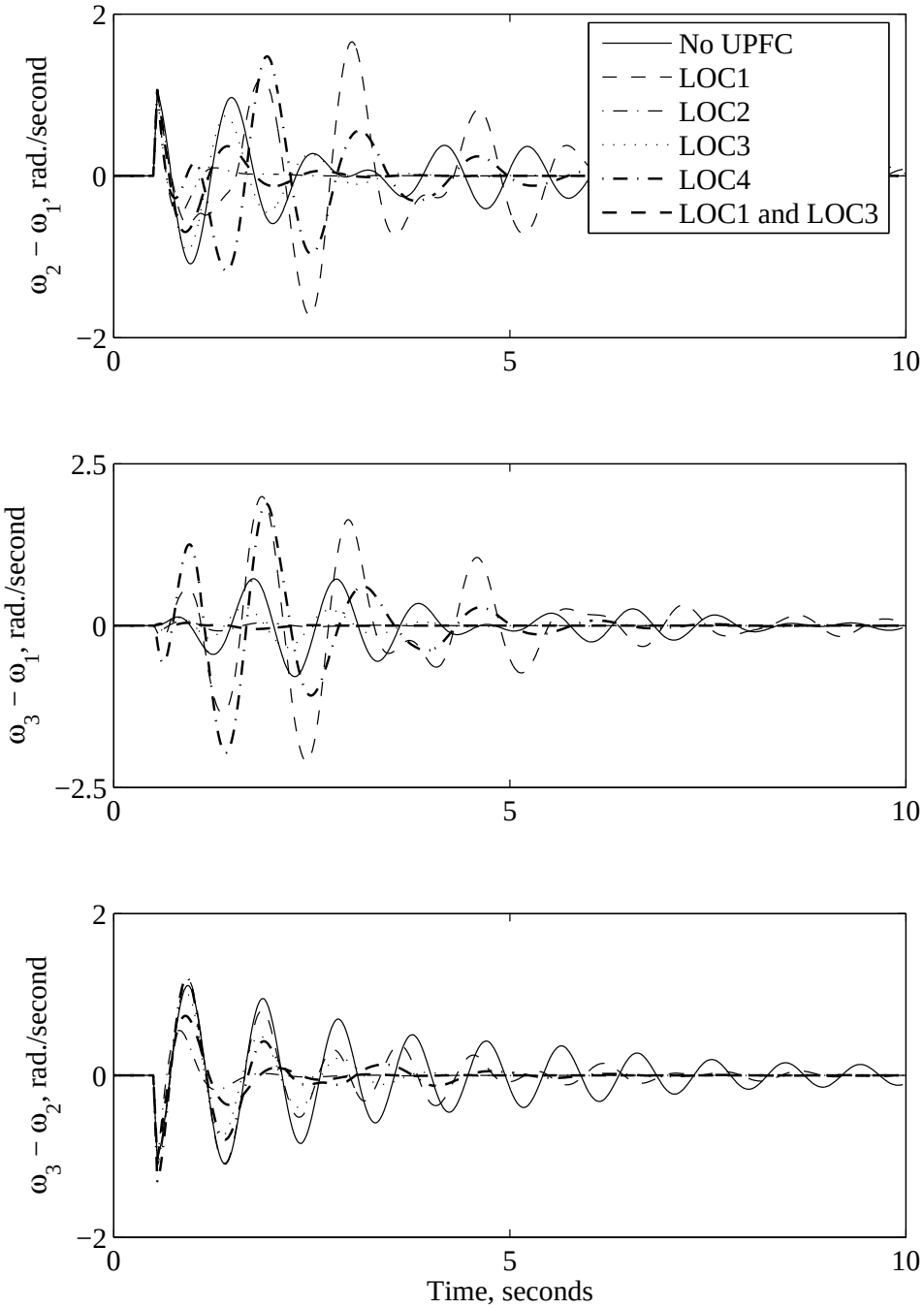

Figure E.2 Relative generator speeds due to a 3-cycle three-phase fault at bus 2 (operating conditions of case2).

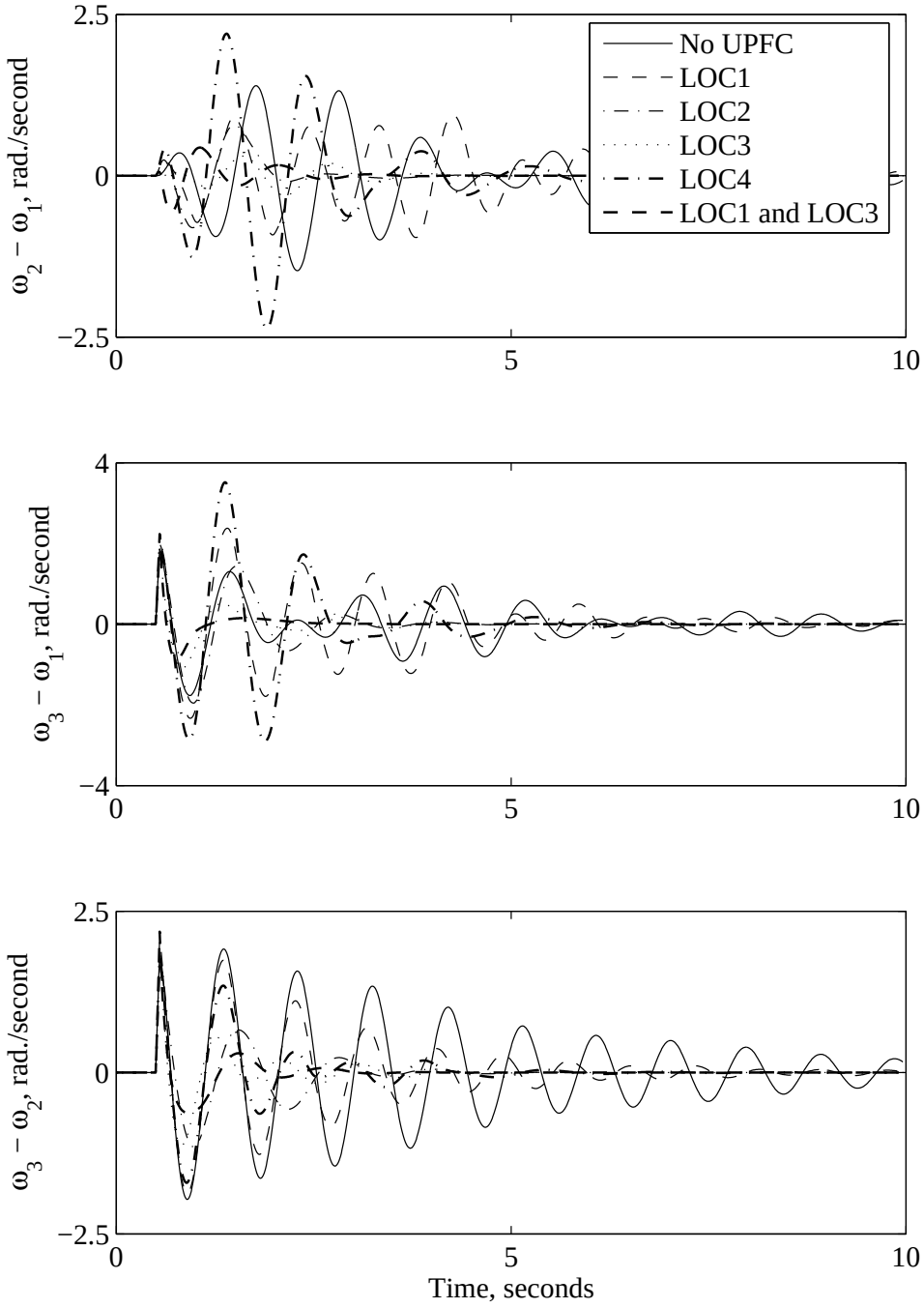

Figure E.3 Relative generator speeds due to a 3-cycle three-phase fault at bus 3 (operating conditions of case2).

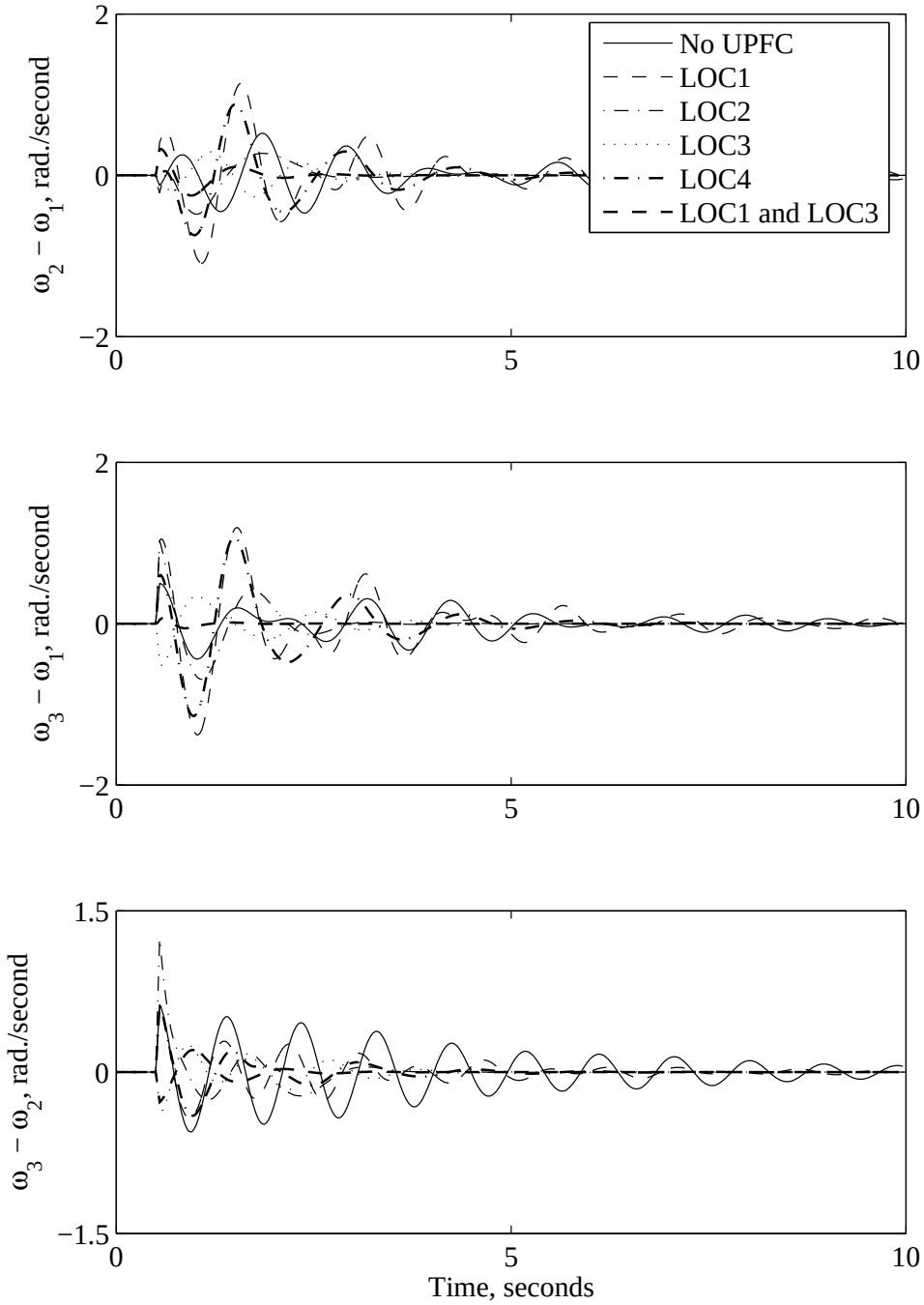

Figure E.4 Relative generator speeds due to a 3-cycle three-phase fault at bus 4 (operating conditions of case2).

APPENDIX F - TIME DOMAIN SIMULATIONS FOR ANOTHER FAULT CLEARING TIME

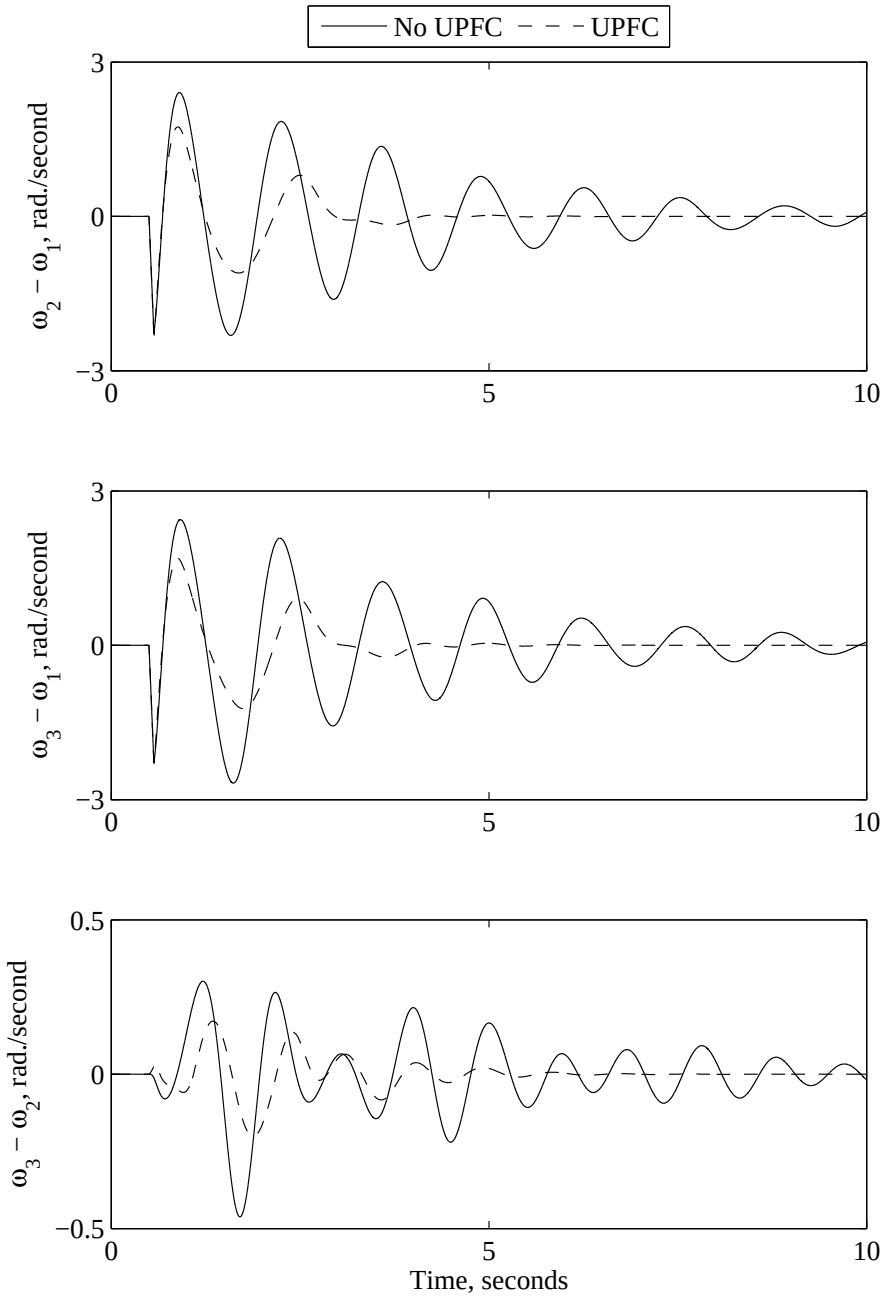

Figure F.1 Relative generator speeds due to a 4-cycle three-phase fault at bus 1 (a UPFC is installed at LOC1).

APPENDIX G - TORSIONAL NATURAL FREQUENCIES AND MODE SHAPES

Turbine-generator A

Rotor	Mode 1	Mode 2	Mode 3
Exciter	1.307	1.683	-102.6
Generator	1.0	1.0	1.0
LP-Turbine	-0.354	-1.345	-0.118
HP-Turbine	-1.365	4.813	0.0544

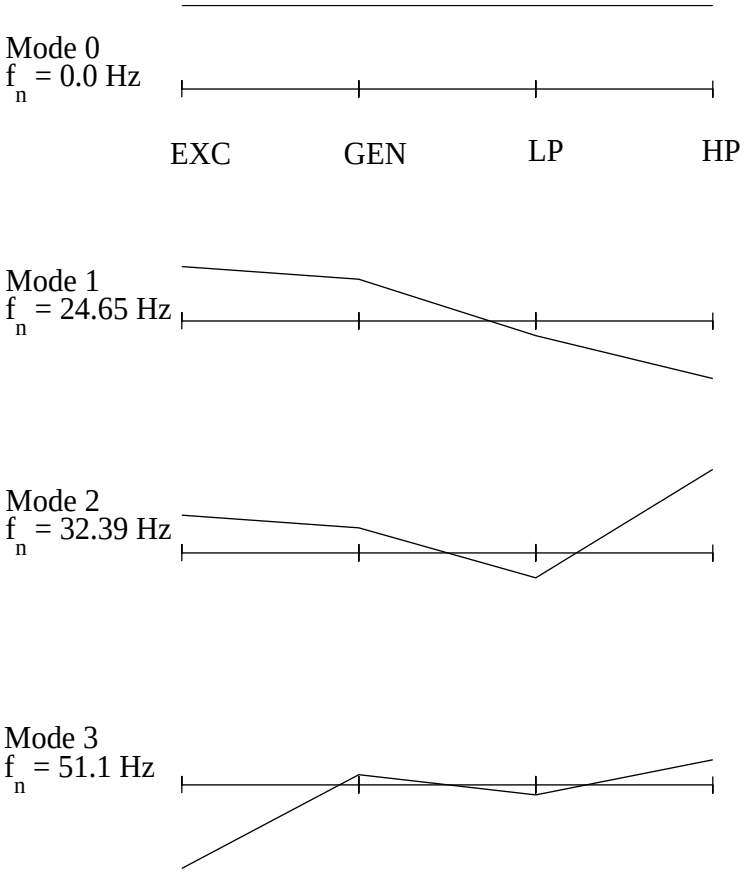

Figure G.1 Typical mode shapes of torsional mechanical system (turbine-generator A).

Turbine-generator B

Rotor	Mode 1	Mode 2	Mode 3	Mode 4	Mode 5
Exciter	2.681	-26.738	-1.5199	-0.6073	-0.2
Generator	1.0	1.0	1.0	1.0	1.0
LPB-Turbine	0.2992	1.0561	-0.5753	-1.6113	-4.6889
LPA-Turbine	0.918	0.4011	1.3831	0.8108	25.1778
IP-Turbine	-1.5646	-1.7299	2.062	0.0696	-222.222
HP-Turbine	-2.0826	-2.9385	6.0241	-1.3941	175.0889

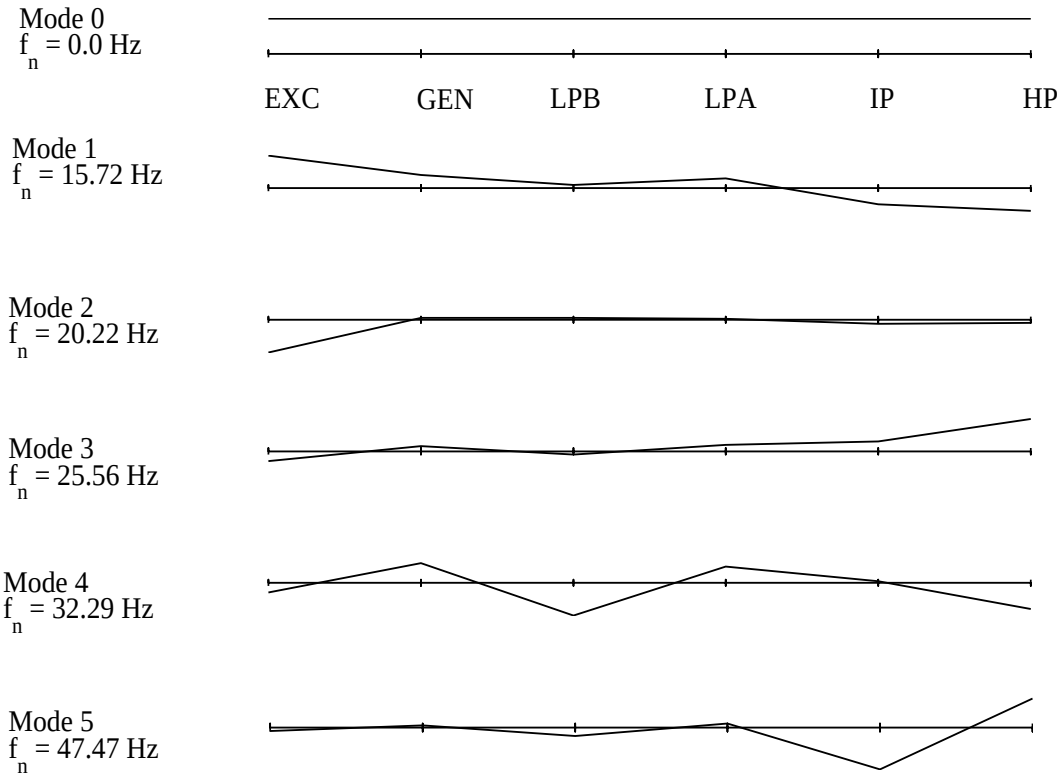

Figure G.2 Typical mode shapes of torsional mechanical system (turbine-generator B).